UNIVERSITAT POLITÈCNICA
DE CATALUNYA
BARCELONATECH

Technical-economic analysis, modeling and optimization of floating off shore wind farms

Markus Lerch

UNIVERSITAT POLITÈCNICA
DE CATALUNYA
BARCELONATECH

IREC

Shaping Energy for a Sustainable Future

PhD Thesis

Technical-Economic Analysis, Modeling and Optimization of Floating Offshore Wind Farms

Author: **Markus Lerch**

Advisors: **Dr. Mikel de Prada Gil**
Dr. Climent Molins Borrell

Program: **Civil Engineering**

Stuttgart, February 2020

Catalonia Institute for Energy Research (IREC)
Electrical Engineering Research Area
Jardins de les Dones de Negre 1 2nd floor,
08930 Sant Adrià de Besòs, Barcelona, Spain

Printed in Stuttgart
First Print, February 2020

UNIVERSITAT POLITÈCNICA DE CATALUNYA
BARCELONATECH
Escola de Doctorat

Curs acadèmic:

Acta de qualificació de tesi doctoral

Nom i cognoms

DNI / NIE / Passaport

Programa de doctorat

Unitat estructural responsable del programa

Resolució del Tribunal

Reunit el Tribunal designat a l'efecte, el doctorand / la doctoranda exposa el tema de la seva tesi doctoral titulada

_____

_____.

Acabada la lectura i després de donar resposta a les qüestions formulades pels membres titulars del tribunal, aquest atorga la qualificació:

☐ APTA/E ☐ NO APTA/E

(Nom, cognoms i signatura) President/a		(Nom, cognoms i signatura) Secretari/ària
(Nom, cognoms i signatura) Vocal	(Nom, cognoms i signatura) Vocal	(Nom, cognoms i signatura) Vocal

_____, _____ d'/de _____ de _____

El resultat de l'escrutini dels vots emesos pels membres titulars del tribunal, efectuat per l'Escola de Doctorat, a instància de la Comissió de Doctorat de la UPC, atorga la MENCIÓ CUM LAUDE:

☐ SÍ ☐ NO

(Nom, cognoms i signatura) Presidenta de la Comissió de Doctorat	(Nom, cognoms i signatura) Secretària de la Comissió de Doctorat

Barcelona, _____ d'/de _____ de _____

To my wife Sally
and my son Liam

Abstract

The offshore wind sector has grown significantly during the last decades driven by the increasing demand for clean energy and to reach defined energy targets based on renewable energies. As the wind speeds tend to be faster and steadier offshore, wind farms at sea can reach higher capacity factors compared to their onshore counterparts. Furthermore, fewer restrictions regarding land use, visual impact, and noise favors the application of this technology. However, most of today's offshore wind farms use bottom-fixed foundations that limit their feasible application to shallow water depths.

Floating substructures for offshore wind turbines are a suitable solution to harness the full potential of offshore wind as they have less constraints to water depths and soil conditions and can be applied from shallow to deep waters. As several floating offshore wind turbine (FOWT) concepts have been successfully tested in wave tanks and prototypes have been proven in open seas, floating offshore wind is now moving towards the commercial phase with the first floating offshore wind farm (FOWF) commissioned in 2017 and several more are projected to be constructed in 2020. This transition increases the need for comprehensive tools that allow to model the complete system and to predict its behavior as well as to assess the performance for different locations.

The aim of this thesis is to analysis from a technical and economic perspective commercial scale FOWFs. This includes the modeling of FOWTs and the study of their dynamic behavior as well as the economic assessment of different FOWT concepts. The optimization of the electrical layout is also addressed in this thesis.

The first model developed is applied to analyze the performance of a Spar type FOWT. The model is tested with different load cases and compared to a reference model. The results of both models show an overall good agreement. Afterwards, the developed model is applied to study the behavior of the FOWT with respect to three different offshore sites. Even at the site with the harshest conditions and largest motions, no significant loss in energy generation is measured, which demonstrates the good performance of this concept.

The second model is used to perform a technical-economic assessment of commercial scale FOWFs. It includes a comprehensive LCOE methodology based on a life cycle cost estimation as well as the computation of the energy yield. The model is applied to three FOWT concepts located at three different sites and considering a 500MW wind farm configuration. The findings indicate that FOWTs are a high competitive solution and energy can be produced at an equal or lower LCOE compared to bottom-fixed offshore wind or ocean energy technologies. Furthermore, a sensitivity analysis is performed to identify the key parameters that have a significant influence on the LCOE and which can be essential for further cost reductions.

The last model is aimed to optimize the electrical layout of FOWFs based on the particle swarm optimization theory. The model is validated against a reference model at first and is then used to optimize the inter-array cable routing of a 500MW FOWF. The obtained electrical layout results in a reduction of the power cable costs and a decrease of the energy losses. Finally, the use of different power cable configurations is studied and it is shown that the use of solely dynamic power cables in comparison to combined dynamic and static cables results in decreased acquisition and installation costs due to the avoidance of cost-intensive submarine joints and additional installation activities.

To conclude, the research work has generated practical models and tools that can be applied to analyze and assess FOWTs. Moreover, the application of the models has demonstrated the high potential of this technology to provide a competitive source of energy in the near future.

Resumen

El sector eólico marino ha crecido significativamente durante las últimas décadas impulsado por la creciente demanda de energía limpia. Los parques eólicos en el mar pueden alcanzar factores de capacidad más altos en comparación a los parques eólicos en la tierra debido a que las velocidades del viento tienden a ser más altas y constantes en el mar. Además, existen menos restricciones con respecto al uso de la tierra, el impacto visual y el ruido. Sin embargo, la mayoría de los parques eólicos actuales utilizan subestructuras fijas que limitan su aplicación factible a aguas poco profundas.

Las subestructuras flotantes para turbinas eólicas marinas (FOWTs en inglés) son una solución adecuada para aprovechar todo el potencial de la energía eólica, ya que tienen menos restricciones para las profundidades del agua y el fondo marino. Dado que varios prototipos de FOWTs se han probado con éxito en el mar, la industria ahora está entrando a la fase comercial con el primer parque eólico flotante (FOWF en inglés) operativo y se proyecta que se pondrán en marcha más en los próximos años. Esta transiciõn aumenta la necesidad de herramientas integrales que permitan modelar el sistema completo y predecir su comportamiento, así como evaluar el rendimiento para diferentes lugares. El objetivo de esta tesis es analizar desde una perspectiva técnica y económica los FOWFs a escala comercial. Esto incluye el modelado de FOWTs, el estudio de su comportamiento dinámico, y la evaluación económica de diferentes conceptos. La optimización del diseño eléctrico también se aborda en esta tesis.

El primer modelo desarrollado se aplica para analizar el rendimiento de un FOWT tipo Spar. El modelo se prueba con diferentes tipos de carga y se compara con un modelo de referencia. Los resultados de ambos modelos muestran una buena concordancia. Posteriormente, el modelo se aplica para estudiar el comportamiento con respecto a tres lugares diferentes. Los resultados muestran que incluso en el sitio con las condiciones más severas, no se mide ninguna pérdida significativa en la generación de energía, lo que demuestra el buen rendimiento de este concepto.

El segundo modelo se utiliza para realizar una evaluación técnico-económica de los FOWF a escala comercial. Esto incluye una metodología integral del costo nivelado de energía (LCOE en inglés). El modelo se aplica a tres conceptos de FOWTs ubicados en tres lugares diferentes y considerando un parque eólico de 500MW. Los resultados indican que los FOWTs son una solución altamente competitiva y que la energía se puede producir con un LCOE igual o inferior en comparación con los parques eólicos con subestructuras fijas o las tecnologías de energía oceánica. Asimismo, se realiza un análisis de sensibilidad para identificar los parámetros claves que tienen una influencia significativa en el LCOE y que pueden ser esenciales para reducciones de costos.

El último modelo se aplica para optimizar el diseño eléctrico en función de la teoría de optimización por enjambre de partículas. Inicialmente el modelo se valida contra un modelo de referencia y luego se utiliza para optimizar la conexión de los cables entre los FOWTs. El diseño eléctrico obtenido da como resultado una reducción de los costos de cables y una disminución de las pérdidas de energía. Finalmente, se estudia el uso de diferentes configuraciones de cables y se demuestra que el uso de cables únicamente dinámicos en comparación con los cables dinámicos y estáticos combinados da como resultado una disminución de los costos de adquisición e instalación debido a que evitan la necesidad de juntas submarinas costosas y costos adicionales de instalación.

Para concluir, el trabajo de investigación ha generado modelos prácticos que pueden ser aplicados para analizar los FOWTs. Adicionalmente, la aplicación de los modelos ha demostrado el alto potencial de esta tecnología para proporcionar una fuente competitiva de energía en un futuro cercano.

Acknowledgements

This thesis has been carried out at the Electrical Engineering Research Area (EERA) of the Catalonia Institute for Energy Research (IREC). The research leading to this work has received funding from the European Union Horizon 2020 program under the grant agreement H2020-LCE-2014-1-640741.

First of all, I would like to express my sincere gratitude to my advisors Dr. Mikel de Prada Gil and Dr. Climent Molins Borrell for their guidance and support, as well as for their valuable scientific and personal advices throughout the PhD period. Also, I would like to say thank you to all my former colleagues from IREC for their help and friendship. I am especially grateful to Gabriela Benveniste, who has been my first contact person at IREC and a great colleague. Thank you for your continuous support, advice and friendship. Likewise, I would like to thank Prof. Oriol Gomis, who has rised my interest in offshore wind energy through his M.Sc. course in Wind Energy and who presented to me the opportunity to do a PhD at IREC.

I would like to acknowledge the LIFES50+ project and thank the consortium for the great collaboration and experience. It has been a pleasure to work in such an inspiring project with leaders from industry and academia and contribute to the further development of floating offshore wind. I am also grateful to InnoEnergy for the participation in the InnoEnergy PhD School, the interesting courses and the financial support received. Furthermore, I would like to thank SINTEF Ocean for providing me the opportunity of a 3-months research stay and welcome me at their facilities.

I greatly appreciate the help and hospitality of Dr. Maxime Thys and Dr. Petter Andreas Berthelsen. Finally, I would like to thank my family for their continuous support and especially my wife Sally for her patience, support and encouragement.

Contents

List of Tables

List of Figures

List of abbreviations

AC	Alternating Current
BOWF	Bottom-fixed Offshore Wind Farm
BOWT	Bottom-fixed Offshore Wind Turbine
CAPEX	Capital Expense
DC	Direct Current
DECEX	Decommissioning Expense
DOF	Degrees of Freedom
EENS	Expected Energy Not Supplied
FOWAT	Floating Offshore Wind Assessment Tool
FOWF	Floating Offshore Wind Farm
FOWT	Floating Offshore Wind Turbine
HVAC	High Voltage Alternating Current
HVDC	High Voltage Direct Current
IRR	Internal Rate of Return
JONSWAP	Joint North Sea Wave Project
LCC	Life Cycle Cost
LCOE	Levelized Cost Of Energy
LF	Low Frequency
LFAC	Low Frequency Alternating Current
MIQCP	Mixed Integer Quadratic Constraint Programmming

MTBF	Mean Time Between Failure
MTTR	Mean Time To Repair
MVAC	Medium Voltage Alternating Current
OPEX	Operating Expense
O&M	Operation & Maintenance
PCC	Point of Common Coupling
PSO	Particle Swarm Optimization
ROV	Remotely Operated Vehicle
TLP	Tension Leg Platform
VSC	Voltage Source Converter
WACC	Weighted Average Cost of Capital
XLPE	Cross-linked Polyethylene

1 Introduction

The offshore wind sector has experienced a significant development path during the last decades since the first offshore wind farm was built in Denmark back in 1991 [1]. Today more than 23.14GW of offshore wind power is installed globally of which the majority, about 79%, is located in European waters [2]. Europe has been pioneer and is still technology leader in offshore wind. However, Asian countries are gaining momentum and investments are rising. In 2018, for the first time China commissioned more offshore wind capacity than any other country [2]. Figure 1.1 presents the annual and cumulative offshore wind installation and highlights the key markets.

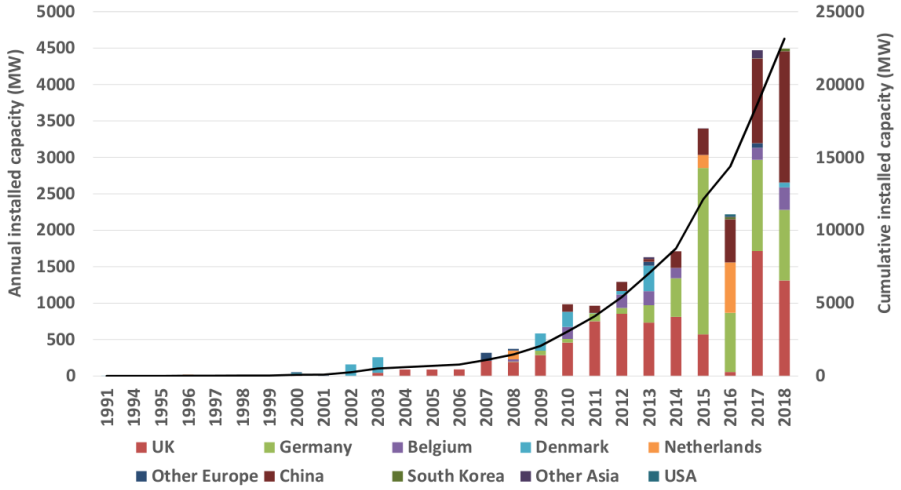

Figure 1.1: Global annual and cumulative offshore wind installations [3, 4].

The exponential increase in offshore wind installation has been driven by several factors. On the one hand, the wind speeds tend to be faster and steadier offshore, which leads to higher capacity factors and thus allowing a steadier supply of energy compared to other renewable energies sources. Furthermore, less restrictions exist regarding land use, visual impact, and noise, which favors the use of larger wind turbines and bigger wind farms [5]. On the other hand, political support and financial incentives combined with the increasing demand for clean energy to reduce carbon emissions and to reach defined national and international energy targets based on renewable energy sources have been key in the formation and rapid growth of the offshore wind sector in Europe [6]. In addition, significant cost reductions have been achieved by the industry along the whole supply chain, which have further increased the attractiveness of the technology for investments. However, the installed offshore wind capacity in Europe in 2018 has only covered 2% of the electricity demand and is still lagging behind its counterpart onshore, which served about 12% of the European electricity consumption [7]. The International Energy Agency estimated that the annual offshore wind installations need to more than quadruple in order to be on track with the Sustainable Development Scenario for 2030 and to meet the targets defined in the Paris Agreement [8].

The majority of offshore wind farms in Europe are located in the shallow waters of the North Sea (70%), followed by the Irish Sea (16%), the Baltic Sea (12%), and the Atlantic Ocean (2%) at an average water depth of 27m [9]. Considering the abundant wind resources available offshore, the industry has the potential to continue to grow. However, the current technology based on bottom-fixed offshore wind turbines (BOWTs) faces technical and economic limitations with increasing water depths [10]. Since shallow waters are scarce around the world, it becomes necessary to develop technical solutions to unlock the wind resources of deep water areas [11].

Floating substructures for offshore wind turbines are a promising solution that has been under development in recent years. They possess lower constraints to water depths and soil conditions and can be applied from shallow to deep waters, thus allowing to take advantage of the full potential of offshore wind [10]. It is estimated that 80% of all the offshore wind resource in Europe is located in water depths greater than 60m and thus favouring the application of floating offshore wind turbines (FOWTs). Moreover, FOWTs enable countries such as Japan, Spain, Portugal and Norway that lack of suitable shallow water sites to construct offshore wind farms and enter the offshore wind market [12].

1.1 Research motivations and objectives

Different concepts for FOWTs have been successfully tested in wind tunnels and wave tanks and several countries have recognized the potential of the technology and have installed prototypes offshore. In addition, the first pre-commercial floating offshore wind farm (FOWF) Hywind Scotland has been commissioned in 2017 and several more are projected to be constructed by 2020 [12]. However, in order to reach commercial application, FOWTs need to solve not only the technological challenges faced by its bottom-fixed counterparts but also provide an economic alternative [11].

The main objective of this thesis is to analyze from a technical and economic perspective novel commercial scale FOWFs. This includes the modeling of FOWTs and the study of their dynamic behavior as well as the economic assessment of different FOWT concepts. The optimization of the FOWF electrical layout is also addressed in this thesis. The specific goals of the thesis are summarized below.

- To develop a simplified numerical model that allows to predict the dynamic response of a FOWT to environmental loads and computes the power generated by the turbine.
- To analyze the dynamic behavior of a specific FOWT with respect to different met-ocean conditions and assess the power generation performance.
- To develop a comprehensive model for the technical-economic assessment of FOWFs in terms of the levelized cost of energy including a detailed computation of the life cycle costs and energy yield.
- To perform a LCOE analysis of large FOWFs located at different offshore sites and to identify the parameters that most influence the LCOE.
- To optimize the electrical layout of a FOWF using a newly developed model that is based on an algorithm that is adapted to the specific optimization problem.

1.2 Scope of the thesis and limitations

The scope of the thesis follows a multi-disciplinary approach as several disciplines are addressed to assess and evaluate FOWFs including subjects of electrical engineering, civil engineering, marine engineering and energy engineering as well as cost engineering. The idea is to study FOWTs from different perspectives to gain a broad understanding of the technology rather than focus on a single topic. This approach results in the division of the research work in three major research lines. The first is the modeling of the FOWT and the analysis of the response of the system to different loads as addressed by Chapter 3 and 4, respectively. The second research line concerns the technical-economic assessment of FOWFs, which is treated by Chapter 5. The last research line deals with the optimization of the electrical layout of the FOWF and is included in Chapter 6. The research lines may approach the topic differently but follow the same objective to provide models to assess and analyze the technology and its performance. As several topics are addressed, limitations have been defined to frame properly the scope of the thesis. For instance, the methodology presented in Chapter 3.2, which provides the theoretical background for the modeling of the system is based on a specific FOWT type. A different concept would require modifications of the equations used in the model. Chapter 5 and 6 focus on the assessment and optimization of FOWFs. The developed models consider the wind turbines, collection grid and transmission to shore. However, relevant issues regarding grid integration are out of the scope.

1.3 Thesis contributions

The main contributions of the thesis are summarized in this section along with their associated publications.

- Development of a simplified numerical model that allows capturing the main motions of a FOWT and computing the energy generation considering the dynamic behavior of the system and the environmental conditions of the site. The model includes a static sizing by calculating the main structural properties of the FOWT and predicts the dynamic response in each degree of freedom by solving the equation of motion. Furthermore, the model computes the power generated by the FOWT considering the additional mean platform tilt angle provoked by the motions of the FOWT and takes into account the relative wind

velocity in the wind force computation. The model has been applied in publications [C1] and [J2] as well as presented in [P4].

- Dynamic response analysis and performance assessment of a Sparbuoy FOWT for three offshore locations using the previously developed model. The influence of the different met-ocean conditions is studied with respect to the motion response and energy yield. In addition, the power production is compared to a BOWT. A sensitivity analysis of defined threshold limits for hub acceleration and platform pitch motion is carried out to study the impact on the capacity factor and downtime of the FOWT. The results have been published in [J2].

- A comprehensive methodology is developed for the calculation of the LCOE of a FOWF including the computation of the life cycle costs and lifetime energy production. The entire life cycle of the wind farm is considered in the cost calculation from development and manufacturing, to transportation, installation, and operation and maintenance until the final decommissioning. Furthermore, the costs are calculated for all components of the FOWF such as wind turbines, floating substructures, power cables and substation. The energy yield of the FOWF is calculated by considering turbine electrical losses, wake losses, availability losses as well as losses in the collection and transmission system. The methodology has been published and applied in [J1] and [O1].

- A technical-economic assessment of three FOWT concepts for three different offshore sites is performed using the previously developed LCOE methodology. In addition, a sensitivity analysis comprising more than 325 inputs parameters is carried out to identify the ones that most influence the LCOE. The results have been published in [J1] and presented in [P2] and [P3].

- An optimization model based on particle swarm theory has been developed to optimize the electrical layout of a FOWF. The model minimizes the cost of the layout considering the acquisition and installation cost as well as the energy losses in the cables and the losses due to unavailability. Furthermore, stochastic wind speed and wind direction are included as well as the entire wind turbine connection possibilities. A comprehensive wake model and different dynamic power cable configurations are also included. The model has been applied in publications [J3] and [C2]. Moreover, results have been presented in [P5].

- A novel tool has been developed with the objective to analyze and assess FOWFs from a technical and economic perspective. The tool named Floating Offshore Wind Assessment Tool (FOWAT) comprises all three major research lines of this thesis with respective modules. The dynamic response analysis and performance assessment of Chapter 4 have been carried out using the Dynamic Analysis module of the tool. The LCOE assessment and sensitivity analysis of Chapter 5 are performed with the Multi-Criteria Evaluation module. The optimization study of Chapter 6 applies the Electrical Layout Optimization module. A description of the tool is provided in Annex B. The tool has been used in the research project LIFES50+ and has been presented at several international conferences [P1, P2, P4, P6].

The publications indicated above are listed in Appendix A.

1.4 Thesis outline

This thesis has been divided into eight chapters organized as follows:

- **Chapter 2** presents the state of the art of the floating offshore wind technology. This chapter includes a description of the main components of a floating offshore wind farm and typical offshore wind configurations for the collection and transmission system, collection grid topologies and considerations for the wind farm layout. Furthermore, a market review is presented including an overview of floating offshore wind projects, a brief analysis of the main markets, as well as key challenges and opportunities of the technology.

- **Chapter 3** introduces into the modeling of floating offshore wind turbines. At first, a description of the offshore environment is given including wind, waves, currents and other environmental conditions such as snow and ice as well as seismic activity and marine growth. Then, the theoretical model is described used for analyzing the structural behavior of a FOWT followed by a description of the main loads acting on a FOWT. The methodology for the computation of the power generation is also given.

- **Chapter 4** presents the validation of a model developed to compute the dynamic response of a FOWT and predict the power performance. The model is based on the methodology presented in Chapter 3. The model is further used in Chapter 4 to compute the dynamic response

for a specific FOWT concept at different offshore sites and to compute the energy generation. A sensitivity analysis of different threshold limits for the operation of the FOWT is also provided.

- **Chapter 5** contains the technical-economic assessment of floating offshore wind farms in terms of a comprehensive LCOE computation. The methodology considered for the life cycle cost and energy yield is explained in detail. A tool has been developed based on the LCOE methodology and is used to perform the calculations. It is shown in Appendix B.1. The tool is applied on a specific case study and the results are presented for the LCOE calculations and for a sensitivity analysis.

- **Chapter 6** includes the optimization of the electrical layout of FOWFs. The applied methodology for the FOWF model is presented as well as the algorithm developed to perform the optimization. Furthermore, the objective function is defined as well as the specific constraints. Different application cases are used to validate the developed model and to perform case studies.

- Finally, the main conclusions of the thesis are given in **Chapter 7** and suggestions for further research work are provided in **Chapter 8**.

1.5 PhD related work and activities

In this section, an overview of PhD related work and activities are mentioned that have been realized and have contributed to the PhD thesis.

Pre-doctoral activities started in February 2016 with an internship at the Catalonia Institute for Energy Research (IREC) to prepare a Master of Science thesis with the title "Levelized cost of energy calculation for floating offshore wind power plants" [13]. The thesis prepared the basis for further work during the PhD related to the technical-economic assessment of floating offshore wind farms and contributed partially to the preparation of Chapters 2 and 6 of this PhD thesis. The PhD work was realized at IREC in the framework of the EU H2020 project LIFES50+ [14]. The project was led by a consortium of 12 leading European institutions and industry partners. It had the objective to develop and assess floating substructure concepts for 10MW offshore wind turbines and water depths greater than 50m. The project started in June 2015 and ended in April 2019.

The participation in the LIFES50+ project allowed to gain comprehensive knowledge about floating offshore wind technology and to connect with key players in the floating offshore wind industry. Furthermore, the project offered the opportunity to present the research work at several international conferences and project meetings as listed in Appendix A.4. Many synergies could be used as the topic of the project and the PhD have been closely related. IREC has led Work Package 2 "Concept Evaluation"and was responsible for the technical and economic evaluation of the substructure concepts. A tool has been developed called "Floating Offshore Wind Assessment Tool - FOWAT", which was used in the LIFES50+ project to evaluate the different FOWT concepts and in the PhD thesis to perform LCOE calculations. A description of the tool is provided in Appendix B. The participation in the project resulted in the publication of several deliverables either as first author or co-author, which are listed in Appendix A.3. Furthermore, the [J1] journal paper has been derived from the project. In addition, the research work concerning this topic has been presented at WindEurope Summit in 2016 [P1] as well as the WindFarms [P2] and WindEurope Conference & Exhibition in 2017 [P3].

The participation in the InnoEnergy PhD School has been a further activity realized during the PhD period. The InnoEnergy PhD School provides high-value complemantary training in innovation, entrepreneurship and business for PhD candidates working in the energy sector [15]. The program enabled to gain specific business skills and to broaden the knowledge on the potential value and application of the performed research. Furthermore, the personal and professional network could be expanded through courses, workshops and conference participations.

The InnoEnergy PhD School supported also the participation in a PhD Summer School and the realization of an international placement. The 8-day PhD Summer School was organized by the Technical University of Denmark (DTU) in August 2017. It had the objective to deepen the knowledge in the analysis, design and testing of floating offshore wind turbine substructures with a particular focus on the modelling and design process of floating substructures [16]. The Summer School provided the fundamental principles required for the modelling of FOWTs and the essential theoretical background for further research on this topic.

The international placement took place after the Summer School and consisted of a 3-months research stay at SINTEF Ocean in Trondheim, Norway. The objective of the research stay was to apply the knowledge gained during the Summer School by developing a tool to model the dynamic behavior of a specific FOWT concept and compute the power generation.

A description of the tool developed during the research stay abroad is given in Appendix B.2. A highlight of the research stay was the experience of the LIFES50+ FOWT model tests in the ocean basin. Results of this research topic have been presented at the ICREN 2018 conference [P4]. Furthermore, journal paper [J2] and conference paper [C1] have been published.

The last research topic of this PhD thesis concerning the electrical layout optimization of FOWFs has been developed in cooperation with the French FOWT concept developer IDEOL, who has also been a participant in the LIFES50+ project. An additional tool has been developed that was used to perform the optimization calculations. A description of the tool is provided in Appendix B. Findings of this research topic have been presented at the DeepWind 2019 conference (P6). Furthermore, journal paper [J3] and conference paper [C2] have been elaborated.

2

State of the art of floating offshore wind

In this chapter, at first the main components of a FOWF are presented. Afterwards different configurations are described regarding the electrical system, cable topology and layout. Finally, an outline of the floating offshore wind market is provided and the latest technological developments are presented. This background information is essential in order to be able to perform an adequate analysis and modeling of the technology.

2.1 Components of a floating offshore wind farm

The main components of a FOWF are the wind turbines, the floating substructures, mooring lines and anchors, as well as the electrical components required for energy transmission such as the cables and the substations. Figure 2.1 presents the main components.

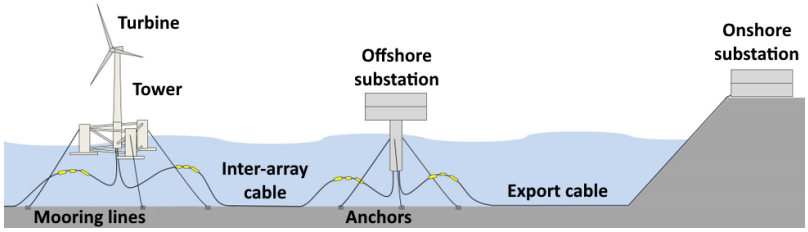

Figure 2.1: Floating offshore wind farm components.

In this section only the structural components of a FOWF are presented, but not the additional vessels and equipment that are required for the installation or maintenance of the wind farm. Those are described in Section 5.3.

2.1.1 Wind turbine

A conventional wind turbine consists of a nacelle, the rotor blades and a hub as well as a tower. Furthermore, each of the main components consists of several subcomponents, which can sum up to more than 8,000 different components in a wind turbine [3]. Figure 2.2 shows the main wind components of a wind turbine. There exist different classifications of wind turbines according to the design or technological concept used. A common classification distinguishes wind turbines regarding the position of the axis of rotation of the wind rotor, which can be horizontal or vertical. Furthermore, wind turbines can be classified according to the number of blades that are used, ranging from a mono blade to triple blades [17].

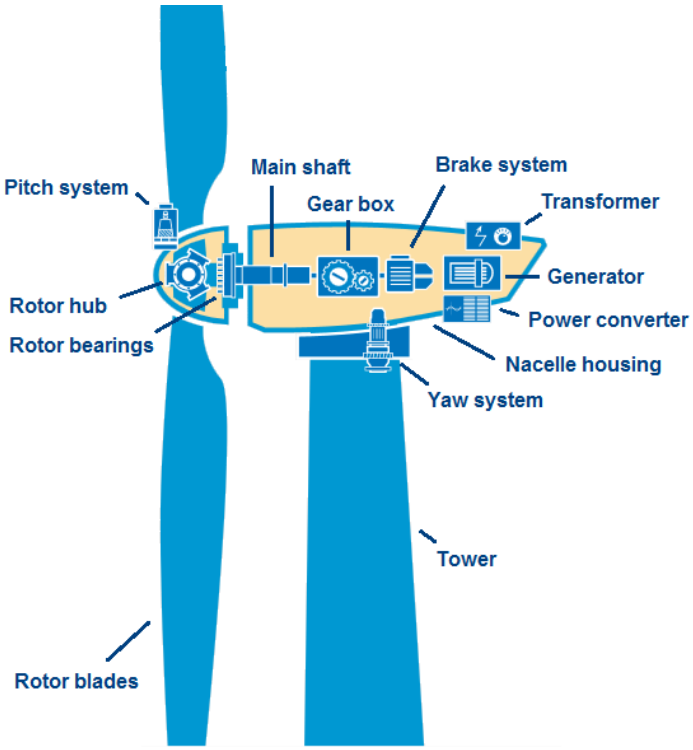

Figure 2.2: Wind turbine components [3].

Besides the before mentioned classifications, the wind turbines can be distinguished by technological differences such as the operation on fixed or variable speed or the application of a gearbox or direct-drive system. The most common wind turbine concept that is applied is the horizontal design with 3 blades and a gearbox in order to take most advantage of the wind resource [17, 18]. Nevertheless, direct drive turbines have gained popularity in recent years because of potential cost savings and increased reliability and are applied by major companies such as Enercon, Goldwind and Siemens [19].

Wind turbines have grown in rotor size and rated power nearly exponential in the past from small 20-60kW turbines in the 1980's to today's multi megawatt power generating units and the trend is expected to continue [20]. The driving motivation is that in higher altitudes higher wind speeds are present that can be harnessed by the wind turbines and with larger rotor diameters and higher mean wind speeds more energy is generated. Besides that, the total production cost per kilowatt hour of electricity produced has generally decreased with increasing turbine size. The tendency to larger turbines is, in particular, the case for offshore wind where higher wind speeds are available far from the cost and fewer constrains exist regarding logistics and visual impact. For instance, onshore manufacturers are constrained by the size of roads and bridges that turbines have to cross to be transported to the installation site [18]. However, offshore wind turbines in comparison to onshore turbines need a higher robustness in order to withstand the extreme offshore conditions and also additional protection to avoid corrosion is required, which in general causes offshore turbines to be more cost intensive. FOWT require, in addition, an adaption of the controller since met-ocean conditions and platform motions would have an effect on the performance of the wind turbine [21].

In 2018, the average capacity rating of newly installed BOWTs in Europe was 6.8MW in comparison to the average size of 5.9MW in 2017. Siemens Gamesa continued to be the top offshore wind turbine supplier with 62% of installed capacity in 2018, followed by MHI Vestas (33%) and General Electric (5%) [9]. These suppliers have also launched first commercial application of larger turbines ranging from 7 to 8MW. For instance, Siemens has introduced in 2015 a 7MW direct-drive turbine and Vestas has installed the V164-8MW wind turbine model at the Burbo Bank extension in the United Kingdom [22, 23]. The trend to larger turbines will likely continue as several wind turbines suppliers have already launched prototype concepts of 10MW to 12MW [24]. For instance, in 2019 General Electric has installed the Haliade-X 12MW prototype in the Netherlands and type certification is

expected for 2020 [25]. However, the further increase of wind turbine size will also implement challenges to infrastructure and vessels that need to be considered and solved [26]. In case of floating offshore wind, where only a few prototypes are installed yet the rated capacity of the turbines ranges from small scale demonstration projects up to units of 6MW to 7MW depending on the specific concept [27].

The tendency to use larger wind turbines applies in the same way to floating wind since the substructures are intended to be built in deep waters where high wind speeds are present [28]. The wind turbine is connected to the floating substructure by the tower, which fits into a transition piece at the substructure. Most developers of floating substructures claim that their concepts are able to accommodate any offshore wind turbine that is used on bottom-fixed foundations. However, the floater motions have an impact on the performance and reliability of the turbine, in particular in form of fatigue on bearings and drive train. Thus, a close collaboration between turbine and floating substructure developers is required [11]. In the following section, the main floating substructure concepts are described.

2.1.2 Floating substructure concepts

Whereas monopiles remain with about 75% by far the most popular substructure type for BOWTs in Europe in 2018, the market of floating substructures is quite diversified [9]. This is due to the numerous floating concepts that are under development and entering the market. Most of the concepts are based on the floating substructure designs that are commonly applied in the oil and gas industry with adaption to the specific requirements and conditions of offshore wind. Despite the variety of designs, it is possible to classify most of the substructures into three main types depending on their method of stabilization [12, 29]. Figure 2.3 illustrates the main classifications.

The spar buoy is based on a ballast stabilized design, which consists of a cylindrical structure that gains its stability from having the center of gravity lower in the water than the center of buoyancy. This platform gains stability by using ballast weights in the lower part of the structure, which creates a righting moment and high inertial resistance to pitch and roll. The fabrication process of this type is relatively simple and the concept provides a high stability. However, due to the large draft requirement the floater concept tends to be applied in waters deeper than 100 meters and the draft causes also challenges in the assembly, transportation and installation phase [11,29].

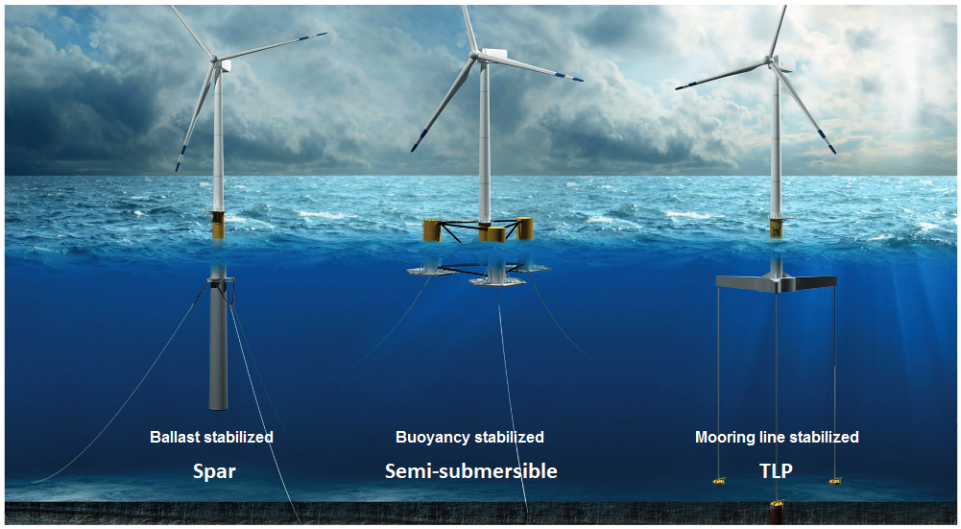

Figure 2.3: Floating offshore wind turbine concepts [12].

The semi-submersible platform concept floats semi-submerged on the surface of the water and is based on buoyancy stabilization. The floater gains stability through distributed buoyancies and uses the weighted water plane area for the righting moment. The concept often requires a heavy and large platform to maintain stability with complex structures that require a more detailed fabrication process. The low draft allows a simple installation and a flexible application also in shallow waters. The concept could be deployed in water depths as low as 25m. However, the design of the catenary mooring system becomes more challenging at lower water depths. The turbine can be assembled to the floating substructure in the port and transported easily by a tug boat to the offshore site, which facilitates the installation process. Another concept that follows a similar design is the barge platform that gains its stability from a pontoon and not by columns as the semi-submersible platform [11, 29].

The tension leg platform (TLP) requires a stabilization of the floating substructure by mooring lines. It consists of a semi-submerged buoyant structure that is anchored to the seabed by tensioned mooring lines. The low draft and high tension stability allows for a smaller and lighter structure and applications in shallow waters, but, on the other hand, the concept increases the stresses on the tendon and anchor system. Furthermore, the design faces challenges in the transportation and installation phase since stability is not given without the tendons. Besides that, it implies a risk in the operation phase in case of a failure of the tendons [29, 30].

Although generally relying on one of the primary sources for stability, most of the floating substructures that are developed today consider stability aspects of all of the three types. The design and the choice of mooring and anchor system are also significantly influenced by the characteristics and requirements of the specific offshore site. Furthermore, the primary material used differs between the concepts and applications. Steel is the most applied material, but a number of concepts have preferred concrete as the primary material due to potential cost savings [11].

Besides the three mentioned types of concepts there are also some concepts that were developed for different purposes. For example, multi-turbine floating platforms were designed to support various turbines or hybrid concepts that combine a floating wind turbine with a wave energy device. The Hexicon multi-turbine platform and the Poseidon P37 hybrid wave wind device are shown below as an example for those concepts [11].

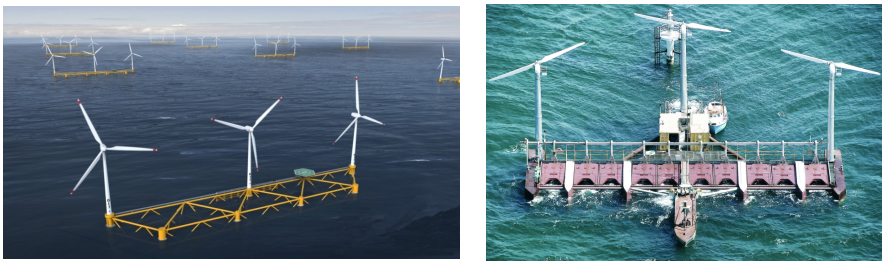

(a) (b)

Figure 2.4: (a) Floating multi-turbine platform [31], (b) Hybrid wind wave device [32].

2.1.3 Mooring system

Mooring lines connect the anchors with the substructure and are used to keep the position of the platform. The most common mooring configurations that are used in floating offshore wind are presented in Figure 2.5. Tension-leg mooring systems are typically used for floating concepts whose stabilization is based on mooring lines like the TLP. The mooring lines are fixed vertically under high tension by anchors in the sea bed in order to maintain stability of the floater. The design is illustrated in Figure 2.5 (a). The cable length is the shortest of all three concepts and it possesses the smallest footprint. It is also characterized by very limited horizontal movements and high vertical loading, as well as more challenging installation conditions [11, 33].

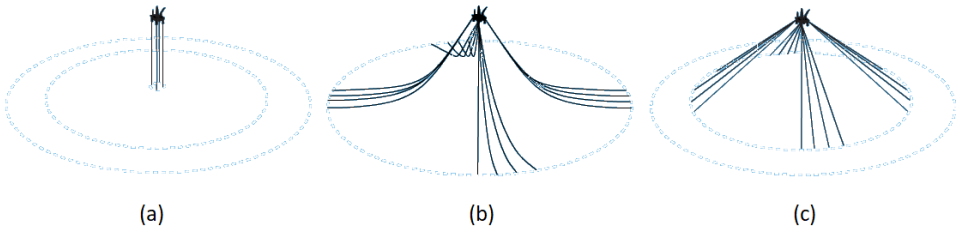

Figure 2.5: Mooring line configurations: (a) Tension-leg mooring, (b) catenary mooring, and (c) taut-leg mooring [33].

Catenary mooring systems are mostly used for ballast and buoyancy stabilized platform concepts and the mooring system is shown in the center of Figure 2.5 (b). The curved shape keeps the floating platform in place by laying the lower section of the mooring lines on the sea bed with their weight and thus supporting the anchor. In case of stormy conditions the catenary mooring lines act as counterweight to displacements of the platform. In contrast to the tension-leg mooring system the catenary system possesses a large footprint and horizontal loadings at the anchor point, as well as some degree of horizontal movement. However, the installation procedure is simpler [11, 33].

Some floating concepts apply a taut-leg mooring system (2.5 (c)), which has characteristics of both other concepts. The major difference is that taut-leg mooring lines arrive at the seabed at an angle and not horizontally as the catenary moorings or vertical as the tension-leg mooring system. The position of the floater is being held by the elasticity of the mooring lines and the footprint is smaller than in the catenary system. However, the taut-leg system has to withstand horizontal and vertical forces [11, 33].

Materials that are used for mooring lines depend on the concept, application and requirements of the offshore site. Commonly, steel chains are used for catenary moorings, where the weight is important in order to keep the platform in position. Wires made of steel fibers are an alternative solution for all three mooring concepts and have the potential of cost saving due to a lower weight and higher elasticity. Synthetic fiber rope is a relatively new material for mooring lines and due its light weight and elasticity an alternative for taut- and tension-leg mooring systems [11, 33].

The mooring line and the anchor are joined by connectors that depend on the application and concept [33]. In the following section, the common types of anchors are presented.

2.1.4 Anchor

The choice of anchor depends on the requirements of the offshore site and in particular on the soil conditions. Furthermore, the directional forces have to be taken into account that act on the anchors based on the type of mooring and substructure. A variety of anchor types exists that are typically used in the oil and gas industry [29]. In the following figure, the main types of anchors are presented that are being employed in the floating offshore wind industry.

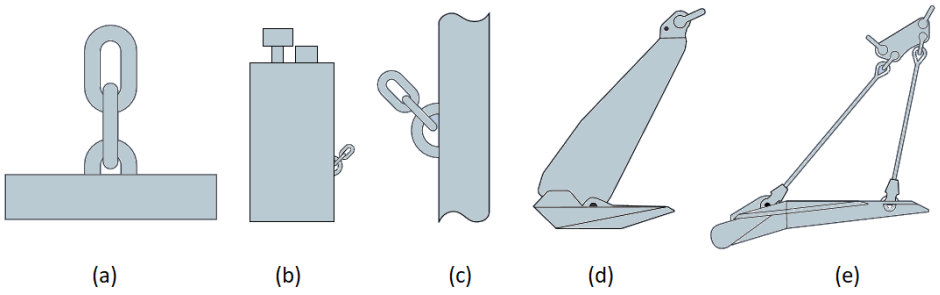

Figure 2.6: Anchors types: (a) Gravity anchors, (b) driven piles, (c) suction anchors, (d) drag-embedded anchors, and (e) vertical load anchors [33].

Gravity anchors are one of the oldest anchors that exist. The holding capacity is mainly based on the weight and material used. Common materials that are used for this type are steel and concrete. However, the large size and weight can increase the installation cost. Gravity anchors are suitable for soft as well as hard soil conditions and are mostly employed with tension-leg systems due to the high holding capacity [11, 33].

Driven piles are hollow steel pipes that are installed into the seabed by using a piling hammer. The holding capacity is based on the friction of the soil along the pile and lateral soil resistance. The driven piles are able to resist both horizontal and vertical loads and are installed generally deep below the seabed in order to obtain the holding capacity. This type of anchor finds application commonly in tension-leg platform configurations, but also in taut-leg mooring systems. Drawbacks of this type are noise impacts during installation due to the use of the piling hammer as well as difficult removal. Driven piles have an advantage in extreme soil conditions since they are forced into the seabed even in the ambiance of stony soils [11, 33].

Suction anchors are as the driven piles hollow steel structures, but unlike the piles are closed at the top and are generally larger in diameter. The

suction anchor is installed by the use of a pump, which extracts the water out of the anchor, which by this means creates a pressure difference forcing the anchor into the sea bed. After the installation the pump is removed. Due to the installation procedure the anchor type is not suitable for hard seabed conditions. However, it can resist both horizontal and vertical loads and has a relatively simple decommissioning. This type of anchor is mostly applied with ballast stabilized floating concepts [11, 33].

Drag-embedded anchors are one of the most common types of anchors. The resistance of the soil in front of the anchor creates the holding capacity. In general this type of anchor is designed for horizontal loads, but not for large vertical loads. It is also characterized by a simple installation and removal procedure. Drag-embedded anchors are commonly employed with catenary mooring configurations and are applied in soft as well as hard seabed conditions [11, 33].

Vertical load anchors are a quite new development and are similar to the drag-embedded anchors, but with the capability to sink deeper into the seabed. Upon installation the anchor changes into a vertical loading mode, which provides the anchor a good resistance to vertical and horizontal loads [11, 33].

2.1.5 Power cables

Power cables are one of the three key elements in the electrical system of an offshore wind farm besides the substations and wind turbine generators. The cable usually consists of one or more conductors surrounded by insulation and jackets in order to conduct electrical power under the sea. Depending on the application different designs and materials are used. Figure 2.7 shows a typical three core cross-linked polyethylene (XLPE) cable for alternating current (AC) application [34].

Figure 2.7: Cross-linked polyethylene (XLPE) cable [35].

In an offshore wind farm two types of cables exist; inter-array cables and export cables. The purpose of inter-array cables is to collect the power generated by the wind turbines and conduct it to the offshore substation [36]. How the wind turbines are inter-connected by the cables is a matter of required reliability and redundancy of the system. The different topologies that exist for cabling the turbines are presented in Section 2.2.2. The collection grid that is formed by the inter-array cables operates typically with medium voltage at 33kV, which has been the standard for many years. However, moving to higher voltages such as 66kV has been under investigation recently in order to enable a more cost-effective power collection and transmission. The benefits of a higher voltage would be an increase of power transmission capacity, lower losses and the reduction of required substations and cables. Nevertheless, the change to a higher voltage demands the development of capable transformers, switch-gears and inter-array cable. Indeed, many of the main developers have initiated research in this area and first prototypes are realized such as the floating offshore wind farm demonstration project FORWARD in Fukushima, Japan that applies 66kV voltage [37].

For the case of floating offshore wind, inter-array cables consist of two different cable sections; a dynamic cable and a static cable. The dynamic cable connects the wind turbine with the static cable, which is buried in the seabed. The dynamic cable is afloat and the tension applied depends on the chosen mooring and anchor concept [35]. Figure 2.8 shows exemplary an inter-array power cable.

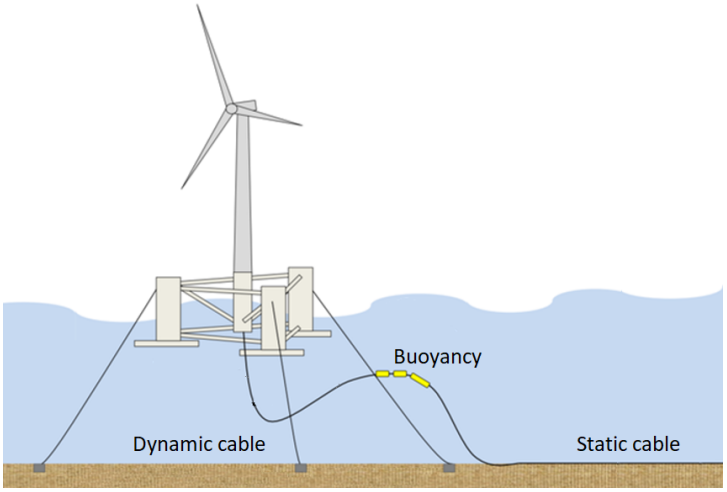

Figure 2.8: Inter-array cable consisting of a dynamic and static cable.

The dynamic cable is especially designed to withstand the movement from the floating substructure. It is subject to torsion and tension particularly at the release point of the cable at the turbine substructure. Furthermore, mechanical stress and friction appear at the connection point of the dynamic and static cable on the seabed. In order to protect the cable against mechanical stresses it can be designed with double wire-armor as cover and wire shield to prevent metallic fatigue caused by the floater. Furthermore, in order to protect the cable from friction against the seabed and to keep it in position, buoyancies are attached to the dynamic cable. By this means, the cable movement is restricted and stresses are reduced [35]. In Chapter 6, the inter-array collection grid is optimized and different wind turbine connection possibilities with dynamic and static cables are studied.

The second type of cables applied in FOWFs are export cables, which are used to conduct the electric power from the offshore to the onshore substation. Those power cables are similar to the static inter-array cables, but are designed for higher voltages such as 100kV or 220kV. The high voltage is applied to reduce energy losses over long distances. The export cables are buried below the seabed in order to ensure long-term reliability by avoiding damage from anchors and the exposure to hydrodynamic loads [18]. Several designs of export cables exist depending on the application. Cross-linked polyethylene cables are usually used for high voltage alternating current (HVAC) applications. However, since wind farms are increasingly built far offshore, it is favorable to apply high voltage direct current (HVDC) for the transmission systen in order to reduce the power losses in the cables [34]. Industry leaders such as Siemens and ABB have already developed the required technology and several HVDC transmission projects have been realized in the North Sea [38]. For HVDC, special submarine cables were developed for the purpose of offshore wind such as the HVDC light cable by ABB or the extruded HVDC submarine cable by Prysmian [39, 40]. The different types of transmission systems are further explained in Section 2.2.1. WindEurope expressed its concerns in 2011 about a potential shortage of submarine cables, especially, high voltage cables since the supply chain capacity was limited and would not be able to satisfy the growing future demand. However, since then the major cable suppliers have significantly invested in new productions facilities in order to match the demand [41, 42]. In 2018, the inter-array cable supplier market has been led by Nexan with 42% of the new energized cables, followed by JDR Cable Systems (32%) and Prysmian (16%). The export cable market, on the other hand, has been more divers with a larger number of companies supplying the offshore wind industry such as NKT, Prysmian, Ls Cable & System, JDR Cable Systems and Nexans [9].

2.1.6 Substations

In the electrical transmission system of an offshore wind farm exist in general a substation onshore and offshore. The type and amount of substations depend on the applied transmission technology and requirements of the specific project. The offshore substation is used to reduce electrical losses by increasing the voltage level with transformers and exporting the power to the shore. In most of the early offshore wind farm projects an offshore substation was not required since those projects were relatively small, close to shore and/or the transmission voltage was at the same level as the collection grid voltage [18]. However, since wind farms are increasingly built far offshore and with higher power ratings the use of offshore substation became necessary. Figure 2.9 shows a typical offshore substation.

Figure 2.9: Walney Phase 2 offshore substation [43].

The electrical equipment installed in the offshore substation is similar to its onshore counterpart, but with additional environmental protection. A handful of companies are dominating the substation market in Europe for the supply of the electrical equipment and technology, which are largely the industry giants Siemens, Alstom and ABB [41]. The offshore substation needs to be very well designed and maintained since a failure or breakdown causes a significant loss of production. In order to reduce the risk of a failure developers have incremented the redundancy in recent projects by increasing the number of export cables and transformers [41].

In most of the offshore wind farms that were constructed the design and installation of the offshore substation was based on references from the oil and gas industry. The substation is typically divided in two main parts; the foundation structure, usually a jacket or monopile structure and the topsides structure that includes all electrical equipment [41]. In case of floating offshore wind, the offshore substation needs to be adapted by installing floating substructures for the deep water applications. So far, only one floating substation has been installed and it is placed at the Fukushima site in Japan. Due to the high weight of the substation the floating substructure needs to be designed heavy enough to sustain the pressure, which results in high costs. Optimizing the design will be an important factor also to avoid blackouts, which could result in high power losses [11].

The onshore substation is the counterpart to the offshore substation and its design is mainly based on the requirements of the network operator. The onshore substation receives the electric power transmitted over the sea and serves as a connection point to the local grid as well as to transform the power to the grid voltage. In general the substation consists of a switchgear, metering, transformers and associated plant [18, 44].

2.2 Configurations

The configuration of an offshore wind farm is considerably more complex than its counterpart on land. Although the same electro-technical considerations apply, the specific offshore conditions require alternative solutions. The main aspects that need to be considered are [34].

- The higher cost of the components and installations in the sea.
- The greater distance for transporting the energy and possible higher losses.
- The higher power that is transmitted by harnessing the vast offshore wind potential.
- The reliability of the system and, in consequence, the redundancy.

The consideration of these aspects is highly important in order to select an adequate configuration and design of the offshore wind farm. Several technical solutions are possible for the configuration of an offshore wind farm and the most applied ones are presented in this section.

At first the electrical configuration of the system is outlined, followed by an explanation of possible collection cable topologies. Finally, important considerations for the configuration of wind turbines in the wind farm layout are presented.

2.2.1 Collection and transmission system

Floating offshore wind is still in its early stage of development. So far, no large scale FOWFs have been built. Only a few projects have been realized ranging from single prototypes up to small pre-commercial wind farms of 5 units [27]. However, the electrical system of a large FOWF would be similar to a bottom-fixed offshore wind farm (BOWF). Therefore, in this section different types of configurations for the collection and transmission system are presented that have been developed for BOWF in order to address the challenges that can appear in the electrical system of an offshore wind farm.

MVAC configuration

The medium voltage alternating current (MVAC) configuration is applied for connecting all wind turbines and to transmit the energy to the onshore substation. A power cable connects a number of turbines in series and exports the generated power in the medium voltage level of the wind turbine transformer, typically about 24kV to 36kV. No offshore substation is used in this configuration. The onshore substation generally contains a transformer, switchgear, reactive power compensator, harmonic filters, metering and the connection to the point of common coupling (PCC). Figure 2.10 illustrates this configuration.

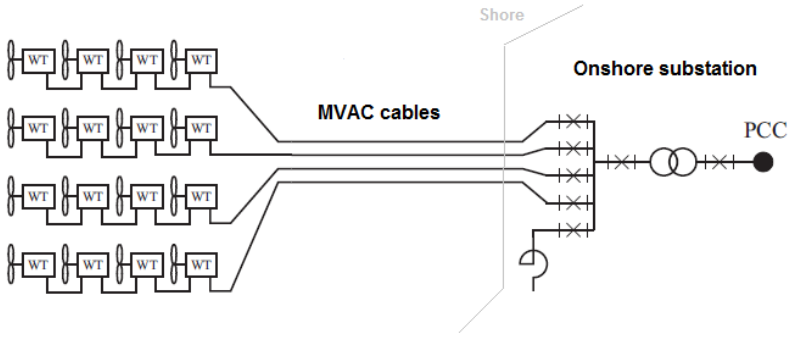

Figure 2.10: MVAC configuration [45].

MVAC was applied in most of the first offshore wind farms that were located near to the shore and had low rated power capacities. For larger wind farms located remotely offshore, alternative technologies need to be applied since the power losses in alternating current transmission typically increase with the distance [45].

MVAC / HVAC configuration

In the MVAC / HVAC configuration, an offshore substation is considered to step up the medium voltage of the wind turbine collection grid to high voltage. The electric power is then transported in HVAC via one or several submarine export cables to the onshore substation. The high voltage applied in the export cables depends on the maximum power to be transmitted and the ability of the power cable. Typical high voltage values are 132kV and 150kV. However, 220kV is also recently studied for new large offshore wind farms. Figure 2.11 illustrates this configuration [46]. The offshore substation contains the transformer, switch gear and reactive power compensation. The onshore substation is similar to the offshore counterpart and is used to adapt the voltage level, frequency and reactive power to the requirements of the local grid in order to integrate the electric power. This configuration is mostly applied today, because due to the high transmission voltage, lower power losses occur along the cables and higher capacities of power are transmittable [45]. However, the construction of the offshore substation involves a large investment and in case of a failure large power losses can occur. Moreover, HVAC seems not technically and economically feasible for very large distances. An exemplary wind farm based on this technology is Walney Extension, which is currently the largest offshore wind farm with a rated power capacity of 659MW [47].

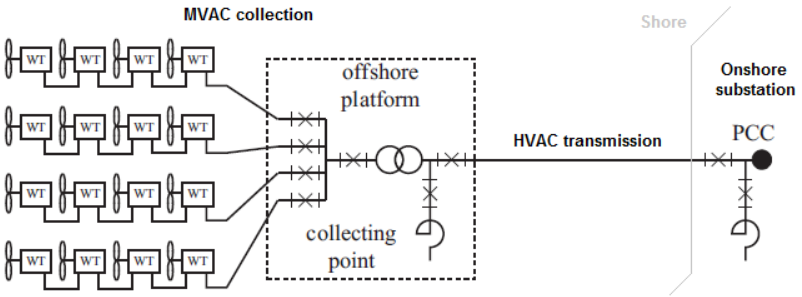

Figure 2.11: MVAC / HVAC configuration [45].

MVAC / HVDC configuration

The transmission of electric power in HVDC is an alternative solution to HVAC for longer distances and larger wind farm capacities. The reason is that in direct current configurations the power transfer capability for long distances is not reduced as much as in HVAC cables, which generate charging currents and reactive power [46]. The break-even distance at which HVDC becomes more feasible than HVAC technology is at about 80km depending on the project circumstances and voltage levels [48]. The drawback of this technology is that large and expensive AC/DC converters are required since the wind farm grid and the onshore distribution grid are operated in AC. In addition, a separate offshore converter station is required besides the AC transformer substation. However, the converters have the benefit of being capable to control both the voltage and the power injected to the main grid in order to fulfill the grid code requirements imposed by the transmission system operator. Figure 2.12 shows a configuration of this technology [49].

The technologies that have been developed for the converters are line commutated converters based on thyristors and voltage source converters (VSC) based on switching devices. Line commutated converters have been widely used in onshore transmission applications, but the drawback of this technology is that it needs a minimum reactive power to work is more affected by to potential AC grid faults than VSC technology. VSC is a relatively new technology and has the advantage that the semiconductors switching is decoupled to the grid voltage and therefore are able to adapt reactive power and provide power system stability. Another benefit is that VSC configurations need fewer filters and therefore require less space on the substation [5, 46]. However, the cost of this technology is higher. VSC has been the preferred technology for offshore wind farm applications in recent years.

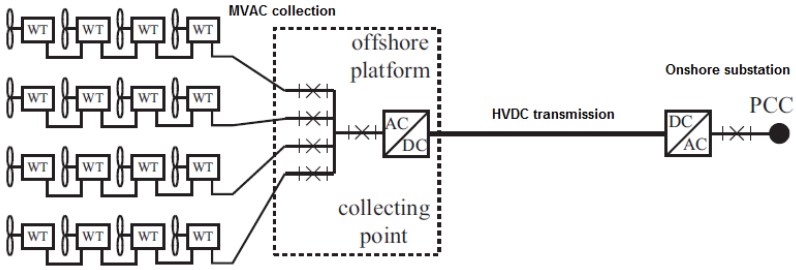

Figure 2.12: MVAC / HVDC configuration [45].

The leading developers are Siemens with the HVDC plus and ABB with the HVDC light solution, both based on VSC configuration [5]. The first HVDC converter station was commissioned in 2009 by ABB and serves to connect the BARD Offshore 1 wind farm with a rated capacity of 400MW to the German national grid [50]. This first project had several technical problems including a shutdown caused by a fire on the platform in 2014 [51]. However, since then, lessons have been learned and several more HVDC transmission links have been built in the North Sea to transfer the electric power generated by the offshore wind farms to the local grid [38].

DC / DC configuration

In light of the increasing power capacities and distances that offshore wind farms are being constructed, researchers aim to find alternative solutions to the conventional transmission configurations in order to reduce power losses and costs. Some of those novel configurations are presented next. Figure 2.13 illustrates a configuration based only on direct current. The DC/DC configuration is an alternative solution that applies direct current both in the turbine collection grid as well as in the export cable. Thus, the internal wind turbine DC/AC converter is replaced by a DC/DC converter. Furthermore, the heavy AC/DC converter and transformer in the offshore substation are replaced by a DC converter that steps up the medium voltage from the wind turbines to the required high voltage transmission voltage. In this way the size of the offshore substation can significantly be reduced and cost saved. Moreover, reactive power compensation is not required [5, 52].

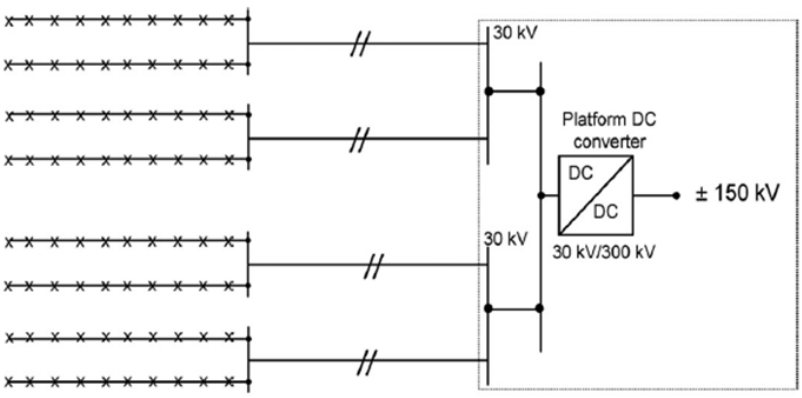

Figure 2.13: DC / DC configuration configuration [52].

However, drawbacks of this configuration are the complex and cost intensive DC/DC converters and a lack of adequate protection methods [5, 52].

LFAC configuration

The LFAC configuration is an alternative solution that suggests using low frequency (LF) in an AC collection and transmission system. Figure 2.14 presents this configuration.

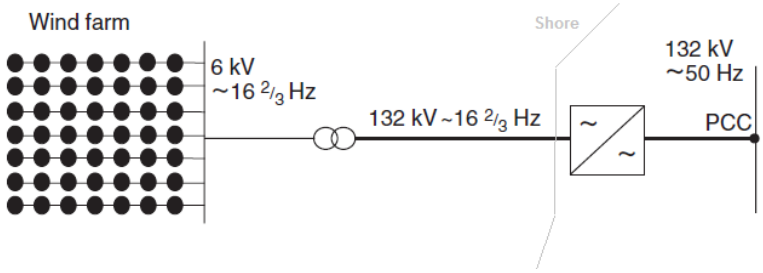

Figure 2.14: LFAC configuration configuration [5].

The LFAC configuration requires a frequency converter onshore to adapt the low frequency of the offshore network to the frequency of the local grid. The lower frequency would also offer the possibility of a simpler, lighter and cheaper design of the wind turbines. Furthermore, the lower frequency reduces significantly the capacity charging current and thus increases the transmission capacity and distance of an AC network. The drawback of this technology is that the transformer size would increase significantly as well as the associated costs. So far this configuration has not been considered by the industry for further development [5].

Multi-terminal HVDC

Most of the current HVDC projects consider only point to point transmission. However, multi-terminal HVDC systems will gain great importance in the near future in order to provide interconnections between countries and increase system stability. In a multi-terminal configuration a link is created between two or more separate transmission systems by increasing redundancy and thus improving system performance. An advancement of this concept is the proposal of a European HVDC super grid that would range from Scandinavia to southern Europe and would combine the generation capacities of all regions [5, 41].

2.2.2 Collection grid topologies

The collection grid consists of the inter-array cables and can be designed differently depending on the wind farm size and preferred level of redundancy. The most common topologies are radial, ring and star connection, which are described next.

Radial connection

The radial or string connection is the most straightforward design. A number of wind turbines are connected to a single cable feeder within a string as illustrated in Figure 2.15. The amount of wind turbines that can be connected depends on the cable capacity and the rated power of the generators. This cable topology is the most common and simplest design, but it involves the lowest redundancy. In case of a failure in the first turbine that is connected, all power generated by the following turbines will be lost [45].

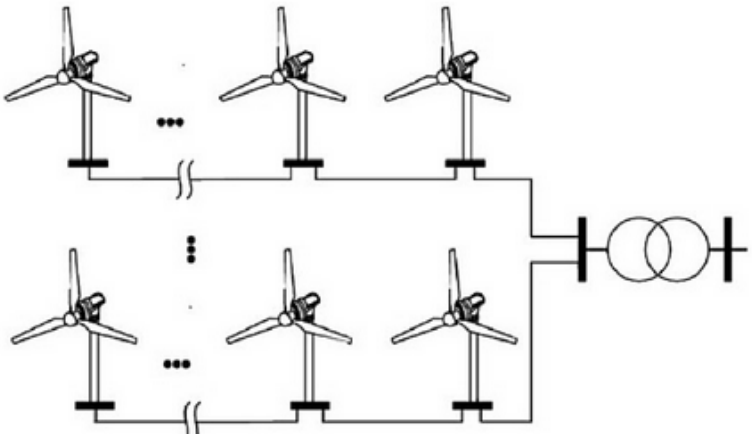

Figure 2.15: Radial configuration [53].

Ring connection

The ring connection is similar to the radial connection but improves the reliability by adding additional cables. Different types of design exist depending on the amount of additional cables. The single-sided ring connection adds a single cable to each feeder in order to connect the last turbine of the row directly to the substation. The double-sided ring configuration, on the other hand, connects two feeders together. Figure 2.16 illustrates this type of connection [53].

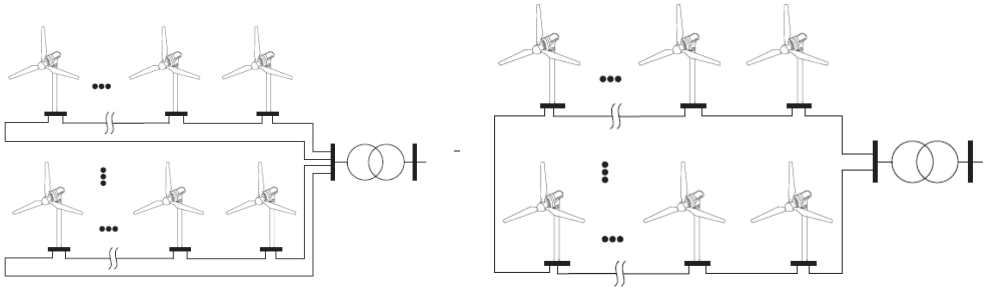

(a) (b)

Figure 2.16: (a) Single-sided and (b) double-sided ring connection [53].

Besides the above mentioned, another ring design exist, which is known as multiple-ring connection that connects each feeder of a multiple row wind farm together. The purpose of all types of ring connections is to increase the redundancy and reliability of the system by adding more power cables to the collection system. However, adding more cables increases also the investment and the cost for operation and maintenance [46]. Moreover, some of the cables need to be oversized in order to allow a power flow in case of a failure [53].

Star connection

The star connection is the last collection cable typology to be mentioned and presented in Figure 2.17. This design aims to reduce the power ratings of the cables by connecting each wind turbine directly to a central connection point. Thus, in case of a single turbine failure the total power losses are kept low. The reliability of this configuration is the highest, but it involves also the highest redundancy and cost of cables. Besides that, since each wind turbine will be connected separately the cable length increases and, therefore, the power losses as well [53]. In practice, redundancy has not been considered as priority in the design of the collection grid. In fact, the cost for additional cable lying as well as operation and maintenance are of more importance to developers. However, the experience that will be gained by the operation of the current offshore wind farms will show whether redundancy will be required in the future [5].

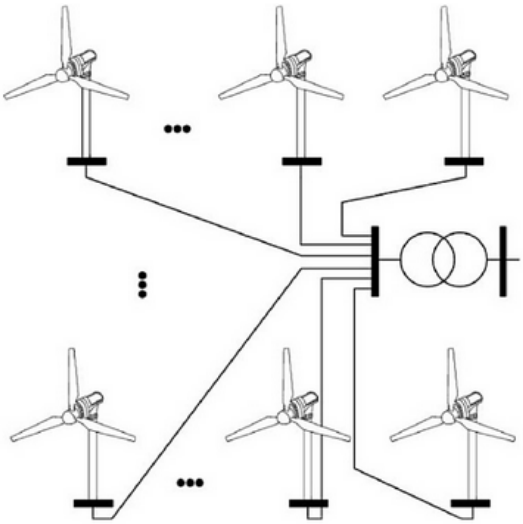

Figure 2.17: Star connection [53].

Besides the standardized topologies mentioned above, research can be performed to optimize the wind turbine connections. Chapter 6 presents the electrical layout optimization of FOWFs by taking into account the costs of the power cables as well as energy losses and reliability.

2.2.3 Wind farm layout

The decision for a wind farm layout is an optimization problem that depends on different constraints. The optimal layout must be a trade-off between those constraints, which are typically technical feasibility, lowest cost, least power losses and the compliance with specific site requirements. The main factors that influence the decision are described next.

Wake is one of the primary concerns in the design of the offshore wind farm layout. It can be defined as the region of circulating wind flow behind the moving rotor blades of a wind turbine. By the rotation of the blades energy is extracted from the incoming wind stream and a turbulent slowed down wind is released in the wake area. The extracted energy is called wake loss and is a typical phenomenon of a rotating wind turbine. The wake effect is highly important for the layout of a wind farm since the turbines are affected by each other. Each turbine will slow down the incoming wind by extracting energy and pass a lower wind speed to next turbine in downwind direction.

The affected turbine will further extract energy of the wind, which causes a sequential reduction in wind energy along a wind flow direction and thus causes a decrease of power generation from one wind turbine to the next. Besides the power loss, wake increases also the turbulences in the rotor with corresponding consequences for the fatigue strength of the turbines [34]. A visualization of the wake effect is presented in Figure 2.18.

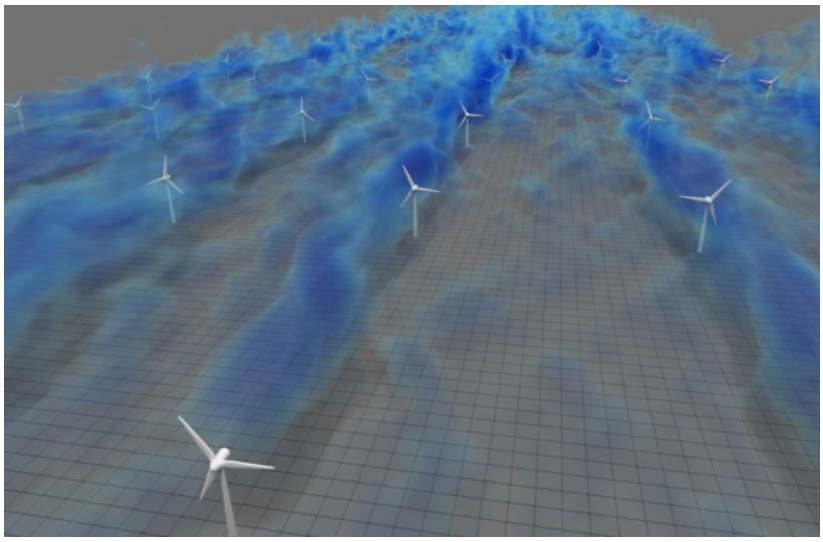

Figure 2.18: Wake visualization [54].

The blue colored wind streams represent the areas affected by turbulences and reduced wind speed. The turbines in a wind farm are not online disturbed by neighbor wind turbines but also by other wind farms nearby. This will become more important in the light of a denser construction of offshore wind farms. The wake effect and associated power losses can be reduced by increasing the distance between turbines and optimizing the operation of the wind turbines. It is common for BOWTs to have a distance of 5 to 9 rotor diameters to each other in the prevailing wind direction and about 3 to 5 rotor diameters in perpendicularly wind direction [55]. For floating offshore wind the distance between turbines will not only be influenced by wake but also by the applied mooring system. The catenary and taut-leg system that possess a larger footprint will certainly require a greater distance between the substructures than the tight tension-leg system. However, an increased distance between turbines will lead, on the other hand, to more cost for inter-array cables [29].

The site conditions are of great importance and need to be taken into account in the wind farm layout. For example wind turbines are certified according to extreme wind speeds. Therefore, the wind speeds need to be measured in order to select the required class of wind turbines [34]. Furthermore, the soil conditions are crucial in order to identify the required anchor system. In particular, for FOWTs the met-ocean conditions, such as wind and waves, are important to consider for a proper design of the floating concept and the wind farm layout [56]. The direction of the wind speed is also an essential factor for the layout definition. The orientation of the wind farm is set towards the prevailing wind direction, which is the direction of the highest occurrence of winds. This will enable generally the highest power production [57].

Permits have a large impact on the layout design especially in the development phase of a project. They may restrict the dimensions and boundaries of the site or place limits to the maximum capacity, tip height or rotor diameter of the wind turbines. Furthermore, restrictions may occur regarding the use of certain technologies or type of foundations. Permits are generally based on an impact assessment that evaluates for example environmental issues, grid constraints, and maritime requirements. It is essential for the success of a project to know well the permits in order to develop a fully compliant layout [34].

Finally, cost matters as always in commercial projects. Most of the constraints can be translated into cost. For example, if different water depths are present at a site different mooring lengths or technologies need to be applied, which causes a variation in costs. Another example of cost is the case of increasing power cable length due to the wake effect reduction. This would result in a higher investment as well as an increase in operation and maintenance cost. Nowadays, computer software such as Windpro and Windfarmer are available that can design wind farm layouts taking into account different constraints and produce cost optimal solutions [17].

Despite the above mentioned constrains, time has also an influence on the design. At the beginning of a project a simple layout is designed based on the current technology, which is used for evaluating the feasibility of the project and applying for tender. It may take several years from the first offer to the final decision in the tender process and the permission to manufacture and construct. During this time, new technologies have been developed or requirements have been changed. Hence, an updated layout is required, which comes typically with a detailed engineering of the wind farm. The layout will be improved regarding the latest know-how and requirements in order to gain an optimal solution.

A further requirement to the layout is the consideration of shipping lines for the maritime traffic as well as the flying routes of birds and crossing routes of sea animals [17]. Finally, the location of the offshore substation has to be considered in the layout, which has an influence on the inter-array cable layout and installation costs. The substation can be located inside or outside of the wind farm collection grid. Project developers will likely look for the most economical solution since offshore platforms are large and involve high transport and installation cost [5].

2.3 Market review

In this section, a review on existing FOWTs is performed as well as a country analysis with associated market barriers. This review is useful in order to understand the current state of development of this technology.

2.3.1 Overview

Floating wind energy is a relatively new technology that has emerged in the recent years within the fast growing offshore wind market. Floating substructures are the essential design to unlock the vast potential of deep waters. Along with favorable incentives and in-depth research and commercialization, this technology could play a key role in the power generation mix of the near future. The first research on floating wind turbines was initiated by the industry in the mid-1990s, followed by the installation of the first prototype Blue H off the Italian cost in the beginning of 2008. The first floating prototype consisted of a small scale TLP with an 80kW wind turbine and was designed by the Dutch company Blue H Engineering [58]. It was only in operation for one year for the purpose of testing and data collection. The first large scale floating wind turbine Hywind was installed by Equinor (former Statoil) [59] in the Norwegian North Sea in 2009 and was capable to carry a 2.3MW Siemens wind turbine. The Hywind design consists of a ballast-stabilized spar floater that is moored by catenary cables. Hywind was the first grid connected floating wind turbine of its kind and is still in operation. The concept has proven its functioning over a long period. The next development was WindFloat by Principle Power [60], which was commissioned in 2011 off the Portuguese coast. This was the first semi-submersible floater installed in open waters and carried a 2MW Vestas wind turbine [28]. The WindFloat FOWT was decommissioned in 2016 as first of its kind and demonstrated the procedures to be used for disconnection of the structure and dismounting of the turbine [60].

Today, a large number of concepts exist that possess different technology readiness levels. Some are in the initial research or development phase and others are already in operation or in construction. A list of commissioned FOWTs is presented in Table 2.1.

Table 2.1: List of commissioned floating offshore wind turbines [9, 27, 61, 62].

Year	Location	Project name	Developer	Type	Size
2009	Norway	Hywind	Equinor	Spar buoy	2.3MW
2011	Portugal	WindFloat 1	Principle power	Semi-submersible	2MW
2013	USA	VolturnUS	University of Maine	Semi-submersible	750kV
2013	Japan	Kabashima	Toda corporation	Semi-submersible	2MW
2013	Japan	Fukushima FORWARD	Mitsui Engineering & Shipbuilding	Semi-submersible	2MW
2015	Japan	Fukushima FORWARD	Mitsubishi Heavy Industries	Semi-submersible	7MW
2015	Sweden	SeaTwirl S1	SeaTwirl	Other	30kW
2016	Japan	Fukushima FORWARD	Japan Marine United	Semi-submersible	5MW
2017	UK	Hywind Scotland	Equinor	Spar buoy	5x6MW
2018	France	Floatgen	Ideol	Barge	2MW
2018	France	Hibiki	Ideol	Barge	3MW
2018	France	Eolink prototype	Eolink	Other	200kW
2018	UK	Kincardine Pilot	Principle power	Semi-submersible	2MW
2019	Spain	W2Power	EnerOcean	Multi-turbine	200kW

The list contains 17 commissioned FOWTs of different size ranging from smaller prototypes of 200kV to large units of up to 7MW. Furthermore, in 2017 the first pre-commercial FOWF has been commissioned consisting of five 6MW units of the Spar buoy concept developed by Equinor. The majority of FOWT concepts are semi-submersibles and barge, which are based on the buoyancy stabilized design. The reason might be that semi-submersible platforms have the benefit of being easier applicable in shallow waters due to the low draft and possess less installation concerns. However, the spar is one of the most advanced concepts as it has been widely studied and extensively proofed offshore [11]. The first floating wind projects have been initiated in Europe by European companies and research institutes based on the support from national incentives and European research and development funds. However, Asian and American companies are catching up and investigating the potential of this technology in their domestic markets. In particular, Japan and the United States are in the focus of major developments [28].

Many of the FOWTs listed in Table 2.1 have been decommissioned after a period of operation since the purpose of the construction was proof of concept and testing in real environmental conditions. However, many more projects are currently in development. Table 2.2 presents a list of planned FOWT projects.

Table 2.2: List of planned floating offshore wind turbines [31, 62–67].

Year	Location	Project name	Developer	Type	Size
2020	Portugal	WindFloat Atlantic	Principle power	Semi-submersible	3x8.4MW
2020	UK	Dounreay Tri	Hexicon	Multi-turbine	1x10MW
2020	UK	Kincardine Wind Farm	Principle power	Semi-submersible	5x9.5MW
2020	France	EFGL	Principle power	Semi-submersible	4x6MW
2020	France	Eolmed	Ideol	Barge	4x6MW
2020	France	Provence Grand Large	SBM Offshore	TLP	3x8MW
2020	France	Groix & Belle-Ile	Eolfi	Semi-submersible	4x6MW
2020	Spain	Flocan 5 Canary	COBRA	Semi-submersible	5x5MW
2020	Spain	Nautilus	Nautilus	Semi-submersible	1x5MW
2020	Spain	DemoSATH	SAITEC Offshore	Other	1x2MW
2020	Norway	TetraSpar	Stiesdal Offshore Technology	Other	1x3.6MW
2020	USA	New England Aqua Ventus I	University of Maine	Semi-submersible	2x6MW
2021	Ireland	Gaelectic I	Ideol	Barge	30MW
2022	Norway	Hywind Tampen	Equinor	Spar	11x8MW

The list shows FOWT projects that are currently developed or to be constructed within the next few years. The list is based on currently available information, but there might be more projects in development that have not been announced publicly. Semi-submersibles are again the most prominent concept that is going to be deployed. However, the first large scale demonstrator of a TLP concept is projected to be installed in 2020. The list reflects also the current development path of floating offshore wind. Whereas so far mostly single prototypes have been constructed, it can be observed that by 2020 several pre-commercial FOWFs will be developed with capacities up to 48MW. Furthermore, the power rating of a single unit is increasing up to the use of 10MW wind turbines. It can also be seen that most of the announced projects are located in Europe, mainly in France and UK, where public tender have been anounced to support floating offshore wind.

However, there are several more countries with a large potential that will likely become important markets for the development of FOWFs. Next, the main markets of floating wind are discussed in more detail.

2.3.2 Country analysis

Europe is the homeland of offshore wind energy with more than 91% of the worlds installed offshore capacity. The development is boosted by national incentives and rich European funds, but on the other hand is mostly based on the benefit of having large shallow waters in the North Sea and nearby Baltic Sea, English Channel and Irish Sea, where the BOWFs are being built. The shallow waters are, however, limited in size and developers will be required to explore alternatives. Floating wind has the potential to enable the exploitation of the vast deep sea areas in the North, Atlantic and Mediterranean Sea [68]. Figure 2.19 shows a map of the North Sea and potential floating wind applications. The areas with lighter color are shallow waters, which are typically close to the shore and suitable for BOWTs. The darker areas are deep waters, where floating turbines are applicable. Around the Norwegian shoreline lies a deep water channel that is suitable for ballast stabilized designs as the Spar.

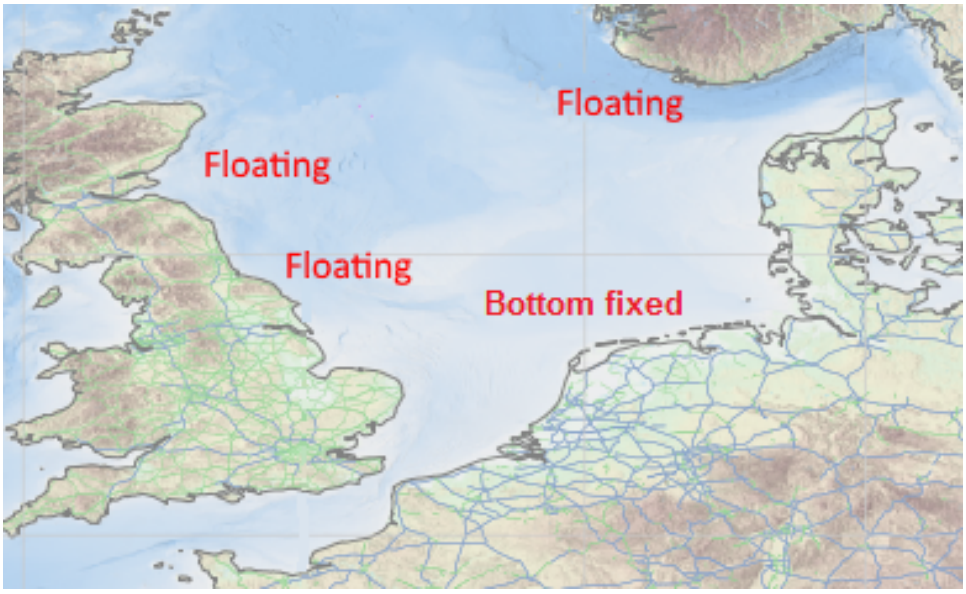

Figure 2.19: Suitable North Sea locations [69].

TLP based designs can applied in medium water depth areas such as close to the English coast. Semi-submersible platforms can be located both from shallow to deep waters [68]. Norway was the first mover in floating wind and installed the world's first floating wind turbine Hywind. Recently, the Ministry of Petroleum and Energy has announced plans to open an area off the coast of Rogaland for floating offshore wind applications as well as a potential site near to the border to Denmark [70]. However, the Norwegian Sea features harsh conditions with rough weather, extreme waves and large depths, which is even for floating wind a challenge. SWAY a Spar buoy prototype, for instance, was installed in 2011 off the Norwegian cost and sunk due to extreme weather conditions [28].

The United Kingdom has shown a strong interest in the development of floating wind. The Crown Estate as well as the Scottish government and UK's Energy Technology Institute have launched major programs to fund deep offshore wind. Hywind Scotland, the world's first floating wind farm has been commissioned in October 2017 and is located off the Aberdeenshire coast in Scotland. Several more floating wind projects are scheduled for construction of the Scottish coast by 2020 [28, 62].

The Mediterranean Sea and the Atlantic Ocean in contrast to the North Sea possess large deep water areas, but the majority is unsuitable for offshore wind applications, even for floating find. The reason is that most areas are too deep and the installation of mooring lines and anchors would not be feasible in terms of cost and technology-wise. However, suitable locations for floating wind can be found in the French waters, around the Spanish and Portuguese cost, as well as in Italian and Greek waters. Figure 2.20 demonstrates the suitable locations.

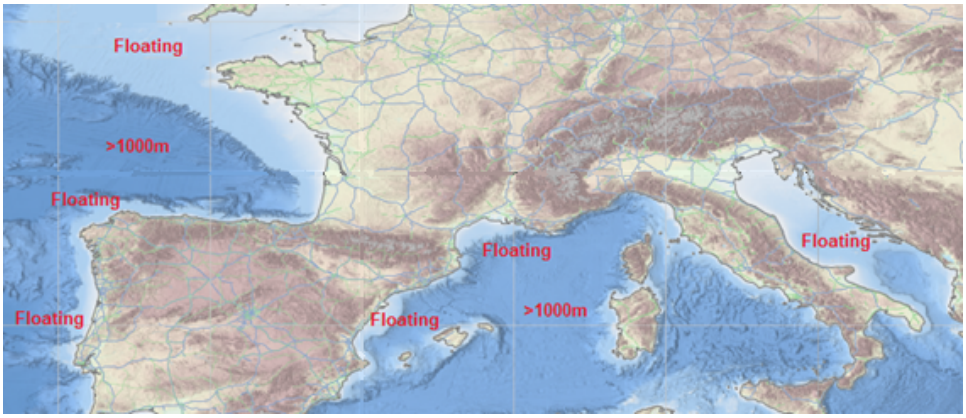

Figure 2.20: Suitable sites in the Mediterranean Sea and Atlantic [69].

France is an active player in floating wind. In early 2019, the European Commission has agreed to support four French floating wind demonstration projects, each consisting of either three or four turbines with a total capacity of 24MW. One project will be located in the Atlantic Ocean, while the other three projects will be located in the Mediterranean Sea. France aims to consume 40% of renewable electricity by 2030 and floating wind has the potential to make its contribution. In particular, the recently released Multiannual Energy Programme has proposed the tendering of around 6GW of fixed and floating offshore wind by 2028 [71]. Prominent demonstration projects that have been realized are WinFlo, Vertiwind and FLOATGEN [28].

Portugal possesses a large exclusive economic zone and has high potential for floating wind with deep waters. The government has recognized the potential and installed WindFloat Europe's second large scale floating system after Hywind. The government plans to extend the project to 27MW in a second phase and up to 150MW in a third phase [28].

Spain has also potential for floating wind and several key players in the floating wind market are of Spanish origin. For instance, promising FOWT concepts that have been developed by Spanish companies are Iberdrola's TLP, the semi-submersible platform by Nautilus, the Windcrete Spar-buoy concept by researchers of UPC-BarcelonaTech or the SATH concept by Saitec Offshore Technologies. Besides that, Spain possesses suitable locations for floating offshore wind employment with deep water sites close to load centers and good wind resources. Only recently, a prototype of a twin-rotored FOWT developed by EnerOcean has been installed off the Canary Islands and the Norwegian developer Equinor has secured a permit to build a 200MW FOWF also close to the Canary Islands [72]. Besides the mentioned countries, prototypes are also being developed in Germany, Sweden and the Netherlands [28].

Japan has a large interest in floating offshore wind development for several reasons. First, the nuclear catastrophe of Fukushima has demonstrated the high risk of nuclear power and the Japanese people are demanding a diversification of the energy mix. Second, the country lacks of suitable sites for onshore wind, since the country is characterized by mountainous terrains and densely populated regions. Lastly, the Japanese coastline falls rapidly off, which causes deep waters near to the coast [11]. The following map shows potential locations for the deployment of FOWTs. Several demonstration projects have been realized in Japan, including conventional floating wind concepts, but also multiple-turbine substructures such as the WindLens project and hybrid systems such as SKWID.

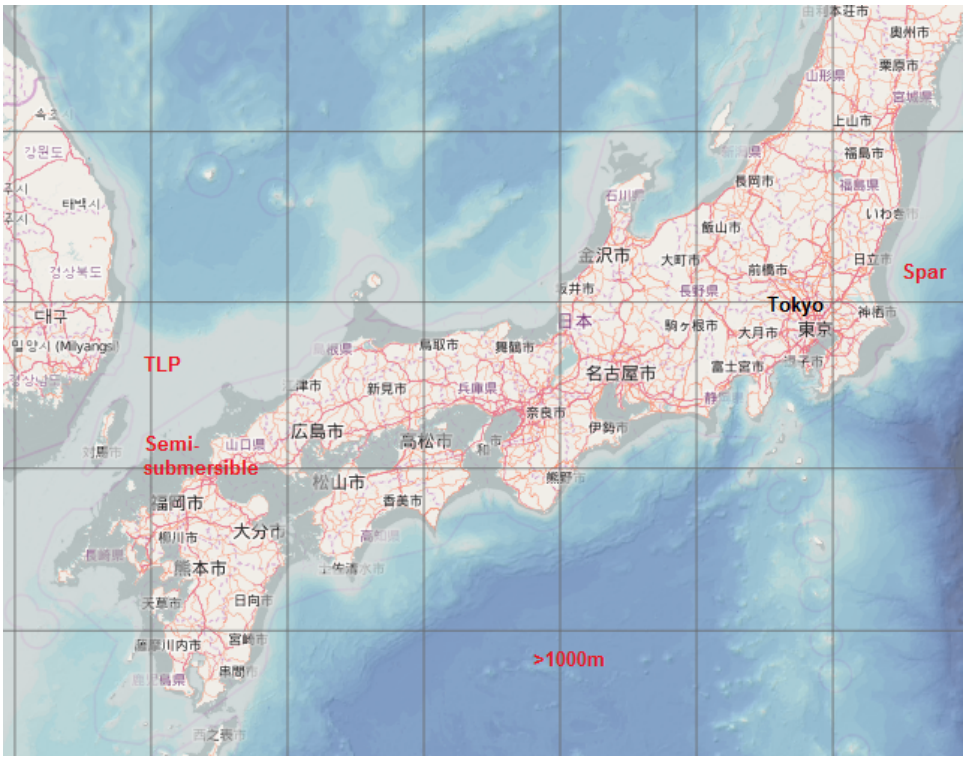

Figure 2.21: Suitable sites in Japan [73].

The most prominent project is Fukushima FORWARD, which is led by a large consortium including Mitsubishi, University of Tokyo, Mitsui, and Marubeni among others. The project includes the construction of two types of semi-submersible floating structures, one spar design and the world's first floating substation. In 2013 one semi-submersible floating turbine with a capacity of 2MW and the floating substation was installed, followed by the installation of the 7MW semi-submersible floating substations in 2015. The advanced spar design with a 5MW turbine has been commissioned in 2016. After, the successful operation of the prototype, the floating offshore wind farm will like be extended to 100MW in phase 3 and possibly 1,000MW in phase 4 [11].

The United States is one of the countries with most onshore capacity installed. However, it has also a large potential for offshore wind at its east and west coast and in particular for floating wind since more than half of the offshore wind resources are estimated to be located in deeper waters.

Furthermore, the most populated parts of the country are located at the coast, which additionally favors the use of offshore wind. So far only one offshore wind farm has been installed located off Rhode Island consisting of BOWTs. However, several more are projected including floating offshore wind. The state of Maine and California have shown in particular interest. A first 20kW FOWT prototype, the VolturnUS, was installed and tested by the consortium DeepCWind for a few months outside of the Castine harbor in 2013 [28].

Other markets that may get popular in the near future are China, Taiwan and South Korea. China the leader in onshore wind energy has so far only two BOWFs installed. More projects are expected in the upcoming years and investigations have been started floating wind as well. However, in contrast to Japan, China does have large shallow waters and they are located near the consumption centers at the cost. Thus, the future will tell who will win the race, bottom-fixed wind, floating wind or a mix of both. Taiwan and South Korea have also shown their interest in floating offshore wind. The French floating substructure designer IDEOL yet has firmed an agreement for collaboration in Taiwan and the German company GICON has been in contact with delegates from South Korea to evaluate the potential application of their floating substructure design [68, 74, 75].

2.3.3 Key challenges and opportunities, market barriers

The most critical market barrier to floating offshore wind is its counterpart the conventional wind technology such as onshore and bottom-fixed offshore wind. In order to be competitive and gain a share in the energy mix, floating wind technology has to demonstrate that it is able to reduce significantly the cost of energy. It might be possible due to the avoidance of large installation works offshore and the harnessing of the most productive sites regardless of water depth constraints. However, an extensive research and development is still required to reduce the cost of the system. Furthermore, long-term political support is necessary, in particular, incentives for floating wind that encourage investments in this technology. Besides that, the floating wind industry is in its infancy and still has to grow. A larger number of manufacturers and suppliers will increase competition and bring down the cost for the components. The funding of demonstration projects is also important in order to test the technology in real environmental conditions and raise the awareness level. Another market barrier might be the available infrastructure. In light of the increasing offshore wind constructions more ports and shipyards are being built to meet the demand.

However, shortages might occur in the use of vessels or the supply of submarine cables. The industry, in particular original equipment manufacturers have to grow in capacity with the rate of installations. The final barriers to consider are new standards and models that need to be developed in order to ensure the commercialization of floating systems [11, 28].

3 Floating offshore wind turbine modeling

The aim of this chapter is to provide the essential theoretical background for the modeling of floating offshore wind turbines. At first, the offshore environment is described in general consisting of wind, waves, currents as well as other important environmental conditions. Then, the model of a typical FOWT is presented including the structural properties and the methodology for the power generation calculation. Finally, the loads acting on a FOWT are described consisting of aerodynamic, hydrostatic and hydrodynamic loads as well as the mooring system.

3.1 The offshore environment

In the offshore environment various environmental loads exist that have an impact on offshore structures. An accurate understanding of the environment is crucial for the design of an offshore structure and its integrity during lifetime [56]. Figure 3.1 presents a FOWT exposed to the main environmental loads: Wind, waves and currents. Depending on the location, icing or seismic activity may occur. Furthermore, the accumulation of marine growth may affect the structure. The following sections describe each of the environmental actors briefly.

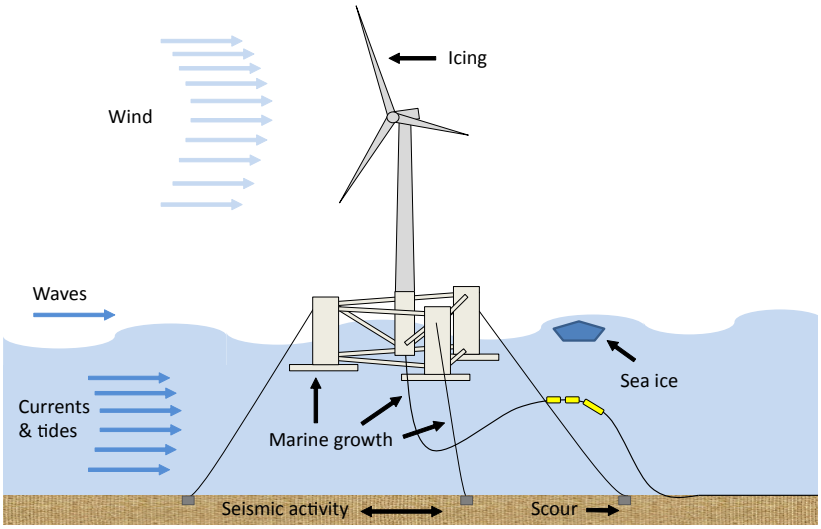

Figure 3.1: Offshore environment impacting a floating offshore wind turbine.

3.1.1 Offshore wind

Wind is the essential fuel required by a wind turbine to generate electricity [76]. The winds existing in the world are caused by the heating of the earth's surface by the sun. Thus wind energy can be considered as a form of solar energy. The air above the surface absorbs the heat, expands and looses pressure. The resulting warm air with lower density rises. As the cool air in higher altitudes has higher pressure based on the higher density, it tends to sink. This circulation of air from high-pressure to low-pressure regions creates the wind [56]. The heating process differs with the location on earth. The equator receives more heat than poles and landmasses tend to heat up faster than the ocean. This uneven heat distribution fuels the creation of wind flows. The rotation of the earth itself also affects the movement of the wind as well as the local topography such as hills, valleys and forests. Furthermore, coastal areas experience breezes caused by the different heating and cooling behavior of land and sea [56, 77].

Offshore the wind is in general higher and more uniform than onshore due to lack of obstacles hindering the free air flow. Furthermore, the surface roughness has an important effect on the wind. The low surface roughness of water causes less friction between the wind and the sea and results in less velocity reduction offshore. In addition, the wind speed tends to increase with height since less frictional and physical influences occur in higher altitudes.

This phenomenon is known as wind shear and is important to consider when assessing offshore sites. For instance, measurements of wind speeds are often taken at a different hight than the hub and need to be converted to the correct hight [56]. The power law is a common method used to determine the wind speed at a specific height and is defined as

$$V = V_0 * \left(\frac{h}{h_0}\right)^{\alpha} \tag{3.1}$$

where V is the speed at height h, V_0 is the speed at the height of the measurement h_0, and α is the power law exponent that depends on the surface roughness [77].

The wind conditions do not only vary in space but also in time. The temporal variation can be short-term, diurnal, seasonal or long-term [77]. Short-term wind speed fluctuations in the scale of seconds to minutes are also known as turbulence [56]. The turbulence characterization of a specific site is an important design requirement since short-term fluctuations pose significant dynamic loads on the structure and rotor and are demanding for the control system of the turbine [77]. The turbulence intensity T_{int} at a given offshore site can be determined by

$$T_{\text{int}} = \frac{\sigma}{V_{\text{mean}}} \tag{3.2}$$

where σ is the standard deviation of the mean wind speed V_{mean}. A power spectra can be used to build time series of wind profiles in case no site specific measurements are available. There exist several power spectra models such as the Davenport, Kaimal, Harris, Frøya, Ochi and Shin, and von Karman spectrum [78, 79]. They generally agree in the high frequency range but may differ in the low frequency range and also on the applicability to offshore sites [78]. The Kaimal wind spectrum is one of the most widely applied models and has also been suggested by the DNV design standard for offshore wind turbine structures [80]. The spectrum is defined by

$$S_{\text{wind}}(f) = \frac{4\ {T_{\text{int}}}^2\ V_{\text{mean}}\ l_{\text{wind}}}{(1 + 6\ \frac{f\ l_{\text{wind}}}{V_{\text{mean}}})^{\frac{5}{3}}} \tag{3.3}$$

where l_{wind} is the integral scale parameter and depends on the height above the seawater level. The frequency is represented by f [80]. The spectrum can then be used to compute the wind time series considering the inverse Fourier transform function to convert from frequency to time domain as demonstrated in [81, 82].

An example of a wind profile obtained with the Kaimal spectrum considering V_{mean} = 12 m/s, T_{int}= 0.14 and l_{wind} =340.2m is presented in Figure 3.2.

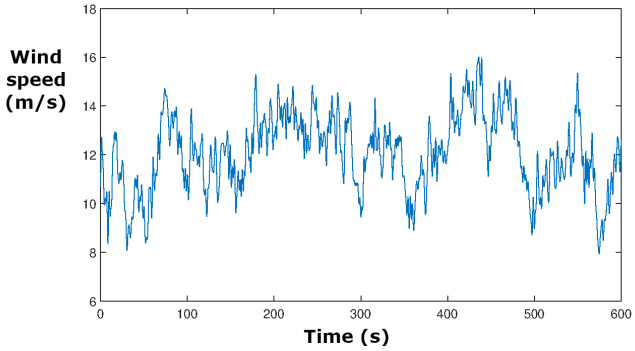

Figure 3.2: Wind speed time series obtained using a Kaimal spectrum.

The diurnal variations of wind are due to the rotation of the earth and corresponding heating of the sun during daytime and cooling at night. Furthermore, it is affected by local geography, proximity to the sea and altitude [77]. The annual variation of wind is defined as the occurrence of seasonal wind speed changes. For instances, in northern Europe generally higher mean wind speeds are present during autumn and winter while lower wind speeds appear in spring and summer [56]. Seasonal variations of wind speeds are important to consider for the scheduling of installation and maintenance work offshore and also for the energy yield assessment for seasonal electricity demand. The long-term wind resource estimation can be of significance for wind farm owners to predict the performance and energy generation of a wind farm over the entire lifetime [77].

The wind resource can be measured in terms of wind speed and wind direction. Typical devices for measuring the wind speed and wind direction are anemometers and vanes, respectively [83]. In recent years alternative methods to the mechanical measurement systems have been developed mainly driven by the increased demand of the offshore wind industry. These are remote sensing systems such as LIDAR and SODAR that apply laser beams or sound waves to measure the wind. The data obtained by long-term wind measurements can be illustrated in form of a wind rose. The wind rose of a specific location is an important tool for developers as it provides information about the wind direction in order to adequately locate the turbines towards the wind and may also provide the wind speed distribution [83].

Figure 3.3 shows a typical wind rose.

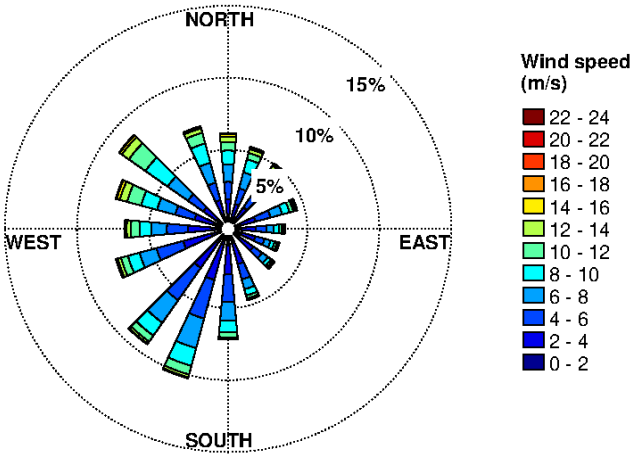

Figure 3.3: Wind rose illustration.

The prediction of the wind speed profile enables the choice of a suitable turbine and the estimation of the energy generation. The Weibull distribution indicates the fraction of time or probability for which a certain wind speed appears. The following equation represents the Weibull distribution function [83].

$$f(V_{\text{mean}}) = \frac{k}{c} * \left(\frac{V_{\text{mean}}}{c}\right)^{k-1} * e^{-(\frac{V_{\text{mean}}}{c})^k} \tag{3.4}$$

The Weibull shape factor is represented by k and the scale factor by c. The wind speed and the scale factor are related by a gamma function as follows [83].

$$c = \frac{V_{\text{mean}}}{\Gamma(1 + \frac{1}{k})} \tag{3.5}$$

Figure 3.4 illustrates Weibull distribution graphs with different shape and scale factors. It can be seen that the most frequent wind speed is in general not the mean wind speed. The reason is that higher wind speeds are typically rarer than lower wind speeds. Thus the graph is not symmetrical rather skewed. A Weibull distribution with a shape factor of 2 is also known as Rayleigh distribution and is often used by wind turbine manufactures for standard performance demonstrations [46].

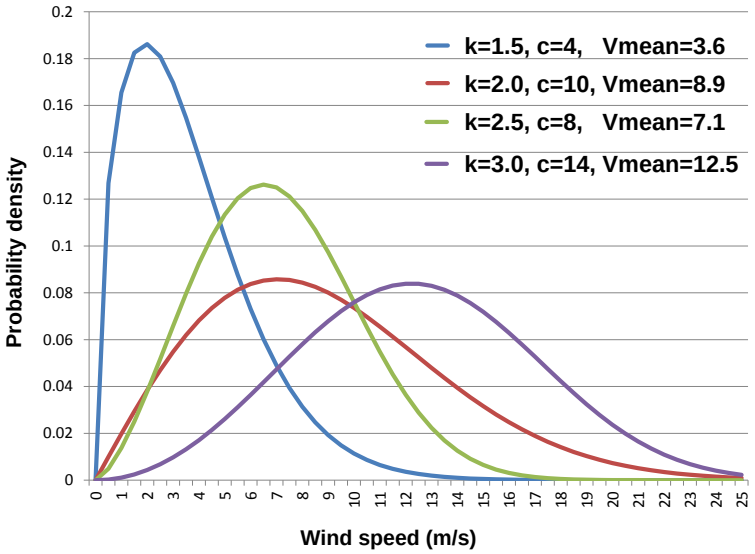

Figure 3.4: Weibull distribution graphs for different shape and scale factors.

The power that can be extracted by a wind turbine with the rotor swept area A is given by

$$P_{\text{wind}} = \frac{1}{2} * C_{\text{p}} * \rho * A * {V_{\text{mean}}}^3 \tag{3.6}$$

where ρ is the density of the wind and C_p represents the power coefficient. The power coefficient is a measure of the wind turbine efficiency and can be calculated by the ratio of the actual electric power produced by the turbine to the total wind power flowing into the rotor swept area. The theoretical maximum power that can be extracted from the wind is defined as the Betz limit with 59% [34]. The power coefficient is often given for a specific wind turbine by the manufacturer to calculate the potential energy generation. Figure 3.5 displays the power coefficient curve for the DTU 10MW Reference Wind Turbine. Furthermore, the power curve is shown representing the maximum power extractable by the turbine for a given wind speed. The figure shows also the cut-in wind speed at which the turbine first starts to rotate and the specific cut-out wind speed at which the rotor is brought to stop due to extreme wind speeds that could damage the structure and the rotor [5]. The power generation equation is slightly adapted in Section 3.2.3 to consider to the dynamic loading from environmental forces as explained further in detail in the following sections.

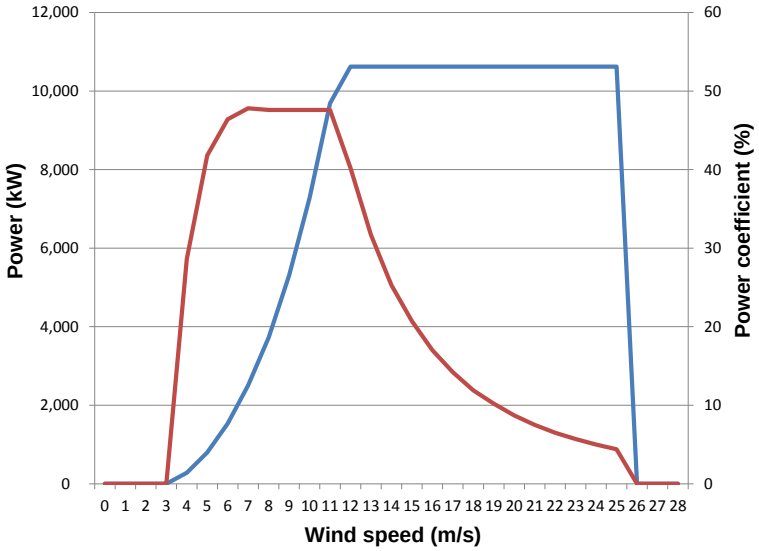

Figure 3.5: DTU 10MW reference wind turbine power curve (blue) and power coefficient (red) [84].

3.1.2 Ocean waves

In general terms, waves can be described as oscillations of the water surface generated by an initial disturbance and compensated by a restoring force. They can be observed in any environment like rivers, lakes, seas or oceans [85]. Ocean waves cause periodic loads on offshore structures such as FOWTs. Understanding the wave loading is crucial to predict the structural response, which can include accelerations, harmonic displacements and internal loads [86]. Furthermore, the accurate characterization of the wave resource contributes to the correct definition of the environmental conditions for the design of the structure at the considered location [56]. Ocean waves occur with different shapes, heights, lengths and speed of propagation [87]. A classification can be made with respect to the wave period and the source that generates the wave [56] as presented in Table 3.1.

The wind is the source for the creation of the waves with the 4 shortest periods, namely capillary, ultra-gravity, ordinary gravity and infra-gravity waves. Storm and earthquakes can cause long-period waves ranging from 5min to 12h. These are also known as tsunamis. The gravitational attraction of sun and moon causes ordinary tides with fixed periods of 12h to 24h.

Table 3.1: Classification of ocean waves [56].

Classification	Period	Source
Capillary waves	Less than 0.1s	Wind
Ultra-gravity waves	0.1s to 1s	Wind
Ordinary gravity waves	1s to 30s	Wind
Infra-gravity waves	30s to 5min	Wind
Long-period waves	5min to 12h	Storm and earthquakes
Ordinary tides	12h to 24h	Sun and moon
Trans-tidal waves	24h and more	Storms, sun and moon

Trans-tidal waves possess the largest wave periods ranging from daily to seasonal variations or more. These can be generated by gravitational forces or other meteorologic factors such as seasonal storms [85]. Besides the creation of waves by natural sources, they can also be generated by a structure moving or oscillating in the ocean [86]. However, the most relevant type of waves and considered in this thesis for the study of wave loading on a floating substructure are ordinary gravity waves with periods ranging from 1s to 30s. The restoring force responsible for returning the wave to its original position depends also on the type of wave. Surface tension is the main restoring force for capillary waves, whereas for ultra-gravity waves both surface tension and gravity can be the source for the returning force. Ordinary gravity, infra-gravity and long-period waves are being returned solely by gravity. However, for long period waves such as ordinary tides and trans-tidal waves both gravity and coriolis force contribute to the restoring effect [88]. Waves generated by wind are highly irregular. However, they can be described as a superposition of regular waves with different amplitudes, frequencies and direction of propagation [86]. In order to analyze irregular waves, it is necessary to understand at first the behavior of an individual harmonic regular wave.

Regular waves

Figure 3.6 illustrates a two-dimensional regular wave and the main defining parameters. The crest represents the highest point of the wave, whereas the lowest point is called through. The wave propagates in positive x-direction and the horizontal distance between two successive crests passing a reference point is defined as wave length λ. Likewise, the time interval between successive crests is called wave period T_w.

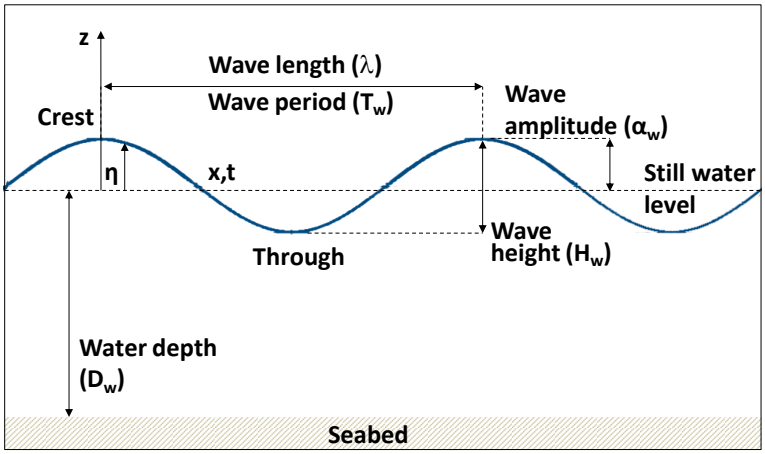

Figure 3.6: Regular wave and main defining parameters.

The still water level defines the height of the water in case no waves are present and the water depth D_w represents the vertical distance between the seabed and the still water level. The wave amplitude α_w describes the vertical distance between the still water level and the wave crest. The wave height H_w measures the distance between through and crest [86]. Linear wave theory or also known as airy wave theory can be used to describe the motions and derived characteristics of a wave. The theory is valid for gravity waves where the wave height is small compared to the wavelength and the water depth. For waves with different shapes one may refer to the appropriate theory for instance stokes, cnoidal, solitary or stream function wave theory [89]. According to the linear wave theory, a regular wave can be described as a sinusoidal function by

$$\eta_{\text{regular}} = \alpha_{\text{w}}\ cos(k_{\text{w}}x - \omega t) \tag{3.7}$$

where $\eta_{regular}$ is the surface elevation and represents the change of the vertical distance between the still water level and the wave surface while the wave propagates. The wave amplitude is half of the wave height for a sinusoidal wave. The wave number is given by k_w and the angular frequency is defined by ω [86]. The wave number and angular frequency are related through the dispersion relationship as follows

$$\omega^2 = g\ k_{\text{w}}\ tanh(k_{\text{w}}\ D_{\text{w}}) \tag{3.8}$$

where g is the acceleration by gravity [90].

The angular frequency is related to the wave period by $\omega = 2\pi/T_w$ and likewise the wave number is related to the wave length by $k = 2\pi/\lambda$ [89]. A further important parameter is the propagation velocity of the wave or also known as wave celerity [86]. For linear waves, the wave celerity c is expressed as follows.

$$c = \frac{\lambda}{T_{\mathrm{w}}} = \frac{\omega}{k_{\mathrm{w}}} = \sqrt{\frac{g}{k_{\mathrm{w}}}\ tanh(k_{\mathrm{w}}\ D_{\mathrm{w}})} \tag{3.9}$$

Finally, the kinematics of a water particle can be defined, which are useful for the further hydrodynamic analysis of a FOWT and the simulation of waves. The velocity components in x- and z-directions are represented by $\mathrm{u_x}$ and $\mathrm{u_z}$, respectively and are defined as follows.

$$u_{\mathrm{x}} = \alpha_{\mathrm{w}}\ \omega\ \frac{cosh(k_{\mathrm{w}}D_{\mathrm{w}} + k_{\mathrm{w}}z))}{sinh(k_{\mathrm{w}}\ D_{\mathrm{w}})}\ cos(k_{\mathrm{w}}x - \omega t) \tag{3.10}$$

$$w_{\mathrm{z}} = \alpha_{\mathrm{w}}\ \omega\ \frac{sinh(k_{\mathrm{w}}D_{\mathrm{w}} + k_{\mathrm{w}}z))}{sinh(k_{\mathrm{w}}\ D_{\mathrm{w}})}\ sin(k_{\mathrm{w}}x - \omega t) \tag{3.11}$$

The water particle accelerations are derived from a differentiation of the velocity components and can be computed as follows.

$$\dot{u_{\mathrm{x}}} = \alpha_{\mathrm{w}}\ \omega^2\ \frac{cosh(k_{\mathrm{w}}D_{\mathrm{w}} + k_{\mathrm{w}}z))}{sinh(k_{\mathrm{w}}\ D_{\mathrm{w}})}\ sin(k_{\mathrm{w}}x - \omega t) \tag{3.12}$$

$$\dot{w_{\mathrm{z}}} = -\alpha_{\mathrm{w}}\ \omega^2\ \frac{sinh(k_{\mathrm{w}}D_{\mathrm{w}} + k_{\mathrm{w}}z))}{sinh(k_{\mathrm{w}}\ D_{\mathrm{w}})}\ cos(k_{\mathrm{w}}x - \omega t) \tag{3.13}$$

It has to be noted that the theory described previously is accurate for shallow waters. For deep waters a few modifications have to be considered as defined in [86]. In this regard, the water is considered to be deep if the water depth is more than half the wave length. Likewise, the water is considered to be shallow if the water depth is less than 1/20 of the wave length [86].

Irregular waves

The actual sea surface is highly irregular. However, it can be described as a superposition of regular waves with different wave heights, frequencies and propagation direction as demonstrated in Figure 3.7 [86].

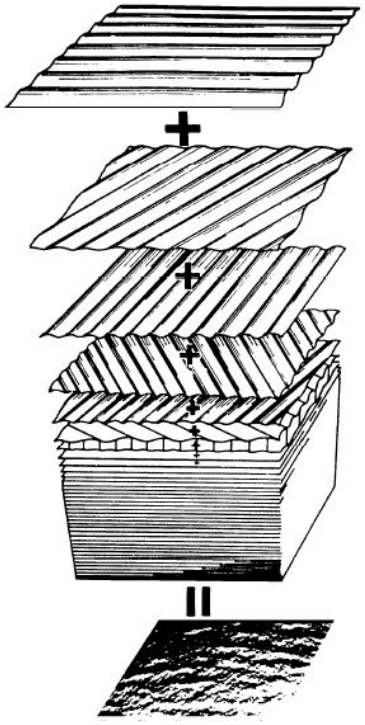

Figure 3.7: Superposition of regular waves to define an irregular sea [91].

The wave resource can be measured by using technologies that are placed in situ for instance wave buoys and acoustic doppler profiles or by using remote sensing systems such as radars and satellites [56]. The measured data is then post processed by statistical means to obtain the wave climate of the site. For instance, a Rayleigh distribution can be used to determine the long-term probability distribution of the wave height as illustrated in Figure 3.8 [92]. The significant wave height H_s is one of the most important statistical wave parameters used in offshore engineering and represents the mean of the highest third of waves measured in a period of time [89]. The wave elevation of an irregular wave $\eta_{irregular}$ can be computed as the sum of a number of regular waves $\mathrm{N_w}$ according to the superposition principle as follows

$$\eta_{\mathrm{irregular}} = \sum_{n_{\mathrm{w}}=1}^{N_{\mathrm{w}}} \alpha_{\mathrm{w}}\ cos(k_{\mathrm{w}}x - \omega t + \varepsilon) \tag{3.14}$$

where ε is a random phase angle [86].

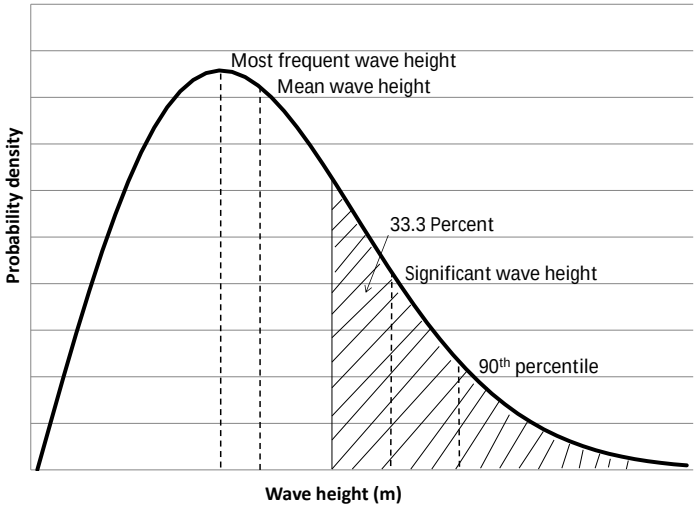

Figure 3.8: Rayleigh wave distribution [92].

The wave amplitude α_w is related to the wave angular frequency ω through the wave energy density spectrum S_{wave} by

$$\alpha_{\mathrm{w}} = \sqrt{2\ S_{\mathrm{wave}}\ \Delta\omega} \tag{3.15}$$

where $\Delta\omega$ is the difference between two successive frequencies [86]. The wave energy density spectrum describes the wave energy distribution over a frequency range of a irregular wave. It is, therefore, dependent on the statistical properties describing the wave such as the significant wave height H_s and the peak period T_p. The peak period represents the period corresponding to the highest density of the spectrum [90]. Different wave spectra exist depending on the conditions of the ocean. The Joint North Sea Wave Project (JONSWAP) spectrum is a widely known model to describe irregular waves generated by wind. It is based on the data collected from an extensive wave measurement carried out in the North Sea between 1968 and 1969 [86]. It can be computed following the recommended practice by DNV-GL [78] as follows

$$S_{\mathrm{wave}} = A_{\mathrm{y}}\frac{5}{16}{H_{\mathrm{s}}}^2{\omega_{\mathrm{p}}}^4\omega^{-5}\ e^{\left(-\frac{5}{4}(\frac{\omega}{\omega_p})^{-4}\right)}\ {\gamma_{\mathrm{p}}}^{e^{\left(-0.5(\frac{\omega-\omega_p}{\sigma_s\ \omega_p})^2\right)}} \tag{3.16}$$

where γ_p is the peak shape parameter, σ_s is the spectral width parameter and A_y is a normalizing factor with $A_y = 1 - 0.287\ ln(\gamma_p)$.

The angular peak frequency ω_p is derived from the peak period by $\omega_p = 2\pi/T_p$ [78]. Figure 3.9 shows exemplary a time series of an irregular wave elevation obtained by using this spectrum.

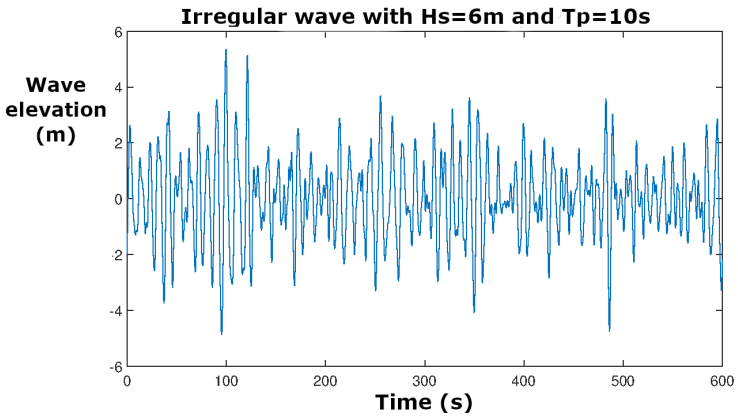

Figure 3.9: Irregular wave obtained with JONSWAP spectrum.

3.1.3 Ocean currents

Ocean currents can be described as a uniform directional flow of sea water. Different types of currents exist that can be classified as follows [78].

- Wind-generated currents
- Tidal currents
- Circulation currents
- Loop and eddy currents
- Longshore currents
- Soliton currents

Wind-generated currents are near surface currents that are caused by the wind force acting parallel to the water surface. Tidal currents are generated by tides and belong to sub-surface currents. They are generally weak in deep water and become stronger in coastal regions. The large currents that exist in the oceans such as the Gulf Stream are called circulation currents and some may break off in smaller loop and eddy currents.

The waves breaking on the shore can also create currents, called longshore currents, which propagate parallel to the shore. Soliton currents are caused by internal waves in the ocean [56]. Floating substructures can be affected in different manners by ocean currents. For instance, the presence of a current can cause additional motions to the floating platform and increase drag and lift forces. Furthermore, the combination of wind and wave loads can change the wave height and periods [78]. Typical devices used to measure currents are doppler current profiles or current meters that are installed in situ [56]. Important measurement parameters are the direction and velocity of the current. The velocity changes with the water depth and can be calculated as the sum of the wind and tide current components. According to the offshore standard by DNV-GL [80], the total current velocity $v_{current}$ at the distance z_c from still water level is obtained by

$$v_{\text{current}}(z_{\text{c}}) = v_{\text{c-wind}}(z_{\text{c}}) + v_{\text{c-tide}}(z_{\text{c}}) \tag{3.17}$$

$$v_{\text{c-wind}}(z_{\text{c}}) = v_{\text{c-wind0}} \left(\frac{D_{\text{w0}} + z_{\text{c}}}{D_{\text{w0}}} \right) \quad for \ -D_{\text{w0}} \leq z_{\text{c}} \leq 0 \tag{3.18}$$

$$v_{\text{c-tide}}(z_{\text{c}}) = v_{\text{c-tide0}} \left(\frac{D_{\text{w}} + z_{\text{c}}}{D_{\text{w}}} \right)^{1/7} \quad for \ z_{\text{c}} \leq 0 \tag{3.19}$$

where $v_{c\text{-}wind0}$ and $v_{c\text{-}tide0}$ represent the wind-generated and tidal current velocity components at still water level, respectively. The reference water depth for the wind-generated current is defined by D_{w0} [80].

3.1.4 Other environmental conditions

There are other environmental conditions depending on the potential offshore site that can have an impact on the performance and the structural integrity of a FOWT. For instance, in a cold climate the accumulation of snow and ice can become an important issue for buoyancy stabilized structures and the potential threat of a collision with floating sea ice should be considered at an early design stage. In case the location of the wind turbine is situated in area with seismic activity, an investigation on the frequency and magnitude of earthquakes is required as well as a study on potential ground motions. An earthquake can cause additional hazards such as tsunamis, liquefaction of the soil, submarine slides, and shock waves. For most of the FOWT designs, hazards arising from seismic actively are of a low significance due to the floatability of the structure.

However, for TLP concepts that are based on a tensioned mooring system, the impact of an earthquake becomes more important [56]. Marine growth, in form of plants and animals attaching to the submerged components of a FOWT, is a further environmental condition to be taken into account. The attachment of marine life to the structure adds additional weight and increases the size. This can have an influence on the hydrodynamic loads and dynamic response of the FOWT as well as impact negatively the accessibility and corrosion rate [80].

3.2 System and model definition

In this section, the theoretical background required to model a FOWT is provided as well as the definition of the structural properties and the computation of the power and energy generation. Furthermore, a specific FOWT concept is presented, which will be used for the subsequent analysis.

3.2.1 Model description

There are two fundamental approaches that can be followed to model the structural behavior of a FOWT [93]. The first approach considers the FOWT as a single rigid body subject to environmental loads and neglects structural deflections by assuming infinite stiffness. This allows for a significant simplification of the model. The second approach is the finite element method, which discretizes the structure in a number of finite elements and takes into account the structural flexibility [94]. Since the structural response and motions are mainly dominated by rigid body motions rather than elastic deformation, the first approach is considered to model the FOWT with enough accuracy [95]. The dynamic analysis of a FOWT is performed by the model by solving the equation of motion in time domain. The equation of motion for a floating structure is given by Equation 3.20, which is based on Newton's second law of motion [93].

$$(\mathbf{M} + \mathbf{A})\ \ddot{\mathbf{x}}(t) + \mathbf{B}\ \dot{\mathbf{x}}(t) + \mathbf{C}\ \mathbf{x}(t) = \mathbf{F_{ext}}(t) \tag{3.20}$$

The motion vector x represents the displacements in each degree of freedom (DOF). The derivatives represent the corresponding velocities and accelerations. The Hywind Spar-buoy FOWT concept is considered in this study for the following analysis. It has typically six rigid-body degrees of freedom as illustrated in Figure 3.10.

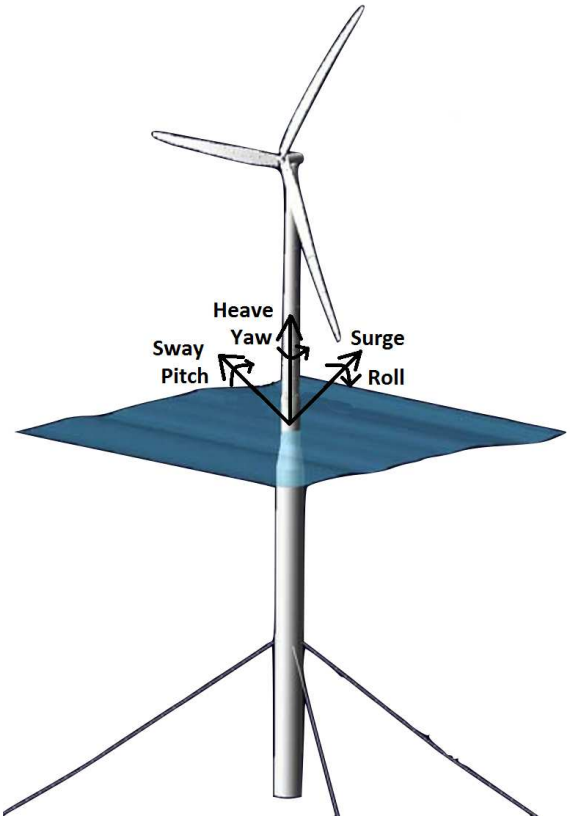

Figure 3.10: OC3-Hywind concept illustration [96].

Due to the symmetry of the Spar-buoy concept and in order to simplify the model only the motions on the XZ-plane will be considered. Hence, the number of degrees of freedom is reduced to three: surge, heave and pitch. M and A represent the mass and added mass of the FOWT. B is the damping and C the hydrostatic stiffness. All those before mentioned are 3 x 3 matrices according to the selected degrees of freedom and including coupling terms. F_{ext} represents the vector of all external forces and moments acting on the FOWT [93]. In order to solve Equation 3.20 all the loads and forces have to be identified. The modeling of the external forces is presented in Section 3.3 and the methodology for computing the structural properties of the left side of the equation is presented in Section 3.2.2. Once the equation of motion is completely defined, it is written in the state-space form in order to eliminate the second order differential equations and ode45 function from MATLAB [97] is used to solve it.

3.2.2 Structural properties

The global mass matrix [89] is determined by

$$\mathbf{M} = \begin{bmatrix} m_{\mathrm{t}} & 0 & m_{\mathrm{t}}\ z_{\mathrm{CoM}} \\ 0 & m_{\mathrm{t}} & -m_{\mathrm{t}}\ x_{\mathrm{CoM}} \\ 0 & -m_{\mathrm{t}}\ x_{\mathrm{CoM}} & I_{\mathrm{yy}} \end{bmatrix} \tag{3.21}$$

where m_t is the mass of the body and I_{yy} is the mass moment of inertia [95]. The non-zero off-diagonal terms result from a slight displacement x_{CoM} of the center of mass to the origin [98]. The added mass is additional mass that the structure appears to have when it is accelerated relative to the surrounding water.

In general, the added mass is dependent on the wave frequency and also on the size and shape of the floating structure. However, in the developed model a constant added mass matrix is considered. Strip theory is used to calculate the added mass for each DOF using added mass coefficients of two dimensional sections and integrating over the length [95]. The added mass matrix is modeled as

$$\mathbf{A} = \begin{bmatrix} \int_{z_{\mathrm{bot}}}^{0} \rho_{\mathrm{w}} C_{\mathrm{a}} A(z) dz & 0 & \int_{z_{\mathrm{bot}}}^{0} \rho_{\mathrm{w}} C_{\mathrm{a}} A(z) z dz \\ 0 & \frac{2}{3}\rho_{\mathrm{w}}\pi R^3 & 0 \\ \int_{z_{\mathrm{bot}}}^{0} \rho_{\mathrm{w}} C_{\mathrm{a}} A(z) z dz & 0 & \int_{z_{\mathrm{bot}}}^{0} \rho_{\mathrm{w}} C_{\mathrm{a}} A(z) z^2 dz \end{bmatrix} \tag{3.22}$$

where C_a represents the added mass coefficient and *A(z)* the cross-sectional area of the Spar structure. The diameter of the Spar changes with the hight and has to be considered in the calculation of the cross-sectional area. As explained in Section 3.3.3, damping due to radiation is neglected in Morison equation. However, Jonkman [96] recommends to add linear damping to capture correctly the response of the OC3-Hywind concept to hydrodynamic loads. The additional damping for surge and heave included as damping matrix is as follows.

$$\mathbf{B} = \begin{bmatrix} 1.000e^5 \mathrm{N\,s/m} & 0 & 0 \\ 0 & 1.300e^5 \mathrm{N\,s/m} & 0 \\ 0 & 0 & 0 \end{bmatrix} \tag{3.23}$$

The hydrostatic stiffness represents the restoring term as effect of the substructure movements in the water in heave and pitch direction.

There is no hydrostatic restoring term in surge or in coupled motions. The variation in heave of the submerged volume will create a force equal in magnitude to the volume of fluid displaced. The restoring moment will arise with the pitch motion from the horizontal displacement of the gravity and buoyancy centers and the water-plane area inertia effects. The restoring torque is written as a sum of the three contributions [99].

$$\mathbf{C} = \begin{bmatrix} 0 & 0 & 0 \\ 0 & \rho_{\mathrm{w}} g A_{\mathrm{wp}} & 0 \\ 0 & 0 & \rho_{\mathrm{w}} g I_{\mathrm{wp}} + \rho_{\mathrm{w}} g V z_{\mathrm{CoB}} - m_{\mathrm{t}} g z_{\mathrm{CoM}} \end{bmatrix} \tag{3.24}$$

A stiffness matrix for the restoring term of the mooring load is defined as follows.

$$\mathbf{K} = \begin{bmatrix} K_{11} & 0 & K_{31} \\ 0 & K_{33} & 0 \\ K_{13} & 0 & K_{55} \end{bmatrix} \tag{3.25}$$

The stiffness parameters represent mean values obtained from the nonlinear quasi-static model. They are used for the computation of the natural frequencies of the FOWT and for comparison of the developed model with FAST. However, in the dynamic model the nonlinear mooring load is considered as an external force for the computation of the Morison equation. Based on the previously defined matrices, the natural frequencies and periods of the FOWT can be obtained from the homogeneous undamped equation of motion, which is presented below [93].

$$(\mathbf{M} + \mathbf{A})\, \ddot{\mathbf{x}} + (\mathbf{C} + \mathbf{K})\, \mathbf{x} = \mathbf{0} \tag{3.26}$$

The solution is considered to be as

$$\mathbf{x} = x_0\, e^{\mathrm{ift}} \tag{3.27}$$

where x_0 is the vector of amplitudes and f is the natural frequency for each DOF. By computing the second derivative and replacing it on Equation 3.26, the eigenvalue problem is obtained and can be solved as

$$\mathbf{C}(\mathbf{M} + \mathbf{A})^{-1} \; - \; f^2\, \mathbf{I} = \mathbf{0} \tag{3.28}$$

3.2.3 Power generation

The power generated by the FOWT can be calculated by Equation 3.29 taking into account the rotor swept area A_{rotor}, the power coefficient C_p and the wind speed v_{wind} at hub height. The power coefficient depends on the blade tip-speed ratio λ and the blade pitch angle β [79].

$$P_{\mathrm{FOWT}} = \frac{1}{2}\ \rho_{\mathrm{a}}\ A_{\mathrm{rotor}}\ C_{\mathrm{p}}(\lambda, \beta)\ {v_{\mathrm{wind\text{-}tilted}}}^3 \tag{3.29}$$

Two considerations have been included in the power equation of the FOWT in contrast to a BOWT. The first is that the motions of the FOWT provoke an additional mean platform tilt angle. This causes the rotor to be slightly tilted against the inflow wind velocity v_{wind}. This effect is taken into account in the power calculation by reducing the inflow wind velocity by the pitch angle θ of the structure as follows [93].

$$v_{\mathrm{wind\text{-}tilted}} = v_{\mathrm{wind}}\ cos(\theta) \tag{3.30}$$

The second consideration is that the model takes into account the relative wind velocity in the wind force computation of the FOWT as defined by Equations 3.32 and 3.33.

3.2.4 Energy generation

The annual energy generation of the FOWT can be obtained by

$$E_{\mathrm{FOWT}} = \sum P_{\mathrm{j,k}} * H_{\mathrm{j,k}} * 8760 \tag{3.31}$$

where $P_{j,k}$ is the power obtained for a specific met-ocean condition, defined by a certain wind speed j and a particular wave height k. The occurrence probability per year of this particular met-ocean condition is considered by $H_{j,k}$.

3.3 Description of loads

The forces that act on the FOWT consist of aerodynamic, hydrostatic and hydrodynamic loads as well as the mooring system. Wind and waves are considered as main environmental loads in this study. However, there are other conditions such as currents, tides, seismic activity or ice that can impact the performance of a FOWT depending on the location, but are out of scope of this thesis [10].

3.3.1 Aerodynamics

The aerodynamic loading on a wind turbine depends mainly on the wind velocity and the rotor characteristics. The wind thrust force acting on the FOWT is given as

$$F_{\mathrm{wind}} = \frac{1}{2}\ \rho_{\mathrm{a}}\ \pi\ {R_{\mathrm{rotor}}}^2\ C_{\mathrm{T}}\ {v_{\mathrm{rel}}}^2 \tag{3.32}$$

where ρ_a represents the air density, R_{rotor} is the radius of the rotor, C_T the thrust coefficient and v_{rel} the relative wind velocity. The relative wind velocity is the velocity seen by the rotor at hub height and can be obtained as presented in the following equation.

$$v_{\mathrm{rel}} = v_{\mathrm{wind}} - v_{\mathrm{hub}} \tag{3.33}$$

v_{wind} represents the incoming wind speed and v_{hub} is the hub velocity due to the motions of the substructure. The wind velocity is considered as uniform and one-directional as seen by the hub. The wind force acting on the tower has been neglected. The thrust coefficient is, in general, a function of the blade tip-speed ratio and the blade pitch angle [79]. This approach has been used in Section 3.2.3 to calculate the power generation. In regard to the modeling of the structural behavior, a simplified approach was used by considering the dependence of the thrust coefficient only on the wind speed as follows

$$C_{\mathrm{T}} = \begin{bmatrix} C_{\mathrm{T0}} & if\ v_{\mathrm{rel}} \leq v_{\mathrm{rated}} \\ C_{\mathrm{T0}}\ e^{\ (\text{-a}\ (\mathrm{v_{rel}}\ \text{-}\ \mathrm{v_{rated}})^{\ \mathrm{b}})} & if\ v_{\mathrm{rel}} > v_{\mathrm{rated}} \end{bmatrix} \tag{3.34}$$

where C_{T0}, a and b are constants with the values 0.75, 0.25 and 0.86, respectively [100]. This approach allows to maximize the thrust force up to rated wind speed v_{rated} by keeping C_T constant. After rated wind speed, the thrust coefficient is exponentially reduced. In addition, a control system is modeled, which limits the C_T variation rate. This simple control provides the system with enough time to include the tower oscillation motion and avoid negative damping, which has occurred in studies performed by Nielsen et al. [101] for the Hywind Spar-buoy concept.

The motions of a floating wind turbine have additional effects on the aerodynamics compared to BOWTs. In this study, two effects have been included. The first is that the motions of the floating wind turbine provoke an additional mean platform tilt angle as outlined in Section 3.2.3 and the second is the relative wind velocity as described above.

Further effects such as the potential occurrence of vortex ring states, time-varying rotor induction, skewed inflow or blade-vortex interactions [93] are not considered and beyond the scope of this thesis. In particular, the interaction between the wind turbine rotor and its wake is a complex phenomenon that requires the application of advanced modeling tools such as free wake vortex methods or computational fluid dynamic simulations [102]. A comprehensive aerodynamic simulation of the floating wind turbine, however, has not been the objective of this study.

3.3.2 Hydrostatics

The hydrostatic loads on the platform refer to the effect of having a submerged body in water and its motions. It can be divided into an undisturbed buoyancy force and a restoring term due to the platform movements. The restoring term is the hydrostatic stiffness C of Equation 3.20 and its computation is defined in Section 3.2.2.

The buoyancy force is a vertical force directed upwards and according to Archimedes' principle possesses a value equal to the volume of fluid displaced by the body and can be obtained by

$$F_{\mathrm{buoy}} = \rho_{\mathrm{w}}\ g\ V \tag{3.35}$$

where ρ_w is the water density, g the gravitational acceleration and V the submerged volume of the Spar [103]. The force that balances the buoyancy is the weight and is obtained by considering the total mass $\mathrm{m_t}$ of the FOWT as follows [96].

$$F_{\mathrm{G}} = -\ m_{\mathrm{t}}\ g \tag{3.36}$$

3.3.3 Hydrodynamics

Morison equation has been applied to calculate the hydrodynamic loads acting on the FOWT. It is one of the widely used methods for slender structures like the Spar and aims to address viscous effects as well as inertial loads by an empirically derived formula [89]. Equation 3.37 presents the Morison equation in conjunction with strip theory by dividing the structure in discrete elements of dz. The total force is obtained by integrating dF over the length of the Spar [103].

$$\begin{aligned} dF_{\mathrm{h}} &= \frac{1}{2}\rho_{\mathrm{w}} C_{\mathrm{d}} D dz |v_{\mathrm{r}}| v_{\mathrm{r}} + C_{\mathrm{a}} \rho_{\mathrm{w}} A(z) dz a_{\mathrm{r}} + A(z) dz \rho_{\mathrm{w}} a_{\mathrm{W}} \\ v_{\mathrm{r}} &= v_{\mathrm{W}} \ - \ v_{\mathrm{B}} \end{aligned} \tag{3.37}$$

C_a and C_d are the hydrodynamic added mass and viscous-drag coefficients and their values for the OC3-Hywind concept are 0.969954 and 0.6, respectively [96]. The model assumes a constant added mass and drag coefficient since the considered Spar concept has demonstrated a low variation across oscillation frequencies and high Reynolds numbers in most environmental conditions [96]. The term Ddz is the frontal area of the strip and Adz is the displaced volume of fluid for the corresponding strip. v_r is the relative velocity between the water particle velocity v_W and the velocity of the body v_B.

The corresponding accelerations are a_r and a_W [103]. The equation does not account for the hydrodynamic heave force experienced by the FOWT. The heave force can be approximated by the change of the hydrostatic pressure caused by the variation of wave elevation η at the water-plane area A_{wp} as follows [96].

$$F_{\mathrm{p}} = \rho_{\mathrm{w}} \ g \ \eta \ A_{\mathrm{wp}} \tag{3.38}$$

3.3.4 Mooring system

There exist several methods to model the mooring loads depending on the level of accuracy and the information required as well as the computational complexity needed as outlined by Chakrabarti [90]. The applied method follows the quasi-static analysis approach, which considers the offset of the floating structure caused by wave-induced motions in time domain and the computation of the non-linear catenary stiffness at each offset within the equation of motions [90].

The mooring line is taken as a continuous cable with homogeneous properties and elasticity is considered to provide the line profile. Forces arising from inertia, viscous drag, internal damping, bending and torsion are neglected [104]. The quasi-static model is applied, because it provides a reasonable approximation of the mooring load and a simple calculation methodology compared with a fully dynamic model. The catenary mooring is modeled as a single line. The mooring line is fixed by the anchor at the bottom at one end. The other end of the line is attached to the structure by the fairlead.

As the structure is being displaced, the fairlead position moves at a height h and length l and provokes a resulting horizontal and vertical force at the fairlead from the mooring load. Equation 3.39 and 3.40 are used to obtain the fairlead forces for a fully suspended mooring line [105].

$$l = \frac{X}{w}\left(ln\left(\frac{Z}{X} + \sqrt{1+\left(\frac{Z}{X}\right)^2}\right) - ln\left(\frac{Z-wL}{X} + \sqrt{1+\left(\frac{Z-wL}{X}\right)^2}\right)\right) + \frac{XL}{EA} \tag{3.39}$$

$$h = \frac{X}{w}\left(\sqrt{1+\left(\frac{Z}{X}\right)^2} - \sqrt{1+\left(\frac{Z-wL}{X}\right)^2}\right) + \frac{1}{EA}\left(ZL - \frac{wL^2}{2}\right) \tag{3.40}$$

X is the horizontal and Z the vertical component of the fairlead force. The unstretched line length is given as L and w represents the weight per unit length of the mooring line in the water. EA is the cross-section axial stiffness. The system of nonlinear equations is solved for a range of possible displacements of the fairlead and by using the solver fsolve from MATLAB [97]. When the vertical force Z is less than the total weight of the cable *(i.e.,* $Z \leq wL$*)*, then a portion of the mooring line will rest on the seabed and Equations 3.41 and 3.42 have to be used [105].

$$l = \frac{X}{w}\left(ln\left(\sqrt{1+\left(\frac{Z}{X}\right)^2} + \frac{Z}{X}\right)\right) + \frac{X}{EA}\ L + L - \frac{Z}{w} \tag{3.41}$$

$$h = \frac{X}{w}\left(\sqrt{1+\left(\frac{Z}{X}\right)^2} - 1\right) + \frac{Z^2}{2\ w\ EA} \tag{3.42}$$

The total mooring load on the structure is obtained by considering the fairlead displacement of all three mooring lines and computing the sum of all fairlead forces.

4 Dynamic response analysis and performance assessment

4.1 Introduction

The transition of floating offshore wind from small demonstration projects towards commercial application increases the need for comprehensive tools that allow to model the complete system and to predict its behavior as well as to assess the performance for different locations. The main objective of this chapter is to study the influence of met-ocean conditions of different sites on the energy yield and downtime of a FOWT. A simplified numerical model with reduced degrees of freedom has been developed based on the methodology presented in Chapter 3. It allows to capture the main motions of the FOWT and to predict the energy generation considering the dynamic behavior of the system and the environment of the site. The model is developed as part of the tool FOWAT (Floating Offshore Wind Assessment Tool), which has been created originally in the H2020 LIFES50+ project to assess both economically and technically floating offshore wind farms [106]. The purpose of the developed model is to contribute with a more realistic annual energy production profile, which can be used for the calculation of the levelized cost of energy. The model considers in the calculation of the energy yield the characteristic motions of the FOWT as well as the downtime due to exceeding operating limits.

To the author's knowledge, not many research papers can be found that investigate the influence of the dynamic response of a FOWT on the long-term energy yield for different offshore sites. The reason might be that many of the FOWT concepts are still in the early development phase and, therefore, the main research effort is given on the correct modeling and experimental testing with different load cases. For instance, a comprehensive comparison of different aero-hydro-servo-elastic modeling codes has been performed in the OC3 (Offshore Code Comparison Collaboration) research project [107] and several studies have been performed on the modeling of the hydrodynamic and aerodynamic response of a FOWT [108–111]. Besides that, the influence of individual degrees of freedom on the power characteristics has been investigated for example in surge [112], pitch [113] and yaw [114]. In 2015, Martini et al. [21] have studied by statistical means the performance of a semi-submersible FOWT considering 20 years of met-ocean data. Hub acceleration and platform pitch motions have been defined as the most relevant operating parameters, which are also applied in this work as selected threshold limits. The model developed applied in this chapter is intended to assess the performance of a Spar-buoy concept at different offshore sites. In addition, a sensitivity analysis of certain threshold limits is carried out to study the impact on the capacity factor and downtime of the FOWT. The model can be useful for early feasibility studies or at the design state and can be of great interest for different stakeholders such as project developers, substructure designers, wind farm operators or investors.

4.2 Floating wind turbine concept

The FOWT concept presented in Chapter 3 is considered for the model validation and dynamic analysis. It consists of the OC3-Hywind concept, which is based on the Spar-buoy developed by Equinor and slightly adapted by the National Renewable Energy Laboratory (NREL) for modeling purposes in the OC3 project [96]. It supports the NREL 5MW wind turbine [115]. The FOWT is illustrated in Figure 3.10. The concept was chosen for the availability of data, the simplicity of the geometry and the relevance of the technology on the market since it is one of the most promising concepts for floating offshore wind [11]. The wind turbine is a three-bladed horizontal-axis wind turbine as defined in [115] and is used in this study considering the modifications introduced for the floating platform by Jonkman in [96]. The mooring system of Equinor's Hywind concept consists of three catenary mooring lines attached to the substructure via a delta connection.

A simplification has been made for the OC3-Hywind concept by removing the delta connection and adding a yaw spring to achieve proper overall stiffness. Furthermore, the multisegment lines are replaced by an equivalent homogenous line with weighted-average properties and damping is neglected [96]. The most relevant properties of the Spar-buoy FOWT are presented in Table 4.1.

Table 4.1: Floating wind turbine main properties [96, 115].

Turbine and tower properties		Spar-buoy substructure properties	
Rated power	5 MW	Total draft below SWL	120 m
Gearbox	multiple-stage	Height to substructure top	10 m
Cut-in, rated, cut-out	3, 11.4, 25 m/s	Depth to top of taper	4 m
Rotor diameter	126 m	Depth to bottom of taper	12 m
Hub height	90 m	Substructure diameter above	6.5 m
RNA mass	350.0 t	Substructure diameter below	9.4 m
Tower mass	249.7 t	Substructure mass	7466.3 t

Mooring system properties	
Number of mooring lines	3
Angle between lines	120 °
Depth to fairleads	70 m
Depth to anchors	320 m
Radius to fairleads	5.2 m
Radius to anchors	853.7 m
Wet mooring line weight	698 N/m
Unstreched line length	902.2 m

4.3 Model validation

The developed model described previously is validated in this section by performing a dynamic analysis on the OC3-Hywind Spar-buoy concept and comparing the results to the ones obtained in the OC3 project by using the FAST software. FAST was developed by NREL and is one of the most widely used tools to perform coupled aero-hydro-servo-elastic simulations of wind turbines. It has been extensively compared and validated against other software solutions in the international research project OC3 and the subsequent continuation in OC4 and OC5 [116, 117]. Furthermore, by Driscoll et al. [118] the accuracy of the FAST simulations has been validated against field measurements of the Hywind-Demo 2.3MW floating offshore wind turbine.

4.3.1 Static sizing

In this section, the obtained static properties of the developed model FOWAT are presented and compared with the ones computed by FAST in the OC3 project. The mass matrices are shown first.

$$\begin{bmatrix} 8.07e^6 kg & 0 & -6.29e^8 \text{kg m} \\ 0 & 8.07e^6 kg & 1.12e^5 \text{kg m} \\ -6.29e^8 \text{kg m} & 1.12e^5 \text{kg m} & 6.80e^{10} \text{kg m}^2 \end{bmatrix} \qquad \begin{bmatrix} 8.07e^6 kg & 0 & -6.29e^8 \text{kg m} \\ 0 & 8.07e^6 kg & 1.12e^5 \text{kg m} \\ -6.29e^8 \text{kg m} & 1.12e^5 \text{kg m} & 6.80e^{10} \text{kg m}^2 \end{bmatrix}$$

Mass computed by FOWAT — Mass computed by FAST

The mass matrix calculated by the developed model agrees well with the one obtained by FAST [96,98]. The obtained added mass matrix is presented next and compared to the results from FAST for zero frequency [96].

$$\begin{bmatrix} 7.98e^6 kg & 0 & -4.94e^8 \text{kg m} \\ 0 & 2.23e^4 kg & 0 \\ -4.94e^8 \text{kg m} & 0 & 3.97e^{10} \text{kg m}^2 \end{bmatrix} \qquad \begin{bmatrix} 8.00e^6 kg & 0 & -4.90e^8 \text{kg m} \\ 0 & 2.00e^4 kg & 0 \\ -4.90e^8 \text{kg m} & 0 & 3.90e^{10} \text{kg m}^2 \end{bmatrix}$$

Added mass computed by FOWAT — Added mass by FAST approximated

The mooring stiffness matrix obtained by FOWAT is shown next. The accuracy of the developed model is quite high for the mooring stiffness calculation in comparison to FAST.

$$\begin{bmatrix} 4.12e^4 \text{N/m} & 0 & -2.82e^6 \text{N/rad} \\ 0 & 1.19e^4 \text{N/m} & 0 \\ -2.82e^6 \text{N/m} & 0 & 3.11e^8 \text{N m/rad} \end{bmatrix} \qquad \begin{bmatrix} 4.12e^4 \text{N/m} & 0 & -2.82e^6 \text{N/rad} \\ 0 & 1.19e^4 \text{N/m} & 0 \\ -2.82e^6 \text{N/m} & 0 & 3.11e^8 \text{N m/rad} \end{bmatrix}$$

Mooring stiffness computed by FOWAT — Mooring stiffness computed FAST

The hydrostatic matrix that has been obtained is shown next.

$$\begin{bmatrix} 0 & 0 & 0 \\ 0 & 3.34e^5 \text{N/m} & 0 \\ 0 & 0 & -5.01e^9 \text{N m/rad} \end{bmatrix} \qquad \begin{bmatrix} 0 & 0 & 0 \\ 0 & 3.33e^5 \text{N/m} & 0 \\ 0 & 0 & -4.99e^9 \text{N m/rad} \end{bmatrix}$$

Hydrostatic stiffness by FOWAT — Hydrostatic stiffness by FAST

The hydrostatic stiffness in pitch considers only the effect of the hydrostatic pressure as defined in the OC3 report [96]. Is it can be noted, the results of both models are in good agreement. Based on the previously presented static matrices, the natural frequencies of the FOWT are computed and presented in Table 4.2.

Table 4.2: Natural frequencies.

	Surge (Hz)	Heave (Hz)	Pitch (Hz)
FAST	0.008	0.032	0.034
FOWAT	0.008	0.033	0.033
Difference	0.000	0.001	0.001

According to the results shown in Table 4.2, the surge frequency obtained from the FOWAT model matches the value calculated in the OC3 report by Jonkman et al. [117]. The frequency in heave is slightly higher than the reference one and the pitch is slightly lower. However, the differences are smaller than 3% and the accuracy of the developed model is seen to be sufficient for the purpose of this study.

4.3.2 Dynamic response to load cases

In this section, the dynamic response of the FOWT to three load cases is computed. The load cases are based on the OC3 Phase IV study [107] where different modeling codes have been compared.

The first load case (LC1) applied on the FOWT is used to obtain the static equilibrium conditions when the system has no initial displacement and is not excited by any load. Figure 4.1 shows the time response of the FOWT to the load case for the 3 degrees of freedom considered in this study. The final stability position of the FOWT achieved by using both the model FOWAT and the software FAST is displayed in Table 4.3.

Table 4.3: Final stability position.

	Surge (m)	Heave (m)	Pitch (°)
FAST	-0.079	-0.000	-0.066
FOWAT	-0.068	-0.000	-0.049
Difference	0.011	0.000	0.017

It can be observed that in both models the stability position of the FOWT is different to zero, which is based on a small initial displacement of the center of mass of the substructure. However, both models respond correctly to the load case by converging to an equilibrium point.

The second load case (LC2) is used to analyze the behavior of the FOWT based on the excitation by a steady wind force of 8m/s and regular airy waves of 6m height and 10s period. The time response for the non-transient part is shown in Figure 4.2.

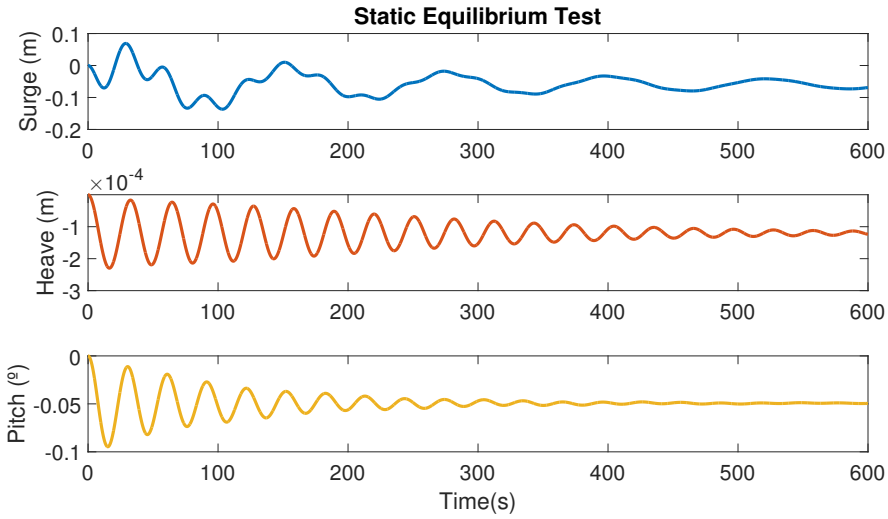

Figure 4.1: Stability test from LC1.

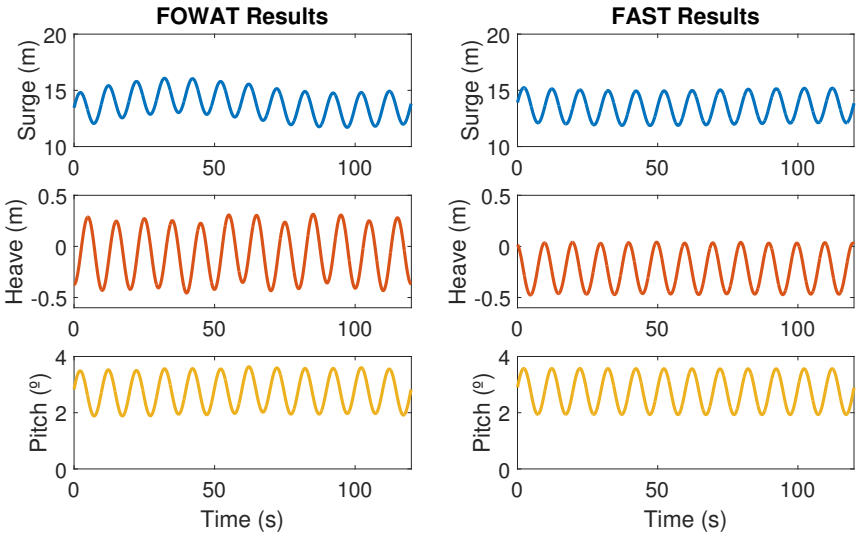

Figure 4.2: Non-transient response.

It can be observed that the system oscillates around the equilibrium position and with the wave frequency in all degrees of freedom. The oscillation with the natural frequencies is also visible.

It can also be seen from the figure that the wind force generates an offset in both the surge and pitch, which causes the equilibrium point to be different than zero for these two DOFs. The average values for the non-transient part obtained with the developed model and FAST are presented in Table 4.4. As it can be seen, the calculated values are close to the ones obtained with FAST, which allows to conclude that the aerodynamic effect is correctly captured by the model.

Table 4.4: Mean displacements.

	Surge (m)	Heave (m)	Pitch (°)
FAST	13.54	-0.22	2.75
FOWAT	13.68	-0.07	2.74
Difference	0.14	0.15	0.01

The third load case LC3 is used to study the effect of irregular waves and turbulent wind. JONSWAP spectrum is considered to create the irregular wave profile with a significant wave height of 6m and a peak-spectral wave period of 10s. The turbulent wind, based on the Kaimal spectrum, has a mean wind speed equal to the rated speed of 11.4m/s and a turbulence intensity of 0.14. Since the irregular wave profile is a superposition of waves with different frequencies, the response of the FOWT is shown as statistical parameters in Table 4.5.

Table 4.5: Response comparison between FOWAT and FAST for LC3.

		Wind (m/s)	Wave (m)	Surge (m)	Heave (m)	Pitch (°)
Minimum	FOWAT	6.28	-4.54	14.67	-0.83	0.18
	FAST	6.60	-5.84	11.38	-1.07	1.33
Mean	FOWAT	11.11	0.01	23.79	-0.21	4.74
	FAST	11.43	0.01	21.19	-0.47	4.25
Maximum	FOWAT	16.16	4.73	31.78	0.23	7.12
	FAST	17.37	4.73	31.13	0.11	6.26
Standard	FOWAT	1.46	1.36	3.84	0.17	1.16
Deviation	FAST	1.96	1.49	4.09	0.22	0.84

For this load case the range of motions shows a good agreement with the mean values calculated by FAST. A slight over- or underestimation is observable for some of the minimum and maximum values, which could be due to the statistical estimation of the loads. The studied load cases have confirmed that the simplified model accounts for the main effects of the FOWT for the motions and accelerations.

4.3.3 Computation time

The computation times by FAST (v8.16.00a-bjj) and FOWAT are measured and compared for the three load cases discussed previously. The comparison is carried out using a computer with an Intel Core i5-6500 processor with 3.2GHz, 8GB memory and Windows 10 operating system. The results are presented in Table 4.6.

Table 4.6: Comparison of computation times between FAST and FOWAT.

Load case	Conditions	Computation time		Difference	
		FAST (s)	FOWAT (s)	(s)	(%)
LC1	Static equilibrium	105.6	7.4	98.2	93.0
LC2	Regular wave and steady wind	157.2	64.6	92.6	58.9
LC3	Irregular wave and turbulent wind	236.4	121.9	114.5	48.4

The results show that the simplified model FOWAT with reduced degrees of freedom provides a significant reduction in computation time for the three load cases in comparison to the more complex simulation code FAST. The simplified model, in its actual implementation in MATLAB, allows reducing about half the computation time of LC2 and LC3 and a reduction of 93% for LC1 with an acceptable accuracy for the purpose of this study.

4.3.4 Power generation results

The power generated by the FOWT has been calculated for a range of wind velocities and wave heights to simulate its specific power curve. The environmental conditions considered are regular waves and a steady wind velocity. A power curve has been computed for each of the wave heights as illustrated in Figure 4.3. The power curves include the specific consideration for a FOWT as explained in Section 3.2.3 and the cut-in and cut-out wind speed limits of the wind turbine.

It is observable that the power production behaves similarly regardless the different wave heights. This behavior is very characteristic for a Spar-type floating substructure, because the deep draft and large inertia result in low heave and pitch motions in operating conditions [119]. Figure 4.4 shows the comparison between the original power curve of the NREL BOWT and the ones obtained by the FOWT.

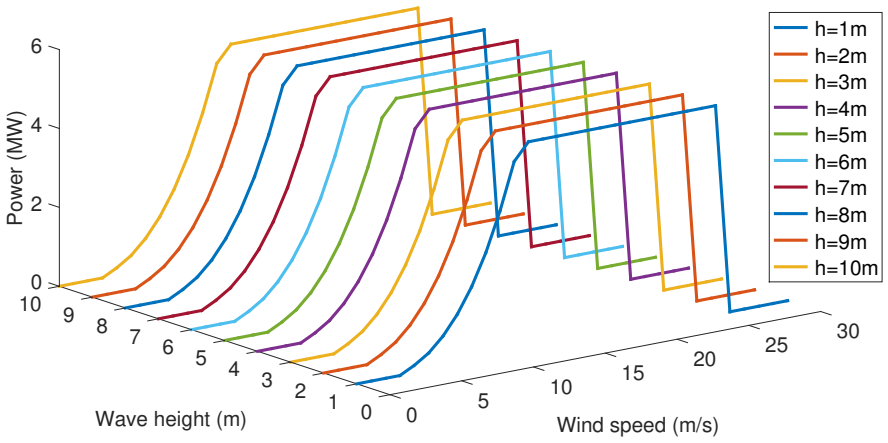

Figure 4.3: Power curve of FOWT for regular waves with different wave heights (h).

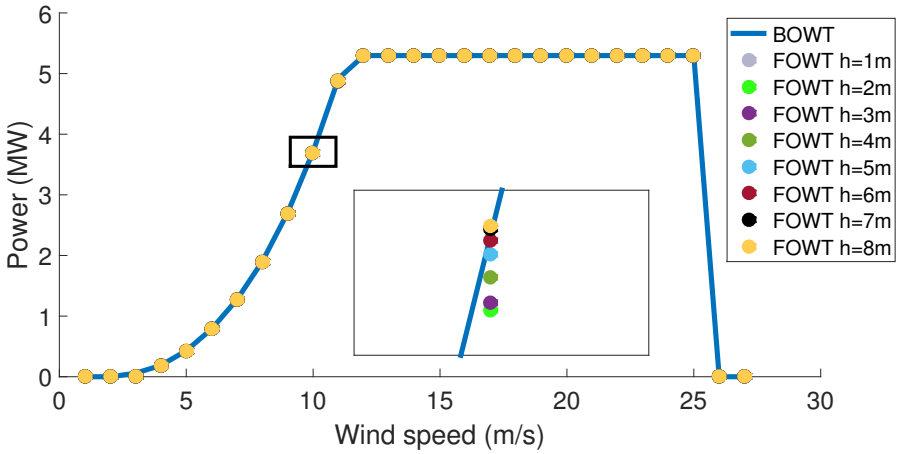

Figure 4.4: Power curve comparison between BOWT (blue line) and FOWT (colored dots for regular waves with wave height (h)).

The blue line represents the power curve of the BOWT. The dots mark the power curves of the FOWT for the different wave heights. The zoom indicates the difference according to the wave heights. As it is shown, the power curve of the FOWT is nearly identical to one obtained by the BOWT.

Even the largest difference between the power curve of the BOWT and the most extreme wave is only smaller than 1%. The power curve is now computed considering an environment with irregular waves and a turbulent wind velocity (Figure 4.5), which represents a more realistic offshore scenario.

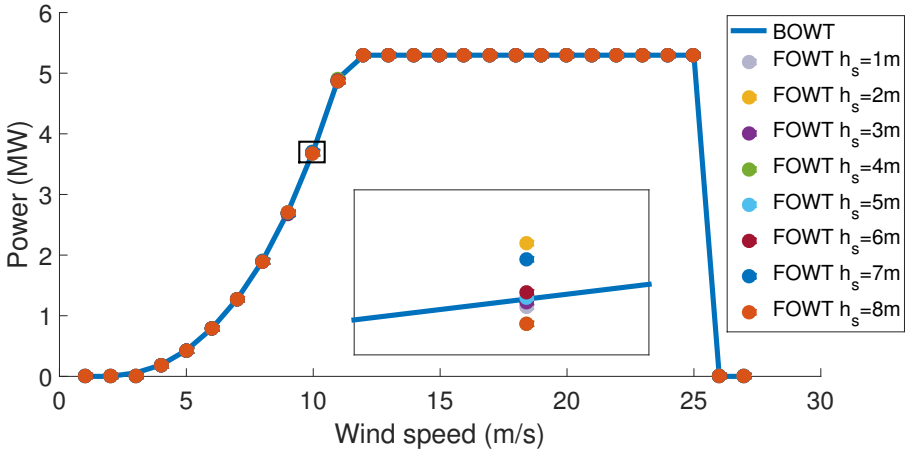

Figure 4.5: Power curve comparison between BOWT (blue line) and FOWT (colored dots for irregular waves with significant wave height (h_s)).

The irregular wave and turbulent wind profiles have been generated by using JONSWAP and Kaimal spectrum, respectively. It is observable that the power curves for the FOWT follow the power curve obtained by the BOWT. The largest difference between the power curve of the BOWT and the most extreme wave is about 1.1% and is, therefore, only slightly higher than compared to the regular wave and steady wind load case. Finally, Figure 4.6 shows the power coefficient obtained for the FOWT and confirms that there is a non-significant difference between the load case and the waves.

It can be concluded that the wind and wave loads have a non-significant effect on the power production performance of the OC3 Spar-buoy FOWT and that the power generation is comparable with a BOWT. This conclusion has also been demonstrated in experimental tests of the Hywind prototype in real offshore conditions [118, 120]. However, the conclusion is only valid for the specific FOWT studied in this paper. For different type of concepts further studies are required.

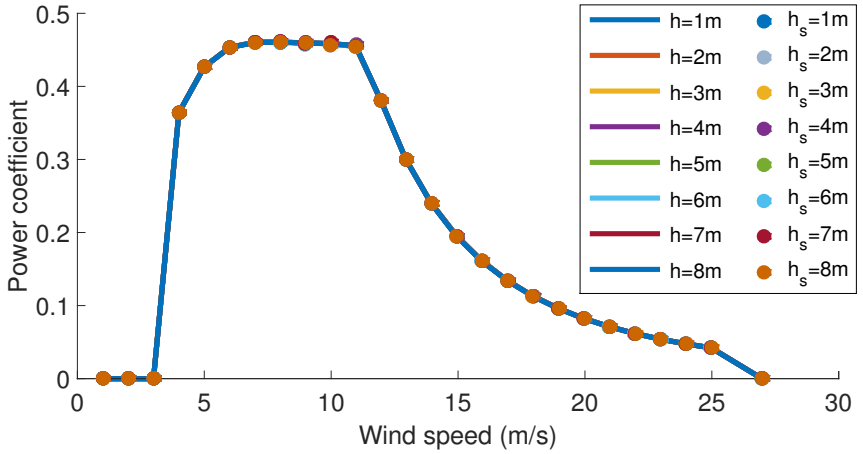

Figure 4.6: Power coefficient comparison of FOWT for regular waves with wave height (h) and irregular waves with significant wave height (h_s).

4.4 Floating offshore wind turbine performance

4.4.1 Definition of offshore sites

Three offshore locations are considered to represent different met-ocean conditions namely Costa Brava in Spain, Gulf of Maine in the USA and West of Barra in Scotland. Costa Brava is located at 42.00°N 3.50°E, 25 km off the city of l'Estartit in the Mediterranean Sea and has a water depth of 200m. The met-ocean conditions are moderate and the corresponding wind and wave profile is taken from the SIMAR 2126144 model point of the Spanish Port System [121].

The Gulf of Maine site is situated 65km east of Portland in the Atlantic Ocean with coordinates 43.33°N 69.27°W and represents medium met-ocean conditions with a water depth of 130m. West of Barra has the harshest conditions together with the highest wind speeds and is located 19km West of Barra Island in the Atlantic Ocean. The coordinates are 56.89°N 7.95°W and the water depth is 150m. The met-ocean data for both sites was prepared within the LIFES50+ project [122]. Figure 4.7 shows the combined wind-wave occurrences at each of the three sites.

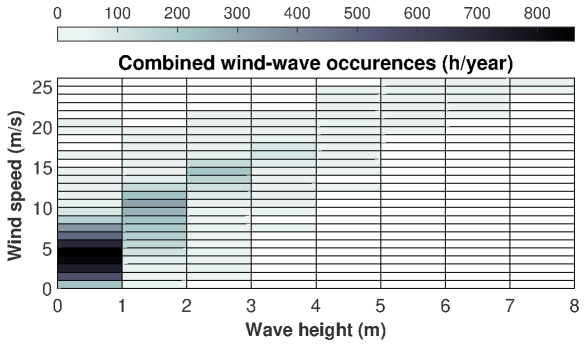

(a) Costa Brava

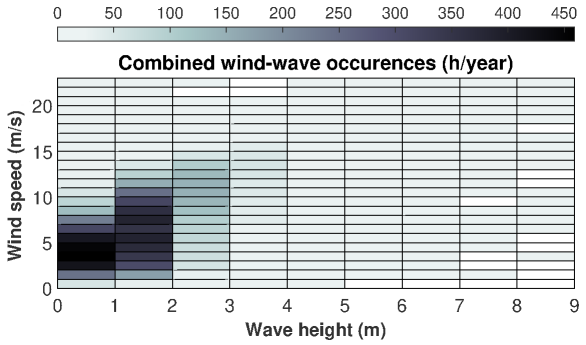

(b) Gulf of Maine

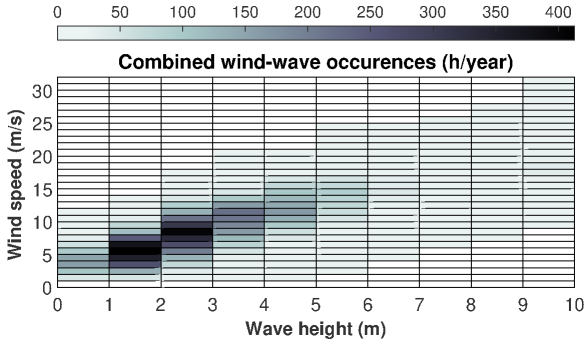

(c) West of Barra

Figure 4.7: Distribution of combined wind-wave occurrences at sites (a) Costa Brava, (b) Gulf of Maine and (c) West of Barra. Wind speed measured at 10m height.

The wind-wave profile of Costa Brava shows that small waves with lower wind speeds are more frequent at this site corresponding to the moderate met-ocean conditions. Larger waves in the range of 5m to 8m only occur with higher wind speeds in the range of 19m/s to 26m/s, but the occurrence of those is rather rarely. The white cells represent non-occurring wind-wave combinations. At Gulf of Maine, a larger distribution of the wind-wave profile is present. However, the most frequent environmental conditions are between wind speeds of 1m/s to 11m/s with up to 2m wave heights. At West of Barra the most frequent environmental conditions are in the range of 3m/s to 13m/s of wind speeds with wave heights of 1m to 6m. In addition, wind speeds larger than 28m/s and waves higher than 9m can occur, which confirm the harsh conditions at this site.

4.4.2 Motion response

The response of the FOWT is computed considering the met-ocean conditions of the three sites. The mean motions of the FOWT in surge, pitch and heave as well as the hub acceleration are presented in Figure 4.8 and Figure 4.9 with respect to the offshore location. The highest response for all degrees of freedom is reached at rated wind speed (11.4m/s). Afterwards, the applied controller acts to reduce the thrust coefficient exponentially and hence the response declines as well. The surge motion is mostly influenced by the wind. However, a slight increase of the peak surge value is also observable for increasing wave heights.

At Costa Brava offshore location, the highest surge experienced is about 26m for wind speeds between 13m/s and 14m/s and wave heights of 3m to 4m. At Gulf of Maine the highest surge motion of 27.4m is reached with the most extreme waves in the range of 8m to 9m and wind speeds between 14m/s and 15m/s. The harsh environmental conditions in West of Barra result in the largest surge motion experienced by the FOWT among the three sites with 29.5m for wind speeds between 18m/s and 21m/s and waves larger than 9m. The surge motions obtained by the model are in good agreement with the mean values of the DeepSpar presented by Karimirad et al. [123].

The pitch response of the FOWT is similar affected by the wind and wave loads as the surge. The highest value at Costa Brava site is 5.2° for waves of 3m to 4m and wind speeds of 12m/s to 14m/s. The magnitude of the pitch response at Gulf of Maine is similar to Costa Brava. However, since larger waves are available at this site the maximum value increases to 5.5° for wind speeds of 14m/s to 15m/s and wave heights of 8m to 9m.

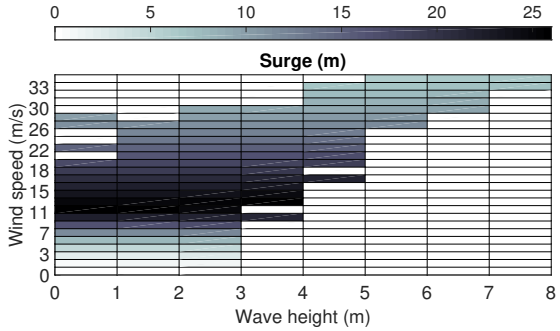

(a) Surge motion at Costa Brava

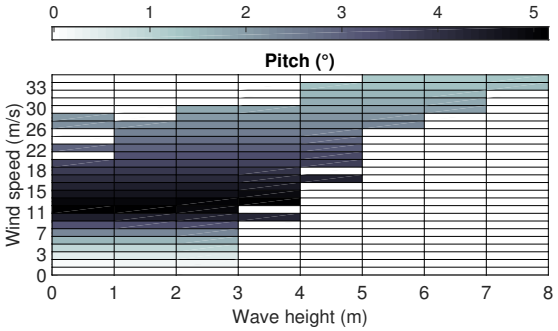

(b) Pitch motion at Costa Brava

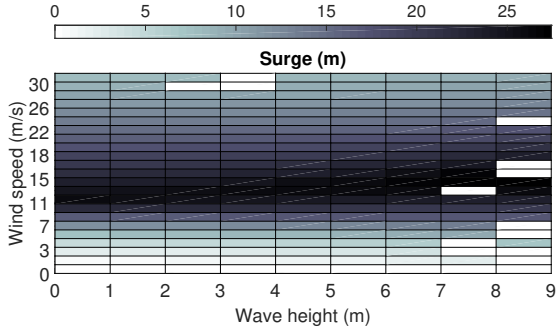

(c) Surge motion at Gulf of Maine

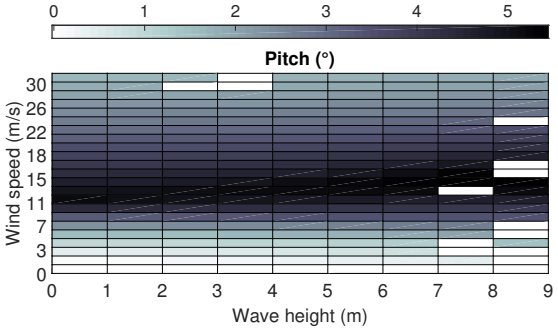

(d) Pitch motion at Gulf of Maine

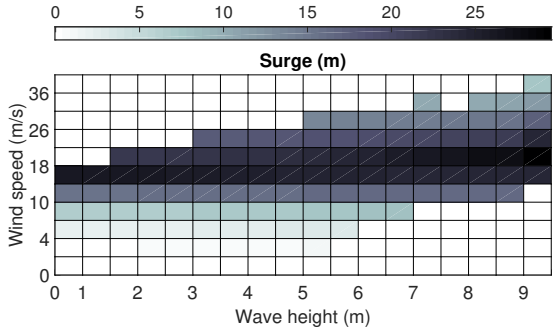

(e) Surge motion at West of Barra

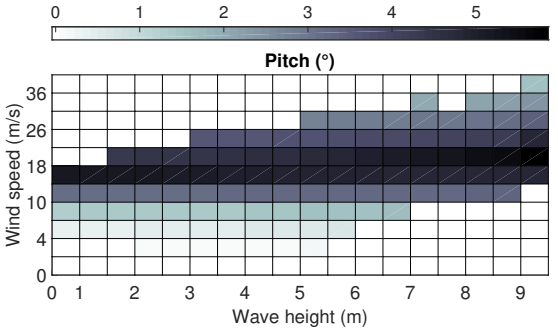

(f) Pitch motion at West of Barra

Figure 4.8: Surge and pitch motions as function of wind speed (at hub) and wave height for the three offshore sites.

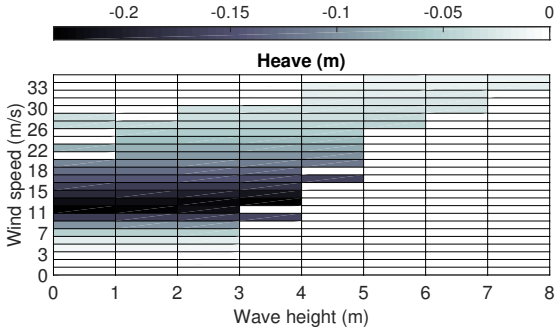

(a) Heave motion at Costa Brava

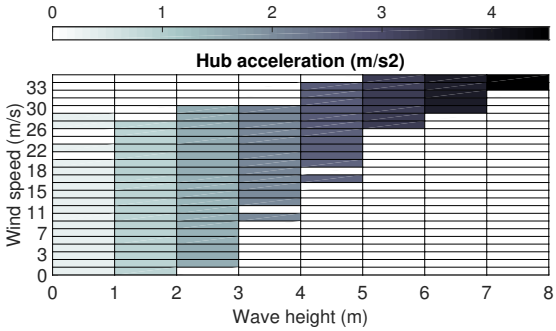

(b) Hub acceleration at Costa Brava

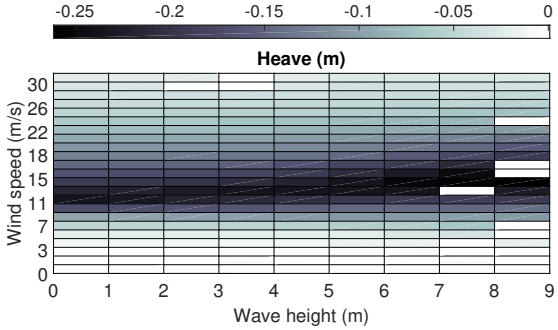

(c) Heave motion at Gulf of Maine

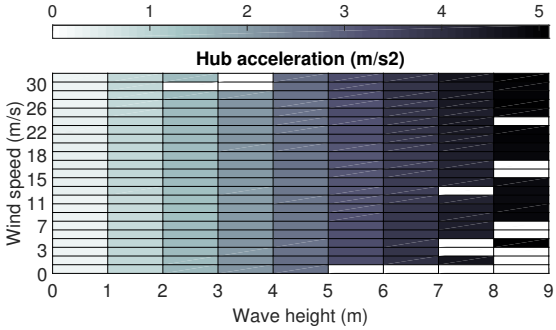

(d) Hub acceleration at Gulf of Maine

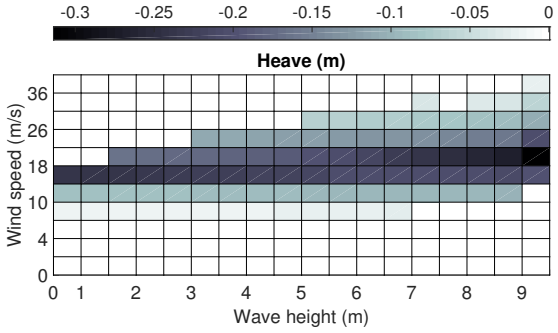

(e) Heave motion at West of Barra

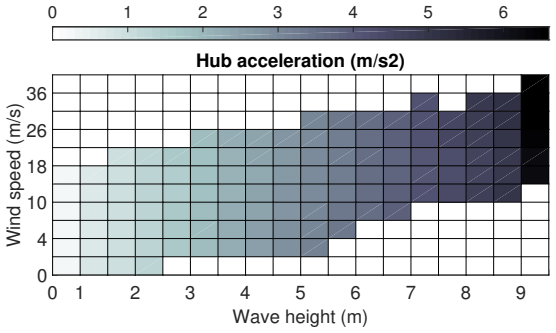

(f) Hub acceleration at West of Barra

Figure 4.9: Heave motions and hub acceleration as function of wind speed (at hub) and wave height for the three offshore sites.

The largest pitch motion is observed again at West of Barra with 5.9° for the largest waves measured at this location of 9m to 10m and wind speeds of 18m/s to 21m/s. The heave motions of the Spar are typically small since the vertical wave exciting forces are low due to the deep draft [124]. As illustrated in Figure 4.9, the heave mean response of the FOWT is lower than -0.3m for all three locations. The hub acceleration is mainly governed by the wave heights. In addition, the largest accelerations are experienced with a combination of highest waves and wind speeds. The maximum hub acceleration values for Costa Brava, Gulf of Maine and West of Barra are 4.5m/s^2, 5.1m/s^2 and 6.6m/s^2, respectively. Besides the before mentioned, the figure shows the distribution of possible motions at the different sites according to the existing met-ocean conditions. For instance, at Gulf of Maine a larger range of combined wind and wave heights is present, which results in a more distributed response of the FOWT from low to very high wind speeds and wave heights in contrast to the other sites.

4.4.3 Energy generation

The annual energy generated by the FOWT is plotted for each of the three sites as function of wind speed (at hub) and wave height in Figure 4.10. The figure shows the characteristic energy generation profile according to the met-ocean conditions of each site. West of Barra demonstrates a larger distribution of energy generation among the available wave heights. Whereas at Costa Brava and Gulf of Maine a larger range of wind speeds is available with lower wave heights, which causes the energy generation profile to be located in the lower wave height section of the figure. Furthermore, it is observable that at West of Barra higher peak generation values are achieved based on more frequent occurrences of high wind speeds. The total annual energy generation is presented in Table 4.7 for the three offshore locations and compared to a BOWT with the same capacity.

Table 4.7: Annual energy production performance comparison.

Location	Energy Generation (GWh) Bottom-fixed	Floating	Difference (%)	Capacity factor (%) Floating
Costa Brava	21.91	21.73	0.82	49.62
Gulf of Maine	24.12	23.98	0.58	54.75
West of Barra	33.32	33.09	0.69	75.54

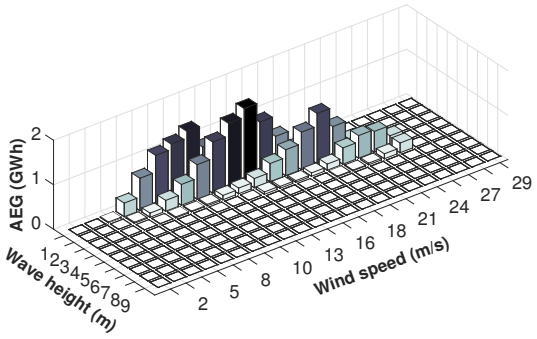

(a) Costa Brava

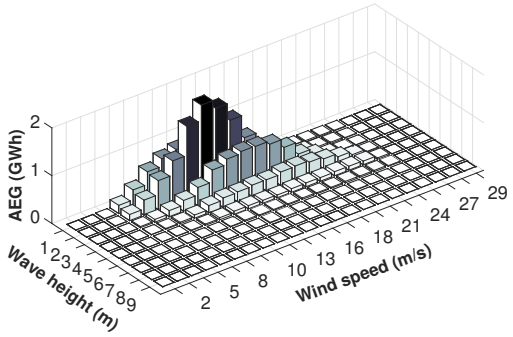

(b) Gulf of Maine

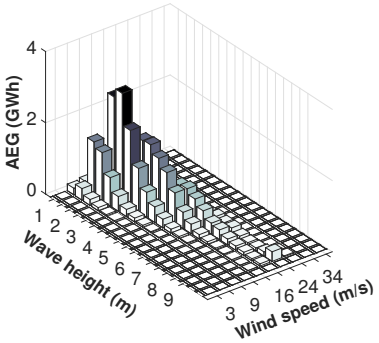

(c) West of Barra

Figure 4.10: Annual energy generation profile considering the wind speed at hub and wave heights of the three offshore sites.

As it is shown in Table 4.7, the difference in the annual energy generation between a fixed and floating wind turbine is below 1% and thus is not very significant. In addition, a BOWT would not be feasible at the three considered sites due to the large water depths. The capacity factor calculated for the FOWT at each site is also shown. It is defined in this paper as the ratio of actual energy generation to the maximum possible per year. The values demonstrate the vast potential of FOWT to be placed in locations where higher wind speeds are available and greater capacity factors can be yielded. For comparison, current BOWFs reach capacity factors of about 30% to 50% and the first floating wind farm installed in Scottish waters has achieved a capacity factor of 56% during the first two years of operation [125, 126]. The high capacity factors demonstrate also the competitiveness of floating offshore wind in terms of power performance in comparison to conventional power plants that typically possess capacity factors of 50% to 60% or more for coal and gas and about 90% for nuclear power plants [127].

4.4.4 Sensitivity analysis

In this section, a sensitivity analysis is carried out to study the effect of applying different threshold limits for the operation of the FOWT. The two parameters that are considered are the hub acceleration and the platform pitch motion, which have been defined by Martini et al. [21] as two of the most relevant operating parameters. In case the defined threshold limit is exceeded by one of the two parameters, the wind turbine is forced to shutdown and stop power generation. The performance of the FOWT under different threshold limits is evaluated in function of capacity factor and downtime as shown in Tables 4.8 to 4.10 for each of the offshore sites. The downtime is defined as the ratio of hours not producing due to exceeding operating limits to total hours per year.

Table 4.8: Capacity factor and downtime in function of hub acceleration and platform pitch limits for Costa Brava.

		Capacity factor (%) Platform pitch (°)								Downtime (%) Platform pitch (°)							
		0.5	1.0	2.0	3.0	4.0	5.0	6.0	7.0	0.5	1.0	2.0	3.0	4.0	5.0	6.0	7.0
Hub acceleration (m/s^2)	0.5	0.0	0.7	2.4	4.9	7.8	13.1	15.2	15.2	82.7	73.3	63.4	55.4	49.9	43.8	41.8	41.8
	1.0	0.0	0.8	2.7	5.8	10.8	29.3	33.9	33.9	81.9	71.7	60.6	50.7	42.2	23.1	18.5	18.5
	1.5	0.0	0.8	2.7	6.8	15.3	36.8	41.7	41.7	81.9	71.6	60.4	49.5	37.6	15.6	10.8	10.8
	2.0	0.0	0.8	2.7	6.8	17.8	39.4	44.3	44.3	81.9	71.6	60.4	49.4	35.1	13.1	8.3	8.3
	3.0	0.0	0.8	2.7	9.1	22.8	44.7	49.6	49.6	81.9	71.6	60.1	45.5	28.6	6.3	1.5	1.5
	4.0	0.0	0.8	2.7	9.1	22.8	44.7	49.6	49.6	81.9	71.6	59.2	44.2	27.3	5.0	0.2	0.2
	5.0	0.0	0.8	2.7	9.1	22.8	44.7	49.6	49.6	81.9	71.6	59.0	44.0	27.1	4.8	0.0	0.0
	6.0	0.0	0.8	2.7	9.1	22.8	44.7	49.6	49.6	81.9	71.6	59.0	44.0	27.1	4.8	0.0	0.0
	7.0	0.0	0.8	2.7	9.1	22.8	44.7	49.6	49.6	81.9	71.6	59.0	44.0	27.1	4.8	0.0	0.0

Table 4.9: Capacity factor and downtime in function of hub acceleration and platform pitch limits for Gulf of Maine.

Hub acceleration (m/s^2)	Capacity factor (%) Platform pitch (°) 0.5	1.0	2.0	3.0	4.0	5.0	6.0	7.0	Downtime (%) Platform pitch (°) 0.5	1.0	2.0	3.0	4.0	5.0	6.0	7.0
0.5	0.0	0.4	1.3	2.9	5.1	9.5	11.0	11.0	91.9	86.6	81.5	76.7	72.8	68.0	66.5	66.5
1.0	0.0	0.7	2.3	5.5	10.8	28.2	34.0	34.0	86.1	76.9	67.6	58.2	49.3	31.0	25.4	25.4
1.5	0.0	0.8	2.5	6.1	14.1	39.0	46.4	46.5	85.7	75.2	65.1	54.6	42.7	16.9	9.8	9.8
2.0	0.0	0.8	2.5	6.1	14.1	40.9	48.8	48.8	85.7	75.2	65.0	54.5	42.6	15.0	7.4	7.4
3.0	0.0	0.8	2.6	6.7	17.6	45.6	53.8	53.8	85.6	74.8	64.2	52.8	37.9	9.2	1.3	1.3
4.0	0.0	0.8	2.6	6.9	18.1	46.4	54.7	54.7	85.6	74.8	64.0	52.4	37.2	8.2	0.1	0.1
5.0	0.0	0.8	2.6	6.9	18.1	46.4	54.8	54.8	85.6	74.8	64.0	52.4	37.1	8.1	0.0	0.0
6.0	0.0	0.8	2.6	6.9	18.1	46.4	54.8	54.8	85.6	74.8	64.0	52.4	37.1	8.1	0.0	0.0
7.0	0.0	0.8	2.6	6.9	18.1	46.4	54.8	54.8	85.6	74.8	64.0	52.4	37.1	8.1	0.0	0.0

Table 4.10: Capacity factor and downtime in function of hub acceleration and platform pitch limits for West of Barra.

Hub acceleration (m/s^2)	Capacity factor (%) Platform pitch (°) 0.5	1.0	2.0	3.0	4.0	5.0	6.0	7.0	Downtime (%) Platform pitch (°) 0.5	1.0	2.0	3.0	4.0	5.0	6.0	7.0
0.5	0.4	0.4	1.0	1.0	1.0	1.0	1.0	1.0	95.7	95.7	94.6	94.6	94.6	94.6	94.6	94.6
1.0	1.2	1.2	5.2	5.2	13.5	13.5	13.9	13.9	89.2	89.2	80.8	80.8	73.0	73.0	72.6	72.6
1.5	1.8	1.8	10.6	10.6	25.9	25.9	28.8	28.8	84.1	84.1	65.3	65.3	50.9	50.9	48.2	48.2
2.0	1.9	1.9	12.2	12.2	35.1	36.1	46.9	46.9	83.0	83.0	61.3	61.3	39.6	38.7	28.4	28.4
3.0	1.9	1.9	12.6	12.6	39.7	53.1	67.5	67.5	82.7	82.7	60.2	60.2	34.6	21.8	8.3	8.3
4.0	1.9	1.9	12.6	12.7	41.3	57.7	72.6	72.6	82.7	82.7	60.1	60.0	32.9	17.4	3.3	3.3
5.0	1.9	1.9	12.6	12.7	41.6	58.8	74.7	74.7	82.7	82.7	60.1	59.9	32.5	16.2	1.2	1.2
6.0	1.9	1.9	12.6	12.7	41.6	58.8	74.7	74.5	82.7	82.7	60.1	59.9	32.4	16.2	1.2	1.2
7.0	1.9	1.9	12.6	12.7	41.7	59.5	75.5	75.5	82.7	82.7	60.1	59.8	32.0	15.2	0.0	0.0

The findings demonstrate that the capacity factor increases non-linearly with higher threshold limits. The maximum capacity factor of 49.6% is reached at Costa Brava with a hub acceleration of $3m/s^2$ and a platform pitch of 6°, which is the same value as presented in Table 4.7 where no threshold limits have been considered. The downtime, on the other hand, decreases with increasing threshold limits towards zero, as expected. According to the findings, Gulf of Maine and West of Barra sites present higher capacity factors, but require at the same time higher hub acceleration limits. It is common practice in the wind industry to set an operational limit for the hub acceleration, which is related to the safety of the turbine components and is about 0.3g ($\approx 3m/s^2$) [128]. Likewise, there is a maximum angle of inclination, which corresponds to the pitch motion and depends largely on the type of FOWT. For instance, Xue [129] has proposed a limit for the inclination angle under the maximum mean wind turbine thrust force of up to 7° for a Spar concept. Considering these parameters, one can find the technical limits for the performance of the FOWT.

For instance, at Gulf of Maine a capacity factor of 53.8% and a downtime of 1.3% would be achievable. The parameters have not only importance for the control strategy but also are essential for the platform design [128]. For example, the maximum angle of inclination $\theta_{\max}$ is related to the minimum rotational stiffness $C_{55,min}$ of the structure by the inclining moment M_I as [130]:

$$C_{55,\min} = \frac{M_{\mathrm{I}}}{\theta_{\max}}. \tag{4.1}$$

In general, the higher the rotational stiffness required, the more expensive the floating substructure will be. Hence, the aim would be to reduce it as much as possible [30]. However, a more rigid structure could be beneficial in harsh conditions such as at West of Barra, because it would reduce the angle of inclination and thus enable to extract energy from more extreme environmental conditions and increase the capacity factor. To resume, the optimal threshold limits should be a trade-off between the maximal energy yield as well minimal downtime and technical feasible limits for a safe operation of the FOWT. This analysis may help to identify suitable threshold limits at design stage and for feasibility studies of different offshore locations.

4.5 Conclusion of the chapter

In this chapter, a methodology has been presented to obtain the dynamic response of a FOWT to different load cases and to assess its performance considering different wind and wave conditions. A simplified model has been built using MATLAB and the system response has been evaluated for the surge, heave and pitch motions. The results have been compared with FAST, which is a well-known complex tool to model and simulate wind turbines. An overall good agreement has been found in the comparison of the structural properties computed by both models. Furthermore, the main motions and system's dynamics could be captured by the simpler model with an acceptable accuracy. The power generated by the FOWT has been computed for an environment with regular waves and steady wind as well as a load case consisting of turbulent wind and irregular waves. It has been found that even for the most extreme wind and wave combination the power loss experienced by the FOWT is less than 1% or 1.1%, respectively the load case studied. Furthermore, the performance of the FOWT has been evaluated for three offshore locations with their specific environmental conditions. Surge and pitch motions are governed by the mean wind speed, whereas the hub acceleration is influenced strongly by the wave height.

The response in heave is only of small magnitude for all three locations, which is typical for a Spar-type FOWT. The peak response has been obtained for all three degrees of freedom at rated wind speed, when the controller starts to reduce the thrust coefficient. Among the offshore locations, the largest motions appear at West of Barra, where the harshest environmental conditions exist, with 29.5m for surge and 5.9°for pitch motion. The highest value for the hub acceleration has also been obtained at West of Barra with 6.6m/s^2. Despite the large motions, no significant loss in energy generation for the FOWT has been found. The difference is smaller than 1% for all three sites.

The highest capacity factor has been reached at West of Barra with up to 75%, which exceeds current BOWFs. This large capacity factors demonstrate the high power performance of the OC3-Hywind Spar FOWT and also coincides with the values achieved by the Hywind floating wind farm. Besides that, it shows that floating offshore wind could be a suitable complement to base load power generation. Finally, a sensitivity analysis has been used to evaluate the effect of different threshold limits, such as hub acceleration and platform pitch, on the performance of the FOWT. Lowering the threshold limits in order to increase the safe operation of the FOWT results in a nonlinear decrease of the capacity factor and nonlinear increase of downtime. The optimal selection of threshold limits should be a trade-off between system reliability and energy generation.

5 Technical-economic assessment of floating offshore wind farms

5.1 Introduction

Floating offshore wind turbines represent a competitive new energy solution by having the ability to harness the best possible wind resources without depth constraints and applying larger wind turbines to increase power generation [12]. Furthermore, the ability to mount the turbine on the floating substructure dockside and to tow the fully assembled structure by tug boats to the offshore site provides a significant potential for cost reduction along the life cycle, because expensive heavy lift jack-up vessels are avoided [10]. However, since only a few prototypes have been constructed so far, there is a lack of information on the cost structure and potential LCOE values of large scale FOWFs. Myhr et al. [131] have estimated in 2013 the LCOE for a number of different FOWT concepts made of steel and supporting a 5MW wind turbine. The findings have shown LCOE values ranging between 106.3€/MWh and 287.8€/MWh, which appear unfavorable in comparison to the cost of current BOWFs [132]. Further research has been proposed to investigate possible cost reductions and to study the impact of different site conditions. Castro et al. [133] have developed in 2013 a methodology for the economic evaluation of FOWFs. The emphasis has been more on the modeling of the life cycle cost and less on the computation of the power generation.

For instance, the power losses due to the wake effect in the wind farm have not been considered. Ebenhoch et al. [134] have calculated in 2015 the LCOE of a FOWF based on a monolithic Spar buoy concept. The LCOE obtained at 175.5€/MWh has been significantly higher than estimated benchmark values for bottom-fixed structures in shallow waters [134]. The high LCOE value may has been due to the lack of information on the cost structure of FOWFs and several assumptions that have been made in the LCOE estimation. For instance, the operation and maintenance costs have been based on estimations for BOWF and the decommissioning cost has been considered as a percentage of the capital expenses. Hence, the advantages that FOWTs provide to reduce costs in these life cycle phases have not been taken into account [28]. Besides that, the energy generation and losses in the system have been based on gross load factors and efficiency rates from literature and have not been optimized for the specific location [135].

Following the work done and the proposal for further investigation, the aim of this chapter is to provide a comprehensive LCOE calculation for commercial scale FOWFs based on cost data provided by industrial and academic FOWT concept developers. The LCOE computation involves both a detailed life cycle cost and energy loss calculation of the system. Furthermore, three different FOWT concepts are analyzed, namely Semi-submersible, TLP and Spar, representing the most promising designs in the sector. Besides that, concrete as well as steel structures are included to represent both manufacturing materials. The calculation is performed for three different offshore locations to study the effect of metocean conditions on the LCOE. Moreover, FOWTs with a rated capacity of 10MW are considered to represent the trend towards larger offshore wind turbines. A sensitivity analysis of 325 input parameters is performed to identify the ones that most influence the LCOE, which provides an useful insight for developers and researchers for further cost reductions.

The analysis is performed by using the tool FOWAT. A description of the tool is given in the Appendix B.1 and the LCOE methodology is presented next.

5.2 Levelized cost of energy

The LCOE calculation is a method used to obtain the cost of one unit energy produced and is typically applied to compare the cost competitiveness of power generation technologies. The LCOE model sets in relation the life cycle costs (LCCs) to the electrical energy provided (E_{el}) as follows [136].

$$LCOE = \frac{LCC}{E_{\mathrm{el}}} = \frac{\sum_{t=1}^{n} \frac{CAPEX_0 + OPEX_{\mathrm{t}} + DECEX_{\mathrm{n+1}}}{(1+i_{\mathrm{rate}})^{\mathrm{t}}}}{\sum_{t=1}^{n} \frac{E_{\mathrm{t}} + L_{\mathrm{t}}}{(1+i_{\mathrm{rate}})^{\mathrm{t}}}} \tag{5.1}$$

The LCCs include all costs occurring in the lifetime of the FOWF such as the capital expense (CAPEX), the cost during the operation and the maintenance phase (OPEX) as well as the decommissioning expense (DECEX) at the end of the lifetime of n years [135]. Since the LCCs occur in different years (t), they have to be discounted to their present value by applying a discount rate i_{rate}. The discount rate has a large influence on the LCOE and should be chosen properly. However, the determination is not always straightforward. An approach is to use the weighted average cost of capital (WACC) as an approximation [136]. The WACC represents the market value of equity and debt and considers project risk and return yield. It can be calculated by

$$WACC = \frac{E}{E+D} * k_{\mathrm{E}} + \frac{D}{E+D} * k_{\mathrm{D}} \tag{5.2}$$

where E is the equity of the company, D is the debt, k_E represents the cost of equity and k_D the cost of debt [137]. A typically value of the discount rate for offshore wind farm investments is between 8% and 12% [131]. In this thesis, the LCOE model is used as a method for the economic evaluation of FOWFs, because it is a common measure to compare the cost of energy across technologies. It represents the minimum price of energy required for a project to become profitable since the LCOE represents the total cost of the power plant per energy generation [52]. There exist other methods to evaluate projects and businesses that consider a slightly different approach. For example, the internal rate of return (IRR) considers not only the costs of a power plant but also the revenues that can be earned as well as other incentives [138]. Furthermore, it has been proposed to extend the LCOE model by considering the cost of external impacts such as environmental damage and health issues or to include the cost of carbon taxes and the impact on the local economy [139]. However, these factors have not been taken into account in this study. In the following sections, the methodology considered to calculate LCCs and energy yield is presented.

5.3 Life cycle costs

The LCCs are the expenses related to the activities performed in each life cycle of an offshore wind farm project as presented in Figure 5.1.

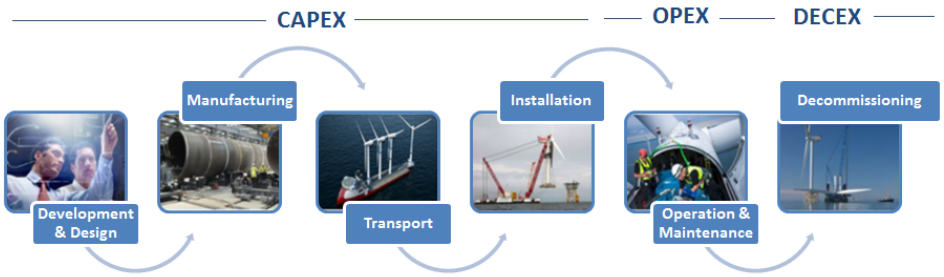

Figure 5.1: Life cycle phases of an offshore wind farm [140].

CAPEX includes the costs related to development, manufacturing, transportation and installation of the wind farm. These costs are also defined as investment costs since they occur at the beginning of the project before the wind farm starts to generate energy. OPEX contains the costs related to operation and maintenance (O&M) activities during the lifetime of the project and DECEX represents the costs occurring at the end of the lifetime for the decommissioning of the wind farm [135]. The total LCCs are obtained as the sum of all phases as follows

$$LCC = TC_{\mathrm{D+D}} + TC_{\mathrm{Manuf}} + TC_{\mathrm{Transp}} + TC_{\mathrm{Instal}} + TC_{\mathrm{O+M}} + TC_{\mathrm{Decom}} \quad (5.3)$$

where TC_{D+D} represents the cost associated to the development and design of the wind farm and TC_{Manuf} includes the cost of manufacturing of each of the wind farm components. The transportation and installation costs are defined by TC_{Transp} and TC_{Instal}, respectively. The cost of operation and maintenance of the wind farm is defined by TC_{O+M}. The final decommissioning and respective costs are included in TC_{Decom}. The calculation of each of the life cycle costs are described further in the following sections.

5.3.1 Development

The development and design phase (C_{D+D}) includes all activities related to the initial development and design of the FOWF up to the point at which the official orders for production and purchasing are made [44].

This first phase is highly important for the projects outcomes since a well-planned design and schedule will enable a construction on time and with low added costs [140]. Typical studies and activities that are performed during the first life cycle stage are presented in Figure 5.2. The list is not exhaustive since the scope of studies is very much project dependent.

Development	Environmental impact study	Assesses any environmental impacts of the wind farm on animals and environment in the sea and air
	Coastal process study	Evaluates the impact of the wind farm on sedimentation and erosion of the coastline
	Met station surveys	Monitor and analyse met ocean conditions
	Sea bed surveys	Analyse sea bed conditions at site
	Human impact study	Impact on community leaving near the site including visual, noise and socio-economic assessment
	Project development and management	Feasibility study, market study, quality control, quality assurance, risk assessment, licensing, management, legal issues
Design	Front end engineering design	Concept development in advance and evaluation of technical uncertainties
	Detailed engineering	Full definition of the design
	Certification cost	Cost of certifying the concept

Figure 5.2: Development life cycle cost components [44].

The total cost of the development phase is affected by the amount of turbines included in the FOWF. Generally, the more turbines are considered the higher is the total cost. Since no large FOWFs have been constructed so far, no information is available regarding the development and design costs. It is expected that the cost for engineering and met-ocean studies will be higher for FOWFs due to the immaturity of the technology and the application in deep waters. However, the cost for environmental and seabed studies will likely be lower due to lower impact by the floaters [140]. The development costs are considered in the LCC calculation as a percentage of the CAPEX. As an approximation, the development costs of a BOWF with the same rated capacity can be assumed. Table 5.1 shows reference development costs in percentage of the CAPEX for a 500MW BOWF that were found in literature. The mean value of the considered reference cost percentages is about 5.7%.

Table 5.1: Reference development costs in percentage of total capital costs for a 500MW bottom-fixed offshore wind farm.

Reference	Crown Estate [44]	Scottish Enterprise [141]	Howard [142]	NREL [143]	Wind Europe [3]	Garrad Hassan [18]	Mean value
Development cost (%)	4%	6.5%	5.8%	4.6%	9.5%	4%	5.7%

5.3.2 Manufacturing

The total manufacturing cost includes the expenses for the acquisition of each of the components of the FOWF such as the wind turbines TC_{WT}, floating substructures TC_{FS}, anchor TC_A and mooring lines TC_{ML} as well as substations TC_{Sub} and power cables TC_{PC} [133]. It can be computed as follows.

$$TC_{\text{Manuf}} = TC_{\text{WT}} + TC_{\text{FS}} + TC_{\text{ML}} + TC_{\text{A}} + TC_{\text{Sub}} + TC_{\text{PC}} \tag{5.4}$$

A brief description of each of the cost components is provided next.

Wind turbine

In contrast to onshore wind farms where wind turbines generally represent the major cost component with up to 70% of the CAPEX, in offshore wind farms the cost composition is more evenly distributed between wind turbines, balance of plant and transportation and installation [144]. The reason for this is that the construction of an offshore wind farm is more complex and requires cost-intensive vessels for the transportation and installation. Furthermore, the balance of plant is significantly higher offshore, since different technologies are used such as offshore substations, submarine cables and offshore foundations. However, a more equally distributed CAPEX does not mean a lower price for the turbines, quite the contrary is the case. Offshore wind turbines possess higher investment cost due to additional corrosion protection, higher robustness against offshore conditions and larger rotors for harnessing the higher wind speeds offshore [136]. Table 5.2 shows reference estimations of the investment cost for a 5MW offshore wind turbine.

Table 5.2: Reference costs for a 5MW offshore wind turbine.

Reference	Crown Estate [44]	RCN [145]	Scottish Enterpise [141]	NVE [146]	Howard [142]	Mean Value
Wind turbine price (K€)	7580	8060	7531	6956	7249	7475
Unit price (M€/MW)	1.516	1.612	1.506	1.391	1.449	1.495

The total manufacturing cost of the wind turbines can be calculated by

$$TC_{\mathrm{WT}} = N_{\mathrm{WT}} * P_{\mathrm{rated}} * C_{\mathrm{WT}} \tag{5.5}$$

where N_{WT} represents the number of wind turbines installed in the FOWF, P_{WT} is the rated power of the turbine and C_{WT} defines the unit price of a single wind turbine.

Floating substructure

The total manufacturing cost of the floating substructures is obtained by

$$TC_{\mathrm{FS}} = N_{\mathrm{WT}} * (C_{\mathrm{FS}} + C_{\mathrm{LO}}) + C_{\mathrm{Area}} \tag{5.6}$$

where C_{FS} represents the manufacturing cost of a single floating substructure, $\mathrm{C_{LO}}$ is the cost associated to the the load-out of the structure and $\mathrm{C_{Area}}$ defines the lease of the required port area. The manufacturing cost accounts for the floating substructures used to carry the offshore wind turbines but does not include the substructure required for the offshore substation, which is taken into account separately. A single substructure consists of several components that have to be manufactured such as columns, pontoons and transition pieces. The composition and amount of components depend on the individual floating substructure concept. Thus, the manufacturing cost of a substructure unit is obtained by the sum of all components cost as follows.

$$C_{\mathrm{FS}} = \sum_{c=1}^{N_{\mathrm{c}}} N_{\mathrm{FS\text{-}c}} * C_{\mathrm{FS\text{-}c}} \tag{5.7}$$

$N_{FS\text{-}c}$ is the quantity of the specific floating substructure component c, $C_{FS\text{-}c}$ is the cost of this component and N_c represents the total number of different

components in a floating substructure. The load-out of the floating substructure on the sea bed by the quay or in a dry dock can be performed with lifting means such as port cranes or crane barges. The associated cost C_{LO} can be calculated as

$$C_{\mathrm{LO}} = N_{\mathrm{means}} * C_{\mathrm{means}} * t_{\mathrm{means}} \tag{5.8}$$

where N_{means} defines the the amount of machines required for the load-out, C_{means} represents the day rate of the crane, barge or vessel and t_{means} accounts for the time period the machine is being used. The lease for the manufacturing area can be computed as shown next.

$$C_{\mathrm{Area}} = A_{\mathrm{lease}} * C_{\mathrm{lease}} * t_{\mathrm{lease}} \tag{5.9}$$

A_{lease} represents the area required for the manufacturing and load-out of the floating substructures, C_{lease} is the lease rate of the area (€/d/m^2) and t_{lease} defines the leasing time in days.

Mooring line

The cost of the mooring lines depends on the type and material as well as the number of mooring lines used. The total mooring line cost is defined by

$$TC_{\mathrm{ML}} = N_{\mathrm{WT}} * N_{\mathrm{ML}} * C_{\mathrm{ML}} \tag{5.10}$$

where N_{ML} is the number of mooring lines per floating substructure and C_{ML} includes the cost of a single mooring line, which depends on the type, weight and length of the mooring [147]. Commonly used are steel chains, steel fiber wires or synthetic fiber rope. The last named is the most cost-intensive type of mooring line, but possesses the lowest weight [148].

Anchor

It is assumed that each mooring line is fixed with an individual anchor in the sea bed. Thus, the total manufacturing cost of the anchors is obtained by considering the cost of a single anchor, the number of mooring lines per floating substructure and the number of turbines to be installed. Consequently, the total manufacturing cost of the anchors is obtained by

$$TC_{\mathrm{A}} = N_{\mathrm{WT}} * N_{\mathrm{ML}} * C_{\mathrm{A}} \tag{5.11}$$

where the anchor unit cost is defined by C_A and depends of the type of anchor used.

Substation

The total substation cost accounts for both the offshore and onshore substation. Consequently, it is calculated by

$$TC_{\mathrm{Sub}} = C_{\mathrm{TS}} * N_{\mathrm{TS}} + C_{\mathrm{CS}} * N_{\mathrm{CS}} + C_{\mathrm{OS}} \tag{5.12}$$

where $\mathrm{C_{TS}}$ is the cost of a single transformer substation, $\mathrm{N_{TS}}$ is the number of transformer substations considered, $\mathrm{C_{CS}}$ is the cost of a single converter substation and $\mathrm{N_{CS}}$ represents the number of converter substations in the wind farm. In case HVAC technology is used, the number of the converter substation is set to zero. The cost of the onshore substation is given by $\mathrm{C_{OS}}$. The cost of an offshore substation includes the transformer or in case of HVDC the converter, switchgears as well as other equipment such as protection devices and reactors. Furthermore, the cost of the substructure is included. The components of the onshore substations are similar to the counterpart offshore, but the facility is simplified [44].

Power cable

Different power cables are used in a FOWF such as dynamic and static cables as well as different cable sections according to the power to be transmitted. Therefore, the total cable cost is computed as follows.

$$TC_{\mathrm{PC}} = \sum_{PC=1}^{N_{\mathrm{PC\text{-}typ}}} N_{\mathrm{PC}} * C_{\mathrm{PC}} * l_{\mathrm{PC}} \tag{5.13}$$

N_{PC} is the quantity of a specific cable, C_{PC} is the unit cost of this cable (€/m) and l_{PC} represents the length of the cable [147]. The number of different cables is defined by $N_{PC\text{-}typ}$.

5.3.3 Transportation

In this section, only the transportation concerning to the construction of the FOWF is considered since it belongs to the CAPEX.

The transportation activities involved in the operation and maintenance as well as the decommissioning of the FOWF are included in the respective sections. Transportation is considered between three locations; the shipyard, the assembly port and the FOWF site. The shipyard is the location where the floating substructure is being manufactured, the port is the location where the pre-assembly takes place and the FOWF site is the actual offshore installation site. It is assumed that all components that have been purchased such as turbines and electrical machines are located in the assembly port. No transportation is considered for delivering the components from the supplier to the port since this cost is already included in the purchasing price. The substructure can be transported either from the shipyard to the port, where it will be assembled to the turbine or directly transported to the wind farm site. In case the floating substructure is manufactured in the port, no transportation from the shipyard will be considered. The total transportation cost accounts for the transportation offshore as well as associated activities in the port as defined by

$$TC_{\text{Transp}} = C_{\text{Offshore}} + C_{\text{Port}} \tag{5.14}$$

where the offshore transportation cost $C_{Offshore}$ consists of the cost for the transportation from the shipyard to the assembly port and to the FOWF site as well as the transportation from the assembly port to the offshore site. It can be calculated by

$$C_{\text{Offshore}} = N_{\text{TV}} * C_{\text{TV}} * t_{\text{SY-Port}} + N_{\text{TV}} * C_{\text{TV}} * t_{\text{SY-Site}} + N_{\text{TV}} * C_{\text{TV}} * t_{\text{Port-Site}} \tag{5.15}$$

where C_{TV} is the day rate of a transportation vessel in (€/d) and N_{TV} is the number of vessels used. $t_{SY\text{-}Port}$ represents the time period in days that the vessel is used for the transportation between shipyard and assembly port, $t_{SY\text{-}Site}$ the time period for the transportation between shipyard and offshore site and $t_{Port\text{-}Site}$ represents the time period for the transportation between port and offshore site. The costs related to port activities C_{Port} are based on crane and auxiliary means utilization as well as the rental of storage area that is required during the loading of the vessels. The cost is obtained by

$$C_{\text{Port}} = N_{\text{Crane}} * C_{\text{Crane}} * t_{\text{Crane}} + N_{\text{Aux}} * C_{\text{Aux}} * t_{\text{Aux}} + A_{\text{Storage}} * C_{\text{Storage}} * t_{\text{Storage}} \tag{5.16}$$

where C_{Crane} represents the rental cost of cranes in (€/d), N_{Crane} is the number of cranes required and t_{Crane} accounts for the time period in days that the crane is used. Similarly, the costs regarding auxiliary means are computed. The computation of the storage area cost is based on the storage area $A_{Storage}$, the rent $C_{Storage}$ in (€/m^2/d) as well as the storage time $t_{Storage}$ in days. The cost of the transportation vessels depends on several factors, such as the kind of vessel used, availability and contract length. Vessel day rates are high volatile and can change from day to day, by season and also with the region.

The cost of a vessel includes besides the day rate also mobilization and demobilization as well as fuel consumption. In the transportation phase vessels are used typically for the transportation of cargo and personnel or tugging operations for the floating structure. These vessels are generally smaller and cheaper than installation vessels [140, 149]. Figure 5.3 shows examples of vessels that are used in the transportation phase.

(a) Tugboat [65].

(b) Heavy lift crane vessel [150].

(c) Supply vessel [151].

Figure 5.3: Typical vessels used in the transportation phase.

Figure 5.3 (a) shows a tugboat towing a FOWT to the offshore installation site and Figure 5.3 (b) displays a heavy lift crane vessel operating in the port.

Figure 5.3 (c) shows a supply vessel transferring equipment to the offshore site. The methodology presented in this section for the calculation of the transportation cost is applied for each component of the FOWF such as the floating substructure, anchor and mooring system, power cables and offshore substation.

5.3.4 Installation

The total installation cost TC_{Instal} consists of the individual cost for the installation of the offshore turbine and the floating substructure $TC_{Turb\text{-}FS_{instal}}$, the pre-installation of the anchor and mooring system $TC_{A\text{-}M_{instal}}$ as well as the electrical system $TC_{ES_{instal}}$. Besides that, the cost for commissioning TC_{Com} of the complete wind farm and insurance TC_{Ins} are also considered in the installation phase. The total installation cost can be obtained as presented in the following equation.

$$TC_{\text{Instal}} = TC_{\text{Turb-FS}_{\text{instal}}} + TC_{\text{A-M}_{\text{instal}}} + TC_{\text{ES}_{\text{instal}}} + TC_{\text{Com}} + TC_{\text{Ins}} \quad (5.17)$$

The calculation of the cost components is presented next.

Floating substructure with turbine

The installation process is closely related to the transportation since the activities to be included depend on the strategy pursued. Figure 5.4 displays four different transportation and installation strategies that are applied typically in offshore wind. The first two strategies refer to the installation process of a FOWT. The last two strategies explain the installation process of BOWTs in order to have a comparison.

The first strategy considers that the floating substructure and turbine are completely assembled and joined together onshore in the port or shipyard, where the construction was carried out. The structure is then towed out to sea by a tugboat and taken to the offshore site where the installation takes place. Since the FOWT is already assembled, only an anchor handling tug vessel is required to perform the final installation, which includes mooring lying and anchor setting [135]. This strategy is commonly applied for semi-submersible or barge substructures, which possess a good floating performance without moorings and are capable to be transported afloat. Costs and risk associated to offshore installations are therefore reduced.

Figure 5.4: Transportation and installation strategies based on [147].

The second strategy considers that the turbine and the substructure are transported separately and assembled offshore. This strategy is applied for ballast and mooring line stabilized substructures, which are not inherently stable. The turbine is transported on a jack-up vessel and the floating substructure is towed by a tugboat. If the turbine itself is assembled before transportation onshore or if the complete assembly is realized offshore depends on the availability of vessels with suitable capacity. The pre-assembly of the components is performed in the port as well as the loading of the transportation vessel. The assembly and final installation of the turbine and floating substructure are performed offshore by an installation vessel that is equipped with a crane for lifting heavy weights [147]. Spar-type floating substructures cannot be erected onshore or in shallow waters due to their deep draft. Therefore, the structure is towed by a tugboat to a suitable location with sufficient water depth or the final installation site, where the assembly of the turbine is performed. Figure 5.5 (a) shows exemplary the Hywind Spar transportation. For the case of mooring line stabilized substructures such as the TLP, companies such as Iberdrola and Glosten have developed supporting means to address the transportation instability issue [152, 153]. For instance, Iberdrola has developed a u-shaped semisubmersible barge, which can be used to transport the floating substructure with an assembled wind turbine as shown in Figure 5.5 (b).

a) Hywind Spar [154]

b) TLPWIND [152].

Figure 5.5: FOWT transportation solutions.

The third strategy applies to BOWTs and considered that the substructures are transported on the deck of a jack-up vessel or barge. If the turbine and substructure can be transported on the same vessel depends on the size and availability of the vessels. The assembly and final installation of the turbine and substructure are performed similar to the second strategy offshore by an installation vessel that is equipped with a crane for lifting heavy weights [147]. Strategy four considers that turbine and substructures are transported and installed by the same crane vessel with a large storage capacity. This would decrease the amount of transportation vessels needed. However, crane vessels with large storage capacity are scarce and more expensive [149]. The four strategies do not cover all possible options of transporting and installing offshore wind turbines, but they show clearly the relation between both life cycle phases and that in some cases one vessel can be used to do both the transportation and installation and thus merging both phases. However, the calculations of both phases are kept separated in order to present a clearer distribution of costs in the life cycle of a FOWF. The total installation cost of the floating substructures with assembled turbine can be obtained by

$$TC_{\text{Turb-FS}_{\text{instal}}} = C_{\text{Turb-FS}_{\text{instal}}} * N_{\text{Turb-FS}_{\text{instal}}} * t_{\text{Turb-FS}_{\text{instal}}} \tag{5.18}$$

where $C_{Turb\text{-}FS_{instal}}$ is the day rate of the installation vessel in (€/d), $N_{Tur\text{-}FS_{instal}}$ the number of vessels used and $t_{Turb\text{-}FS_{instal}}$ is the time period in (d) the vessel is in operation. Floating substructures have the potential to reduce significantly the cost of installation, in particular if strategy 1 can be applied, which considers the assembly of turbine and floating substructure in the

port. This reduces the risk associated to offshore operations and the need of using expensive installation vessels [28].

Anchor and mooring system

An anchor handling vessel is usually used to install the anchor and mooring system. It is a powerful vessel that has a large deck area to carry the mooring line and anchors as well as an open stern to launch the anchor to the water [149]. Figure 5.6 (a) displays the vessel. It can additionally be used to tow the floating substructure from the port to the offshore location and thus combining the transportation of the floating substructure with the anchor handling operation, which reduces the cost of additional vessels. However, another method based on the experience from oil and gas business suggests pre-installing the mooring system and highlighting it with buoyancies for the later assembly to the floating substructure. This would reduce the installation time of the floating substructure offshore and avoid possible weather window limitations [33]. The anchor handling vessel carries the anchor already connected to the mooring. At the offshore location the anchor with the connected mooring line are then launched into the water with the help of a powerful winch. The positioning of the anchor by the vessel is realized regarding the requirements of the individual anchor. The anchor positioning procedure is explained exemplary for the drag-embedded and suction anchor. The simplest method for the drag-embedded anchor is to lower the anchor to the seabed by using the mooring line. When the anchor reaches the ground, the vessel should move slowly forward to ensure a correct immersion of the anchor into the seabed. Attention has to be paid that the anchor does not turn around while sinking. Additionally, a chaser can be connected to the anchor for an optimal positioning of the anchor. Figure 5.6 displays the anchor laying procedure [33].

a) Anchor handling vessel [155]

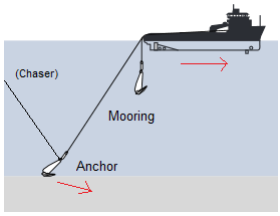

b) Anchor laying [33].

Figure 5.6: Anchor and mooring installation.

The setting of the suction pile anchor is more complex. A pump connected to the top of the pile creates a pressure difference, which forces the suction anchor into the seabed. Afterwards, the pump is removed and the anchor is hold in its final position [156]. Figure 5.7 shows the installation of a suction pile anchor.

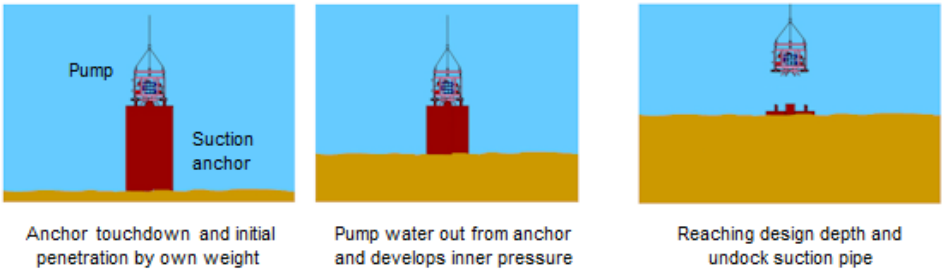

Figure 5.7: Suction pile anchor installation [156].

For this type of installation a remotely operated underwater vehicle (ROV) is often additionally used for monitoring the installation process [140]. In some cases also divers are required and the associated costs have to be considered in the total installation costs. The total anchor and mooring installation costs can be calculated by

$$TC_{\text{A-M}_{\text{instal}}} = C_{\text{A-M}_{\text{instal}}} * N_{\text{A-M}_{\text{instal}}} * t_{\text{A-M}_{\text{instal}}} + C_{\text{ROV}} * t_{\text{ROV}} + C_{\text{Diver}} * t_{\text{Diver}} \tag{5.19}$$

where $C_{A\text{-}M_{instal}}$ is the day rate of the anchor and mooring installation vessel in (€/d), $N_{A\text{-}M_{instal}}$ the number of vessel used and $t_{A\text{-}M_{instal}}$ is the time period in days the vessel is in operation. C_{ROV} represents the day rate of a ROV in (€/d) and t_{ROV} the time of usage. C_{Diver} represents the labor cost of a diver in (€/d) and t_{Diver} is the working time in days.

Electrical system

The electrical system is referred to the inter-array cables installed in the collection grid, the export cables and the substations. The total cost for the installation of the electrical system is calculated as

$$TC_{\text{ES}_{\text{instal}}} = TC_{\text{Cables}_{\text{instal}}} + TC_{\text{OffSub}} + TC_{\text{OnSub}} \tag{5.20}$$

where $TC_{Cables_{instal}}$ is the installation cost of the power cables and TC_{OffSub} is the installation cost of the offshore substation.

TC_{OnSub} represents the respective cost for the onshore substation. In case the construction of the onshore substation is realized by a third party or already exists, then the cost is set to zero. The installation of the power cables is realized by the use of a cable laying vessel. Those vessels contain on-deck carousels for storing the cable, cable guiding sheaves as well as remotely operated vehicles for trenching activities. Modern vessels also possess dynamic positioning devices to keep steady position under harsh weather conditions [80]. The power cable installation cost can be computed by

$$TC_{\text{Cables}_{\text{instal}}} = \frac{C_{\text{Cables}_{\text{instal}}} * l_{\text{Cables}_{\text{instal}}}}{I_{\text{Cables}_{\text{instal}}}} \tag{5.21}$$

where $C_{Cables_{instal}}$ represents the day rate of the installation vessel in (€/d), $I_{Cables_{instal}}$ the installation rate at which the vessels performs the cable laying in (m/d) and $l_{Cables_{instal}}$ the total length of cables in (m). In case of FOWTs, where the inter-array cable consists of a static and dynamic component, a joint unit has to be considered for connecting both cables. The joint can be pre-installed in the factory or can be installed offshore. A procedure to install the submarine joint offshore is presented in Figure 5.8.

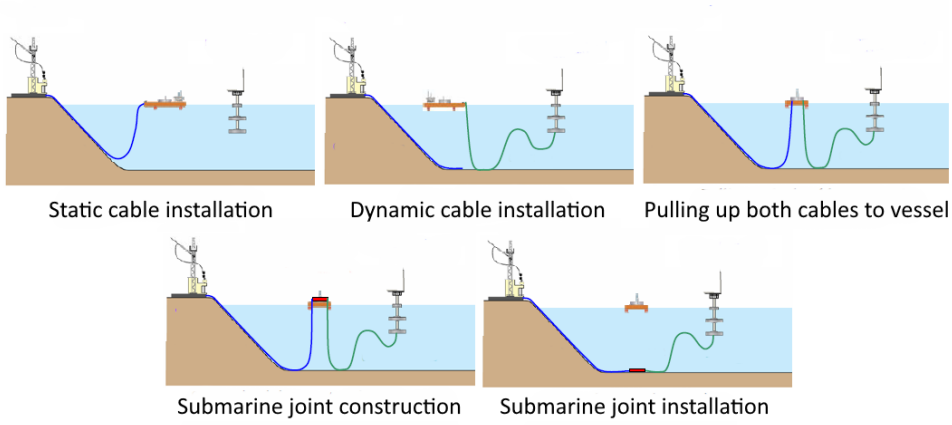

Figure 5.8: Submarine joint installation in Fukushima project [157].

The offshore substation consists typically of the foundation structure and the topside structure. The foundation structure might be a jacket or monopile substructure or a floating substructure depending on the application. The topside includes all electrical equipment and components. It is considered that the topside is fully assembled onshore and transported to the site, where it is mounted on the foundation structure.

The submarine cables are then connected to the substation and the final commissioning is completed. The installation process generally requires large and expensive crane vessels [41]. Figure 5.9 displays the installation of an offshore substation with a heavy crane vessel.

Figure 5.9: Offshore substation installation with crane vessel [158].

The cost of the offshore substation installation is computed by

$$TC_{\text{OffSub}} = C_{\text{OSS}_{\text{instal}}} * N_{\text{OSS}_{\text{instal}}} * t_{\text{OSS}_{\text{instal}}} \tag{5.22}$$

where $C_{OSS_{instal}}$ is the day rate of the vessel that performs the installation of the substation, $t_{OSS_{instal}}$ represents the time in days required for installing one offshore substation and $N_{OSS_{instal}}$ is the number of substations that will be installed. The installation cost of the onshore substation can be calculated by

$$TC_{\text{OnSub}} = C_{\text{OnSub}_{\text{Prep}}} + C_{\text{OnSub}_{\text{Cement}}} + C_{\text{OnSub}_{\text{Instal}}} \tag{5.23}$$

where $C_{OnSub_{Prep}}$ is the preparation cost of the area, $C_{OnSub_{Cement}}$ represents cementation cost for the building and $C_{OnSub_{Instal}}$ includes the total cost for installation with cranes [147].

Commissioning

Commissioning contains the activities performed after all components of the FOWF are installed. This can include electrical tests of the turbine and substation as well as inspections of the civil works. A comprehensive testing is essential in order to deliver a full functioning plant and satisfy the customer. The commissioning may take up to several days. After the commissioning the FOWF is handed over to the operator, who will be responsible for the operation and maintenance of the FOWF [18]. For the installation cost calculation a fixed value TC_{Com} is considered. This includes also the fee for the grid connection, which varies between countries.

Insurance

The construction and operation of an offshore wind farm is a complex and capital-intensive endeavor that involves risks and uncertainties. A careful planning of each life cycle stage is highly important to avoid delays in the construction of the wind farm. However, not everything can be planned and some events are unavoidable. Thus, insurances are important to provide financial protection from cost overruns. They are most commonly applied in the construction and operation phase, where delays or failures can result in high costs. The construction insurance provides financial protection against delays and damage in the assembly, transport and installation phase of the FOWF. Insurances are highly important to potential investors since they take the risk of cost overruns, which would otherwise negatively affect the cash flow. The price of the construction insurance policy is considered per installed capacity (€/MW) [140].

5.3.5 Operation and maintenance

The operation and maintenance begins after the commissioning of the FOWF. The costs associated to this phase include fixed costs that occur annually for operating the FOWF as well as costs related to maintenance activities. The total operation and maintenance cost TC_{O+M} is obtained by

$$TC_{\mathrm{O+M}} = (C_{\mathrm{Operation}} + C_{\mathrm{Prevent}} + C_{\mathrm{Corrective}}) * t_{\mathrm{lifetime}} \tag{5.24}$$

where $C_{Operation}$ represents the annual operation costs and $C_{Prevent}$ and $C_{Corrective}$ the preventive and corrective maintenance costs per year, respectively. The lifetime of the wind farm is defined by $t_{lifetime}$ in years.

In this section, at first the operational costs are outlined and afterwards the maintenance of the FOWF explained.

Operation cost

Typically, it is assumed that an offshore wind farm has an operational lifetime of 20 to 25 years mainly based on the lifetime expectation of the offshore wind turbine. However, many floating substructure designs, both steel and concrete, are expected to last longer and experiences from the oil and gas industry prove the long durability of floating substructures. This enables alternatives to a simple decommissioning of the FOWF such as continuing operation or repowering of turbines. In particular, this is crucial facing the complexity and costs related to the replacement of mooring lines and floating substructure [11]. However, it has to be considered that turbine technology is developing fast and in 20 years the floating substructure might not be suitable anymore to carry the state of the art turbines. Besides that, it might also not economically be feasible to continue operate an aged FOWF and the construction of a new wind farm at the same location might be more favorable. The operation costs refer to expenses occurring by monitoring, sales and administration activities. These costs represent normally a smaller part of the total O&M costs [159]. A list of possible cost components is presented in Table 5.3.

Table 5.3: Operation cost components [143].

Insurance	Transmission charge	Offshore land lease	Onshore land lease	General management	Monitoring
Generation planning	Operating facilities	Sales expenses	Turbine consumption	Marine management	Weather forecasting

The table represents an exemplary list of operation cost components. In practice it depends on the individual project, which services and activities are required to operate the FOWF. The operation phase insurance is an important part since it covers costs occurring from failures of the components that cause a loss of power production such as turbines and substations. It does not cover the actual repair of the components since this belongs to maintenance cost, rather it covers the financial claims due to the contract that arise from a power loss [140]. Further costs that might occur in the operation phase include leases for land and buildings onshore, for instance workshops and storage areas in the port and offshore land lease.

Furthermore, expenses typically occur for sales activities, general management and monitoring of the FOWF. Charges can also occur for power consumption of the turbines and substation during the operation and services for monitoring of met-ocean conditions [143]. For the operation cost a constant annual value $C_{Operation}$ is considered that covers the activities and services required for operating a FOWF.

Maintenance cost

The objective of maintenance is to ensure a high availability of the FOWF and reduce downtimes. It consists of preventive and corrective maintenance. Preventive maintenance considers all planned activities that aim to avoid the failure of a machine or component. This includes minor and major maintenance activities. Minor activities such as inspections and replacements of wear parts or lubricants are routinely performed at the offshore site. Major maintenance, on the other hand, involves the replacement of larger components, which are performed either offshore or in the port. An accurate planning of the maintenance activities is crucial to limit maintenance cost and prevent breakdowns of the machines. Thus, a maintenance plane is prepared that schedules the maintenance activities. Minor maintenance is performed routinely, whereas major activities are scheduled on a yearly, three or five year basis [160]. The maintenance plan has to consider all components of the FOWF including mooring system, substructure, turbine, power cables and substations. However, it is expected that the turbine will require a more frequent maintenance for its mechanical-electrical components compared to the floating substructure, which consists mainly of structural components and a balance system [28].

Corrective maintenance responds to the failure of a component of the FOWF. In contrast to preventive maintenance, corrective maintenance is carried out after a failure has happened and includes the repair or replacement of the components. The corrective maintenance can be scheduled even when the failure was unplanned. For example, in case a single component fails that has only a low impact on the overall performance of the FOWF, its repair can be coordinated with a scheduled maintenance activity or postponed until a larger component fails [159].

The maintenance of an offshore wind farm is much more complex than onshore, because of the harsh offshore conditions. FOWTs add another level of difficulty to it due to the floating motion of the substructure. Thus, the maintenance activity requires a careful planning. Important factors that have to be considered are listed in Table 5.4.

Table 5.4: Considerations for maintenance activities.

Maintenance strategy		Port infrastructure
Vessel availability	Weather windows	Accessibility

The maintenance strategy refers to how major maintenances activities are performed such as the replacement of large components. This might be done offshore with the use of heavy Jack-up vessels or in the port by towing back the whole floating substructure with cheaper tugboats. However, this depends on the capability of the floating substructure to be towed with the turbine mounted on top. Besides that, it depends also on the mooring system and power cables to be designed for a quick disconnection and reinstallation without impacting the performance of nearby floating turbines [11]. The power cable connection technology typically used in bottom-fixed offshore wind consists of pulling the cable into the substructure through a J-tube and a disconnection is generally not foreseen only in the low probability event of a cable failure [160]. Thus, new concepts have to be developed for floating wind application. Since so far only a few prototypes of floating turbines are installed, no answer can be given to which maintenance strategy to choose. The practice will show which strategy will be more applicable and result in the lowest cost.

The availability of ports is also important to consider in a maintenance plan, in particular, the distance from the port to the offshore site since it impacts the transportation time and cost [159]. Suitable ports for offshore wind require generally a water depth of at least 10m, long quayside length and sufficient area for storage and assembly [41]. The consideration of a suitable port is not only important in the operation and maintenance phase but has significance in all life cycle phases of the FOWF. Many ports and coastal cities have benefited from the offshore wind growth due to large investments, creation of jobs and revitalizing of local industry [28].

The vessels that are used for maintenance activities have a large influence on the maintenance costs based on the volatile charter rates, which are related to the market dynamics. A main bottleneck in the offshore wind industry is the availability of vessels. Thus, in high season, typically in the summer when weather conditions are best for constructing offshore, the demand rises and suitable vessels are becoming scarce, which results in high charter rates. Therefore, companies charter vessels often well in advanced and for longer periods [149].

Weather windows are defined as the time frame in which certain weather conditions, such as wind speed and wave height, are below a certain threshold value. Weather windows have a large influence on the maintenance activities since vessels can only go offshore below certain wave heights. Each vessel has a different limitation to the wave height and it depends on the size and type of the vessel. Thus, the maintenance activities have to be scheduled accordingly to the existing weather windows and vessel application. Wind speed has also an impact on the maintenance since too extreme wind speeds might not allow certain repair or maintenance activities at the floating turbine [160].

Accessibility is related to the weather conditions and is especially important to consider for floating turbines. It is defined as the proportion of time a turbine can be accessed and is restricted by threshold values for wind speeds and wave heights [159]. The accessibility depends also on the design of the floating substructure and the easiness to access it by vessel. Helicopters might also be used in the operation and maintenance phase for transporting technicians to the offshore site. Technicians can be transported and winched down directly to the nacelle of the turbine or substation. Helicopters have the advantage of transporting crew rapidly to the site over long distances and being less effected by wave heights. However, helicopters possess a small transport capacity, involve high charter rates and their operation is restricted by visibility due to clouds [159]. Besides that, the application to a floating turbine has not been tested yet. The cost associated to preventive maintenance activities can be calculated as follows

$$C_{\text{Prevent}} = \sum_{PA=1}^{N_{\text{PA-type}}} (C_{\text{Vehicle}_{\text{PA}}} * N_{\text{Vehicle}_{\text{PA}}} * t_{\text{Vehicle}_{\text{PA}}} + C_{\text{Material}_{\text{PA}}} + C_{\text{Diver}_{\text{P}}} * t_{\text{Diver}}) * N_{\text{PA}} \tag{5.25}$$

where $C_{Vessel_{PA}}$ is the day rate for the vehicle used for the maintenance, which can be a vessel or helicopter and includes labor cost. $t_{Vehicle_{PA}}$ represents the time in days required for the activity and depends on the type of maintenance activity PA. $N_{PA\text{-}type}$ is the number of different preventive maintenance activities. $N_{Vehicle_{PA}}$ is the amount of vehicles used. $C_{Material_{PA}}$ is the material cost, which also depends on the type of maintenance. In case of minor maintenance the cost consists of the replacement of tear parts or lubricants. In case of major maintenance activities, where larger components are replaced the cost is associated to the new component.

When divers are required, a cost is added consisting of personnel cost C_{Diver_P} and duration t_{jDiver_P}. The number of activities carried out per year of a specific preventive maintenance activity is defined by N_{PA}.

Corrective maintenance responds to the breakdown of a component. FOWTs posses the ability to be towed back to port for major corrective maintenance [160]. This allows the use of smaller tug boats instead of heavy lift jack-up vessels. The corresponding calculation method of the corrective maintenance costs is similar to the preventive maintenance with the difference that the failure rate is used as an indicator for the maintenance frequency [147]. In addition, costs are considered that occur when maintenance is performed in the port such as the use of cranes. The corrective maintenance costs is obtained by

$$C_{\text{Corrective}} = \sum_{CA=1}^{N_{\text{CA-type}}} (C_{\text{Vessel}_{\text{CA}}} * t_{\text{Vessel}_{\text{CA}}} * N_{\text{Vessel}_{\text{CA}}} + C_{\text{Aux}_{\text{CA}}} * t_{\text{Aux}_{\text{CA}}} * N_{\text{Aux}_{\text{CA}}} + C_{\text{comp}_{\text{CA}}} + C_{\text{Diver}_{\text{CA}}} * t_{\text{Diver}_{\text{CA}}}) * F_{\text{rate}_{\text{CA}}} \tag{5.26}$$

where the day rate, duration and number of vessels used for the corrective maintenance type CA is defined by $C_{Vessel_{CA}}$, $t_{Vessel_{CA}}$ and $N_{Vessel_{CA}}$, respectively. The day rental cost of auxiliary means used in the port as well as the duration and amount are given by $C_{Aux_{CA}}$, $t_{Aux_{CA}}$ and $N_{Aux_{CA}}$, respectively. The replacement cost of the component is defined by $\text{C}_{\text{comp}_{\text{CA}}}$ and the failure by $F_{rate_{CA}}$ in (failures/year). The methodology for the preventive and corrective maintenance cost calculation is applied to each component of the FOWF such as the wind turbine, the floating turbines, the mooring and anchors as well as the power cables and substations. When maintenance of several components is realized with one transport vehicle and in a single shift then the cost related to the transportation is considered only once [147].

5.3.6 Decommissioning

The projected lifetime of a wind farm can be extended by repowering of the turbines or a continuing operation. However, at a certain lifetime it will not be technical or economical feasible anymore to operate the wind farm and a decommissioning is required. Decommissioning can be considered as a reversed installation process and includes the disassembly of the FOWF as well as the transportation back to the port. Besides that, the final treatment of the various components of the FOWF is considered as well as the cleaning

of the site [140]. The owner of an offshore wind farm is in general obligated to remove all structures that were built and clear the complete offshore site after the lifetime ends. Typically, the developer is required to present a preliminary decommissioning plan already in the development phase to prove its ability for decommissioning and in some case financial securities. However, it also depends on national regulations and in some cases a decommissioning of all components might not be required when associated risks are too high or the impacts of remaining structures are not significant [161]. So far, no large offshore wind farm has been decommissioned. However, several smaller offshore wind turbine decommissioning projects have been realized during the last years. The reasons for decommissioning have been varied including research projects that have not been intended for extended operation or turbines that have reached already the end of lifetime [162]. Table 5.5 shows a list of decommissioned offshore wind turbines.

Table 5.5: Decommissioned offshore wind turbines [162, 163].

Name	Country	Size	Foundation	Built	Removed
Nogersund	Sweden	1x220kW	Tripod	1991	2007
Yttre Strengrund	Sweden	5x2MW	Monopile	2001	2015
Robin Rigg	UK	2x3MW	Monopile	2010	2015
Lely	Netherlands	4x500kW	Monopile	1994	2016
Hooksiel	Germany	1x5MW	Triple	2008	2016
WindFloat	Portugal	1x2MW	Floating	2011	2016
Vindeby	Denmark	11x450kW	Gravity	1991	2017
Blyth	UK	2x2MW	Monopile	2000	2019

In 2016, for the first time a FOWT has been decommissioned demonstrating the successful procedure to be used in future commercial projects. The WindFloat floating substructure was detached from its mooring lines and electrical cable and towed back to the port where the wind turbine was dissembled [164]. The total decommission cost can be calculated as follows

$$TC_{\text{Decom}} = C_{\text{DP}} + C_{\text{Turb-FS}_{\text{Decom}}} + C_{\text{A-M}_{\text{Decom}}} + C_{\text{Cable}_{\text{Decom}}} + C_{\text{Substation}_{\text{Decom}}} + C_{\text{Clear}} + C_{\text{FT}} \tag{5.27}$$

where C_{DP} is the cost associated to the planning of the decommissioning, $C_{Turb\text{-}FS_{Decom}}$ is the disassembly cost related to the turbine and floating substructure, $C_{Anchor\text{-}Mooring_{Decom}}$ accounts for the disassembly cost related to the anchor and mooring system, $C_{Cable_{Decom}}$ is the respective cost for the power cables and $C_{Substation_{Decom}}$ is the decommissioning cost related to the

substations. C_{Clear} represents the total cost for clearance of the offshore site after disassembly and C_{FT} is the cost resulting from the final treatment of the components [161]. A more detailed description of the individual cost components is presented next.

Decommissioning planing

The first activity in decommissioning consists of a proper planning. A scope of work has to be defined as well as a strategy for the disassembly. Furthermore, permits have to be secured for the decommissioning and clearing of the site. Finally, the market has to be analyzed for possible selling and disposal options of the components [161].

Turbine and floating substructure

Floating substructures possess the potential benefit of a simpler disassembly procedure in comparison to BOWTs and thus saving time and costs. While bottom-fixed substructures require special equipment and vessels to be removed, floating substructures have the advantage to be towed back to shore by a simple tug vessel after disconnecting from the mooring system [11]. However, the procedure depends on the individual floating design and different strategies for disassembling the turbine and floating substructure exist.

The first strategy considers the disassembly in the port. At first, the floating structure is disconnected from the mooring lines and power cable and then towed back to port by tug boats with the turbine still mounted on top. The disassembly of floating structure and turbine is realized in the port by cranes and barges. This strategy saves costs for the avoidance of large vessels, decreases the risk associated to offshore operations and lowers the dependency on weather windows. However, not all floating substructure designs allow transportation with the assembled turbine.

The second strategy considers the disassembly offshore. It begins with the removal of the turbines. The power cables are disconnected from the turbine and then all lubricants and hazardous materials are removed. The turbine itself can be dismantled into various components depending on the requirements and capacity of the transport vessel. Crane vessels or Jack-up vessels can be used for the disassembly activity. The time required for disassembling the turbine will probably be less than for the installation since the turbine has already reached its lifetime end and, therefore, less cautiousness regarding damage is needed [161].

After disassembly of the turbine, the wind turbine components are transported to the port. The remaining floating substructure is then disconnected from the anchor system and towed back to the port by a tug vessel. In the port the components of the turbine are unloaded by means of a crane and the floating substructure is fully disassembled. The costs resulting from the decommissioning of the wind turbine and floating substructure can be modeled as

$$C_{\text{Turb-FS}_{\text{Decom}}} = C_{\text{Disassembly}_{\text{Decom}}} + C_{\text{Transport}_{\text{Decom}}} + C_{\text{Port}_{\text{Decom}}} \tag{5.28}$$

where $C_{Disassembly_{Decom}}$ is the cost resulting from the disassembly of the turbine and floating substructure, $C_{Transport_{Decom}}$ represents the offshore transportation cost and $C_{Port_{Decom}}$ includes the costs associated activities in the port such as unloading, handling, transporting and storing of components. In case the first decommissioning option is used where turbine and floating substructure are transported fully assembled and the disassembly takes place in the port, then the disassembly cost $\text{C}_{\text{Disassembly}_{\text{Decom}}}$ accounts for the dismantling performed in the port. The cost associated to the disassembly can be calculated as presented next.

$$C_{\text{Disassembly}_{\text{Decom}}} = C_{\text{Vessel}_{\text{Disassembly}}} * N_{\text{Vessel}_{\text{Disassembly}}} * t_{\text{Vessel}_{\text{Disassembly}}} \tag{5.29}$$

where $C_{Vessel_{Disassembly}}$ is the day rate of the vessel used for the disassembly process, $N_{Vessel_{Disassembly}}$ is the number of vessels used and $t_{Vessel_{Disassembly}}$ represents the time period in days the vessel is in operation. The transportation cost of the disassembled components can be calculated as

$$C_{\text{Transport}_{\text{Decom}}} = C_{\text{Vessel}_{\text{DecomTransp}}} * N_{\text{Vessel}_{\text{DecomTransp}}} * t_{\text{Vessel}_{\text{DecomTransp}}} \tag{5.30}$$

where $C_{Vessel_{DecomTransp}}$ represents the day rate of a transportation vessel, $N_{Vessel_{DecomTransp}}$ the number of vessels used and $t_{Vessel_{DecomTransp}}$ is the charter time of the vessel in days. The costs regarding port activities can be calculated as

$$\begin{aligned} C_{\text{Port}_{\text{Decom}}} = {} & C_{\text{Vehicle}_{\text{DecomPort}}} * N_{\text{Vehicle}_{\text{DecomPort}}} * t_{\text{Vehicle}_{\text{DecomPort}}} + \\ & C_{\text{Store}} * A_{\text{Store}} * t_{\text{Store}} \end{aligned} \tag{5.31}$$

where $C_{Vehicle_{DecomPort}}$ is the day rate of a vehicle used in the port such as a crane or transportation vehicle in (€/d).

$N_{Vehicle_{DecomPort}}$ is the number of machines used and $t_{Vehicle_{DecomPort}}$ is time in days it is used. Since some components need to be stored for a while, a storage area has to occupied and the associated day rate is C_{Store} in (€/m^2/d). A_{Store} is the required storage area in (m^2) and t_{Store} is the respective storage period in (d).

Anchor and mooring system

Since there is no specific information available regarding mooring and anchor decommissioning of FOWTs, the principles of the oil and gas industry are considered. Two decommissioning strategies have been investigated. The first assumes that the mooring lines are disconnected at first from the floating substructure and laid down on the seabed before being recovered and brought ashore [165]. The mooring lines and anchors can be highlighted with buoyancies for an easier position finding. Once the floating substructure is towed back to the port, the disassembly of the mooring system can begin. The decommissioning of the mooring and anchor system is a reversed process of the installation. Typically, an anchor handling tug vessel is used to load the mooring lines with the anchor on deck. Remote operated underwater vehicles (ROV) and divers can also be applied in the decommissioning process. The second decommissioning strategy considers that the floating substructure keeps connected to the mooring system. A chaser is used to catch the anchor and lift it up on the vessel. The mooring is then disconnected from the floating substructure and lifted to the vessel [33]. Additional tug vessels might be required in this strategy to hold the floating substructure in position. Figure 5.10 illustrates the decommissioning with a chaser.

Depending on the type of anchor, it might also be left in place as a removal could impact the integrity of the seabed. It could cause the seabed to be unstable and unsuitable for new anchor settings [165]. The decommissioning cost of anchor and mooring system are computed by

$$C_{\text{A-M}_{\text{Decom}}} = C_{\text{A-M}_{\text{Decom}}} * N_{\text{A-M}_{\text{Decom}}} * t_{\text{A-M}_{\text{Decom}}} + C_{\text{A-M}_{\text{ROV}}} * t_{\text{A-M}_{\text{ROV}}} + C_{\text{A-M}_{\text{Diver}}} * t_{\text{A-M}_{\text{Diver}}} \tag{5.32}$$

where $C_{A\text{-}M_{Decom}}$ represents the day rate of an anchor handling vessel, $N_{A\text{-}M_{Decom}}$ the number of vessel used and $t_{A\text{-}M_{Decom}}$ the time period in days the vessel is in operation. $C_{A\text{-}M_{ROV}}$ is the day rate of a ROV and $\text{t}_{\text{A-M}_{\text{ROV}}}$ the time of usage. $C_{A\text{-}M_{Diver}}$ represents the labor cost of a diver in (€/d) and $t_{A\text{-}M_{Diver}}$ the working time in days.

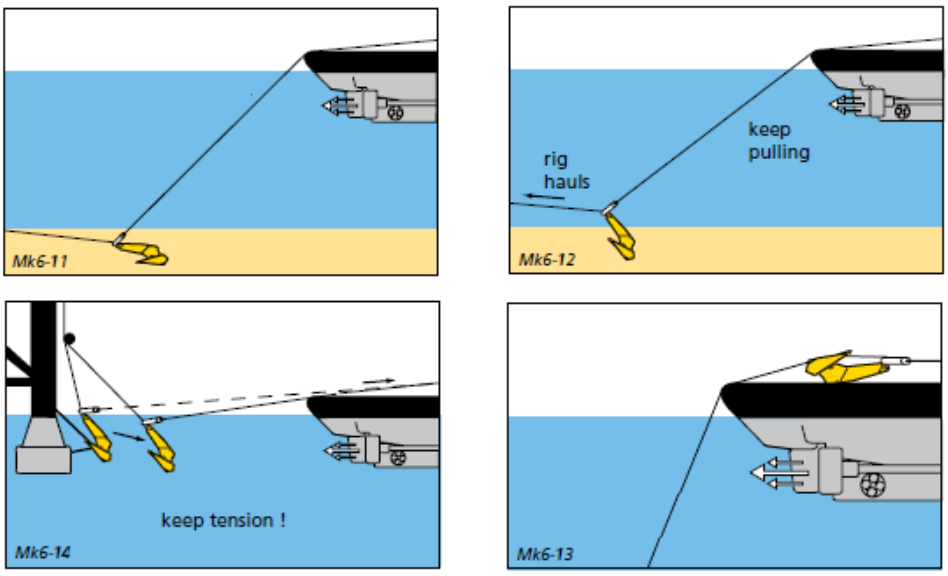

Figure 5.10: Decommissioning of anchor and mooring with chaser [33].

Power cables

The environmental impact of submarine power cables is not well known. Some studies state that the electromagnetic field generated by electric power transmission can disturb the behavior of marine species and the heat loss could increase locally the sea bottom temperature. However, these studies also state that the environmental impacts are generally limited close to the cable routes and are temporarily [166]. The uncertainty about the environmental impact of submarine power cables causes that there is no clear regulation on the decommissioning. It depends often on the specific case and circumstances if a removal of the power cables is required. For instance, when power cables are located in trawling fishing areas or not deeply buried, it is most likely that the removal is desired. The cable removal process involves typically a cable laying vessel, a ROV and if needed a diver. The ROV recovers at first the submarine cable and attaches it to the winch of the vessel. Then, the cable is winded up by the engine of the winch until the entire cable is loaded on the deck of the vessel. The cable might be cut in pieces for easier transportation. The explained cable removal procedure is applied for both, the inter-array cables as well as the export cables [161].

The associated decommissioning costs can be calculated as follows

$$C_{\text{Cable}_{\text{Decom}}} = \frac{C_{\text{Cable}_{\text{Decom}}} * l_{\text{Cable}_{\text{Decom}}} *}{I_{\text{Cable}_{\text{Decom}}}} \tag{5.33}$$

where $C_{Cable_{Decom}}$ is the day rate of the vessel in (€/d) and $l_{Cable_{Decom}}$ the total length of the cable to be removed in (m). The rate at which the vessels performs the cable removal in (m/d) is given by $I_{Cable_{Decom}}$.

Substations

The offshore substation is likewise disassembled as it was installed. The topside is removed and transported separately to the port. In case the foundation is made of a bottom-fixed substructure, then it will be cut below the mud line, lifted up with a crane vessel and transported to the port [161]. When the foundation consists of a floating substructure, then the same procedure is applied as for the FOWT. The mooring system and topside have to be separated at first and then a tug boat can tow the floater to the port. The decommissioning cost of the offshore substation is obtained by

$$C_{\text{OffshoreSub}_{\text{Decom}}} = C_{\text{OffshoreSub}_{\text{Decom}}} * t_{\text{OffshoreSub}_{\text{Decom}}} * N_{\text{OffshoreSub}_{\text{Decom}}} \tag{5.34}$$

where $C_{OffshoreSub_{Decom}}$ is the day rate of the vessel that performs the disassembly of the substation in (€/d), $t_{OffshoreSub_{Decom}}$ represents the time in (d) required for disassemble one offshore substation and $N_{OffshoreSub_{Decom}}$ is the number of offshore substations that will be removed. The decommissioning cost of the onshore substation can be calculated as

$$C_{\text{OffshoreSub}_{\text{Decom}}} = C_{\text{OnshoreSub}_{\text{Decom}}} * t_{\text{OnshoreSub}_{\text{Decom}}} * N_{\text{OnshoreSub}_{\text{Decom}}} \tag{5.35}$$

where $C_{OnshoreSub_{Decom}}$ is the day rate of the crane that perform the demolition of the onshore substation area in (€/d), $t_{OnshoreSub_{Decom}}$ represents the time in (d) required and $N_{OnshoreSub_{Decom}}$ is the number of cranes used. The total cost for the decommissioning of the substations is finally obtained by the sum of offshore and onshore substation decommissioning costs.

$$C_{\text{Substation}_{\text{Decom}}} = C_{\text{OffshoreSub}_{\text{Decom}}} + C_{\text{OnshoreSub}_{\text{Decom}}} \tag{5.36}$$

Site clearance

Site clearance is the last activity in the offshore decommissioning process. After all components of the FOWF are disassembled and transported back to the port, the offshore site has to be cleaned, which involves the removal of debris on the sea floor. Offshore regulations and lease terms require generally that the offshore site is left in a state similar to how it was found before. In the oil and gas industry a common practice is to drag a trawl net across the construction site and thus clean the sea floor. Furthermore, side scan sonars might be used to look for remaining components. However, considering the large area of a FOWF to be cleared it would be reasonable to develop alternative methods to clean the site accurately and cost-effective [161]. The total cleaning cost can be calculated by

$$C_{\text{Clear}} = C_{\text{Clean}} * A_{\text{site}} \tag{5.37}$$

where the cleaning cost in (€/m^2) is defined by $C_{AreaClean}$ and the total area of the offshore construction site is given by A_{site} in (m^2).

Final treatment

The final treatment of the disassembled components of the FOWF consists of reusing, selling or disposal. It is expected that the potential to reuse some of the components such as power cables, tower or machineries will be low due to the age of the components and likely high corrosion. Components that have a value such as steel structures can be sold at steel scrap prices to the market. However, the selling price has to consider that costs occur for cutting the steel component into saleable units as well as for potential transportation. The last option would be to simple dispose the components in a landfill. However, this method also involves costs for the transportation and the disposal [161]. The cost of the final treatment can be calculated as

$$C_{\text{FT}} = C_{\text{Disposal}} + C_{\text{Sell}} \tag{5.38}$$

where $C_{Disposal}$ represents the disposal costs and C_{Sell} the selling costs. The disposal cost consists of the cost demanded by the landfill and the transportation cost and is computed by

$$C_{\text{Disposal}} = C_{\text{Landfill}} * m_{\text{Disposal}} + C_{\text{Vehicle}_{\text{Disposal}}} * t_{\text{Vehicle}_{\text{Disposal}}} * N_{\text{Vehicle}_{\text{Disposal}}} \tag{5.39}$$

where $C_{Landfill}$ is the cost for disposal in the landfill in (€/t) and $m_{Disposal}$ is the total weight of the components to be disposed in (t). $C_{Vehicle_{Disposal}}$ represents the day rate of the transportation vehicle used for transporting the components to the landfill in (€/d), $t_{Vehicle_{Disposal}}$ is the required time for transportation in (d) and $N_{Vehicle_{Disposal}}$ is the amount of vehicles used. The selling of a component generates an income to the company and is treated as a negative cost. It can be calculated by

$$C_{\text{Sell}} = -C_{\text{Material}_{\text{Sell}}} * m_{\text{Material}_{\text{Sell}}} + C_{\text{Vehicle}_{\text{Sell}}} * t_{\text{Vehicle}_{\text{Sell}}} * N_{\text{Vehicle}_{\text{Sell}}} + C_{\text{Material}_{\text{Processing}}} * m_{\text{Material}_{\text{Processing}}} \tag{5.40}$$

where $C_{Material_{Sell}}$ is the selling price of a material in (€/t) and $m_{Material_{Sell}}$ is the total weight to be sold in (t). $C_{Vehicle_{Sell}}$ represents the day rate of a transport vehicle used for transporting the components to the scrap yard in (€/d), $t_{Vehicle_{Sell}}$ is the required transportation time in (d) and $N_{Vehicle_{Sell}}$ the amount of vehicles used. $C_{Material_{Processing}}$ represents the cost for processing the components into sellable units in (€/t) and the $m_{Material_{Processing}}$ is the weight of components to be sold. It is assumed that a reuse of a component would not result in costs to be included in the life cycle of the FOWF.

5.4 Lifetime energy production

The energy provided is the denominator of the LCOE equation (Equation (5.1)). It refers to the total energy generated (E_t) during the lifetime minus the energy losses (L_t) that occur in generation, collection and transmission of the energy [147]. Figure 5.11 displays the losses in the system that are considered in the model.

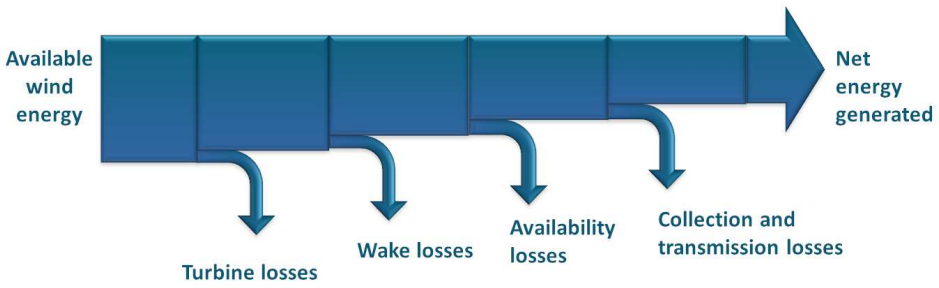

Figure 5.11: Energy losses considered in the LCOE calculation.

The available wind energy $E_{available}$ is the amount of energy extractable by the FOWT based on the characteristics of the wind turbine and the metocean conditions. It is been defined previously by Equation 3.31 in Section 3.2.4. The turbine losses account for the mechanical and electrical losses occurring by wind extraction and power generation of the wind turbine, which are considered by the power coefficient. A further energy loss taken into account is based on the wake effect from neighboring wind turbines in the wind farm. The wake losses for the whole wind farm are computed in this section by using the software WAsP and included as efficiencies. A comprehensive model has been considered in Chapter 6 and a detailed description of the methodology is given in Section 6.2.2. The availability is the proportion of time a wind farm is capable to produce energy due to downtime caused by failures and breakdowns of components in the wind farm such as the wind turbines, power cables and substations [34]. The total loss in energy production based on the availability of the FOWF is considered as an efficiency rate in this section. Since so far no floating offshore wind farms exists that have been operated for a longer period, the availability rate of BOWFs is considered. In Section 6.2.4, a more detailed approach to the availability assessment of the electrical components of a FOWF is presented. The collection and transmission losses represent the cumulative energy losses that occur in the power cables due to the resistive heating. The power loss of a generic cable can be computed by

$$P_{\mathrm{cable_{loss}}} = {I_{\mathrm{cable}}}^2 * R_{\mathrm{cable}} * l_{\mathrm{cable}} \tag{5.41}$$

where I_{cable} represents the current flowing through the cable, R_{cable} the resistance and l_{cable} the length of the cable [167].

5.5 Case study

The LCOE methodology presented previously is used in this case study to assess three FOWT concepts located at different locations. At first, the FOWT concepts and offshore sites are presented and information is given regarding the FOWF configuration. Afterwards, the results of the study are provided and discussed.

5.5.1 Floating offshore wind turbine concepts

In this study, the three most common types of floating substructures are investigated. These are the Semi-submersible, Tension Leg Platform (TLP) and Spar. The cost data used for this study has been provided by the respective concept designer. Figure 5.12 illustrates the FOWT designs.

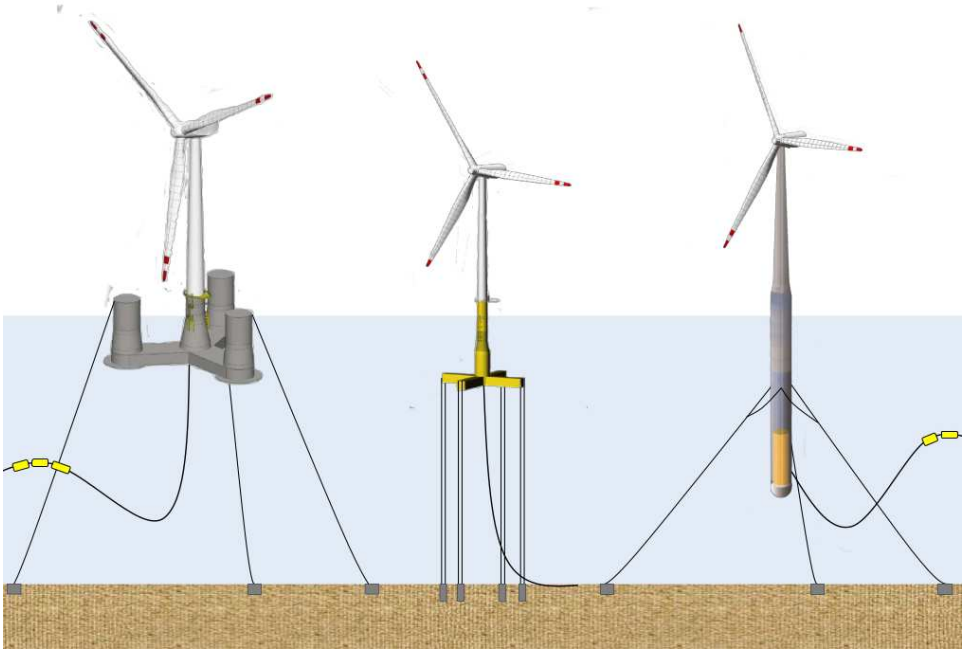

Figure 5.12: Illustration of floating offshore wind turbine concepts. From left: Semi-submersible Concrete based on OO-Star Wind Floater [168], TLP Steel based on TLPWIND [169] and Spar Concrete based on Windcrete [170].

All three concepts support the DTU 10MW reference wind turbine. The horizontal upwind turbine has been developed by the Technical University of Denmark (DTU) and consists of a 3-bladed rotor, medium speed drivetrain with a multiple stage gearbox and a variable speed collective pitch control. The hub height is 119m and the rotor has a diameter of 178.3m. Further information about the wind turbine is provided by Bak et al. [84]. The tower and associated costs have been adjusted to each of the FOWT designs.

The semi-submersible floating substructure concept considered in this study is made of concrete and can be constructed locally worldwide [171].

Fabrication of the hull can be done on floating barges, in a dry dock or on a quay. The installation of the turbine is performed at quayside, which allows to avoid the use of expensive offshore cranes. The low draft allows a simple transportation with tug boats of the complete FOWT and a flexible application also in lower water depths [171]. As soon as it arrives at the offshore site, the floater will be connected to the pre-installed mooring system at the offshore site, which consists either of catenary or taut spread mooring lines. The drag anchor is commonly applied to these mooring systems, but the final choice depends on the soil conditions at the specific site [172]. The concrete structure requires few on-site inspections and the required preventive maintenance activities can be performed along with the turbine maintenance, which reduces costs. In addition, it can be towed back to shore by tug boats in case of a major repair due to its floatability. The decommissioning follows the same principle as the installation and disassembled concrete components may be reused at a suitable location [171].

The TLP concept considered in this study uses steel as main construction material [173]. It consists of a semi-submerged buoyant structure that is anchored to the seabed by tension leg moorings. The low draft and high stability allows for a smaller and lighter structure. However, the dependence on the taut moorings for stabilization requires a special purpose-built vessel for transportation and installation [11]. After the decommissioning of the floating substructure, the steel components can be processed and sold as recycled material [174].

The Spar concept considered in this study is made of concrete and encourages the use of low cost materials, local construction processes and low maintenance needs. The substructure can be built in a dry dock and in a horizontal position by using a slipform, which avoids the presence of concrete joints. After floating the dock, tug boats tow the substructure to the installation site. The erection of the Spar and the installation of the wind turbine are performed offshore by submerging the structure and exchanging the ballast material. A catamaran ship can be applied for this process instead of heavy floating cranes, which reduces installation costs. After erection, the SPAR is connected to the pre-installed mooring system, which consists of three catenary mooring lines [175]. The decommissioning follows the same principal as the installation process and concrete material may be reused or sold for other purposes [175]. Further information about the specific floating wind turbine concepts can be found on the respective websites of the concept developers, which are listed in the references [168–170].

5.5.2 Offshore sites

The metocean conditions of an offshore site have a significant influence on the design, cost and performance of FOWTs [176]. For instance, the type of seabed influences the choice of anchor and the mooring line length depends largely on the water depth. Furthermore, the dimensions and design of the floating substructure have to be carefully chosen in order to withstand even the most extreme environmental loads of a specific site [30]. Besides that, the available wind resources are highly important in order to maximize energy generation. In this study, three offshore locations are considered to represent different metocean conditions namely Golfe de Fos (moderate), Gulf of Maine (medium) and West of Barra (severe). In addition, the sites are chosen based on potential deployment areas of the three FOWT concepts and where political support is expected for offshore wind. The availability of metocean data has also been essential for the selection process. Table 5.6 summarizes the characteristics and Figure 5.13 (a,c,e) displays the location of the wind farm with relevant water depths.

Table 5.6: Offshore sites characteristics.

	Golfe de Fos	Gulf of Maine	West of Barra
Country	France	USA	Scotland
Reference location	Marseille	Portland	Barra
Ocean	Mediterranean Sea	Atlantic	Atlantic
Metocean conditions	Moderate	Medium	Severe
Design water depth (m)	70	130	100
Wind speed 50 years (m/s)	37	44	50
Mean wind speed at 100m (m/s)	>10	10.18	11.26
Sign. wave height 50 years (m)	7	10.48	14.27
Transmission length* (km)	38	57.8	180
Soil type	Sand/Clay	Sand/Clay	Rock/Basalt

*Distance between offshore and onshore substation

Golfe de Fos has been chosen to represent moderate metocean conditions with a design water depth of 70m and a 50-year wind speed at hub of 37m/s [122]. Despite not having deployed any BOWTs to date, France is increasingly promoting the development of floating wind technology. A 2MW full-scale prototype has been installed in May 2018 and four pre-commercial FOWFs are expected to be commissioned by 2020/21. Having suitable offshore sites in both the Mediterranean Sea and the Atlantic Ocean, France has proposed in his current multi-annual energy program to develop up to 6GW of bottom-fixed offshore wind and 2GW of floating wind and tidal

projects by 2025/26 [177].

Gulf of Maine site is located about 57.8km off Portland in the Northeast coast of the USA. It represents medium metocean conditions with 44m/s of 50 years wind speed and a water depth of 130m [122]. Floating wind activity can be tracked back in the state of Maine as early as 2013, where a small prototype of the VolturnUS concrete Semi-submersible concept was installed. It represented also the first offshore wind turbine deployed in US waters. Two 6MW full-scale models of this concept are expected to be commissioned by 2020 off the coast of Maine followed by a potential commercial deployment [177].

West of Barra site is situated 19km West of Barra Island in the Atlantic Ocean. It has the harshest conditions and highest wind resources with a 50-year wind speed of 50m/s and 100m design water depth. Furthermore, basalt is present at this location, whereas the soil of the other two sites consists of a mixture of sand and clay [122]. Scotland has large potential for floating wind deployment with attractive near-shore deep water sites and suitable metocean conditions. It is home to the world's first floating wind farm Hywind Scotland, which was commissioned in 2017 and a second project consisting of the 50MW Kincardine floating wind farm is expected to be completed by 2019/20. Floating wind could benefit from the experience and supply chain of UK's offshore wind industry and could play a large part in Scotland's target to generate all of its electricity from renewable sources by 2020 [177]. A detailed description of the three offshore sites and environmental conditions is given by Gomez et al. [122].

5.5.3 Wind farm definition and general parameters

A FOWF is considered with 50 offshore wind turbines and a nominal power capacity of 500MW. The selected transmission technology is HVAC with the collection grid voltage operating at 66kV and the transmission voltage at 220kV. The position of the wind turbines within the wind farm layout is the same for all concepts and, therefore, provokes the same wake losses. However, the connection of the floating wind turbines and the position of the offshore substation are defined individually by each concept designer, which cause the total power cable losses to be slightly different. Figure 5.13 (b,d,f) presents the wind farm layouts of the three offshore sites. The wind turbines are placed in direction to the prevailing winds at each site.

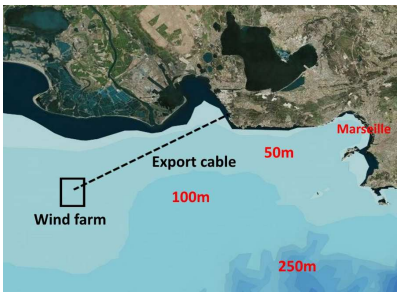

(a) Golfe de Fos site

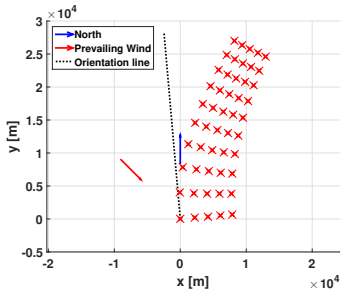

(b) Golfe de Fos layout

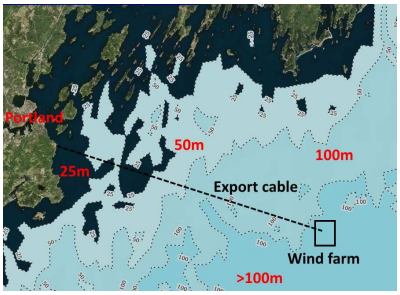

(c) Gulf of Maine site

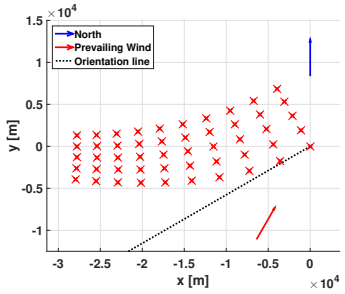

(d) Gulf of Maine layout

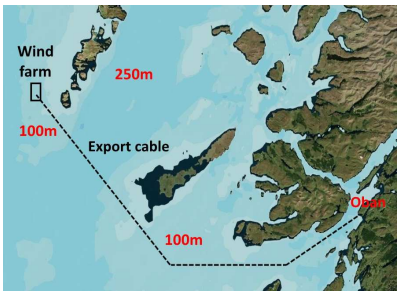

(e) West of Barra site

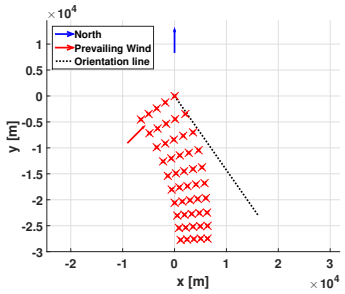

(f) West of Barra layout

Figure 5.13: Offshore sites and layouts.

The interconnection of the wind turbines is realized by a combination of dynamic and static power cables, where the dynamic part is connected to the turbines and the static part is laying on the seabed. The cost of the offshore substation is estimated for different water depths and reactive power compensation is adjusted according to the distance to shore. Advantage is taken of existing electrical infrastructure concerning the onshore substation. However, for the case of West of Barra a larger investment is required, be-

cause no suitable infrastructure exists at the location. In addition, common parameters are defined that are used for all study cases. For instance, the discount rate is set to 10%, which represents a typical value for offshore wind farm projects and a lifetime of 25 years is chosen.

5.5.4 LCOE results

The input data used in study has been provided by the respective concept designer and thus the results are affected by the accuracy and source of the data. Furthermore, a general conclusion for FOWT concepts cannot be given since they vary widely by their technical specifications and cost composition. Besides that, the concepts compared in this study are on different technical and commercial readiness levels, which involve a different degree of uncertainty in the data. Therefore, the objective of this study is not to assess the feasibility of the concepts nor the LCOE values, but rather to analyze the sensitivity of the LCOE in relation to input parameters.

The results of the levelized cost of energy calculation for the different offshore sites and floating offshore wind turbine concepts are presented in Figure 5.14. The Spar buoy concept could not be analyzed for Golfe de Fos because of the deep draft and the low water depth available at this offshore site. The LCOE values are shown with and without offshore transmission cost to consider the different policies that are in place in the countries regarding transmission assets. Besides that, this allows a better comparison of the FOWT concepts since the transmission assets are considered as common components and possess similar costs.

The values for the FOWF obtained in this study range from as low as 77€/MWh for the TLP FOWT concept in Golfe de Fos including offshore transmission costs to 119€/MWh for the Semi-submersible FOWT concept in West of Barra. A significant portion of the LCOE represents the cost of the offshore transmission assets, which is influenced by the different sites and highlighted in the figure. For instance, for the West of Barra case the portion of the transmission cost reaches up to 37% for the Spar concept, 34% respectively for the Semi-submersible FOWT concept and 33% for the TLP concept. The high portion is based on the long export cable needed for the remote offshore site with respective investment costs and energy losses. Furthermore, the cost of the substation increases with the distance due to the larger investment required for reactive power compensation in the HVAC transmission. The difference in the offshore transmission costs among the three FOWF designs is based on the different positioning of the offshore substation within the wind farm layout. It influences the distance to shore

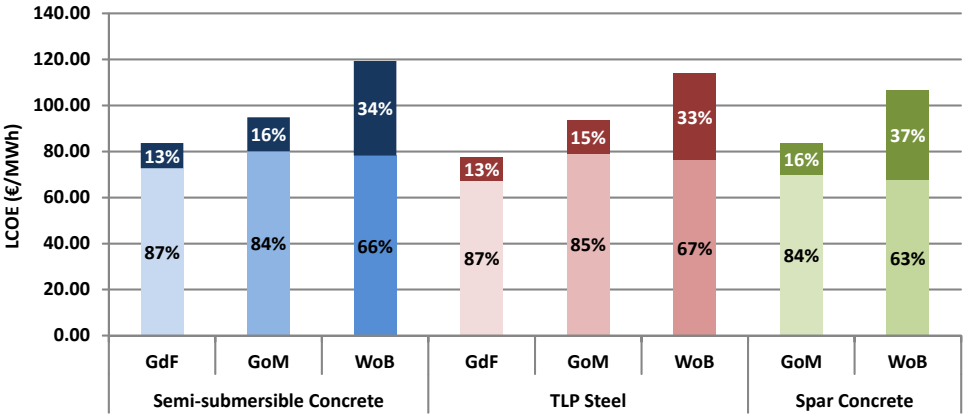

Figure 5.14: LCOE results for each concept and offshore site. The upper parts of the bars represent the portion of transmission asset costs of the LCOE.

and consequently the length of the export cable, the cost of the offshore substation as well as other LCCs such as transportation, maintenance and decommissioning. The LCOE results without offshore transmission assets demonstrate values, for instance, as lows as 67€/MWh for the TLP FOWT concept in Golfe de Fos. Next, Figure 5.15 shows a LCOE comparison between different energy generation technologies.

The LCOE values calculated for the three offshore sites and for each of the floating wind turbine concepts are highlighted by colored symbols. Myhr et al. [131] has estimated the LCOE values for a number of different FOWT concepts and the results are taken as a reference range. It can be seen that the obtained LCOE values are in the lower part or even below the reference range, which demonstrates the high cost effectiveness of the studied concepts. Furthermore, Figure 5.15 shows that floating offshore wind power can be a high competitive solution to conventional bottom-fixed offshore wind, where the LCOE is currently between 73€/MWh and 142€/MWh [132]. In addition, the obtained values are comparable to Contracts for Difference auction results recently published in the United Kingdom with commissioning years expected to be between 2021 and 2023 [180]. However, in order to be competitive in the long-term, floating wind energy needs to follow the cost reduction pathways that onshore and offshore wind energy have already experienced. Floating wind can also benefit from economies of scale of the well developed bottom-fixed offshore wind sector since many components are shared by both technologies.

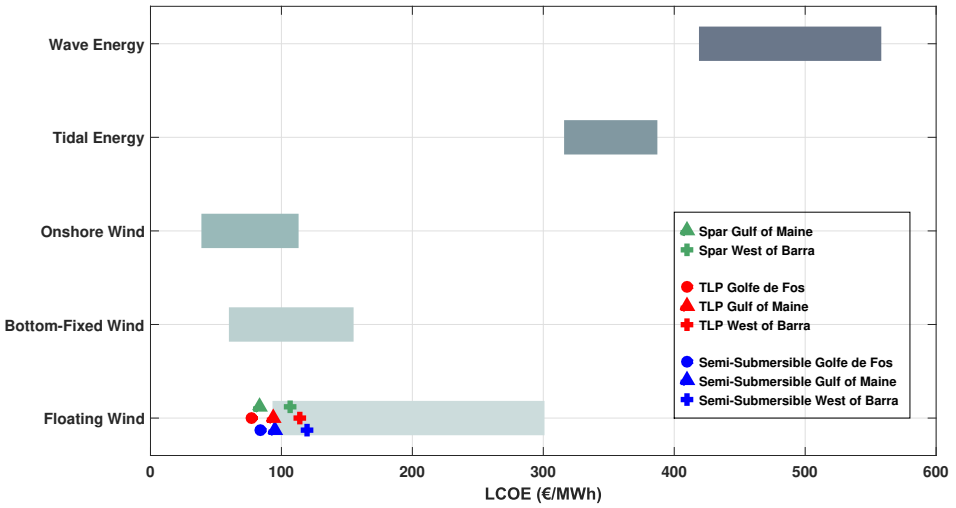

Figure 5.15: LCOE comparison between energy generation technologies. Calculated values of TLP in red, Semi-submersible in blue and Spar in green. The reference LCOE range for floating offshore wind is based on Myhr et al. [131]. The range for wave and tidal energy is taken from the Carbon Trust [178], for bottom-fixed offshore wind from Kausche et al. [132] and for onshore wind from Duan [179].

In addition, FOWTs have the advantage to be placed in locations with the best possible wind resources without depth constraints, which improves the capacity factor and leads to a lower LCOE [12]. Moreover, floating wind does not necessarily need to compete with bottom-fixed offshore wind, because FOWTs possess its full potential at deep water locations (more than 60m), where conventional bottom-fixed substructures are unsuitable from a cost and technical perspective [11].

Ocean energy technologies, such as tidal and wave energy converters, are still at an early stage of development and have in comparison the highest cost of energy [181]. The Carbon Trust [178] has estimated the LCOE of tidal and wave energy at 329€/MWh to 374€/MWh and 432€/MWh to 545€/MWh, respectively. The higher cost of energy results from both lower capacity factors and a higher capital investment [182]. Furthermore, the rate of cost reduction is potentially lower since ocean energy can not benefit as much as floating offshore wind from an existing supply chain [178].

Figure 5.16 shows a breakdown of the LCCs including offshore transmissions assets for the different FOWF concepts and offshore sites. The LCCs are represented by differently colored bars and the value for each of the offshore sites is highlighted by the horizontal lines. Manufacturing contributes by far the highest portion to the LCC for all sites and concepts. This could be expected because it includes the manufacturing cost of large components such as the wind turbines, substructures, power cables and substation. Besides that, it includes the storage cost in the port as well as the load-out process. The larger investment required for the offshore transmission in West of Barra contributes to an increased manufacturing cost for this site.

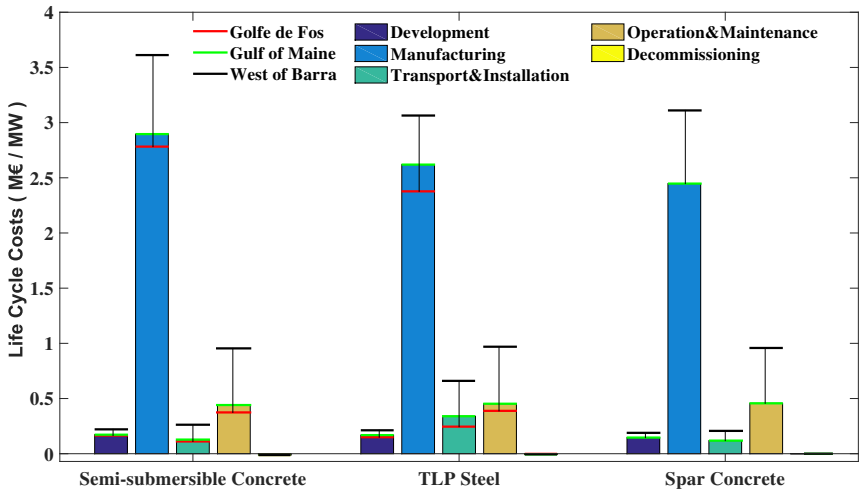

Figure 5.16: Life cycle costs including transmission assets.

Furthermore, it can be observed that transportation and installation costs have increased for West of Barra. Concerning the comparison among the FOWT concepts, the Spar obtains the lowest LCC due to the manufacturing cost reduction potential of concrete structures, simple anchor and mooring lines and a cost effective installation process. However, due to the large draft the Spar concept is not suitable for water depths below 90m, such as in Golfe de Fos. The Semi-submersible concept possesses larger manufacturing costs due to the greater dimensions but lower transportation and installation costs, since it can be towed by simple tug boats. Furthermore, parallel transportation and installation activities have been considered during the transportation and installation process.

Thus, by slightly increasing the number of less costly tug boats, the rental time and overall cost could be reduced significantly. The TLP concept, on the other hand, requires a special purpose built barge for the offshore transportation due to its instability, which construction cost is included in the manufacturing life cycle. By comparing West of Barra with Golfe de Fos and Gulf of Maine, it can be seen that this site requires a more robust substructure due to the severe metocean conditions. However, the required robustness of the floating substructures does not necessarily result in a significant cost increase. Only a 10% higher investment for the substructures is observable on average among the concepts. The site's environmental conditions have certainly a significant influence on the installation cost, because a larger and more specialized installation spread is required to install within reduced weather windows. Moreover, soil conditions in West of Barra are more challenging because the seabed consists of rocks while at the other sites it is basically sand and mud. This requires a different anchor type and depending on the FOWT concept, it can impact the manufacturing and especially the installation cost of anchor and mooring lines.

5.5.5 Sensitivity analysis

A sensitivity analysis is generally used to identify how the output of a model reacts to variations in model inputs given by variables or parameters [183]. In this study, output is defined as the value of the LCOE of a FOWF in €/MWh. The inputs are parameters that are needed for the calculation of the LCOE such as costs, financial variables and energy related parameters. The quantification of uncertainty in the input is given by a specific range of variation, which is in this study 50% above and below the mean value. The specific range must be, however, the same for all input parameters to ensure that the results are comparable. There exist also a number of different methods to perform a sensitivity analysis [183]. The type that is applied in this analysis is the One-at-a-time (OAT) method. OAT is one of the simplest and most common approaches, which implies to vary one parameter at a time while holding the others fixed. This approach is repeated for all input parameters considering the defined uncertainty range [184].

The obtained results can then be filtered by a defined threshold value. For example, in this analysis a minimum variation of 1% is required to be counted as a significant input parameter. The filtered results are further studied by defining reasonable variation ranges in order to obtain the actual influences on the LCOE and to examine the output based on best and worst case scenarios [185].

This analysis can be of great interest for the floating wind technology in order to highlight the performance limits and to identify potential cost reductions. In this analysis, 325 parameters such as costs, financial variables and energy related parameters have been considered as sensitivity parameters to assess their influence on the LCOE of a FOWF. The parameters are based on the input data provided by the concept designers for the design specific components and other parameters are defined for the common components. A complete list of the parameters is provided by Benveniste et al. [O2]. The parameters that most influence the LCOE, based on the minimum 1% criteria, are shown in Tables 5.7 and 5.8. The results are shown at first for floating design dependent parameters and afterwards for the common parameters, which are based on the balance of plant, energy related and economic parameters.

Table 5.7: LCOE variation (%) by change of design dependent parameters.

Offshore site	Concept / Parameter variation	Semi-submersible Concrete -50%	Semi-submersible Concrete +50%	TLP Steel -50%	TLP Steel +50%	Spar Concrete -50%	Spar Concrete +50%
Golfe de Fos	Substructure cost	-12.41	+12.41	-8.24	+8.24		
	Inter-array cable length	-3.14	+3.15	-2.15	+2.16		
	Inter-array cable cost	-2.40	+2.40	-0.89	+0.89		
	Mooring cost	-1.61	+1.61	-1.42	+1.42		
	Installation vessel day rate	-1.07	+1.07	-2.75	+2.75		
	Anchor cost	-0.38	+0.38	-1.93	+1.93		
	Anchor&Mooring installation time	-0.29	+0.29	-1.67	+1.67		
Gulf of Maine	Substructure cost	-11.44	+11.44	-8.85	+8.85	-5.26	+5.26
	Inter-array cable length	-3.13	+3.14	-1.94	+1.95	-3.12	+3.16
	Inter-array cable cost	-2.45	+2.45	-0.94	+0.94	-1.88	+1.88
	Mooring cost	-1.99	+1.99	-1.47	+1.47	-4.42	+4.42
	Anchor cost	-0.43	+0.43	-2.00	+2.00	-0.88	+0.88
	Installation vessel day rate	-0.99	+0.99	-2.94	+2.94	-1.00	+1.00
	Anchor&Mooring installation time	-0.26	+0.26	-2.02	+2.02	-0.25	+0.25
West of Barra	Substructure cost	-9.15	+9.15	-7.15	+7.15	-4.11	+4.11
	Mooring cost	-3.01	+3.01	-1.03	+1.03	-4.10	+4.10
	Inter-array cable length	-2.28	+2.29	-1.30	+1.31	-2.60	+2.65
	Inter-array cable cost	-1.71	+1.71	-0.64	+0.64	-1.39	+1.39
	Anchor cost	-0.20	+0.20	-0.55	+0.55	-0.93	+0.93
	Installation vessel day rate	-1.03	+1.03	-5.12	+5.12	-0.79	+0.79
	Anchor&Mooring installation time	-0.43	+0.43	-4.67	+4.67	-0.25	+0.25

Table 5.7 shows that the parameters that most vary the LCOE across all concepts and offshore sites are capital cost related. This includes the cost of the substructure, inter-array power cable cost and length as well as mooring and anchor cost. However, it is also observable that the installation vessel day rate has an important influence on the LCOE.

An increase or decrease of the substructure cost has by far the highest impact on the LCOE with a variation on the LCOE value ranging from 4.11% for the Spar buoy concept in West of Barra to over 12.41% for the Semi-submersible in Golfe de Fos. Furthermore, the higher variation by the Semi-submersible concept reflects the higher construction cost needed for that type of floating substructure. The mooring cost of the Spar buoy concept has also a significant influence on the LCOE based on the specific type of mooring line used for holding the structure in place.

The results for the common parameters are presented in Table 5.8. The common parameters show that there is no large difference among the concepts on the LCOE variation. However, there is a difference among the offshore sites. Turbine and offshore substation cost cause clearly a large influence on the LCOE based on the capital intensive investment. The LCOE variation based on the export cable increases among the offshore sites. West of Barra requires the longest and thus most expensive export cable. The influence on the LCOE is, therefore, the highest for this location. The discount rate has by far the largest influence among all input parameters studied. A 50% increase or decrease of the mean value causes a variation of the LCOE by more than 30% for all study cases. Thus, a well-chosen discount rate is of significant importance for the LCOE calculation. Energy related parameters that were analyzed such as the overall net production, availability loss and turbine electrical losses possess also a larger impact on the LCOE. For this reason, energy losses in the system should tried to be minimized. Besides that, the maintenance has a larger impact on the LCOE. In particular, the number of preventive maintenance activities and the component repair cost. The corrective maintenance failure rate has also significant influence on the LCOE. For West of Barra, the operation cost shows a larger influence since transmission charges are required to be included at this site.

Table 5.8: LCOE variation (%) based on change of common parameters.

	Concept	Semi-submersible Concrete		TLP Steel		Spar Concrete	
Site	Parameter variation	-50%	+50%	-50%	+50%	-50%	+50%
Golfe de Fos	Discount rate	-32.24	+36.34	-31.28	+35.49		
	Turbine cost	-20.09	+20.09	-21.75	+21.75		
	Energy production	+11.08	-9.07	+11.05	-9.04		
	Offshore substation cost	-3.75	+3.75	-4.06	+4.06		
	Turbine electrical losses	-3.08	+3.28	-3.07	+3.27		
	Availability loss	-2.56	+2.70	-2.56	+2.70		
	Operation cost	-2.56	+2.56	-2.76	+2.76		
	Development cost	-2.41	+2.41	-2.37	+2.37		
	Export cable length	-2.20	+2.34	-1.96	+2.04		
	Export cable cost	-1.58	+1.58	-1.44	+1.44		
	Preventive maintenance activities	-1.17	+1.17	-1.27	+1.27		
	Corrective maintenance failure rate	-1.14	+1.14	-1.23	+1.23		
	Lifetime	+1.85	-2.12	+1.90	-2.15		
Gulf of Maine	Discount rate	-31.76	+35.82	-31.33	+35.46	-30.50	+34.62
	Turbine cost	-18.95	+18.95	-19.22	+19.22	-21.68	+21.68
	Energy production	+11.08	-9.07	+11.06	-9.05	+11.11	-9.09
	Offshore substation cost	-3.80	+3.80	-3.85	+3.85	-4.35	+4.35
	Turbine electrical losses	-3.08	+3.29	-3.07	+3.28	-3.05	+3.25
	Export cable length	-3.57	+4.25	-3.40	+3.99	-3.19	+3.58
	Preventive maintenance activities	-2.48	+2.48	-2.51	+2.51	-2.84	+2.84
	Export cable cost	-2.40	+2.40	-2.31	+2.31	-2.26	+2.26
	Development cost	-2.38	+2.38	-2.36	+2.36	-2.31	+2.31
	Preventive maintenance repair cost	-2.14	+2.14	-2.17	+2.17	-2.45	+2.45
	Operation cost	-1.88	+1.88	-1.90	+1.90	-2.15	+2.15
	Corrective maintenance failure rate	-1.07	+1.07	-1.09	+1.09	-1.23	+1.23
	Lifetime	+1.83	-2.10	+1.86	-2.12	+1.86	-2.11
West of Barra	Discount rate	-29.19	+32.98	-28.73	+32.53	-27.95	+31.74
	Export cable length	-19.10	+73.23	-17.40	+58.21	-19.71	+73.15
	Turbine cost	-13.64	+13.64	-14.02	+14.02	-15.39	+15.39
	Energy production	+11.08	-9.06	+11.04	-9.04	+11.11	-9.09
	Export cable cost	-5.81	+5.81	-5.68	+5.68	-6.50	+6.50
	Operation cost	-4.96	+4.96	-5.10	+5.10	-5.60	+5.60
	Availability loss	-4.17	+4.55	-4.17	+4.55	-4.17	+4.55
	Turbine electrical losses	-3.49	+3.75	-3.41	+3.66	-3.44	+3.71
	Preventive maintenance activities	-3.04	+3.04	-3.12	+3.12	-3.43	+3.43
	Preventive maintenance repair cost	-2.71	+2.71	-2.79	+2.79	-3.06	+3.06
	Offshore substation cost	-2.64	+2.64	-2.71	+2.71	-2.98	+2.98
	Development cost	-2.19	+2.19	-2.17	+2.17	-2.12	+2.12
	Export cable installation vessel	-1.16	+1.16	-1.14	+1.14	-1.30	+1.30
	Lifetime	+1.71	-1.95	+1.72	-1.96	+1.72	-1.94

5.5.6 LCOE variation potential

This study is complementary to the previous section as it presents the variation of the LCOE by applying uncertainty ranges defined by the FOWT concept designers and common ones. The ranges are applied on the parameters that most influence the LCOE and that were obtained in the previous section. This serves to identify how much the LCOE could actually vary based on uncertainty ranges defined by the designers. The parameter variation and LCOE results are listed in Table 5.9. Zero values in the table imply that no uncertainty ranges were defined for this parameter. The offshore site Golfe de Fos shows that the discount rate has the largest influence on the LCOE. For example, a 13.5% decrease of the LCOE is achievable by lowering the discount rate by 20%. However, when the discount rate is chosen too high, for example with a 20% increase, the LCOE can rise by about 14%. Furthermore, it can be observed that a decrease of 5% of the LCOE value can be reached by increasing the energy production by 5%.

The turbine supply costs and availability loss rate are also of significance for the LCOE. By lowering the turbine costs by 8% or reducing by half the availability loss rate, a reduction of up to 3% of the LCOE is achievable. The lifetime has also a significant influence. By extending the lifetime by 12%, the LCOE can be lowered by 2.7% because of the higher energy production. In case of a further expansion of the lifetime, investments would be required such as wind turbine component replacements that would negatively affect the LCOE. Besides that, the mooring system and floating substructure have been designed to a lifetime of 25 years and would require, depending on the concept, a redesign. The maximum parameter variation of the offshore substation is assumed to be 20%, which results in a LCOE decrease of 1.5% to 1.6% among the different concepts. However, according to a study performed by ORE Catapult [186], it is more likely that the cost of the offshore substation will increase than decrease. A 20% higher cost would result, for example, in the case of the Semi-submersible concrete floating wind turbine concept to a 1.5% increase of the LCOE.

Since the substructure cost represents a larger part of the CAPEX, it has also a significant influence on the LCOE. For instance, for the floating wind farm based on the Semi-submersible Concrete concept, a 20% cost reduction in the substructures can result into a 5% decrease of the LCOE value. Furthermore, it can be seen that based on the defined variation ranges for the cost of anchor and mooring as well as the power cables, a variation of the LCOE is not very significant (below 1%).

Table 5.9: LCOE variation (%) based on change of individually defined parameters.

Site	Concept / Parameter Variation	Semi-submersible Concrete LCOE % *(Parameter %)*	Semi-submersible Concrete LCOE % *(Parameter %)*	TLP Steel LCOE % *(Parameter %)*	TLP Steel LCOE % *(Parameter %)*	Spar Concrete LCOE % *(Parameter %)*	Spar Concrete LCOE % *(Parameter %)*
Golfe de Fos	Discount rate	-13.5 *(-20)*	+14.1 *(+20)*	-13.1 *(-20)*	+13.8 *(+20)*		
	Turbine cost	-3.1 *(-8)*	+6.2 *(+15)*	-3.4 *(-8)*	+6.2 *(+15)*		
	Substructure cost	-5.0 *(-20)*	+5.0 *(+20)*	0.0 *(0)*	0.0 *(0)*		
	Anchor cost	-0.1 *(-10)*	+0.1 *(+10)*	0.0 *(0)*	0.0 *(0)*		
	Mooring cost	-0.3 *(-10)*	+0.3 *(+10)*	0.0 *(0)*	0.0 *(0)*		
	Substation cost	-1.5 *(-20)*	+1.5 *(+20)*	-1.6 *(-20)*	+1.6 *(+20)*		
	Energy production	+5.3 *(-5)*	-4.8 *(+5)*	+5.2 *(-5)*	-4.7 *(+5)*		
	Availability loss	-2.6 *(-50)*	+2.7 *(+50)*	-2.6 *(-50)*	+2.7 *(+50)*		
	Turbine elec.loss	-1.1 *(-17)*	+1.1 *(+17)*	-1.1 *(-17)*	+1.1 *(+17)*		
	Export cable cost	-0.5 *(-17)*	+0.5 *(+17)*	-0.5 *(-17)*	+0.5 *(+17)*		
	Export cable length	-0.4 *(-10)*	+0.4 *(+8)*	-0.4 *(-10)*	+0.3 *(+8)*		
	Inter-array length	-2.0 *(-31)*	+0.9 *(+15)*	-1.3 *(-31)*	+0.6 *(+15)*		
	Inter-array cost	-0.7 *(-15)*	+0.7 *(+15)*	0.0 *(0)*	0.0 *(0)*		
	Instal.vessel day rate	-0.6 *(-30)*	+0.4 *(+20)*	-0.4 *(-7)*	+0.4 *(+7)*		
	Corr.maint.failure rate	-0.5 *(-20)*	+0.5 *(+20)*	-0.5 *(-20)*	+0.5 *(+20)*		
	Prev.maint.activities	-0.5 *(-20)*	+0.5 *(+20)*	-0.5 *(-20)*	+0.5 *(+20)*		
	Lifetime	+3.0 *(-12)*	-2.7 *(+12)*	+3.0 *(-12)*	-2.7 *(+12)*		
Gulf of Maine	Discount rate	-13.3 *(-20)*	+14.0 *(+20)*	-13.1 *(-20)*	+13.8 *(+20)*	-12.8 *(-20)*	+13.5 *(+20)*
	Turbine cost	-2.9 *(-8)*	+5.8 *(+15)*	-3.0 *(-8)*	+5.9 *(+15)*	-3.3 *(-8)*	+6.7 *(+15)*
	Substructure cost	-4.6 *(-20)*	+4.6 *(+20)*	0.0 *(0)*	0.0 *(0)*	-0.9 *(-9)*	+2.3 *(+22)*
	Anchor cost	-0.1 *(-10)*	+0.1 *(+10)*	0.0 *(0)*	0.0 *(0)*	-0.9 *(-50)*	+0.9 *(+50)*
	Mooring cost	-0.4 *(-10)*	+0.4 *(+10)*	0.0 *(0)*	0.0 *(0)*	-1.8 *(-20)*	+2.7 *(+30)*
	Substation cost	-1.5 *(-20)*	+1.5 *(+20)*	-1.5 *(-20)*	+1.5 *(+20)*	-1.7 *(-20)*	+1.7 *(+20)*
	Energy production	+5.3 *(-5)*	-4.8 *(+5)*	+5.2 *(-5)*	-4.7 *(+5)*	+5.3 *(-5)*	-4.8 *(+5)*
	Availability loss	-3.1 *(-50)*	+3.3 *(+50)*	-3.1 *(-50)*	+3.3 *(+50)*	-3.1 *(-50)*	+3.3 *(+50)*
	Turbine elec.loss	-1.1 *(-17)*	+1.1 *(+17)*	-1.1 *(-17)*	+1.1 *(+17)*	-1.1 *(-17)*	+1.1 *(+17)*
	Export cable cost	-0.8 *(-17)*	+0.8 *(+17)*	-0.8 *(-17)*	+0.8 *(+17)*	-0.8 *(-17)*	+0.8 *(+17)*
	Export cable length	-0.8 *(-11)*	+1.0 *(+12)*	-0.8 *(-11)*	+0.9 *(+12)*	-0.7 *(-11)*	+0.8 *(+12)*
	Inter-array length	-2.0 *(-31)*	+0.7 *(+12)*	-1.2 *(-31)*	+0.5 *(+12)*	-2.0 *(-31)*	+0.7 *(+12)*
	Inter-array cost	-0.7 *(-15)*	+0.7 *(+15)*	0.0 *0)*	0.0 *(0)*	-0.8 *(-20)*	+0.8 *(+20)*
	Instal.vessel day rate	-0.6 *(-30)*	+0.4 *(+20)*	-0.4 *(-7)*	+0.4 *(+7)*	-0.3 *(-15)*	+1.0 *(+50)*
	Corr.maint.failure rate	-0.4 *(-20)*	+0.4 *(+20)*	-0.4 *(-20)*	+0.4 *(+20)*	-0.5 *(-20)*	+0.5 *(+20)*
	Prev.maint.activities	-1.0 *(-20)*	+1.0 *(+20)*	-1.0 *(-20)*	+1.0 *(+20)*	-1.1 *(-20)*	+1.1 *(+20)*
	Lifetime	+3.0 *(-12)*	-2.7 *(+12)*	+3.0 *(-12)*	-2.7 *(+12)*	+3.0 *(-12)*	-2.7 *(+12)*
West of Barra	Discount rate	-12.3 *(-20)*	+12.9 *(+20)*	-12.1 *(-20)*	+12.7 *(+20)*	-11.8 *(-20)*	+12.4 *(+20)*
	Turbine cost	-2.1 *(-8)*	+4.2 *(+15)*	-2.1 *(-8)*	+4.3 *(+15)*	-2.4 *(-8)*	+4.7 *(+15)*
	Substructure cost	-3.7 *(-20)*	+3.7 *(+20)*	0.0 *(0)*	0.0 *(0)*	-0.7 *(-9)*	+1.8 *(+22)*
	Anchor cost	-0.1 *(-10)*	+0.1 *(+10)*	0.0 *(0)*	0.0 *(0)*	-0.9 *(-50)*	+0.9 *(+50)*
	Mooring cost	-0.6 *(-10)*	+0.6 *(+10)*	0.0 *(0)*	0.0 *(0)*	-1.6 *(-20)*	+2.5 *(+30)*
	Substation cost	-1.1 *(-20)*	+1.1 *(+20)*	-1.1 *(-20)*	+1.1 *(+20)*	-1.2 *(-20)*	+1.2 *(+20)*
	Energy production	+5.3 *(-5)*	-4.8 *(+5)*	+5.2 *(-5)*	-4.7 *(+5)*	+5.3 *(-5)*	-4.8 *(+5)*
	Availability loss	-4.1 *(-50)*	+4.6 *(+50)*	-4.2 *(-50)*	+4.6 *(+50)*	-4.1 *(-50)*	+4.6 *(+50)*
	Turbine elec.loss	-1.2 *(-17)*	+1.2 *(+17)*	-1.2 *(-17)*	+1.2 *(+17)*	-1.2 *(-17)*	+1.2 *(+17)*
	Export cable cost	-2.0 *(-17)*	+2.0 *(+17)*	-1.9 *(-17)*	+1.9 *(+17)*	-2.2 *(-17)*	+2.2 *(+17)*
	Export cable length	-2.2 *(-4)*	+1.0 *(+2)*	-1.9 *(-4)*	+0.9 *(+2)*	-2.2 *(-4)*	+1.0 *(+2)*
	Inter-array length	-1.6 *(-34)*	+0.8 *(+18)*	-0.9 *(-34)*	+0.5 *(+18)*	-1.8 *(-34)*	+1.0 *(+18)*
	Inter-array cost	-0.5 *(-15)*	+0.5 *(+15)*	0.0 *(0)*	0.0 *(0)*	-0.6 *(-20)*	+0.6 *(+20)*
	Instal.vessel day rate	-0.6 *(-30)*	+0.4 *(+20)*	-0.7 *(-7)*	+0.7 *(+7)*	-0.3 *(-15)*	+0.8 *(+50)*
	Corr.maint.failure rate	-0.3 *(-20)*	+0.3 *(+20)*	-0.4 *(-20)*	+0.4 *(+20)*	-0.4 *(-20)*	+0.4 *(+20)*
	Prev.maint.activities	-1.2 *(-20)*	+1.2 *(+20)*	-1.3 *(-20)*	+1.3 *(+20)*	-1.4 *(-20)*	+1.4 *(+20)*
	Lifetime	+2.8 *(-12)*	-2.5 *(+12)*	+2.8 *(-12)*	-2.5 *(+12)*	+2.7 *(-12)*	-2.5 *(+12)*

Gulf of Maine shows similar results for the common parameters as the site Golfe de Fos, since the general site characteristics and consequently the common components are not significantly different. The discount rate, for example, has by far the highest effect on the LCOE value. By a decline of 20%, a reduction of the LCOE of more than 13% can be achieved for all FOWT concepts. The parameters offshore substation and turbine cost, as well as turbine availability, energy production and lifetime show similar variation ranges as in Golfe de Fos. However, some differences are observable. For instance, for the Semi-submersible Concrete concept the substructure cost possesses a larger parameter variation and consequently a larger influence on the LCOE than for the other concepts. A 20% variation of the substructure cost can lead to a 4.6% increase or decrease of the LCOE. The Spar concept, on the other hand, is less sensitive to the substructure cost. The maximum variation ranges supposed by the concept designer are -9% and +22%, but cause only a decrease of -0.9% and increase of 2.3%, respectively. The cost of the anchor and mooring system shows only a larger importance for the Spar Concrete concept, which is mainly based on the higher cost of the system for this design and the perception of the concept designer for the uncertainty in the costs. A parameter variation of -20% and +30% is assumed for the mooring cost of the Spar Concrete concept, which results in a LCOE decline of -1.8% and an increase of 2.7%, respectively. The parameters that possess a low influence on the LCOE (below 1%) for this offshore site are corrective maintenance failure rate, inter-array cable and export cable cost.

For the offshore site West of Barra the most predominant parameters are the the discount rate, substructure cost, availability rate and offshore substation cost as well as lifetime and energy production. However, the effect of some parameters has slightly diminished while other parameters have increased their impact on the LCOE compared to the previous discussed offshore sites. For instance, by lowering the turbine costs by 8% a LCOE reduction of around 2.1% to 2.4% is achievable. This is lower compared to the other two offshore sites, where a LCOE reduction of more than 3% was reached. The case of West of Barra shows also a lower share of turbine and substructure cost in reference to the total capital cost since the prices in other components are increased. Furthermore, it can be seen that the Semi-submersible Concrete concept has the larger LCOE variation based on the provided uncertainty values. Regarding the turbine availability, a reduction by half of the rate results in a decline of more than 4% of the LCOE for all three floating wind turbine concepts.

Based on the larger distance to shore at this particular site, the parameters that are related to the distance have a larger influence on the LCOE than in the previous cases. For instance, by reducing the export cable length by 4% or the export cable cost by 17%, a reduction of the LCOE of more than 2% can be reached. The preventive maintenance activities show also a larger influence for this offshore site with a cost reduction potential of up to 1.3%, whereas in the previous sites the influence was 1% or lower. Concerning the inter-array cable cost, no significant influence on the LCOE has been observed based on the defined parameter variations in all three offshore sites. For instance, for the Spar Concrete concept a 20% variation in cable cost would result only in an 0.6% increase or decrease of the LCOE. On the other hand, a 34% shorter inter-array power cable would cause a 1.8% LCOE decline. However, a reduction of the cable length would require further modification of the system design such as the mooring configuration and the wind farm layout. Next, Figure 5.17 demonstrates the potential minimum and maximum LCOE limits for the parameters with the defined variation ranges.

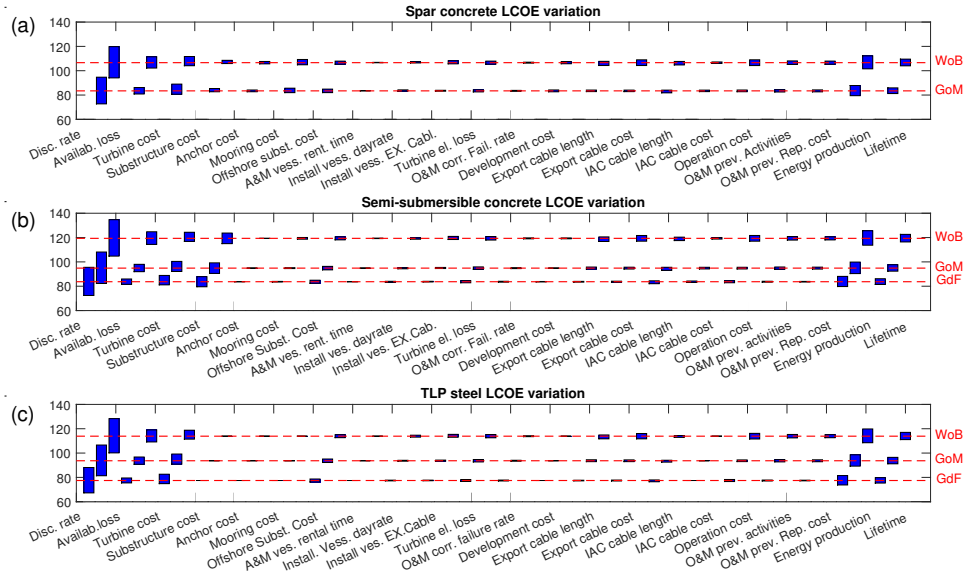

Figure 5.17: LCOE variation based on defined parameters for (a) Semi-submersible concrete concept, (b) TLP steel concept and (c) Spar concrete concept.

The upper bars in Figure 5.17 represent the LCOE variation for the offshore site West of Barra (WoB), the central bars represent the Gulf of Maine (GoM) and the lower bars in line Golfe de Fos (GdF). The LCOE values are shown including offshore transmission cost. The figure shows the parameters that have been identified as the most influencing ones on the LCOE and they are presented with their actual LCOE variation potential. For instance, it can be observed that the common parameters such as the turbine and offshore substation cost, as well as the energy related and financial parameters, i.e., availability loss, energy production, lifetime and discount rate, have the largest influence on the LCOE for all three floating wind turbine concepts. From the design dependent parameters the substructure component cost has by far the most influential factor on the LCOE value. However, for the Spar Concrete concept the mooring system is also a significant parameter. Besides that, the figures can serve to identify possible maximum and minimum LCOE values for the defined parameters. The Semi-submersible Concrete concept, for example, could reach based on the provided uncertainty ranges a LCOE as low as 72€/MWh or as high as 135€/MWh depending on the site. The LCOE of the TLP Steel concept, on the other hand, could drop as low as 67€/MWh or reach a maximum value of 128€/MWh. The Spar Concrete concept possesses LCOE values ranging between 72€/MWh and 119€/MWh. However, it should be noted that these values are based only on the variation of one parameter the discount rate and, therefore, are not directly design dependent. In contrast, if the substructure component cost is considered solely one can see that the parameter variation would cause for the Semi-submersible Concrete FOWT concept a minimum LCOE of 72€/MWh and a maximum of 124€/MWh. For the Spar Concrete concept possible LCOE values would be as low as 83€/MWh and as high as 109€/MWh considering only the parameter variation of the substructure component cost. It should also be noted that in this cost estimation no cost reductions based on economies of scale or a large scale employment of the technology are considered.

5.6 Conclusion of the chapter

In this chapter, three floating offshore wind turbine concepts have been studied, located at three different sites and considering a 500MW floating offshore wind farm. At first, the LCOE values for the different FOWT concepts have been obtained. Afterwards, a sensitivity analysis has been conducted on 325 input parameters by considering a deterministic variation.

Finally, based on the uncertainty values provided by the concept designers, a complementary study has been performed to highlight actual LCOE variation limits for the different concepts and sites. The findings indicate that FOWTs are a high competitive solution and energy can be produced at an equal or lower LCOE compared to bottom-fixed offshore wind or ocean energy technologies. Several key parameters have been identified that have a significant influence on the LCOE and which can be essential for further cost reductions. For instance, the parameters that most vary the LCOE across all three concepts and offshore sites are manufacturing cost related, such as the cost of the wind turbine, substructure and mooring system. Thus, a cost optimized design involving all components of a FOWT is important and should be considered already in the early design stage. Floating wind specific construction and assembly facilities may also help to reduce costs especially in the manufacturing phase.

Steel as well as concrete floating substructures have been studied. The Spar Concrete FOWT has obtained one of the lowest manufacturing cost by combining the advantage of simple manufacturing processes with a low cost of concrete material, but the large draft of the Spar restricts the concept to offshore locations with water depths greater than 90m and requires more expensive offshore cranes for mating the turbine with the floating structure. The TLP Steel concept has obtained the lowest LCOE value in this study by having a light structure combined with tense mooring lines. However, the instability of the concept during transportation requires bespoke vessels or buoyancy collars as additional investment to the FOWT. Investigation on TLP designs that are self-stable in the towing process could potentially further reduce the LCOE. The low draft of the Semi-submersible Concrete concept provides a flexible application in both shallow and deep waters. The ability to float independently allows for a simple transportation, which reduces costs along the life cycle. However, the large surface structure results in comparably higher manufacturing costs.

The discount rate plays an important financial parameter since it has the highest influence on the LCOE. The further development of floating wind energy to a commercial technology and the reduction of financial and technological risks can allow to optimize this value. The power cable parameters have also shown a larger influence on the LCOE in the sensitivity analysis. The trend towards bigger turbines requires further development and verification of dynamic cables with higher power capacities and the corresponding electrical connectors. An advantage exists during installation because the cables can be installed before turbine installation, which allows the performance of parallel installation processes with a decreased installation time.

Parameters related to the decommissioning have a smaller influence on the LCOE due to the low share on the total LCC. Nevertheless, the decommissioning of FOWTs has the potential of cost savings in comparison to BOWTs. The cost savings are in particular true for FOWT concepts that do not require heavy lift vessels and can be towed back to shore by simple tug boats.

Regarding the end of life management, steel floating substructures could benefit from a greater recyclability, whereas concrete substructures may benefit from their longer lifetime and potential reuse. However, further investigation is required on the recyclability and reuse of offshore concrete structures. The offshore substation accounts for a larger portion of the capital cost and thus a variation in the costs has an important influence on the LCOE. Since only one floating substation prototype has been developed so far, further research is needed to study the mutual behavior of the floating substructures and substation in order to reduce technological risks and costs.

The metocean conditions at the different offshore sites possess a significant influence on the LCOE of FOWFs. For instance, West of Barra has increased severe conditions and requires a more robust substructure and higher specialized vessel spreads for installing the anchor and mooring system in reduced weather windows. Installation times could be decreased with higher experience in the sector once the technology reaches a commercial stage and following lessons learned. The maintenance cost, which is based on the failure rate and repair cost, shows also a larger influence for West of Barra. However, since only a few prototypes have been tested for a longer period so far, there is a large uncertainty involved in the assumption of the maintenance cost. A better understanding of the motions and loads acting on the components of FOWTs together with an increased testing period in offshore conditions can help to reduce the uncertainty and optimize costs. West of Barra is the most remote location among the offshore sites studied, which impacts the cost of the export cable and the resulting power losses as well as the transportation cost. Therefore, suitable offshore sites should be selected considering not only the best wind resources, but also the distance to shore and accessibility.

The floating offshore wind technology can be a commercially competitive solution and an excellent component in the energy mix in Europe. However, in order to reach the required cost reductions and economies of scale, a clear policy commitment and support mechanism are required. Funding of research programs and collaborative innovation programs can support the development of key components of the system that are essential for cost reductions.

Moreover, by acknowledging the potential and setting target values for FOWT installations, private investments are attracted that are required for the commercialization of the technology. Besides that, floating wind energy can take advantage of the cost reductions that are achieved in bottom-fixed offshore wind, since many areas of the supply chain are in common use.

6 Electrical layout optimization of floating offshore wind farms

6.1 Introduction

The cost of the electrical system of BOWFs can take up to 15% to 30% of the total investment in which the cost of cables takes a large portion [187]. For FOWFs the costs might be even higher since new technologies and installations procedures are applied. For instance, dynamic power cables are used that include additional buoyancy components and joints. Furthermore, floating substations are needed, which represent a crucial component of the electrical system. Besides that, commercial scale FOWFs will likely include wind turbines with power ratings ranging from 6MW to 12MW or more, which require dynamic power cables with higher voltage levels. Hence, it is desirable to optimize the electrical layout to obtain the most cost-effective solution. The electrical layout optimization is defined in this thesis as the determination of the optimal connection configuration of FOWTs by the use of power cables based on a pre-defined wind turbine placing. The locations of the offshore substation and the export cable are also considered. The electrical layout impacts both the energy yield and the costs. The energy yield of the wind farm takes into account the energy generation by each wind turbine and the losses appearing in the power cables.

The energy generation is based on the wind speed available at the location and is also impacted by the wake effect occurring within the wind farm. The costs are a function of the length and the configuration of the cable as well as the installation procedure [188]. The optimization methods applied in literature to this kind of problem can be classified in deterministic and metaheuristic methods. The deterministic approach has been used in [189–195]. A common approach for deterministic methods is to solve the cable routing optimization problem as a minimum spanning tree. However, it has been found that the computational time increases significantly with the amount of turbines. The problem becomes essentially complex to unsolvable as more turbines and, therefore, connections possibilities are added [188]. Besides that, as the power loss calculation is based on a nonlinear equation of the current flowing in the cable, the problem becomes more difficult to solve by, for instance, a mixed integer linear programming method [196]. Power losses have been included in [193–195], however, in order to solve the problem for a larger wind farm new constraints have been added to reduce the complexity of problem. For instance, in [195] the amount of possible cables entering a turbine has been reduced to one and in [193] the connection is restricted to the subsequent turbine in a row. Moreover, the stochastic characteristics of wind speed and direction are not taken into account.

Due to the complexity, a number of studies have investigated the use of metaheuristic methods [197–201] or a combination [188, 196, 202, 203]. Due to the nature of a heuristic model, the studies have therefore opted to a model that may not find a proven optimal solution but a feasible one in a reasonable time with very few constraints [188]. In [198] a genetic algorithm (GA) has been the metaheuristic method of choice and has been used to optimize the electrical system of an offshore wind farm considering the capital cost of the cables, energy production and availability of system components due to failures. However, a clustering of turbines has been considered to reduce the complexity and the wake effect is not taken into account. In [197] particle swarm optimization (PSO) model has been applied as well as a single wake model considered. However, the fluctuations in wind speed and wind direction have not been considered as well as no installation cost and reliability of the system. PSO possesses many similarities with evolutionary optimization methods such as GA but differs in the optimization algorithm, which is based on swarm intelligence. The implementation of PSO tends to be simpler with less parameters to adjust [204].

The previous work has addressed mainly the optimization of the electrical layout of BOWFs. The objective of this chapter is to solve the electrical layout problem of a FOWF by applying an adapted particle swarm optimization model. The complexity is increased by considering the stochasticity of wind speed and wind direction and taking into account the entire wind turbine connection possibilities. Besides that, a comprehensive wake model is included. Furthermore, dynamic power cables used for the connection of FOWTs are considered as well as their respective acquisition and installation costs. The availability assessment of the electrical components and the influence on the energy generation are also taken into account.

6.2 Floating Offshore Wind Farm Model

In this section, the FOWF model is described including the electrical system, wake effect model and the computation of the energy losses in the cables. Furthermore, the availability assessment due to failures is outlined.

6.2.1 Electrical system

The electrical system of an offshore wind farm includes the inter-array cables, offshore substation and the export cable as illustrated in Figure 6.1.

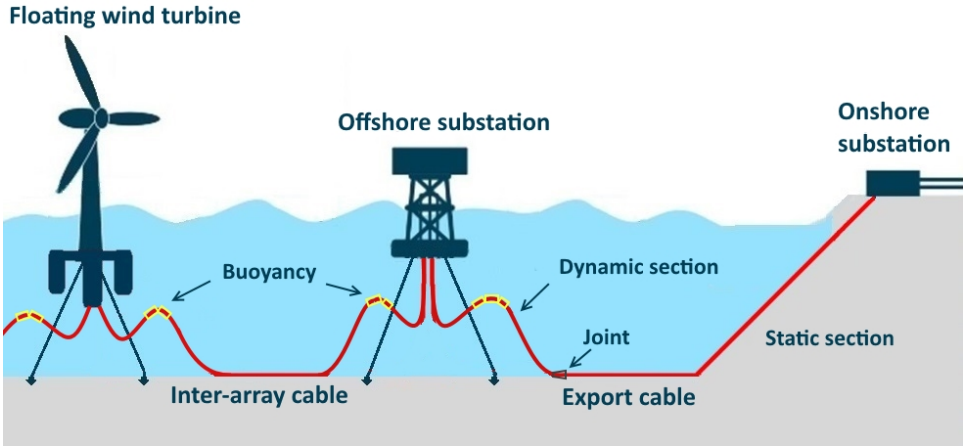

Figure 6.1: Electrical system of a floating offshore wind farm with a lazy wave dynamic cable configuration.

Inter-array cables are used to connect the FOWTs and to transmit the generated energy to the offshore substation. They are typically three-core copper conductors with steel wire armored and insolation components as shown in Figure 2.7. The nominal operating voltage of the inter-array cable system of current offshore wind farms is typically 33kV. However, with the development of larger wind turbines with higher power ratings, higher voltage levels are required such as 66kV [205]. The offshore substation is equipped with a transformer to increase the medium voltage of the collection grid to high voltage in order to reduce losses during transmission to the shore. In a floating offshore wind farm the topside of the substation is also mounted on a floating substructure. The export cable transmits the collected energy from the offshore to the onshore substation and may operate with HVAC or HVDC technology depending on the distance and power rating of the wind farm [205].

While power cables for BOWFs are buried under the seabed and connected to the structure by a J-tube or J-tubeless interface, the cables for FOWTs have a dynamic section that moves with the floating substructure [206]. The dynamic cable requires a high level of flexibility and mechanical strength in order to withstand the combined impacts of waves, currents, seabed interactions and floater motions [205]. Potential configurations of dynamic cables can be derived from offshore risers used in the oil and gas industry and include, e.g. lazy wave, steep wave, lazy S or other [207]. The lazy wave has been the preferred configuration in demonstration projects such as Hywind Scotland [208] and Fukushima [157] and is shown in Figure 6.1. This configuration applies buoyancy modules to reduce the load on the cable by providing mid-water suspension. In this way, the substructure motion is decoupled from the cable touchdown at the seabed and the dynamic responses and tension of the cable are reduced [205]. A single dynamic cable can be used for a FOWT connection or a combination of static and dynamic cables. Static cables might be lower priced, but a submarine joint is required to connect both cable types. Section 6.5.4 analyzes and compares the two connection options. The optimization of the electrical layout of FOWTs gains additional importance because the length of a power cable is increased due to the dynamic cable section, spatial requirements of the mooring system and the offset of the floating substructure. For BOWTs a common approach in literature is to simply calculate the geometric distance between wind turbines without considering the water depth [193, 197, 209]. The length of the power cable used for the connection of FOWTs can be obtained by

$$L_{\text{cable}} = 1.05 * D_{\text{FOWTs}} + 2 * (L_{\text{dynamic}} - D_{\text{x}}) \tag{6.1}$$

where D_{FOWTs} is the distance between FOWTs, $L_{dynamic}$ represents the length of the dynamic cable section and D_x accounts for the horizontal distance from the substructure to the touchdown point at the seabed. It is considered a 5% increase of the static part of the cable to allow for routing around the mooring system anchors. For the sack of clarity, the variables are illustrated in Figure 6.2

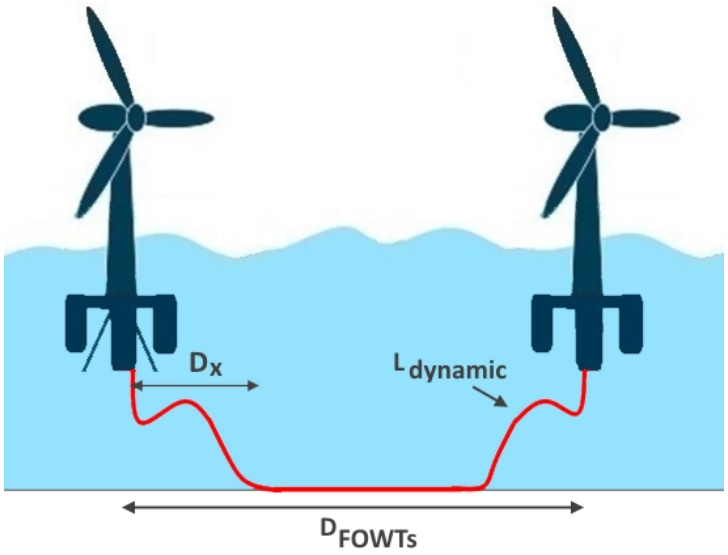

Figure 6.2: Power cable length illustration.

The length of the dynamic cable part can be determined by a segmentation into three catenary lines and calculating the arc length of each catenary assuming the curvature as a hyperbolic cosine function. The numerical modeling of deep sea risers has been widely discussed in marine engineering literature. For the computation of the lazy wave catenary riser length one may refer to [210].

6.2.2 Wake model

A comprehensive wake model has been included in the optimization model to calculate the wind speed v_{ws} for the power generation calculation at each FOWT. The wake model has been developed previously by De-Prada-Gil and has been applied for instance as part of a control strategy to maximize the energy yield of offshore wind farms [211]. The model considers single, partial and multiple wake effects among turbines. Besides that, it takes into

account the wind direction of the free-stream wind speed. Furthermore, global momentum conservation in the wake downstream of the wind turbine is considered as well as an linear expansion of the wake downstream. However, turbulent behavior caused by wakes is neglected. The model is based on the wake concept developed by Jensen [212], which is a well-known and widely applied model that provides adequate accuracy with a reduced computational time. A detailed description of the applied model is provided in [55]. For the sake of completeness, an outline of the methodology is presented next.

- Single wake:
  The downstream wind speed of a single turbine is described as

$$v_2 = v_1 \left[1 - (\frac{D_{\text{rotor}}}{D_{\text{rotor}} + 2 * k_{\text{wake}} * x})^2 * (1 - \sqrt{1 - C_{\text{t}}})\right] \tag{6.2}$$

  where v_2 is the wind speed at distance x from the FOWT, D_{rotor} is the diameter of the turbine rotor, C_t is the thrust coefficient, v_1 is the free-stream wind and k_{wake} is the wake decay constant [212].

- Partial wake:
  Partial wake is a phenomenon which occurs when one or more wind turbines cast a single shadow on a downstream turbine. The wind speed entering into the turbine m affected by the upstream wind turbine n is then given by [213]

$$v_{\text{m}} = v_1 \left(1 - \sqrt{\sum_{n=1}^{N} \beta_{\text{T}_\text{m},\text{T}_\text{n}} * (1 - \frac{v_{\text{T}_\text{n}}}{v_1})}\right), \tag{6.3}$$

  where v_m is the wind speed of the downstream turbine m. v_1 is the initial wind speed entering into the wind turbine n. v_{T_n} is the shadow of n falling on the mth wind turbine and β_{T_m,T_n} is the ratio of the shadow area by the wake to the total rotor area.

- Multiple wakes:
  In a wind farm with a large number of turbines, a single wind turbine can be affected by several wakes. The multiple wake model takes this effect into account. It assumes that the kinetic energy deficit of interacting wakes is equal to the sum of the energy deficits of the individual wakes [55]. Thus, the velocity at the intersection of several wakes can be determined by [214]

$$1 - \frac{v_{\mathrm{x}}}{v_1} = \sqrt{\sum_{n=1}^{N} (1 - \frac{v_{\mathrm{n}}}{v_1})^2}, \tag{6.4}$$

where v_1 is the initial free-stream velocity, N is the total number of upstream influencing turbines, v_n is the wind speed affected by the individual wake n and v_x is the wind speed such that all the wakes are taken into account [211]. Figure 6.3 illustrates multiple wakes occurring in an offshore wind farm for a specific wind direction.

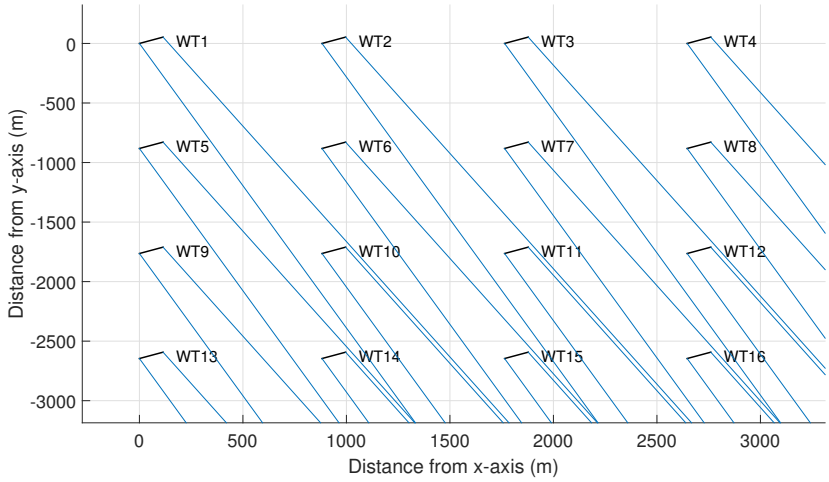

Figure 6.3: Multiple wakes in an offshore wind farm for 25° wind direction.

6.2.3 Energy loss computation

The power generated by a wind turbine can be calculated as follows

$$P_{\mathrm{gen}} = \frac{1}{2}\ \rho_{\mathrm{a}}\ A_{\mathrm{rotor}}\ C_{\mathrm{p}}(\lambda, \beta)\ {v_{\mathrm{ws}}}^3 \tag{6.5}$$

where A_{rotor} accounts for the rotor swept area and ρ_a for the density of air. C_p is the power coefficient and v_{wind} represents the wind speed at hub height. The power coefficient depends on the blade tip-speed ratio λ and the blade pitch angle β [79]. The power loss in any power cable of the FOWF can be determined by

$$P_{\text{loss}} = 3(\frac{P_{\text{gen}} + P_{\text{trans}}}{\sqrt{3} * U})^2 * R_{\text{cable}} * L_{\text{cable}} \tag{6.6}$$

where P_{gen} is the power generated by the FOWT from which the cables exists. P_{trans} represents the power that has been transmitted to this FOWT from another wind turbine. U is the voltage applied, for example, medium voltage for inter-array cables and high voltage for the export cable. The resistance of the power cable is represented by R_{cable} and L_{cable} defines the length of the cable. The energy loss can, finally, be obtained by

$$E_{\text{loss}} = \sum_{v_{\text{min}}}^{v_{\text{max}}} \sum_{0^\circ}^{360^\circ} P_{\text{loss}} * H_{\text{ws}} * H_{\text{wd}} * T \tag{6.7}$$

where T is the expected lifetime of the FOWF. Wind speed and wind direction are included as stochastic variables. The occurrence probabilities of wind speed and wind direction are defined by H_{ws} and H_{wd}, respectively. The total energy losses are obtained as the sum of energy losses according to different wind speeds and wind directions.

6.2.4 Availability assessment

Certain components of the electrical infrastructure of an offshore wind farm may fail and interrupt partially or completely the energy generation. These unexpected losses due to unforseen equipment failures are very important in offshore wind farms since severe weather conditions can lead to a long downtime for maintenance [55]. The resulting energy losses are defined as expected energy not supplied (EENS) and the calculation of these losses is based on reliability multi-state models as explained in detail in [215]. The models consider that each component has several states of service with a respective probability of occurrence. In this study, the availability assessment is carried out for the inter-array cables connecting to the offshore substation, the export cable as well as the transformers in the offshore substation. The states of operation are available and unavailable. The probability of being available is given by

$$A = \frac{MTBF}{MTBF + MTTR} = \frac{1}{1 + \lambda * MTTR} = \frac{\mu}{\mu + \lambda} \tag{6.8}$$

where $MTBF$ is the mean time between failure and $MTTR$ represents the mean time to repair with $MTBF{=}\lambda^{-1}$ and $MTTR{=}\mu^{-1}$. The failure rate of a component is defined by λ and the repair rate is μ [215, 216].

Consequently, the unavailability probability is expressed as *U=1-A* and the EENS can be obtained as

$$EENS = \sum_{k=1}^{n} {P_{\mathrm{k}}}^{\mathrm{cons}} * U_{\mathrm{k}} * T \tag{6.9}$$

where ${P_k}^{cons}$ is the power constrained or not delivered in each system state due to a failure. A system state is defined by a specific event, e.g., failure of power cable 1. Each system state is considered to have, at most, one component unavailable. The number of system states is defined by n [55, 193]. Similar to the calculation of EENS considers the unavailability rate, the computation of the energy losses takes into account the availability rate of the components.

6.3 Problem statement

6.3.1 Objective problem

The objective is to minimize the cost of the electrical layout considering the cost of acquisition $C_{aquisition}$, the installation cost $C_{installation}$ as well as the costs associated to the energy losses in the cables C_{loss} and the cost of EENS C_{EENS}. Therefore, the objective of this optimization problem can be stated for a single particle as

$$min(C_{\mathrm{acquisition}} + C_{\mathrm{installation}} + C_{\mathrm{loss}} + C_{\mathrm{EENS}}) \tag{6.10}$$

The acquisition cost takes into account the initial investment cost for the inter-array and export power cables as well as the transformer in the offshore substation. Furthermore, amortization is included considering the expected lifetime T of the FOWF as follows

$$\begin{aligned} C_{\mathrm{acquisition}} = \Big(\sum_{i=1}^{N_{\mathrm{iac}}} (C^i_{iac} * L^i_{iac} + C^i_{iac-aux}) + \sum_{j=1}^{N_{\mathrm{exc}}} (C^j_{exc} * L^j_{exc} + C^j_{exc-aux}) \\ + \sum_{l=1}^{N_{\mathrm{t}}} C^l_t \Big) * \Big(T \frac{i_{\mathrm{rate}}(1+i_{\mathrm{rate}})^{\mathrm{T}}}{(1+i_{\mathrm{rate}})^{\mathrm{T}} - 1} \Big) \end{aligned} \tag{6.11}$$

where C_{iac} represents the cost per meter of the inter-array cables and L_{iac} the length of the cables used to connect between the FOW turbines and the

offshore substation. Likewise, C_{exc} defines the cost of the export cable and L_{exc} the length of the export cable. The dynamic power cable requires auxiliary equipment such as buoyancies, bend stiffners and connectors, which cost is taken into account by $C_{iac\text{-}aux}$ and $C_{exc\text{-}aux}$, respectively. The cost of the transformer is given by C_t. The number of inter-array, export cables and transformers are defined by N_{iac}, N_{exc} and N_t, respectively. The interest rate used for the calculation of the amortization is defined by i_{rate}. The installation cost includes the cost for installing the power cables and is obtained as

$$C_{\text{installation}} = \Big((\sum_{i=1}^{N_{\text{iac}}} L_{iac}^{i} + \sum_{j=1}^{N_{\text{exc}}} L_{exc}^{j}) * C_{\text{vessel}} * r_{\text{instal}} + C_{\text{Mob/Demob}} \Big) * \Big(T \frac{i_{\text{rate}}(1+i_{\text{rate}})^{\text{T}}}{(1+i_{\text{rate}})^{\text{T}} - 1} \Big) \tag{6.12}$$

where C_{vessel} is the day rate of the cable laying vessel and r_{instal} represents the installation rate in days per meter. The mobilization and demobilization costs of the vessel are defined by $C_{Mob/Demob}$. The cost associated to the energy losses in the cables can be determined by

$$C_{\text{loss}} = (\sum_{1}^{N_{\text{iac}}} E_{loss-iac}^{i} + \sum_{1}^{N_{\text{exc}}} E_{loss-exc}^{i}) * C_{\text{energy}}, \tag{6.13}$$

where $Eloss_{iac}$ and $Eloss_{exc}$ are the energy losses in the inter-array and export cables, respectively. The energy losses have been defined previously by Equation 6.7. N_{iac} and N_{exc} are the number of inter-array and export cables. The total cost of energy losses is obtained as the sum of energy losses multiplied by the cost per unit of energy C_{energy}. The cost of EENS can be obtained as follows.

$$C_{\text{EENS}} = T \sum_{k=1}^{n} {P_{\text{k}}}^{\text{cons}} * U_{\text{k}} * C_{\text{energy}} \tag{6.14}$$

6.3.2 Constraints

The optimization model includes several constraints that have to be satisfied in order to count as a suitable solution.

- The energy leaving a turbine must be supported by a single cable.
- A maximum of one cable can be placed between two turbines.
- The crossing of power cables is not allowed due to potential damages.
- The building of a closed loop connection is not allowed, which is a connection between several FOWTs that does not end in the offshore substation.
- The power transmitted by a cable cannot exceed the capacity of the installed cable.

6.4 Numerical Optimization Model

6.4.1 Particle swarm optimization algorithm

PSO is a population-based metaheuristic optimization algorithm that has been chosen due to its simplicity and high computational efficiency in solving non-linear complex problems [202]. In PSO, a possible solution is defined as a particle and is randomly initialized at the beginning. Each particle has its own position vector $x_{\mathrm{j}} = (x_{\mathrm{j1}}, x_{\mathrm{j2}}, ..., x_{\mathrm{jd}})$ and velocity vector $v_{\mathrm{j}} = (v_{\mathrm{j1}}, v_{\mathrm{j2}}, .., v_{\mathrm{jd}})$, where j refers to the number of particles and d to the amount of dimensions [217]. A set of particles is called population and moves around in a multi-dimensional search space. The velocity and position of the particles are updated every iteration k according to Equations 6.15 and 6.16 in order to move the particles through the search space to find new and better solutions. Similar to how a bird of a swarm reconfigures its behavior based on its own experience and the experience of the rest of the birds, each particle updates its position based on its personal best solution *Pbest* found so far, the global best solution *Gbest* found by all particles and according to its velocity of the subsequent iteration $\mathrm{v_j}^{\mathrm{k+1}}$ [217].

$$v_{\mathrm{j}}^{\mathrm{k+1}} = w^{\mathrm{k}} * v_{\mathrm{j}}^{\mathrm{k}} + c_1 * r_1 * (Pbest_{\mathrm{j}}^{\mathrm{k}} - x_{\mathrm{j}}^{\mathrm{k}}) + c_2 * r_2 * (Gbest_{\mathrm{j}}^{\mathrm{k}} - x_{\mathrm{j}}^{\mathrm{k}}) \quad (6.15)$$

$$x_{\mathrm{j}}^{\mathrm{k+1}} = x_{\mathrm{j}}^{\mathrm{k}} + v_{\mathrm{j}}^{\mathrm{k+1}} \quad (6.16)$$

w^k represents the inertia weight. c_1 and c_2 are positive constants and r_1 and r_2 are randomly distributed numbers in the range from zero to one [218].

The first term of Equation 6.15 is called inertia and ensures that the particle moves in its path and does not change too abruptly. The second represents the memory of a particle and ensures that it moves towards its personal best solution (*Pbest*). The last term includes the cooperation and attracts the particle to a global best solution (*Gbest*), which is the one found by all particles [217]. The inertia weight changes with the iterations and can be determined as follows

$$w^{\mathrm{k}} = w_{\max} - \frac{w_{\max} - w_{\min}}{k_{\max}} * k \tag{6.17}$$

where w_{max} and w_{min} are the maximum and minimum inertia coefficients and k_{max} represents the maximum number of iterations [219]. The PSO algorithm updates within an iteration loop the particles position, velocity and *Pbest* as well as *Gbest* until convergence is obtained or a maximum number of iterations is reached [209].

6.4.2 Model implementation

The optimization model, based on PSO theory, has been implemented using MATLAB programming language and has been adapted in order to solve the collection grid optimization problem. The model has been developed as part of the tool FOWAT (Floating Offshore Wind Assessment Tool), which has been created originally in the H2020 LIFES50+ project to assess both economically and technically floating offshore wind farms [106]. The algorithm of the optimization model is illustrated in Figure 6.4.

The developed PSO model initializes with the definition of the main parameters and information about the wind farm layout such as the location of the wind turbines. Afterwards, an initial population is created consisting of particles with a three-dimensional position matrix.

$$x(a, 4, b), a \in \{1, 2, ..., N_{\mathrm{wt}}\}, b \in \{1, 2, ..., j\} \tag{6.18}$$

where $\mathrm{N_{wt}}$ is the number of FOWTs and j the number of particles. In the second dimension of the matrix four types of essential information are saved, which are represented by the parameter 4. This information includes the type of cable used for a connection, the two turbines connected by a cable and the power transmitted. After the initialization, each particle is checked if it provides a feasible solution to the problem by complying with a set of pre-defined constraints. In case a particle does not comply with a specific constraint, the model reallocates the connection of the FOWTs until the constraint is satisfied.

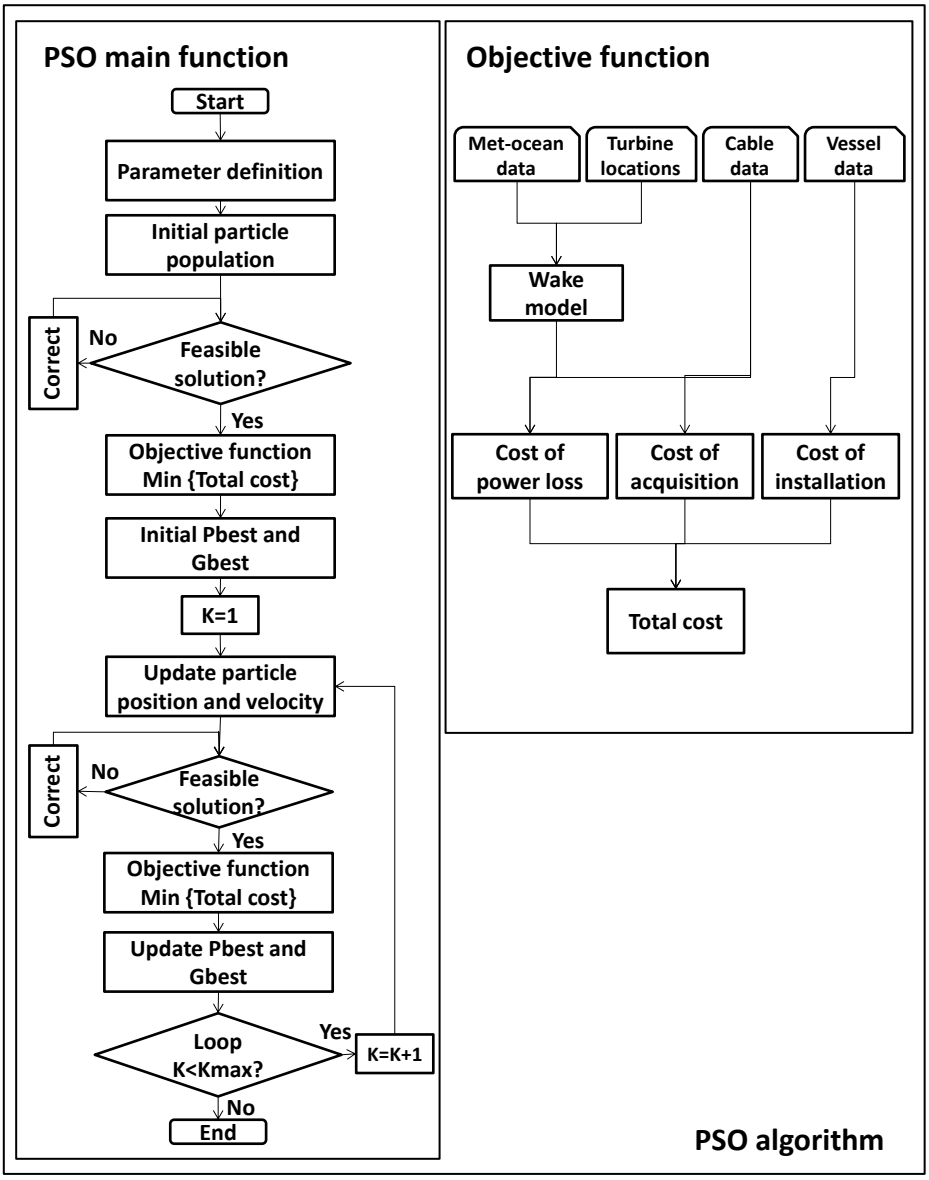

Figure 6.4: PSO algorithm applied.

The constraints presented in Section 6.3.2 are included in the optimization model. When the feasibility of all particles is ensured, the population is searched for the best solution. This can be mathematically described by

the minimization of a function, called objective function. This subroutine computes the costs of each particle's solution and determines the one with the lowest total cost, which is then proposed as the initial *Pbest* and *Gbest*. The computation of the objective function is based on the methodology presented in Section 6.3.1. In the next step, the PSO algorithm updates the position and velocity of all particles according to Equations 6.15 and 6.16 and enters into a loop until a maximum number of iterations is reached. At each iteration the feasibility of the particles is checked as well as *Pbest* and *Gbest* updated by using the objective function.

6.5 Application

6.5.1 Validation case

At first, the developed optimization model is validated against an existing model used in [193]. In [193] the electrical layout of the Barrow BOWF was optimized by the use of a mixed integer quadratic constraint programming (MIQCP) method. Several constraints and restrictions were included in order to reduce the complexity of the problem. However, these constraints cause the solution to be less realistic. For instance, cable crossing was allowed, which is not recommended in practice due to potential cable damages [196]. Furthermore, wake effect as well as wind direction were not considered and the range of wind speeds was reduced to 5 scenarios with corresponding power generations. Besides that, the wind turbine connection possibilities were restricted to the adjacent wind turbine of its row and no installation costs were taken into account. In order to validate and compare the developed PSO model, a simplified version is created containing the before mentioned constraints. At first, the simplified model is used to solve the optimization problem and the results are compared with the reference. Then, the full PSO model is applied to search for a more realistic solution. The power cable information used as input data for this case study is presented in Table 6.1.

The Barrow BOWF consists of 30 wind turbines with each having a rated capacity of 3MW. The collection grid is operated at 33kV and the export cable transmits the energy at 132kV. Two possible locations are considered for the offshore substation as shown in Figure 6.5. Furthermore, two different transformer capacities (60MVA and 120MVA) are considered with respective costs and availability values. A complete description of the case study and the input data is provided in [193].

Table 6.1: Power cable information [193, 220].

	Inter-array 33kV			Export 132kV	
Cross section (mm^2)	95	120	300	400	630
Power capacity (MW)	17.9	19.43	30.29	134.89	163.47
Resistance (Ω/km)	0.246	0.196	0.079	0.063	0.042
Cable cost (€/m)	210	258	354	450	578
Failure rate (failures/km)	0.149	0.149	0.149	0.179	0.179
Repair rate (total repairs/lifetime)	912.5	912.5	912.5	347.6	347.6

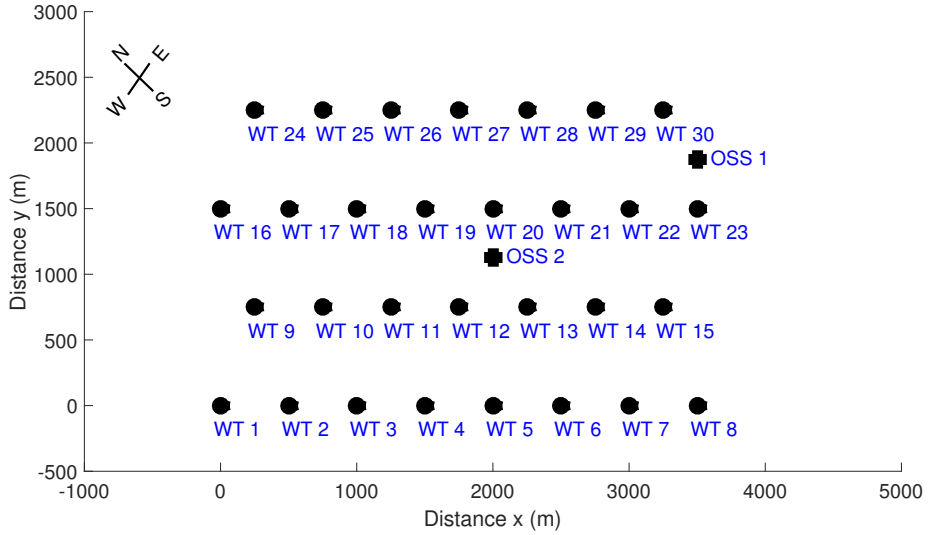

Figure 6.5: Wind turbine (WT) placements and offshore substation (OSS) locations at Barrow offshore wind farm.

The simplified PSO model is applied on the Barrow BOWF. The number of particles is set to 10 and 20 iterations are considered. The cable routing layout obtained from solving the optimization problem is presented in Figure 6.6. As expected the optimization model has obtained a cable routing where the turbines are connected in a straight row due to the constraint to connect to adjacent wind turbines. The model has selected offshore substation 1, because costs and energy losses are reduced since less cable length of the more expensive export cable is used. Despite 2 smaller transformers are slightly more expensive than a single larger transformer, the optimization

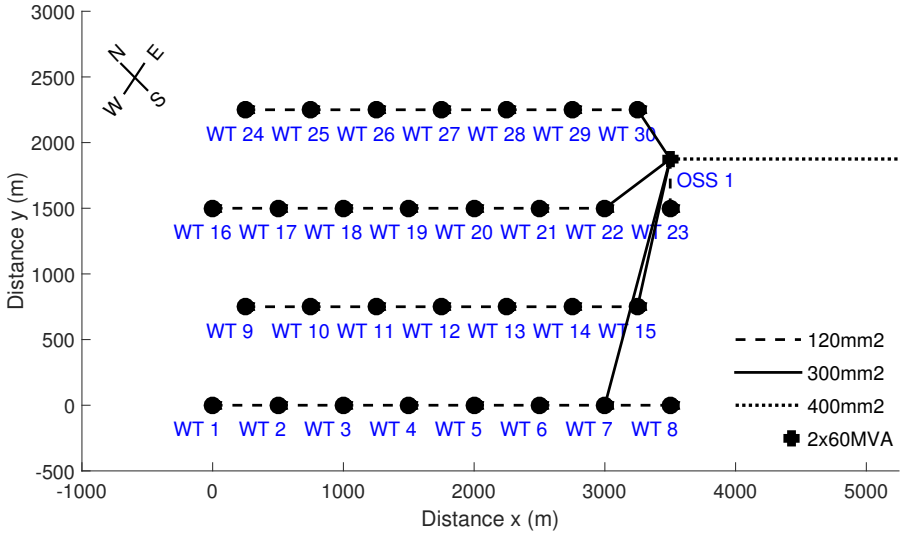

Figure 6.6: Optimized layout obtained from simplified PSO model.

model has chosen to install 2 units of each having 60MVA. This is mainly based on the lower costs of EENS due to failure of the transformers. In case a single large transformer fails, all the power generated by the wind farm would be lost and when a smaller transformer fails still half of the total power can be served. The electrical layout obtained by the simplified PSO model equals the one obtained in [193]. Table 6.2 presents the costs for this collection grid layout and compares to the results obtained by the MIQCP model of the reference study.

Table 6.2: Comparison of costs.

	MIQCP [193]	Simplified PSO	Full PSO
Acquisition cost (M€)	25.23	25.23	24.71
Cost of EENS (M€)	5.29	6.39	6.36
Cost of energy loss (M€)	4.09	4.19	4.17
Total cost (M€)	34.61	35.81	35.24
Inter-array length (km)	17.04	17.04	16.60

The acquisition cost determined by the developed PSO model matches the value obtained by the MIQCP model. A slight difference is observable in the cost of EENS and the cost of energy losses, which is based on differ-

ences in the methodology to calculate the power losses and how the wind speed distribution is considered in the calculation of the energy production. Nevertheless, the PSO model has correctly obtained the optimized electrical layout of the reference study with the same turbine connections and the offshore substation selection. Hence, the developed PSO model is considered as validated. The computation time of the simplified PSO model has been 14 seconds using a Intel Core i5 processor with 2.53 GHz, 4 GB memory and Windows 7 operating system. In comparison, the MIQCP model requires 26 hours for the same optimization problem [193]. This demonstrates the high efficiency in solving complex problems by the developed PSO model. As it can be observed in Figure 6.6, a cable crosses the connection between wind turbine 14 and 15, which would not be a recommended practice in a real offshore wind farm. Therefore, the full PSO model is applied next on the case study to obtain a more realistic solution. The solution obtained by the full PSO model is presented in Figure 6.7.

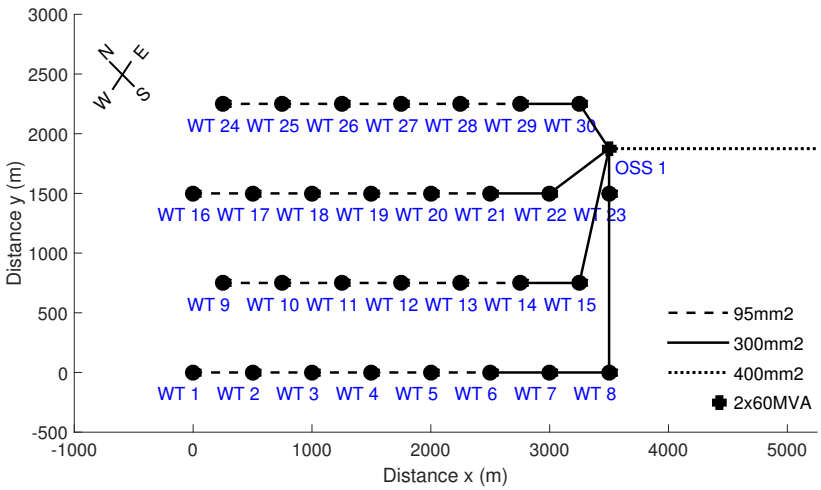

Figure 6.7: Optimized layout obtained from full PSO model.

It is observable that cable crossing is avoided. Furthermore, the model has chosen to use a smaller cable cross section for the first 5 wind turbines in a row, which allows to reduce the cost of cable acquisition by 2% as presented in Table 6.2. In addition, the optimized layout has provided a reduction of the total length of inter-array cables by about 2.6%, which causes both a decrease in acquisition costs and energy losses.

6.5.2 Floating offshore wind case study

A 500MW FOWF has been considered for the application of the optimization model to the case of floating offshore wind. It consists of 50 FOWTs with each having a rated power capacity of 10MW. The DTU 10MW reference wind turbine has been considered and related specifications are given in [84]. Golfe de Fos has been chosen as offshore site. It is located in the south of France in the Mediterranean Sea. The reference water depth is about 70m and the environmental conditions are moderate. The wind rose of the offshore site is presented in Figure 6.8 and shows how wind speed and wind direction are distributed at the location.

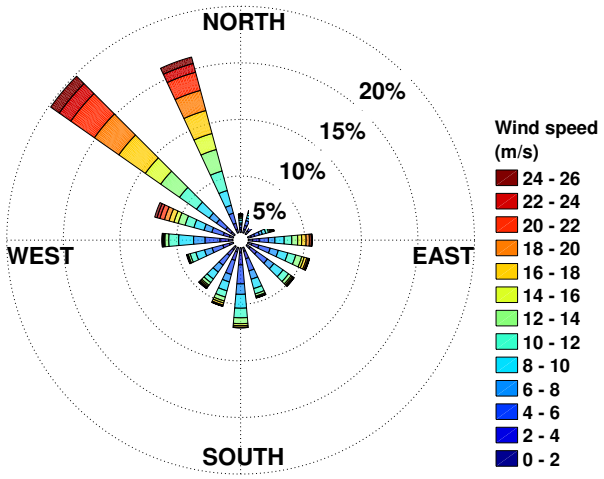

Figure 6.8: Wind speed and wind direction distribution at Golfe de Fos.

More information about the offshore site is provided in [122]. The collection grid of the FOWF is operated at 66kV and the transmission voltage is 220kV. Figure 6.9 presents the FOWF and the electrical layout. The FOWTs are placed in direction to the prevailing winds. The offshore substation is located to the east of the FOWF. The present layout is based on work performed in the LIFES50+ project [14]. The objective is to optimize the inter-array cable layout by applying the developed PSO model.

The offshore substation and export cable are not taken into account in the optimization. The power cable specifications and costs that are considered for the study are presented in Table 6.3. Additional parameters for the calculation of the installation cost and the availability are shown in Table 6.4.

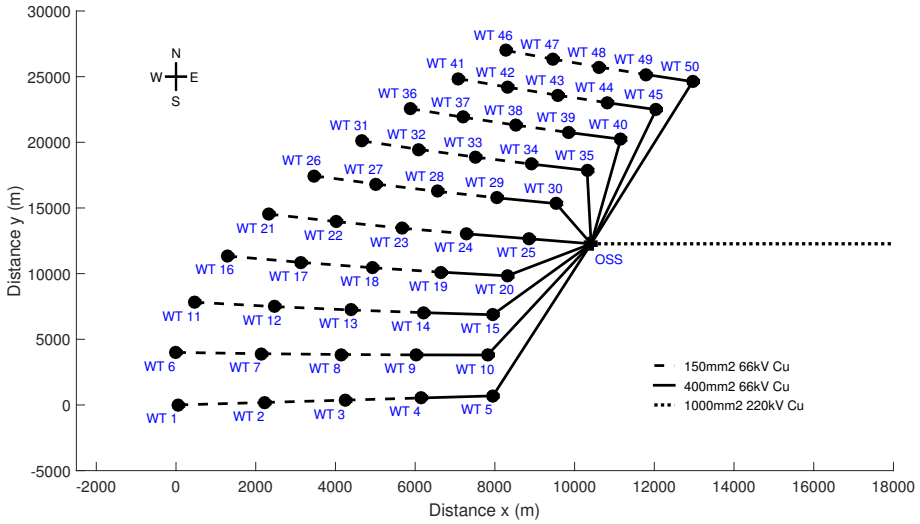

Figure 6.9: Golfe de Fos initial electrical layout.

Table 6.3: 66kV inter-array power cable information [221].

Cross section (mm^2)	95	150	300	400	630	800
Power capacity (MW)	23	30	40	50	63	71
Resistance (Ω/km)	0.25	0.16	0.08	0.06	0.04	0.03
Static cable cost (€/m)	219	300	423	474	554	689
Dynamic cable cost (€/m)	238	323	456	512	603	748
Buoyancy components (T€)	59	63	81	90	126	159
Stiffner and connectors (T€)	135	145	172	190	231	262

Table 6.4: Installation and availability parameters [221–223].

Installation rate (d/km)	1.5
Vessel day rate (€/d)	60,000
Vessel mobilization (€)	400,000
Vessel demobilization (€)	400,000
Submarine joints per WT connection (€)	200,000
66kV cable failure rate (failures/km/year)	0.0094
66kV cable mean time to repair (months)	2

The full optimization model is applied on the FOWF case. The number of particles is set to 15 and a total of 40 iterations is considered. The inter-array connection layout obtained from the optimization is presented in Figure 6.10.

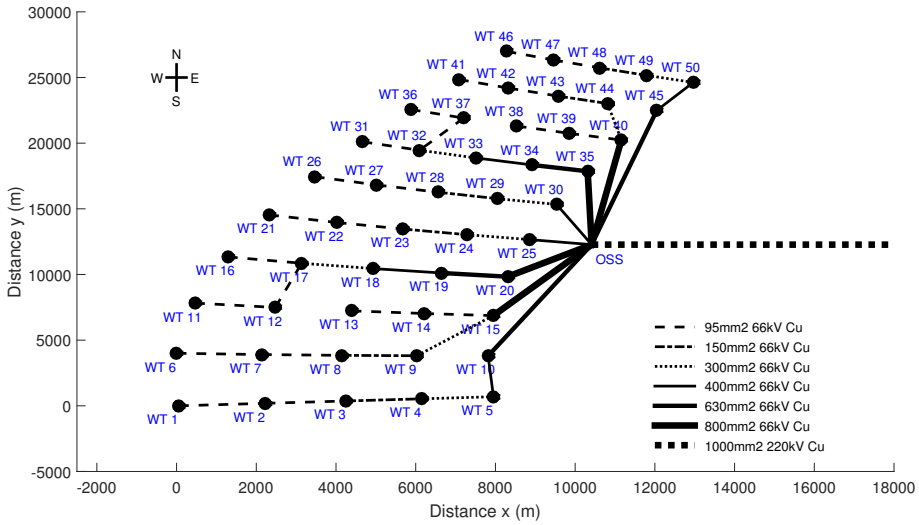

Figure 6.10: Golfe de Fos optimized collection grid.

The optimized collection grid is similar to the initial layout but some changes are observable. For instance, the number of FOWTs connected to the offshore substation has decreased from 10 to 8. Furthermore, there exist strings of cables where a higher number of FOWTs are connected. For example, a string of 7 FOWTs exists that requires the use of inter-array cables with larger cross sections up to 800mm^2.

Figure 6.11 presents the result for the total cost corresponding to each iteration of the optimization model. It can be seen that the optimization model obtains a final result and converges after 18 iterations.

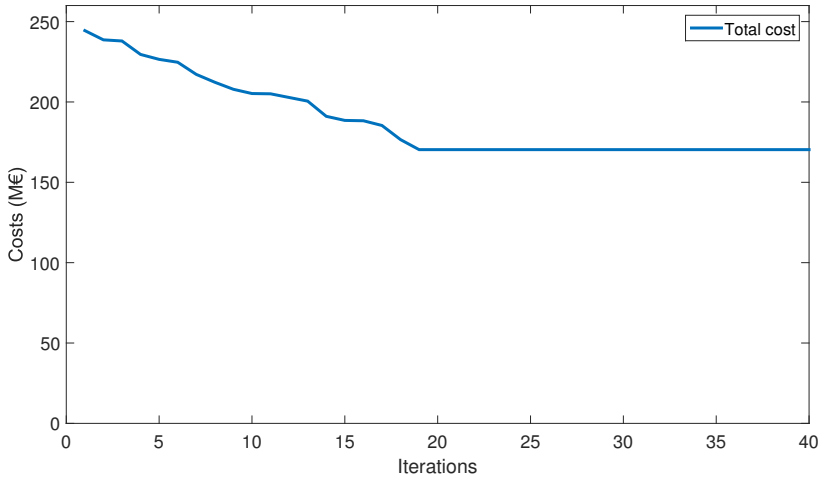

Figure 6.11: Total cost corresponding to each iteration for optimized collection grid layout.

Table 6.5 presents the costs and energy losses for this collection grid layout and compares to the initial one. In comparison to the initial layout, it can be seen that the total cost of the inter-array cables has decreased by more than 4.5% and the energy losses by about 6.4% despite the use of more expensive larger cross sections. This is mainly due to the decrease in the total length of the cables since fewer cables are used and less connections to the offshore substation exist. Consequently, the shorter total length of cables has resulted in a decrease in acquisition and installation cost as well as cost of energy losses.

Table 6.5: Comparison of results for initial and optimized collection grid layout.

	Initial	Optimized	Difference (%)
Acquisition cost (M€)	122.75	118.17	-3.73
Installation cost (M€)	22.82	20.85	-8.63
Cost of energy loss (M€)	23.90	22.39	-6.32
Cost of EENS (M€)	8.93	8.92	-0.11
Total cost (M€)	178.40	170.33	-4.52
Annual energy loss (GWh)	14.94	13.99	-6.36
Total length of cables (km)	150.41	136.75	-9.08

6.5.3 Reduced power cable type usage

In the wind industry it is quite common that a supplier of power cables provides a discount on the purchase of a large amount of cables. Developers often prefer to use less different cables and apply larger cross sections for the connection of the wind turbines in the wind farm. Hence, it is of interest to analyze the effect of such a discount. Therefore, based on the layout obtained from the previous optimization, the number of available power cables is reduced to the 2 largest cross sections (630mm^2 and 800mm^2) and a discount of 15% on the price is applied. Figure 6.12 shows the comparison of the results for the inter-array cables and the total cost.

It is observable that despite the discount of 15%, the acquisition cost of the inter-array cables is higher since more cables with larger cross sections and higher unit costs are used. However, the use of solely larger cross sections allows to reduce the energy losses and thus the cost of energy loss, which outweighs the acquisition cost increase and results in a decrease of the total cost of the collection grid could by about 2%. A sensitivity analysis of different discount rates has found that a discount of at least 10% is required to equal the total cost. The results obtained for this discount rate are shown in green in Figure 6.12 for the sake of completeness.

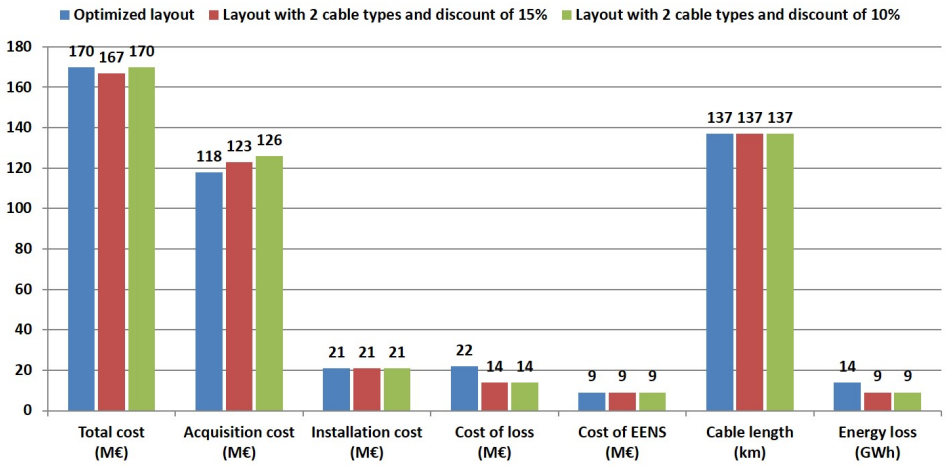

Figure 6.12: Comparison of inter-array costs and energy losses for quantity discount

6.5.4 Power cable configuration study

The electrical connection of two FOWTs is made by a combination of a dynamic cable that is designed to withstand the stresses applied by the moving structure and a static cable that is buried in the seabed and transports the power between the turbines [28]. The dynamic cable section has typically a larger outer sheath and increased armor resulting in a higher cost in comparison to the static cable [224]. Both cable sections are shown in Figure .

(a) (b)

Figure 6.13: (a) Dynamic and (b) static power cable sections [224].

The connection of the static and dynamic cable can be made through either a permanent factory splice or a submarine joint that enables a separation and reconnection. The submarine joint can be further classified in dry-mate or wet-mate connectors depending on the ability to perform the connection on board of a vessel or under water [222]. Theoretically, the connection of the FOWTs could be done by using only dynamic cables without a static section and by burying a section of the dynamic cable. This would avoid the use of submarine joints, but would lead to higher costs for the cables. In this section, a comparison is made between the two configurations of cable connections. One option is to use only dynamic power cables for the entire collection grid. The second option would be to use the combination of dynamic and static cable sections with a dry-mate connector as submarine joint. Figure 6.14 presents the two wind turbine connection configurations.

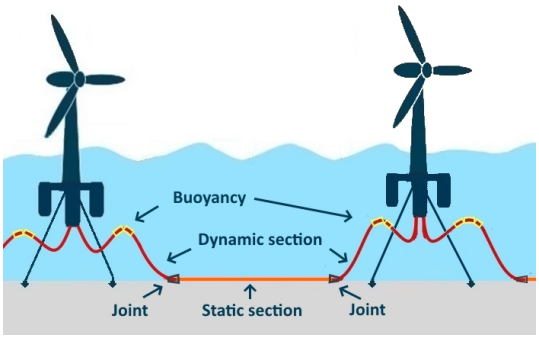

(a) Dynamic with static cable configuration.

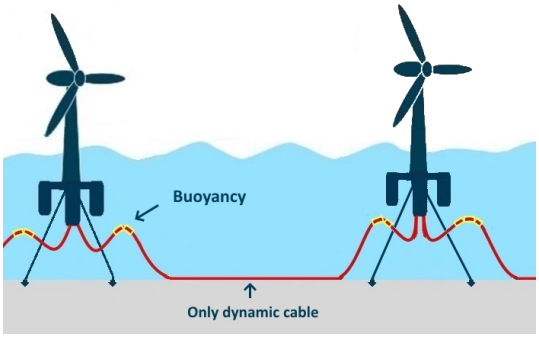

(b) Dynamic cable only configuration.

Figure 6.14: Power cable configurations.

The cost of cable acquisition and installation differs slightly between two power cable configurations. The cost calculations associated to a single power cable for each configuration (C1 and C2) without taking into account amortization are shown next.

$$C_{\text{acquisition-C1}} = C_{\text{static}} * L_{\text{static}} + C_{\text{dynamic}} * L_{\text{dynamic}} + C_{\text{buoy}} + C_{\text{stiff}} + C_{\text{joint}} \tag{6.19}$$

$$C_{\text{installation-C1}} = L_{\text{iac}} * C_{\text{vessel}} * r_{\text{instal}} * 1.1 + C_{\text{Mob/Demob}} \tag{6.20}$$

$$C_{\text{acquisition-C2}} = C_{\text{dynamic}} * L_{\text{dynamic}} + C_{\text{bouy}} + C_{\text{stiff}} \tag{6.21}$$

$$C_{\text{installation-C2}} = L_{\text{iac}} * C_{\text{vessel}} * r_{\text{instal}} + C_{\text{Mob/Demob}} \tag{6.22}$$

$C_{dynamic}$ and C_{static} represent the cost per meter of the dynamic and static cable with the associated length of the cable $L_{dynamic}$ and L_{static}, respectively. The cost of the buoyancies required for the dynamic section are defined by C_{buoy} and the cost of bend stiffners and connectors are represented by C_{stiff}. The cost of the submarine joints required by cable configuration C1 is defined by C_{joint}. Furthermore, as the connection of the static and dynamic cable section is performed offshore, an increase of 10% is taken into account for the installation cost of C1. The optimized collection grid layout obtained in Section 6.5.2 is considered and the cable configuration C2 is applied and compared to the results of C1 that have been obtained in the previous section. Figure 6.15 shows the comparison of the results for both cable configurations.

It is observable that the acquisition cost of the cable configuration C2 has decreased despite using solely the slightly more expensive dynamic power cables. This is based on the avoidance of the submarine joints, which are required for cable configuration C1. Furthermore, the installation cost has decreased for C2, because no additional cost for the installation of the submarine joint is required. The energy losses are not influenced by the type of cable configuration since the same resistance is assumed for both dynamic and static cable. The total cost of the collection grid has decreased by 6.5% considering the use of only dynamic power cables.

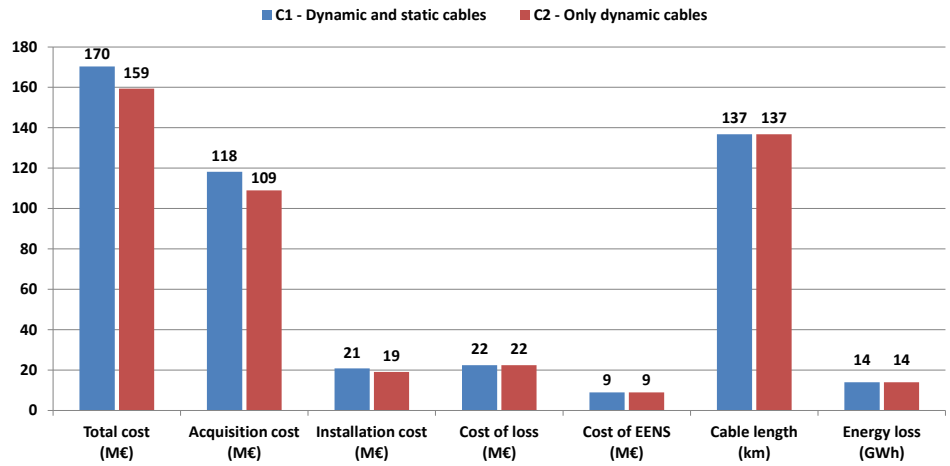

Figure 6.15: Comparison of inter-array costs and energy losses for different cable configurations.

6.6 Conclusion of the chapter

In this chapter, an optimization model based on an adapted metaheuristic PSO algorithm has been presented for the electrical layout planning of FOWFs. The model possesses a high complexity by considering the stochasticity of wind speed and wind direction and taking into account the entire wind turbine connection possibilities. Besides that, a comprehensive wake model is included. Furthermore, dynamic power cables used for the connection of FOWTs are considered as well as their respective acquisition and installation costs. The availability assessment of the electrical components and the influence on the energy generation are also taken into account. The developed PSO model has been applied on different case studies.

The first application has been used to validate the model. The validation case consisted of a 90MW BOWF and the results obtained by the developed model have been compared to a reference optimization model from literature. For this purpose, at first a simplified version of the PSO model has been used containing the restrictions and assumptions included in the reference model. The simplified PSO model has obtained the same electrical layout as the reference model but with a significant reduction in computation time. Furthermore, the acquisition cost determined by the developed model has matched the value from the reference model.

A slight difference has been observed for the cost of EENS and energy losses, which is based on a different approach for the energy loss calculation. Hence, the model has seen to be validated. Then the full PSO model has been applied with all its functionalities. The model has successfully avoided a cable crossing in the obtained layout and provided an optimized layout with a shorter total length of cables and a decrease in acquisition costs and energy losses. The second application case concerned a 500MW FOWF. The inter-array cable layout has been optimized by applying the full PSO model. The total cost of the inter-array cables could be decreased by 4.5% and the energy losses by 6.4% in comparison to the reference case. The reductions are due to the smaller amount of cables that are used in the optimized layout and fewer connections to the offshore substation.

It can be concluded, that the developed optimization model has demonstrated its ability to optimize the electrical layout of FOWFs. As the PSO algorithm by nature does not guarantee to find the optimal solution it involves a risk of premature convergence. However, for the purpose of this study the model has fulfilled its objective by providing an optimized layout in an acceptable time frame. A study on the application of a quantity discount has shown that from a certain discount rate on (10% for the case studied) it becomes worthwhile to consider less types of different power cables but with a larger cross section and a discount on the acquisition cost. Finally, the use of two different power cable configurations have been studied. The first configuration considered a combination of dynamic and static power cables for the collection grid whereas the second considered only dynamic power cables. It has been shown that the use of solely dynamic power cables results in decreased acquisition costs and installation costs due to the avoidance of cost-intensive submarine joints and additional installation activities.

7 Conclusion

Floating offshore wind is currently developing from prototype testing towards the commercial phase, where there is a need for comprehensive tools that allow to assess commercial FOWFs for different offshore sites. This thesis was aimed to respond to this need by the development and application of models to analyze FOWFs both from a technical and economic perspective. The main research work of the thesis has been divided into three research lines in order to cover several aspects and disciplines of this technology. The first is the modeling of the FOWT and the analysis of the response of the system to different met-ocean conditions. The second concerns the technical-economic assessment of FOWFs and the last research line consists of the optimization of the electrical layout of the FOWF. The main important remarks of each research topic are drawn in the following. More detailed conclusions can be found at the end of each chapter.

The theoretical background for the modeling of FOWTs has been provided in Chapter 3. This includes a description of the main environmental conditions and loads acting acting on the system. Furthermore, the methodology has been provided for defining the structural properties and solving the equation of motion in order to perform the dynamic analysis of the FOWT. In addition, the power generation equation has been adapted to consider the motions of the structure.

The methodology has been implemented in a model that has been used in Chapter 4 to study and analyze the performance and behavior of a Spar-type FOWT. At first, the developed model has been tested with a set of predefined load cases and and the results have been compared to a reference model.

An overall good agreement has been found in the comparison of the structural properties computed by both models. In addition, the main motions and system's dynamics could be captured by the developed model with an acceptable accuracy. The analysis of the power generation has shown that even for the most extreme wind and wave combination the power loss experienced by the FOWT is less than 1% or 1.1% compared to a BOWT and demonstrates the high performance of the system. The FOWT model has been further tested with regards to three offshore sites and associated met-ocean conditions ranging from moderate to severe. The largest motions have appeared at the site with the harshest conditions. However, despite the large motions no significant loss in energy generation was measured, which has also let to reach high capacity factors up to 75%.

In Chapter 5, a technical-economic assessment of commercial scale FOWFs has been performed. A comprehensive LCOE methodology has been presented including life cycle cost estimation for all components of the FOWF as well as the energy yield considering wind farm power generation and losses. Three FOWT concepts have been included in the study, located at three different sites and considering a 500MW wind farm configuration. At first, the LCOE values for the different concepts have been obtained. Afterwards, a sensitivity analysis has been conducted on 325 input parameters by considering a deterministic variation. Finally, based on the uncertainty values provided by the concept designers, a complementary study has been performed to highlight actual LCOE variation limits for the different concepts and sites. The findings indicate that FOWTs are a high competitive solution and energy can be produced at an equal or lower LCOE compared to bottom-fixed offshore wind or ocean energy technologies. Furthermore, the sensitivity analysis has identified several key parameters that have a significant influence on the LCOE and which can be essential for further cost reductions. For instance, the parameters that most vary the LCOE across all three concepts and offshore sites are manufacturing cost related, such as the cost of the wind turbine, substructure and mooring system. Thus, a cost optimized design involving all components of a FOWT is important and should be considered already in the early design stage.

In Chapter 6 an optimization model based on an adapted metaheuristic PSO algorithm has been proposed for the electrical layout planning of FOWFs. The model has been applied on different case studies. The first application has been used to validate the model. The second application case has concerned the optimization of the inter-array cable routing of a 500MW FOWF.

The optimized electrical layout resulted in a reduction of the inter-array cable costs of 4.5% and a decrease of the energy losses by 6.4% in comparison to the reference case. The reductions are due to the smaller amount of cables that are used in the optimized layout and fewer connections to the offshore substation.

A further study that has been performed has demonstrated that the use of less different cable types but with larger cables cross sections and a discount on the acquisition cost can result in a decrease of the total cost of the collection grid due to lower total energy losses in the cables. Finally, it has been shown that the use of solely dynamic power cables in comparison to the use of combined dynamic and static cables can result in decreased acquisition and installation costs due to the avoidance of cost-intensive submarine joints and additional installation activities.

To sum up, it can be concluded that the research work has generated practical models and tools that can be of great interest for concept designers, project developers and researchers of this industry that require adequate methods to analyze and assess FOWTs. Moreover, the application of the models has demonstrated the high potential of this technology to provide a competitive source of energy in the near future. In the next chapter, further research work is proposed that can be derived from this thesis.

8 Further work

From this thesis, future research work can be derived, which is proposed below.

- Regarding the methodology proposed in Chapter 3 for the modeling of a FOWT, several improvements could be included:
  - Increase the degrees of freedom from three to six to obtain the complete representation of the substructure motions.
  - Consider the impact of marine growth.
  - Adapt the methodology to study different FOWT concepts.
  - Include an advanced controller scheme.
  - Investigate the interaction between the wind rotor and its wake.
- With respect to the dynamic analysis of a FOWT presented in Chapter 4, the following additional research work could be of interest:
  - Compare the performance and motions response of several FOWT concepts.
  - Change the dimensions of a FOWT design and analyze the impact on the performance.

- From the technical-economic assessment performed in Chapter 5, it could be of interest to study the following tasks:
  - Include an advanced wake model that considers the motions of the floating substructure
  - Compute the LCOE for FOWFs located far offshore and transmit energy by using HVDC technology.
  - Include dielectric, screen, and armour losses in the computation of the power cable losses.
  - Study the influence on the LCOE when more than one parameter changes at a time.
- Further research work concerning the optimization model of Chapter 6 could contain:
  - Optimization of the turbine and substation locations.
  - Apply the optimization algorithm to wind farms with different sizes and distances from shore.
  - Include power cable laying restrictions around moorings.
  - Sensitivity analysis of input parameters and influence on layout.
  - Include submarine hubs as a connection point of power cables.
  - Improve coding and reduce calculation time.
- Finally, one proposal is the connection of the dynamic analysis tool and the optimization tool to the technical-economic assessment tool. This would enable the calculation of the LCOE for a FOWF considering an optimized layout and a more accurate computation of the energy yield taking into account the motions of the FOWT.

Bibliography

[1] EY. Offshore wind in Europe. Technical report, 2015. 1

[2] GWEC. Global wind report 2018. Technical report, 2019. 1

[3] WindEurope. The economics of wind energy. Technical report, 2009. 1, 12, 94

[4] GWEC. Global wind reports 2006-2018. Technical report. 1

[5] T. Ackermann. *Wind power in power systems*. 2005. 2, 26, 27, 28, 30, 34, 48

[6] A. McDonald and J. Carroll. *Offshore wind farms: Technologies, design and operation*, chapter Design of generators for offshore wind turbines, pages 159–192. Elsevier, 2016. 2

[7] WindEurope. Wind energy in Europe in 2018. Technical report, 2019. 2

[8] IEA. Offshore wind - Tracking clean energy progress, https://www.iea.org/tcep/power/renewables/offshorewind/, Accessed 15.09.2019. 2

[9] WindEurope. Offshore wind in Europe - Key trends and statistics 2018. Technical report, 2018. 2, 13, 14, 21, 35

[10] M. Atcheson and A. Garrad. *Floating offshore wind energy: The next generation of wind energy*, chapter Looking Back, pages 1–20. Springer, 2016. 2, 61, 89

[11] Carbon Trust. Floating offshore wind: Market and technology review. Technical report, 2015. 2, 3, 14, 15, 16, 17, 18, 19, 23, 35, 39, 40, 42, 68, 108, 110, 114, 123, 129

[12] WindEurope. Floating offshore wind vision statement. Technical report, 2017. 2, 3, 14, 15, 89, 129

[13] M. Lerch. Levelized cost of energy calculation for floating offshore wind power plants. Master's thesis, Universitat Politècnica de Catalunya, 2016. 7

[14] LIFES50+. Innovative floating offshore wind energy, https//lifes50plus.eu, Accessed 20.12.2018. 7, 160

[15] InnoEnergy. PhD School, http://www.innoenergy.com/education/phd-school, Accessed 23.07.2019. 8

[16] DTU. PhD Summer School: Analysis, design and testing of floating offshore wind turbine structures, https://www.vindenergi.dtu.dk/english/kalender/2017/08/summerschool-analysis-design-and-testing-of-floating-offshore-wind-turbine-structures?showcalendaradd=false, Accessed 23.07.2019. 8

[17] A. P. Talayero Navales and E. Telmo Martínez. *Energía eólica*. Prensas de la Universidad de Zaragoza, 2011. 12, 13, 33, 34

[18] WindEurope. Wind energy - The facts: A guide to the technology, economics and future of wind power. Technical report, 2012. 13, 21, 22, 23, 94, 107

[19] OffshoreWIND. Report on wind turbine gearbox and direct-drive systems out now, https://www.offshorewind.biz/2014/09/19/report-on-wind-turbine-gearbox-and-direct-drive-systems-out-now, Accessed 01.06.2019. 13

[20] S. R. Awasthi. *Wind Power: Practical Aspects*. The Energy and Resources Institute, 2018. 13

[21] M. Martini, R. Guanche, J. A. Armesto, I. J. Losada, and C. Vidal. Met-ocean conditions influence on floating offshore wind farms power production. *Wind Energy*, 19(3):399–420, 2016. 13, 68, 84

[22] WindPowerOffshore. Siemens 7MW lined up for Walney Extension, https://www.windpoweroffshore.com/article/1337868/siemens-7mw-lined-walney-extension, Accessed 01.06.2019. 13

[23] MHI Vestas. First V164-8.0 MW turbine installed at Burbo Bank Extension, http://www.mhivestasoffshore.com/first-v164-8-0-mw-turbine-installed-burbo-bank-extension-2, Accessed 01.06.2019. 13

[24] Riviera Maritime Media. Siemens Gamesa joins 10 MW+ club as GE makes plans to test Haliade-X prototype, https://www.rivieramm.com/opinion/siemens-gamesa-joins-10-mw-club-as-ge-makes-plans-to-test-haliade-x-prototype-22061, Accessed 03.03.2019. 13

[25] Wind Kraft Journal. Die Haliade-X 12 MW von GE, die leistungsstärkste Offshore-Windenergieanlage der Welt, produziert ersten Strom, https://www.windkraft-journal.de/2019/11/08/die-haliade-x-12-mw-von-ge-die-leistungsstaerkste-offshore-windenergieanlage-der-welt-produziert-ersten-strom/141792 Accessed 14.01.2020. 14

[26] W. Musial, P. Beiter, P. Schwabe, T. Tian, T. Stehly, P. Spitsen, and V. Gevorgian. Offshore wind technologies market report. Technical report, 2016. 14

[27] Carbon Trust. Floating wind joint industry project - Phase I summary report. Technical report, 2018. 14, 24, 35

[28] WindEurope. Deep Water: The next step for offshore wind energy. Technical report, 2013. 14, 34, 35, 38, 39, 41, 42, 90, 103, 109, 110, 165

[29] S. Gonzalez and V. Diaz-Casas. *Floating offshore wind farms*, chapter Present and Future of Floating Offshore Wind, pages 1–23. Springer, 2016. 14, 15, 18, 32

[30] A. Henderson, M. Collu, and M. Masciola. *Floating offshore wind energy: The next generation of wind energy*, chapter Overview of floating offshore wind technologies, pages 87–132. Springer, 2016. 15, 86, 124

[31] Hexicon. Hexicon, https://www.hexicon.eu/hexicon, Accessed 04.04.2019. 16, 36

[32] Floating Power Plant. P37, http://www.floatingpowerplant.com/products, Accessed 08.06.2019. 16

[33] Vryhof. Anchor manual 2015 - the guide to anchoring. Technical report, 2015. 16, 17, 18, 19, 103, 116, 117

[34] E. Hau and H. von Renouard. *Wind turbines: Fundamentals, technologies, application, economics*. Springer, 2006. 19, 21, 23, 32, 33, 48, 121

[35] R. Taninoki, D. Azuma, I. Sato, T. Utsunomiya, S. Ishida, and K. Kokubun. Development of dynamic cable system for floating offshore wind power. In *CIGRE AORC Technical meeting*, 2014. 19, 20, 21

[36] C. Ng and L. Ran. *Offshore wind farms: Technologies, design and operation*, chapter Introduction to offshore wind energy, pages 3–8. Elsevier, 2016. 20

[37] DNV-GL. 66 kV systems for offshore wind farms. Technical report, 2015. 20

[38] J. Glasdam, L. Zeni, M. Gryning, J. Hjerrild, L. Kocewiak, B. Hesselbaek, K. Andersen, T. Sørensen, M. Blanke, P. E. Sørensen, and Others. HVDC connected offshore wind power plants: review and outlook of current research. In *12th Wind Integration Workshop*, 2013. 21, 27

[39] ABB. HVDC Light - It's time to connect. Technical report, 2012. 21

[40] Prysmian. Extruded cables for HVDC power transmission, https://www.prysmiangroup.com/sites/default/files/atoms/files/BR-HVDC-2018-rev12.pdf, Accessed 01.06.2019. 21

[41] WindEurope. Wind in our sails - The coming of Europe's offshore wind energy industry. Technical report, 2011. 21, 22, 23, 28, 106, 110

[42] ABB. ABB to invest $400 million on expansion of cable production capacity in Sweden, https://new.abb.com/news/detail/13788/abb-to-invest-400-million-on-expansion-of-cable-production-capacity-in-sweden, Accessed 04.03.2018. 21

[43] 4COffshore. Walney phase 2 offshore substation, https://www.4coffshore.com/transmission/substation-walney-phase-2-substation-sid7.html, Accessed 05.06.2019. 22

[44] Crown Estate. A guide to an offshore wind farm. Technical report, 2010. 23, 92, 93, 94, 95, 97

[45] S. Lundberg. *Wind farm configuration and energy efficiency studies-series DC versus AC layouts*. PhD thesis, Chalmers University of Technology, 2006. 24, 25, 26, 29

[46] M. Zubiaga and S. Aurtenetxea. *Energy transmission and grid integration of AC offshore wind farms*. INTECH, 2012. 25, 26, 30, 47

[47] Ofgem. Preliminary information memorandum - Walney Extension. Technical report, 2016. 25

[48] C. Ng and L. Ran. *Offshore wind farms: Technologies, design and operation*. 2016. 26

[49] A. Curvers and J. Pierik. WP 3: Technologies state of the art - Task 3: Grid integration aspects. Technical report, ORECCA, 2011. 26

[50] O. Anaya-Lara. *Offshore wind farms: Technologies, design and operation*, chapter Offshore wind farm arrays, pages 389–418. Elsevier, 2016. 27

[51] Offshore wind industry. Troubleshooting continues, http://www.offshorewindindustry.com/news/troubleshooting-continues Accessed 13.06.2019. 27

[52] P. Lakshmanan, J. Liang, and N. Jenkins. Assessment of collection systems for HVDC connected offshore wind farms. *Electric Power Systems Research*, 129:75–82, 2015. 27, 28

[53] M. de Prada Gil, J. L. Domínguez-Garcia, F. Díaz-González, and A. Sumper. *HVDC Grids: For Offshore and Supergrid of the Future*, chapter Offshore Wind Power Plants (OWPPS). 2016. 29, 30, 31

[54] D. Bock. Wind Energy: On the grid, Off the Checkerboard, https://www.aip.org/publishing/journal-highlights/wind-energy-grid-checkerboard Accessed 01.06.2017. 32

[55] M. de Prada Gil. *Design, operation and control of novel electrical concepts for offshore wind power plants*. PhD thesis, Universitat Politécnica de Catalunya, 2014. 32, 148, 150, 151

[56] L. Cradden, P. Laporte Weywada, and M. Atcheson. *Floating offshore wind energy: The next generation of wind energy*, chapter The Offshore Environment, pages 21–87. Springer, 2016. 33, 43, 44, 45, 46, 49, 50, 53, 56, 57

[57] M. S. Courtney and C.B. Hasager. *Offshore wind farms: Technologies, design and operation*, chapter Remote sensing technologies for measuring offshore wind, pages 59–82. Elsevier, 2016. 33

[58] Blue H Engineering. Technology, https://www.bluehengineering.com/tablet/technology.html Accessed 25.01.2020. 34

[59] Equinor. Hywind, https://www.equinor.com/en/what-we-do/hywind-where-the-wind-takes-us.html, Accessed 25.01.2020. 34

[60] Principle Power. Globalizing offshore wind, http://www.principlepowerinc.com/en, Accessed 25.01.2020. 34

[61] 4COffshore. W2Power platform unveiled, https://www.4coffshore.com/news/w2power-platform-unveiled-nid12505.html, Accessed 02.06.2019. 35

[62] WindEurope. Floating offshore wind energy: A policy blueprint for Europe. Technical report, 2018. 35, 36, 38

[63] Ideol. Our projects, https://www.ideol-offshore.com/en/our-projects, Accessed 03.06.2019. 36

[64] Maine Aqua Ventus. New England Aqua Ventus I, http://maineaquaventus.com/index.php/the-project/ Accessed 03.06.2019. 36

[65] Principle Power. Key markets and projects, http://www.principlepowerinc.com/en/key-markets-projects?location=9, Accessed 03.06.2019. 36, 99

[66] Energy Live News. EU approves support for French floating offshore wind farms, https://www.energylivenews.com/2019/02/25/eu-approve-support-for-french-floating-offshore-wind-farms, Accessed 03.06.2019. 36

[67] Sener. Press releases, http://www.poweroilandgas.sener/press-releases/sener-in-cobra-kincardine-offshore-floating-wind-farm-in-scotland, Accessed 03.06.2019. 36

[68] A. R. Henderson, D. Witcher, and C. A. Morgan. Floating support structures enabling new markets for offshore wind energy. In *European Wind Energy Conference (EWEC)*, volume 1619, 2009. 37, 38, 41

[69] EMODnet. Bathymetry, http://portal.emodnet-bathymetry.eu, Accessed 04.04.2016. 37, 38

[70] The Maritime Executive. Norway Proposes Areas for Floating Offshore Wind, https://www.maritime-executive.com/article/norway-proposes-areas-for-floating-offshore-wind, Accessed 06.08.2019. 38

[71] OffshoreWIND. France to set 1GW annual offshore wind tendering target, https://www.offshorewind.biz/2019/06/13/france-to-set-1gw-annual-offshore-wind-tendering-target/, Accessed 02.08.2019. 39

[72] Recharge. Spain grants Equinor ok for world's biggest floating wind farm, https://www.rechargenews.com/wind/1798896/spain-grants-equinor-ok-for-worlds-biggest-floating-wind-farm, Accessed 08.08.2019. 39

[73] Openseamap. Openseamap, http://map.openseamap.org/, Accessed 01.08.2019. 40

[74] OffshoreWIND. Ideol, CSC Hook Up for Taiwanese Floating Offshore Wind, https://www.offshorewind.biz/2015/11/13/ideol-csc-hook-up-for-taiwanese-floating-offshore-wind/, Accessed 05.08.2019. 41

[75] GICON. GICON, http://www.gicon.de/en/aktuelles/nachrichtenliste-aktuell/newsdetails/archive/2015/november/26/article/south-korean-delegation-gathers-information-at-gicon-about-compatibility-of-the-offshore-wind-energy-and-fishing-industries.html, Accessed 05.08.2019. 41

[76] B.H. Bailey. *Offshore wind farms: Technologies, design and operation*, chapter Wind resources for offshore wind farms: characateristics and assessment, pages 29–58. Elsevier, 2016. 44

[77] P. A. Lynn. *Onshore and offshore wind energy: an introduction*. John Wiley & Sons, 2012. 44, 45, 46

[78] DNV. Recommended practice DNV-RP-C205 - Environmental conditions and environmental loads. Technical report, 2017. 45, 54, 55, 56

[79] F. D. Bianchi, H. de Battista, and R. J. Mantz. *Wind turbine control systems: Principles, modelling and gain scheduling design*. Springer, 2006. 45, 61, 62, 149

[80] DNV. Offshore Standard DNV-OS-J101 - Design of Offshore Wind Turbine Structures. Technical report, 2014. 45, 56, 57

[81] E. Branlard. Generation of time series from a spectrum: generation of wind time series from the Kaimal spectrum, generation of wave time series from Jonswap spectrum. Technical report, Technical University of Denmark, 2010. 45

[82] S. Rose and J. Apt. Generating wind time series as a hybrid of measured and simulated data. *Wind Energy*, 15(5):699–715, 2012. 45

[83] M. Sathyajith. *Wind energy: fundamentals, resource analysis and economics*. Springer, 2006. 46, 47

[84] C. Bak, F. Zahle, R. Bitsche, T. Kim, A. Yde, L. C. Henriksen, M. H. Hansen, and A. Natarajan. The DTU 10 MW Reference Wind Turbine. Technical report, Technical University of Denkmark (DTU), 2013. 49, 122, 160

[85] A. Toffoli and E. M. Bitner-Gregersen. Types of Ocean Surface Waves, Wave Classification. *Encyclopedia of Maritime and Offshore Engineering*, pages 1–8, 2017. 49, 50

[86] J. M. J. Journée and W. W. Massie. *Offshore hydromechanics*. 2001. 49, 50, 51, 52, 53, 54

[87] L. Perez. Design, testing and validation of a scale model semisubmersible offshore wind turbine under regular/irregular waves and wind loads. Master's thesis, University of Strathclyde, 2014. 49

[88] M. P. M. Reddy. *Descriptive physical oceanography*. 2001. 50

[89] M. Karimirad. *Offshore energy structures: For wind power, wave energy and hybrid marine platforms*. Springer, 2014. 51, 52, 53, 59, 63

[90] S. Chakrabarti. *Handbook of Offshore Engineering*. Elsevier, 2005. 51, 54, 64

[91] W. J. Pierson, G. Neumann, and R. W. James. Practical methods for observing and forecasting ocean waves by means of wave spectra and statistics. Technical report, 1971. 53

[92] C. L. Bretschneider. Generation of waves by wind. State of the art. Technical report, National Engineering Science Co Washington DC, 1965. 53, 54

[93] D. Matha, J. Cruz, M. Masciola, E. Bachynski, M. Atechson, A. Goupee, S. Gueydon, and A. Robertson. *Floating offshore wind energy: The next generation of wind energy*, chapter Modelling of floating offshore wind technologies, pages 133–240. Springer, 2016. 57, 58, 60, 61, 63

[94] C. Curfs. Dynamic behaviour of floating wind turbines: A comparison of open water and level ice conditions. Master's thesis, Delft University of Technology, 2015. 57

[95] M. Karimirad and T. Moan. A simplified method for coupled analysis of floating offshore wind turbines. *Marine Structures*, 27(1):45–63, 2012. 57, 59

[96] J. Jonkman. Definition of the Floating System for Phase IV of OC3. Technical report, National Renewable Energy Laboratory (NREL), 2010. 58, 59, 63, 64, 68, 69, 70

[97] MathWorks. Matlab, https://de.mathworks.com/products/matlab.html Accessed 25.01.2020. 58, 65

[98] J. Jonkman. Inertial Moments of OC3-Hywind Components, https://wind.nrel.gov/forum/wind/viewtopic.php?t=748, Accessed 05.09.2016. 59, 70

[99] E. Bachynski and T. Moan. Design considerations for tension leg platform wind turbines. *Marine Structures*, 29(1):89–114, 2012. 60

[100] M. Borg and H. Bredmose. Dynamic Analysis - PhD Summer School lecture: Analysis, design and testing of floating offshore wind turbine structures. Technical report, Technical University of Denmark, 2017. 62

[101] F. G. Nielsen, T. D. Hanson, and B. Skaare. Integrated dynamic analysis of floating offshore wind turbines. In *Proceedings of the 25th International Conference on Offshore Mechanics and Arctic Engineering*, pages 671–679, 2006. 62

[102] T.-T. Tran and D.-H. Kim. The platform pitching motion of floating offshore wind turbine: A preliminary unsteady aerodynamic analysis. *Journal of Wind Engineering and Industrial Aerodynamics*, 142:65–81, 2015. 63

[103] J. Jonkman. Dynamics modeling and loads analysis of an offshore floating wind turbine. Technical report, National Renewable Energy Laboratory (NREL), 2007. 63, 64

[104] M. Masciola, J. Jonkman, and A. Robertson. Implementation of a multisegmented, quasi-static cable model. Technical report, National Renewable Energy Laboratory (NREL), 2013. 64

[105] M. Masciola. Instructional and Theory Guide to the Mooring Analysis Program. Technical report, National Renewable Energy Laboratory (NREL), 2013. 65

[106] G. Benveniste, M. Lerch, and M. de Prada Gil. Deliverable 2.2: LCOE tool description, technical and environmental impact evaluation procedure. Technical report, LIFES50+, 2016. 67, 154, 201, 202

[107] J. Jonkman and W. Musial. Offshore code comparison collaboration (OC3) for IEA Task 23 offshore wind technology and deployment. Technical report, 2010. 68, 71

[108] X. Shen, J. Chen, P. Hu, X. Zhu, and Z. Du. Study of the unsteady aerodynamics of floating wind turbines. *Energy*, 145:793–809, 2018. 68

[109] R. Farrugia, T. Sant, and D. Micallef. A study on the aerodynamics of a floating wind turbine rotor. *Renewable Energy*, 86:770–784, 2016. 68

[110] M. Shen, Z. Hu, and G. Liu. Dynamic response and viscous effect analysis of a TLP-type floating wind turbine using a coupled aero-hydro-mooring dynamic code. *Renewable Energy*, 99:800–812, 2016. 68

[111] L. Sethuraman and V. Venugopal. Hydrodynamic response of a stepped-spar floating wind turbine: Numerical modelling and tank testing. *Renewable Energy*, 52:160–174, 2013. 68

[112] B. Wen, X. Tian, X. Dong, Z. Peng, and W. Zhang. Influences of surge motion on the power and thrust characteristics of an offshore floating wind turbine. *Energy*, 141:2054–2068, 2017. 68

[113] B. Wen, X. Dong, X. Tian, Z. Peng, W. Zhang, and K. Wei. The power performance of an offshore floating wind turbine in platform pitching motion. *Energy*, 154:508–521, 2018. 68

[114] T. Sant and K. Cuschieri. Comparing three aerodynamicmodels for predicting the thrust and power characteristics of a yawed floating wind turbine rotor. *Journal of Solar Energy Engineering*, 138(3):31004, 2016. 68

[115] J. Jonkman, S. Butterfield, W. Musial, and G. Scott. Definition of a 5-MW reference wind turbine for offshore system development. Technical report, National Renewable Energy Laboratory (NREL), 2009. 68, 69

[116] A. Robertson, F. Wendt, J. Jonkman, W. Popko, H. Dagher, S. Gueydon, J. Qvist, F. Vittori, J. Azcona, E. Uzunoglu, and Others. OC5 project phase II: Validation of global loads of the DeepCwind floating semisubmersible wind turbine. *Energy Procedia*, 137:38–57, 2017. 69

[117] J. Jonkman, T. Larsen, A. Hansen, T. Nygaard, K. Maus, M. Karimirad, Z. Gao, T. Moan, and I. Fylling. Offshore code comparison collaboration within IEA wind task 23: Phase IV results regarding floating wind turbine modeling; Preprint. Technical report, 2010. 69, 71

[118] F. Driscoll, J. Jonkman, A. Robertson, S. Sirnivas, B. Skaare, and F. G. Nielsen. Validation of a FAST Model of the Statoil-Hywind Demo Floating Wind Turbine. *Energy Procedia*, 94:3–19, 2016. 69, 76

[119] S Nallayarasu and NS Kumar. Experimental and numerical investigation on hydrodynamic response of buoy form spar under regular waves. *Ships and Offshore Structures*, 12(1):19–31, 2017. 74

[120] D. Roddier, C. Cermelli, J. Weinstein, E. Byklum, M. Atcheson, T. Utsunomiya, J. Jorde, and E. Borgen. *Floating offshore wind energy: The next generation of wind energy*, chapter State-of-the-Art, pages 271–332. Springer, 2016. 76

[121] Spanish Government - Ministry of Development. Puertos del Estado, http://www.puertos.es/en-us/oceanografia/Pages/portus.aspx, Accessed 12.09.2019. 77

[122] P. Gonzalez, G. Sanchez, A. Llana, and G. Gonzalez. Deliverable 1.1 Oceanographic and meteorological conditions for the design. Technical report, LIFES50+, 2015. 77, 124, 125, 160

[123] M. Karimirad and T. Moan. Feasibility of the application of a spar-type wind turbine at a moderate water depth. *Energy Procedia*, 24:340–350, 2012. 79

[124] T. Liu, X. Chen, J. Wu, and K. Huang. Global performance and mooring analysis of a truss spar. In *The Thirteenth International Offshore and Polar Engineering Conference*. International Society of Offshore and Polar Engineers, 2003. 82

[125] World Energy Council. World Energy Resources Wind 2016, https://www.worldenergy.org/wp-content/uploads/2017/03/WEResources_Wind_2016.pdf, Accessed 03.05.2017. 84

[126] Equinor. Facts abou the Hywind Scotland Pilot Park, https://www.equinor.com/en/news/2019-11-28-hywind-scotland-data.html, Accessed 27.01.2020. 84

[127] U.S. Energy Information Administration (EIA). Electric Power Monthly. Technical report, 2018. 84

[128] A. R. Nejad, E. E. Bachynski, and T. Moan. On Tower Top Axial Acceleration and Drivetrain Responses in a Spar-Type Floating Wind Turbine. In *ASME 36th International Conference on Ocean, Offshore and Arctic Engineering*, 2017. 85, 86

[129] W. Xue. Design, numerical modelling and analysis of a spar floater supporting the DTU 10MW wind turbine. Master's thesis, NTNU, 2016. 85

[130] M. Borg and M. Collu. A comparison between the dynamics of horizontal and vertical axis offshore floating wind turbines. *Philosophical Transactions of the Royal Society A: Mathematical, Physical and Engineering Sciences*, 373(2035), 2015. 86

[131] A. Myhr, C. Bjerkseter, A. Ågotnes, and T. A. Nygaard. Levelised cost of energy for offshore floating wind turbines in a life cycle perspective. *Renewable Energy*, 66:714–728, 2014. 89, 91, 128, 129

[132] M. Kausche, F. Adam, F. Dahlhaus, and J. Großmann. Floating offshore wind - Economic and ecological challenges of a TLP solution. *Renewable Energy*, 126:270–280, 2018. 89, 128, 129

[133] L. Castro-Santos and V. Diaz-Casas. Life-cycle cost analysis of floating offshore wind farms. *Renewable Energy*, 66:41–48, 2014. 89, 94

[134] R. Ebenhoch, D. Matha, S. Marathe, P. C. Muñoz, and C. Molins. Comparative levelized cost of energy analysis. *Energy Procedia*, 80:108–122, 2015. 90

[135] R. Ebenhoch. Comparative levelized cost of energy analysis for a floating offshore wind turbine concept. Master's thesis, Student research paper at Stuttgart Wind Energy (SWE), 2014. 90, 91, 92, 100

[136] IRENA. Renewable energy technologies: Cost analysis series wind power. Technical report, 2012. 90, 91, 94

[137] C. Breyer. *Economics of Hybrid Photovoltaic Power Plants*. PhD thesis, University of Kassel, 2012. 91

[138] M. Percoco and E. Borgonovo. A note on the sensitivity analysis of the internal rate of return. *International Journal of Production Economics*, 135(1):526–529, 2012. 91

[139] J. Aldersey-Williams and T. Rubert. Levelised cost of energy–A theoretical justification and critical assessment. *Energy Policy*, 124:169–179, 2019. 91

[140] C. Bjerkseter and A. Ågotnes. Levelised cost of energy for offshore floating wind turbine concepts. Master's thesis, Norwegian University of Life Sciences, 2013. 92, 93, 99, 104, 107, 108, 113

[141] Scottish Enterprise. A guide to offshore wind and oil & gas capability. Technical report, 2011. 94, 95

[142] Howard, R. Offshore wind cost reduction pathways project: Simple levelised cost of energy model. Technical report, The Crown Estate, 2012. 94, 95

[143] C. Moné et al. Cost of wind energy review. Technical report, Nation Renewable Energy Laboratory (NREL), 2013. 94, 108, 109

[144] BVG Associates. Value breakdown for the offshore wind sector. Technical report, 2010. 94

[145] Westwood, D. Offshore Wind Assessment for Norway. Technical report, 2010. 95

[146] Multiconsult. Technological and cost development trends of renewable offshore energy production. Technical report, 2010. 95

[147] L. Castro-Santos. *Methodology related to the development of the economic evaluation of floating offshore wind farms in terms of the analysis of the cost of their life-cycle phases.* PhD thesis, University of A Coruña, 2013. 96, 97, 101, 102, 106, 112, 120

[148] Rodríguez Arias, R. and Rodrǵuez Ruiz, A. and González de Lena Alonso, V. *Floating offshore wind farms*, chapter Mooring and Anchoring, pages 89–120. Springer, 2016. 96

[149] Navigant. Global evaluation of offshore wind shipping opportunity. Technical report, 2013. 99, 102, 103, 110

[150] Ugland Companies. Operated Fleet, http://www.jjuc.no/crane-vessels, Accessed 1.04.2016. 99

[151] Shipping and Marine. Lifting & shifting, http://www.shippingandmarine.co.uk/articlepage.%0Aphp?contentid=14528&issueid=430, Accessed 25.04.2016. 99

[152] Amate, J. et al. How to install a TLP substructure for offshore wind? TLPWIND case study. Technical report, Iberdrola, 2015. 101, 102

[153] Pelastar. PelaStar Installation, https://pelastar.com/?page_id=55, Accessed 11.06.2019. 101

[154] Statoil. Hywind Demo, http://www.statoil.com/en/Technology Innovation/NewEnergy/RenewablePowerProduction/Offshore/Hywind/Pages/HywindPuttingWindPowerToTheTest.aspx, Accessed 26.04.2016. 102

[155] MarineLink. Van Oord Contracts Damen for DP2 Cable Laying Vessel, http://www.marinelink.com/news/contracts-laying-damen360604.aspx, Accessed 29.04.2016. 103

[156] CLP. Suction Caisson Technology, https://www.clp.com.hk/offshorewindfarm/hongkongoffshorewindfarm/suctiontech.html, Accessed 29.06.2019. 104

[157] K. Yagihashi, Y. Tateno, H. Sakakibara, and H. Manabe. Dynamic cable installation for Fukushima floating offshore wind farm demonstration project. In *Proceeding Jicable 15–International Conference on Insulated Power Cables*, 2015. 105, 146

[158] Scira Offshore Energy. Sheringham Shoal offshore substations in place, http://scira.co.uk/news/news13_05_11.php,. 106

[159] GL Garrad Hassan. A guide to UK offshore wind operations and maintenance. Technical report, 2013. 108, 109, 110, 111

[160] C. Brons-Illing. Analysis of operation and maintenance strategies for floating offshore wind farms. Master's thesis, University of Stavanger, 2015. 109, 110, 111, 112

[161] Mark J Kaiser and Brian Snyder. *Offshore wind energy cost modeling: Installation and decommissioning*, volume 85. Springer Science & Business Media, 2012. 113, 114, 117, 118, 119

[162] Smith, G. and Lamont, G. Decommissioning of Offshore Wind Installations - What we can Learn. Technical report, DNV GL. 113

[163] 4COffshore. E.ON decommissioning Blyth, https://www.4coffshore.com/news/e.on-decommissioning-blyth-nid11363.html, Accessed 12.06.2019. 113

[164] Principle Power. WindFloat, http://www.principlepowerinc.com/en/windfloat, Accessed 13.06.2019. 113

[165] BP. Schiehallion and loyal decommissioning programmes Phase 1. Technical report, 2013. 116

[166] T. Merck and R. Wasserthal. Assessment of the environmental impacts of cables. *Biodiversity series: OSPAR Commission*, 2009. 117

[167] I. Sarajcev, M. Majstrovic, and I. Medic. Calculation of losses in electric power cables as the base for cable temperature analysis. *WIT Transactions on Engineering Sciences*, 27, 2000. 121

[168] Dr. Techn. Olav Olsen, OO-Star Wind Floater, http://www.olavolsen.no/en/node/149, Accessed 03.02.2019. 122, 123

[169] Iberdrola Engineering & Construction, TLPWind, Website: https://www.iberdrolaingenieria.com/ibding/pagina?id=119&itemMenu=50&locale=en, Accessed 10.09.2017. 122, 123

[170] Windcrete. Concrete floating platform for wind turbines, http://www.windcrete.com, Accessed on 14.09.2017. 122, 123

[171] Dr. Techn. Olav Olsen. OO-Star Wind Floater - An innovative and robust semi-submersible for offshore floating wind. Technical report, 2017. 122, 123

[172] IRENA. Floating foundations: A game changer for offshore wind power. Technical report, 2016. 123

[173] K. Mueller, D. Matha, M. Karch, S. Tiedemann, and R. Proskovics. Deliverable 7.5: Guidance on platform and mooring line selection, installation and marine operations. Technical report, LIFES50+, 2016. 123

[174] L. Castro-Santos and V. Diaz-Casas. *Floating offshore wind farms*, chapter Life-cycle cost of a floating offshore wind farm, pages 23–38. Springer, 2016. 123

[175] A. Campos, C. Molins, X. Gironella, and P. Trubat. Spar concrete monolithic design for offshore wind turbines. In *Proceedings of the Institution of Civil Engineers-Maritime Engineering*, volume 169, pages 49–63, 2016. 123

[176] K. Mueller, R. Faerron-Guzman, A. Manjock, and M. Borg. Deliverable D.7.7 Identification of critical environmental conditions and design load cases, 2018. 124

[177] Carbon Trust. Floating wind joint industry project - Phase I summary report. Technical report, 2018. 125

[178] Carbon Trust. Accelerating Marine Energy. Technical report, 2011. 129

[179] F. Duan. Wind Energy Cost Analysis CoE for offshore Wind and LCOE financial modeling. Master's thesis, Helsinki Metropolia University of Applied Sciences, 2017. 129

[180] UK Department for Business, Energy & Industrial Strategy, Contracts for Difference Results, https://www.gov.uk/government/publications/contracts-for-difference-cfd-second- allocation-round-results, Accessed 12.09.2017. 128

[181] S. Astariz, A. Vazquez, and G. Iglesias. Evaluation and comparison of the levelized cost of tidal, wave, and offshore wind energy. *Journal of Renewable and Sustainable Energy*, 7:53–112, 2015. 129

[182] E. D. Stoutenburg, N. Jenkins, and M. Z. Jacobson. Power output variations of co-located offshore wind turbines and wave energy converters in California. *Renewable Energy*, 35(12):2781–2791, 2010. 129

[183] A. Fassò and P. F. Perri. Sensitivity analysis. *Encyclopedia environmetrics*, 2002. 131

[184] D. M. Hamby. A review of techniques for parameter sensitivity analysis of environmental models. *Environmental monitoring and assessment*, 32(2):135–154, 1994. 131

[185] E. Borgonovo. *Sensitivity Analysis: An Introduction for the Management Scientist*. Springer, 2017. 131

[186] ORE Catapult. Offshore transmission benchmarking and cost monitoring. Technical report, 2016. 135

[187] H. Ling-Ling, C. Ning, Z. Hongyue, and F. Yang. Optimization of large-scale offshore wind farm electrical collection systems based on improved FCM. *IET*, 2012. 143

[188] A. C. Pillai, J. Chick, L. Johanning, M. Khorasanchi, and V. de Laleu. Offshore wind farm electrical cable layout optimization. *Engineering Optimization*, 47(12):1689–1708, 2015. 144

[189] P. Fagerfjäll. Optimizing wind farm layout: more bang for the buck using mixed integer linear programming. Master's thesis, Chalmers University of Technology and Gothenburg University, 2010. 144

[190] H. G. Svendsen. Planning tool for clustering and optimised grid connection of offshore wind farms. *Energy Procedia*, 2013. 144

[191] M. Lindahl, N. F. Bagger, T. Stidsen, S. Ahrenfeldt, and I. Arana. OptiArray from DONG energy. *12th Workshop Large-Scale Integration of Wind Power into Power Systems*, 2013. 144

[192] C. Berzan, K. Veeramachaneni, J. McDermott, and U.-M. O'Reilly. Algorithms for cable network design on large-scale wind farms. *Massachusetts Institute of Technology*, 2011. 144

[193] M. Banzo and A. Ramos. Stochastic optimization model for electric power system planning of offshore wind farms. *IEEE Transactions on Power Systems*, 26(3):1338–1348, 2011. 144, 146, 151, 156, 157, 158, 159

[194] A. Cerveira, A. de Sousa, E. J. S. Pires, and J. Baptista. Optimal cable design of wind farms: The infrastructure and losses cost minimization case. *IEEE Transactions on Power Systems*, 31(6):4319–4329, 2016. 144

[195] J. Bauer and J. Lysgaard. The offshore wind farm array cable layout problem: a planar open vehicle routing problem. *Journal of the Operational Research Society*, 66(3):360–368, 2015. 144

[196] M. Fischetti and D. Pisinger. Optimizing wind farm cable routing considering power losses. *European Journal of Operational Research*, 270(3):917–930, 2018. 144, 156

[197] P. Hou, G. Yang, We. Hu, C. Chen, M. Soltani, and Z. Chen. Cable Connection Scheme Optimization for Offshore Wind Farm Considering Wake Effect. In *2018 IEEE Congress on Evolutionary Computation*, pages 1–8, 2018. 144, 146

[198] M. Zhao, Z. Chen, and F. Blaabjerg. Optimisation of electrical system for offshore wind farms via genetic algorithm. *IET Renewable Power Generation*, 2009. 144

[199] F. M. Gonzalez-Longatt, P. Wall, P. Regulski, and V. Terzija. Optimal electric network design for a large offshore wind farm based on a modified genetic algorithm approach. *IEEE Systems Journal*, 6:164–172, 2011. 144

[200] M. Zhao, Z. Chen, and F. Blaabjerg. Optimization of Electrical System for a Large DC Offshore Wind Farm by Genetic Algorithm. 144

[201] S. Dutta and T. J. Overbye. A clustering based wind farm collector system cable layout design. In *2011 IEEE Power and Energy Conference at Illinois*, pages 1–6, 2011. 144

[202] P. Hou, W. Hu, and Z. Chen. Optimisation for offshore wind farm cable connection layout using adaptive particle swarm optimisation minimum spanning tree method. *IET Renewable Power Generation*, 10(5):694–702, 2016. 144, 153

[203] D. D. Li, C. He, and Y. Fu. Optimization of internal electric connection system of large offshore wind farm with hybrid genetic and immune algorithm. In *Third International Conference on Electric Utility Deregulation and Restructuring and Power Technologies*, pages 2476–2481, 2008. 144

[204] K. O. Jones. Comparison of genetic algorithm and particle swarm optimization. In *Proceedings of the International Conference on Computer Systems and Technologies*, pages 1–6, 2005. 144

[205] N. Srinil. *Offshore wind farms: Technologies, design and operation*, chapter Cabling to connect offshore wind turbines to onshore facilities, pages 419–440. Elsevier, 2016. 146

[206] R. Taninoki, A. B. E. Kazutoshi, T. Sukegawa, D.e Azuma, and M. Nishikawa. Dynamic cable system for floating offshore wind power generation. *SEI Technical review*, (84):53–58, 2017. 146

[207] S. Chandrasekaran. *Dynamic analysis and design of offshore structures*. Springer, 2015. 146

[208] R. Yttervik. Hywind Scotland–status and plans. Technical report, 2015. 146

[209] P. Hou, W. Hu, M.n Soltani, and Z. Chen. Optimized placement of wind turbines in large-scale offshore wind farm using particle swarm optimization algorithm. *IEEE Transactions on Sustainable Energy*, 6(4):1272–1282, 2015. 146, 154

[210] S. Li and C. Nguyen. Dynamic response of deepwater lazy-wave catenary riser. *Deep Offshore Technology International*, 2010. 147

[211] M. De-Prada-Gil, C. G. Alías, O. Gomis-Bellmunt, and A. Sumper. Maximum wind power plant generation by reducing the wake effect. *Energy Conversion Management*, 101:73–84, 2015. 147, 149

[212] N. O. Jensen. *A note on wind generator interaction*. 1983. 148

[213] M. Ali, J. Matevosyan, J. V. Milanović, and L. Söder. Effect of wake consideration on estimated cost of wind energy curtailments. In *8th International Workshop on Large Scale Integration of Wind Power*, pages 14–15, 2009. 148

[214] Z. Bie, X. Zou, Z. Wang, and X. Wang. *Studies on models and algorithms of the power system probabilistic production simulation integrated with wind farm*, chapter 2009 IEEE Power & Energy Society General Meeting, pages 1–7. 2009. 148

[215] A. Lisnianski, I. Frenkel, and Y. Ding. *Multi-state system reliability analysis and optimization for engineers and industrial managers*. Springer Science & Business Media, 2010. 150

[216] H. Bukowski. *Engineering design handbook - Maintainability engineering theory and practice*. 1976. 150

[217] M. Dauer, J. Meyer, J. Jaeger, T. Bopp, and R. Krebs. EPSO DE algorithm for system-wide protection coordination. In *2016 Power Systems Computation Conference (PSCC)*, pages 1–7, 2016. 153, 154

[218] M. A. Abido. Optimal power flow using particle swarm optimization. *International Journal of Electrical Power & Energy Systems*, 24(7):563–571, 2002. 153

[219] S. Boubaker, M. Djemai, N. Manamanni, and F. M'sahli. Active modes and switching instants identification for linear switched systems based on discrete particle swarm optimization. *Applied Soft Computing*, 14:482–488, 2014. 154

[220] J. Green, A. Bowen, L. J. Fingersh, and Y. Wan. Electrical collection and transmission systems for offshore wind power. Technical report, 2007. 157

[221] LIFES50+. Data based on information collected in the LIFES50+ project. 161, 162

[222] F. Sharkey, M. Conlon, and K. Gaughan. Practical analysis of key electrical interfaces for wave energy converter arrays. In *International Conference on Ocean Energy*, 2012. 162, 166

[223] A. Ferguson, P. de Villiers, B. Fitzgerald, and J. Matthiesen. Benefits in moving the inter-array voltage from 33 kV to 66 kV AC for large offshore wind farms. *EWEA Annual Event Copenhagen*, 2012. 162

[224] O. Vold, G. Hakon, T. Guttormsen, and L. Delp. Hywind Scotland Pilot Park Project Plan for Construction Activities 2017. Technical report, Statoil, 2017. 165

A

List of Publications and Presentations

In this chapter, the journal and conference papers that have been derived from the development of the thesis are listed. In addition, publications are presented that have been prepared in the associated research project as well as the presentations that have been made at relevant conferences.

A.1 Journal articles

[J1] M. Lerch, M. De-Prada-Gil, C. Molins, and G. Benveniste. Sensitivity analysis on the levelized cost of energy for floating offshore wind farms. Sustainable Energy Technologies and Assessments. December 2018; 30:77-90. DOI: https://doi.org/10.1016/j.seta.2018.09.005

[J2] M. Lerch, M. De-Prada-Gil, and C. Molins. The influence of different wind and wave conditions on the energy yield and downtime of a Spar-buoy floating wind turbine. Renewable Energy. June 2019; 136:1-14. DOI: https://doi.org/10.1016/j.renene.2018.12.096

[J3] M. Lerch, M. De-Prada-Gil, and C. Molins. A meta-heuristic optimization model for the electrical layout planning of floating offshore wind farms. Submitted to International Journal of Electrical Power & Energy Systems.

A.2 Conference articles

[**C1**] M. Lerch, M. De-Prada-Gil, and C. Molins. A simplified model for the dynamic analysis and power generation of a floating offshore wind turbine. In E3S Web of Conferences, 2018; 61:1-8. DOI: https://doi.org/10.1051/e3sconf/20186100001

[**C2**] M. Lerch, M. De-Prada-Gil, and C. Molins. Collection grid optimization of a floating offshore wind farm using particle swarm theory. In Journal of Physics: Conference Series. IOP Publishing, 2019; 1356:1-10. DOI: https://doi.org/10.1088/1742-6596/1356/1/012012

A.3 Other publications

Other relevant publications not directly related to the thesis are listed in this section.

[**O1**] G. Benveniste, M. Lerch, and M. De-Prada-Gil. Deliverable 2.2: LCOE tool description, technical and environmental impact evaluation procedure. LIFES50+, 2016.

[**O2**] G. Benveniste, M. Lerch and M. De-Prada-Gil. Deliverable 7.6: Framework for LCOE, uncertainty and risk considerations during design. LIFES50+, 2017.

[**O3**] G. Benveniste, M. Lerch, and M. De-Prada-Gil. Deliverable 2.6: Economical, technical, and environmental evaluation of phase 1. LIFES50 plus, 2017.

[**O4**] M. Lerch, G. Benveniste, and M. De-Prada-Gil. Deliverable 2.7: Evaluation report phase 2. LIFES50+, 2019.

[**O5**] G. Benveniste, M. Lerch, and M. De-Prada-Gil. Deliverable 2.8: Expected LCOE for floating wind turbines of 10MW and for 50m water depth. LIFES50+, 2019.

[**O6**] G. Benveniste and M. Lerch. Deliverable 2.9: Presentation of the methodology and results of the WP at a relevant conference. LIFES50+, 2019.

A.4 Presentations

Oral and poster presentations related to the PhD work are listed in this section.

[P1] M. Lerch, Multi-criteria assessment tool for floating offshore wind power plants. WindEurope Summit 2016, Hamburg, Germany, Oral presentation

[P2] M. Lerch, Sensitivity analysis of floating foundations for offshore wind power plants. WindFarms Conference 2017, Madrid, Spain, Oral presentation

[P3] M. Lerch, M. De-Prada-Gil, and G. Benveniste, Sensitivity analysis of floating offshore wind power plants. WindEurope Conference & Exhibition 2017, Amsterdam, The Netherlands, Poster presentation

[P4] M. Lerch, A simplified model for the dynamic analysis and power generation of a floating offshore wind turbine. The International Conference on Renewable Energy (ICREN) 2018, Barcelona, Spain, Oral presentation

[P5] M. Lerch, M. De-Prada-Gil, and C. Molins, Collection grid optimization of a floating offshore wind farm using particle swarm theory. DeepWind Conference 2019, Trondheim, Norway, Poster presentation

[P6] M. Lerch, Concept evaluation and expected LCOE for floating wind. WindEurope Conference & Exhibition 2019, Bilbao, Spain, Oral presentation

B

Floating offshore wind assessment tool

The Floating Offshore Wind Assessment Tool (FOWAT) has been developed in the H2020 LIFES50+ project for the purpose of evaluating FOWFs based on a multi-criteria evaluation approach [106]. In the course of the thesis work two more modules have been developed as part of the FOWAT tool, which are the Dynamic Analysis module and the Electrical Layout Optimization module. All modules are explained in more detail in the next section. Figure B.1 shows the main screen and the modules selection window.

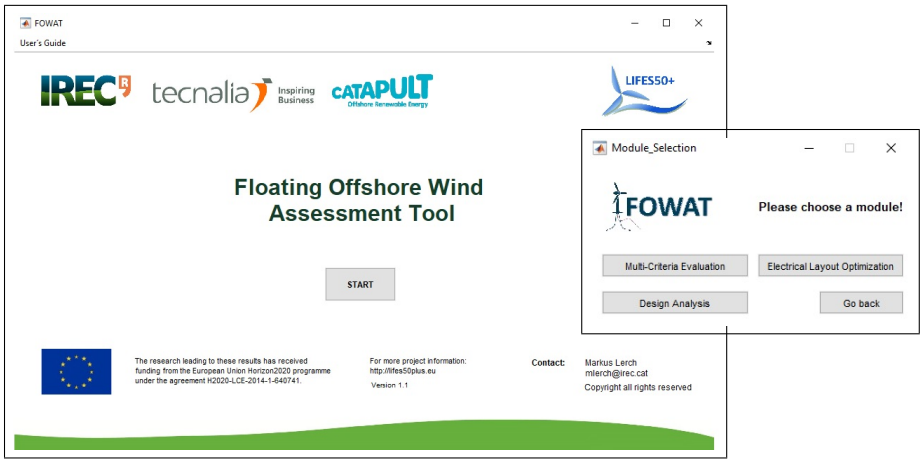

Figure B.1: Main Screen and Modules Selection.

B.1 Multi-Criteria Evaluation module

The Multi-criteria Evaluation module has been used in the LIFES50+ project to assess FOWFs economically in terms of a comprehensive LCOE calculation, a life cycle assessment and a risk evaluation. A description of the multi-criteria evaluation approach is provided in [106]. In this section only the LCOE calculation model is described further in detail as it has been used in Chapter 5 to perform the calculations. After selecting the Multi-criteria Evaluation module, a new window opens that contains a world map with the available offshore locations (Figure B.2). The user has to choose one of the available sites for the calculation and click next.

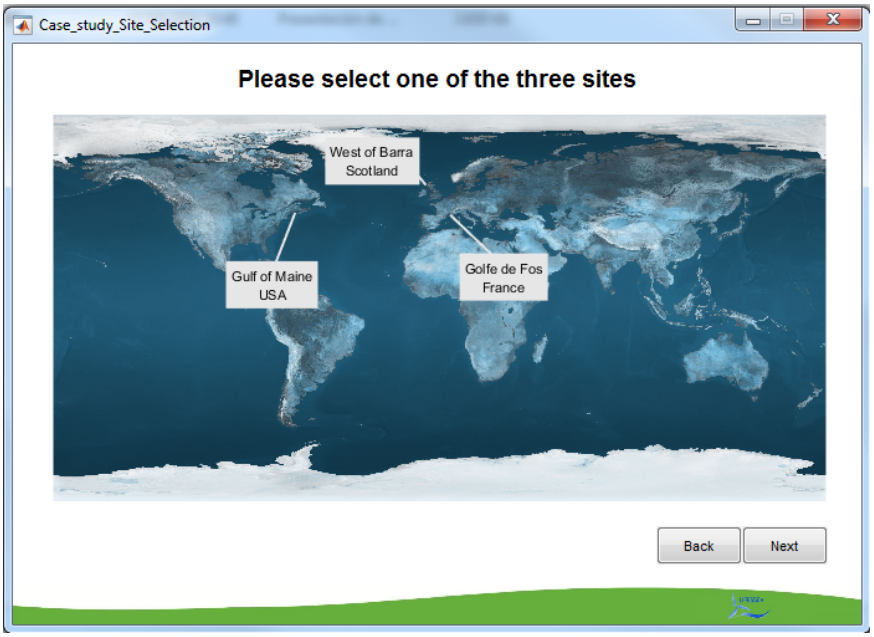

Figure B.2: Site selection.

In the following window (Figure B.3) the user has to choose a floating substructure concept from a drop-down list. All the FOWT concepts that have been studied in this thesis are available in the list. Next, the wind farm capacity is selected from a predefined list. After all criteria for the calculation are defined, the user is required to load the input data, which includes all required technical information and costs. The data is loaded from a comprehensive Excel questionnaire that has to be filled out previously. Figure B.4 presents this section of the tool.

Figure B.3: Concept selection.

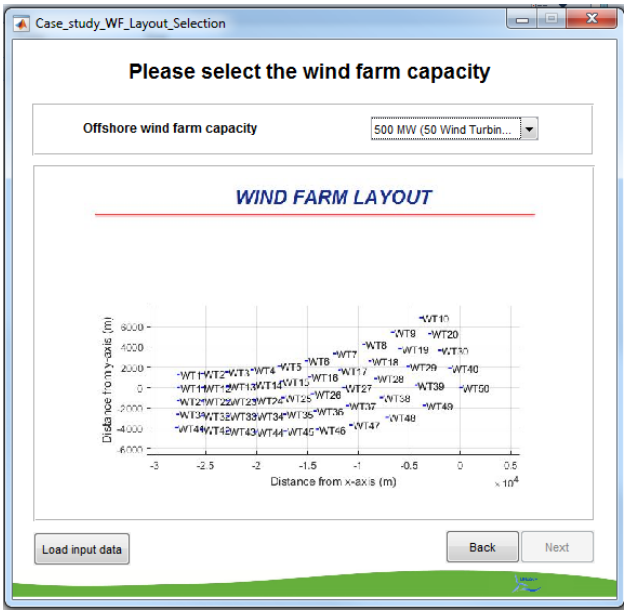

Figure B.4: Capacity selection.

After completion of the data upload, the user reaches the main menu of the Multi-criteria Evaluation module as illustrated in Figure B.5.

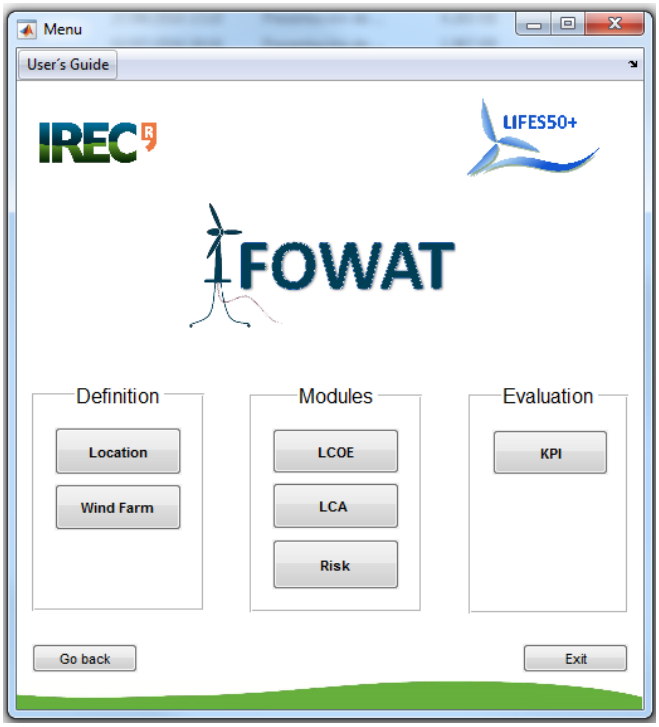

Figure B.5: Main menu.

The main menu consists of the sections: Definition, Modules and Evaluation. The Location Definition is used to define the location of the FOWF including General Data and Wind Conditions. General Data contains for example the name of the related country and ocean, the latitude and longitude as well as location specifications such as type of soil, distance to shore and water depths. In Wind Conditions, the wind speeds are defined according to their probability of occurrence at the site and a Weibull distribution is shown for each wind direction. Figure B.6 and Figure B.7 present these sections.

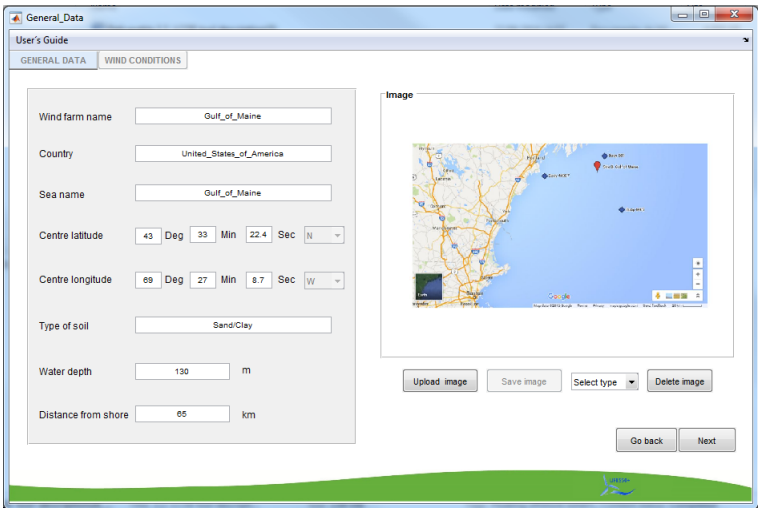

Figure B.6: General data.

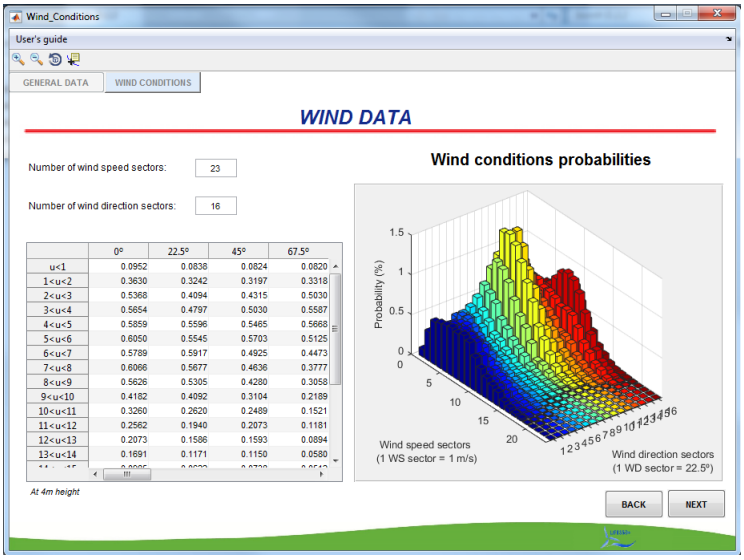

Figure B.7: Wind conditions.

The second part of the Definition section concerns the wind farm and contains the sections Wind Turbine, Wind Farm Layout and Grid Connection. Wind Turbine contains information regarding the wind turbine and the floating substructure. The section Wind Farm Layout presents the predefined wind farm layout according to the chosen location and capacity.

Figure B.8 and Figure B.9 show these sections of the tool.

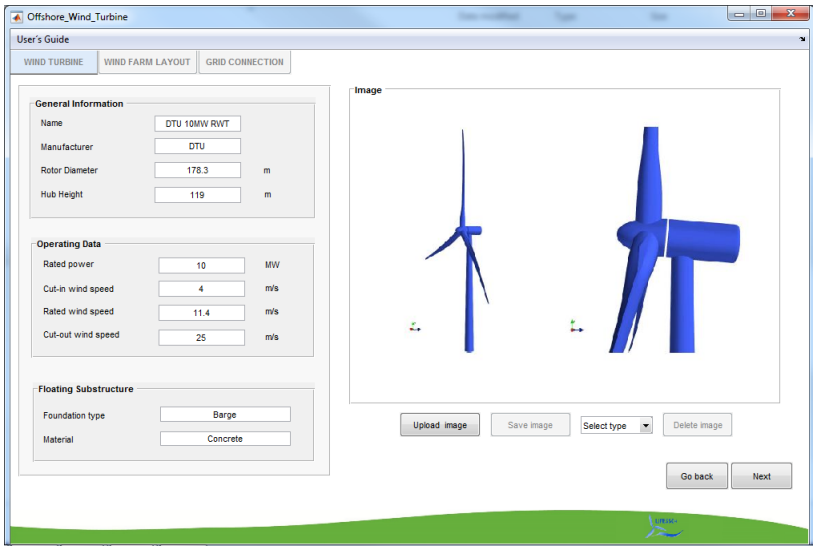

Figure B.8: Wind turbine model.

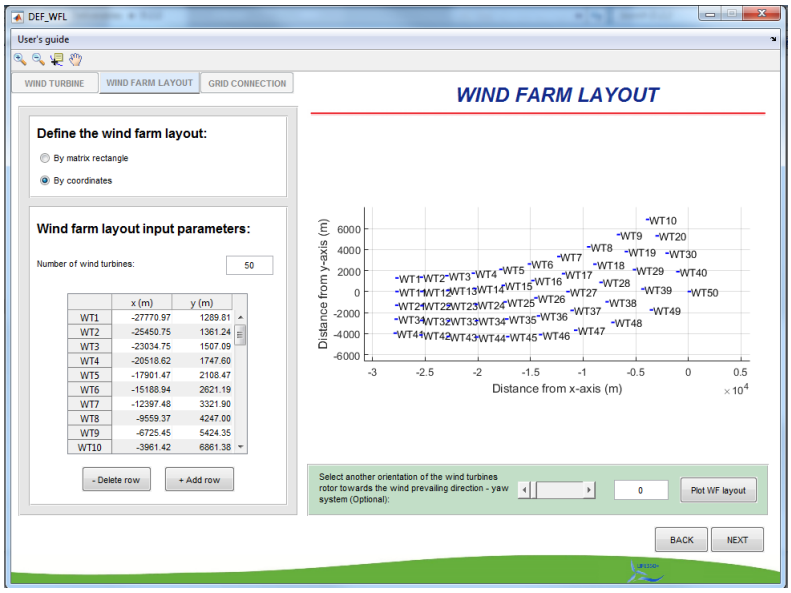

Figure B.9: Wind farm layout.

The section Grid Connection contains all necessary data concerning the collection grid, offshore substation and transmission grid such as nominal voltage, frequency, number of power cables, etc. An illustration of the collection grid and the location of the substation are also included. This section of the tool is presented in Figure B.10.

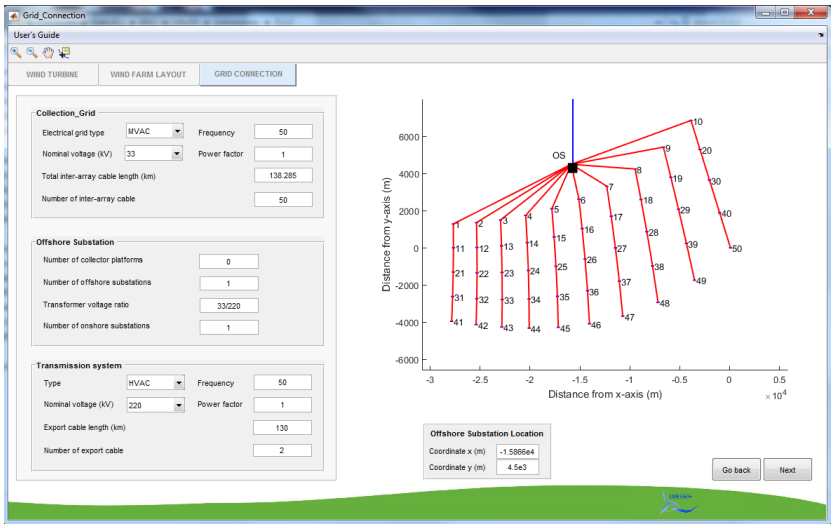

Figure B.10: Grid connection.

The LCOE module, presented in Figure B.11, consists of the Energy Production section and Life Cycle Cost section as well as the Results section. The LCOE module is used to calculate the LCOE value for the respective FOWF. The section energy production includes all parameters that are used to calculate the energy generation and losses in all components of the wind farm as well as the consideration of wake. Figures B.12 to B.15 illustrate this features of the tool.

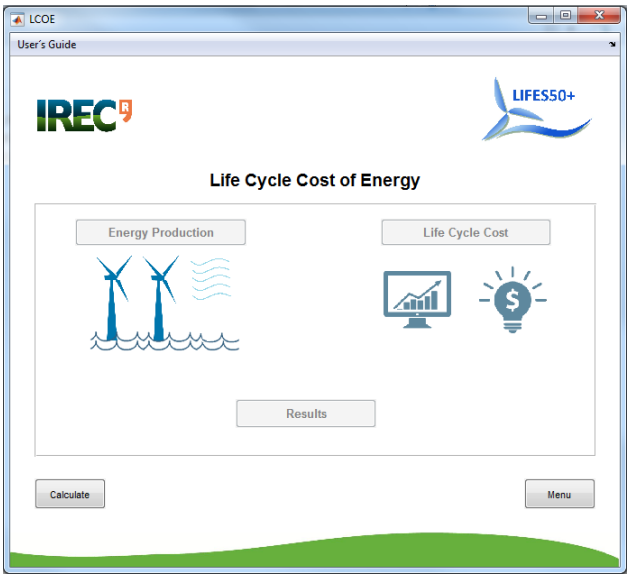

Figure B.11: LCOE calculation.

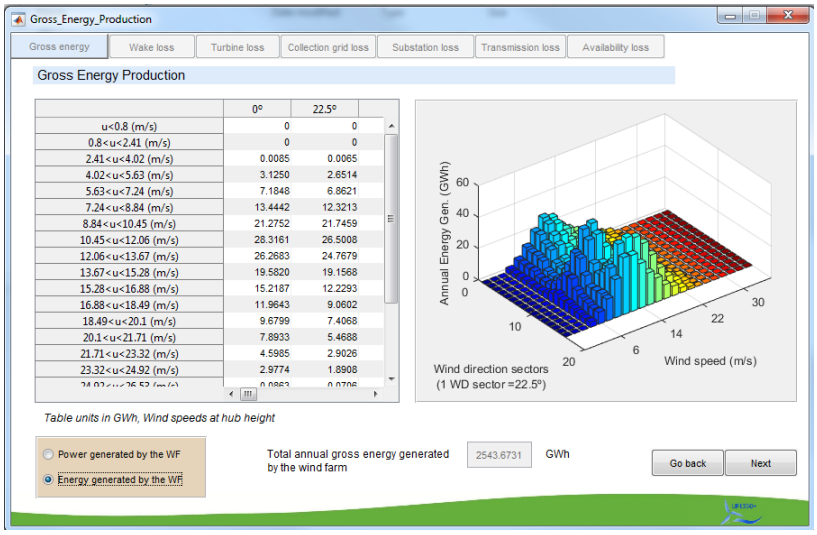

Figure B.12: Gross energy production.

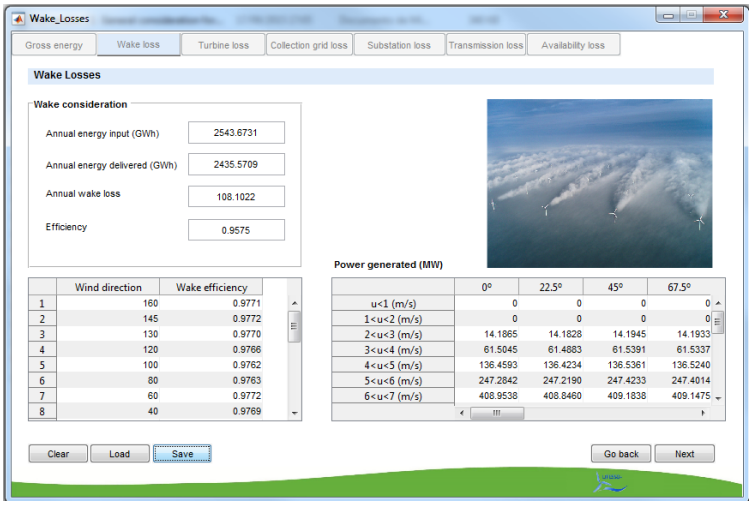

Figure B.13: Wake losses.

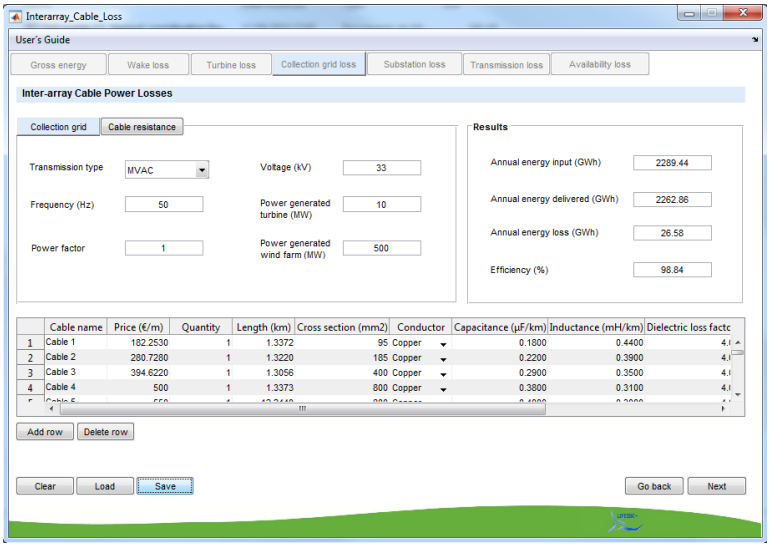

Figure B.14: Collection grid losses.

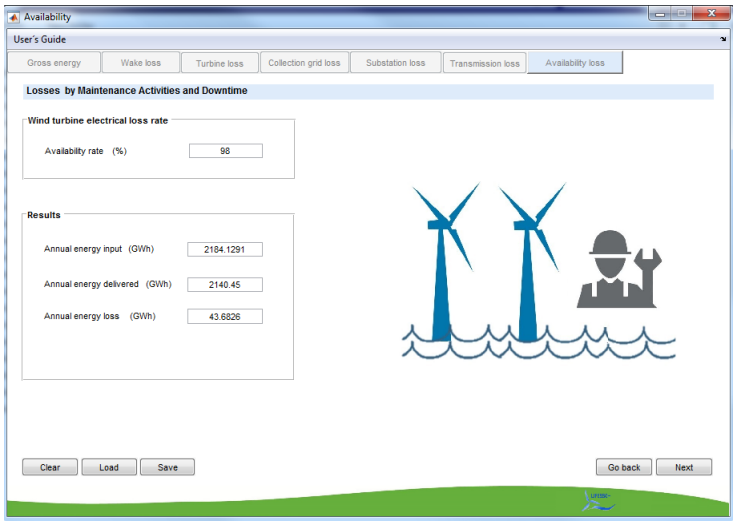

Figure B.15: Availability losses.

The section Life Cycle Costs contains all cost parameters that are used for the calculation and that occur during the different life cycle phases. Some exemplary images of these sections are presented in Figures B.16 to B.21.

Figure B.16: Life cycle cost.

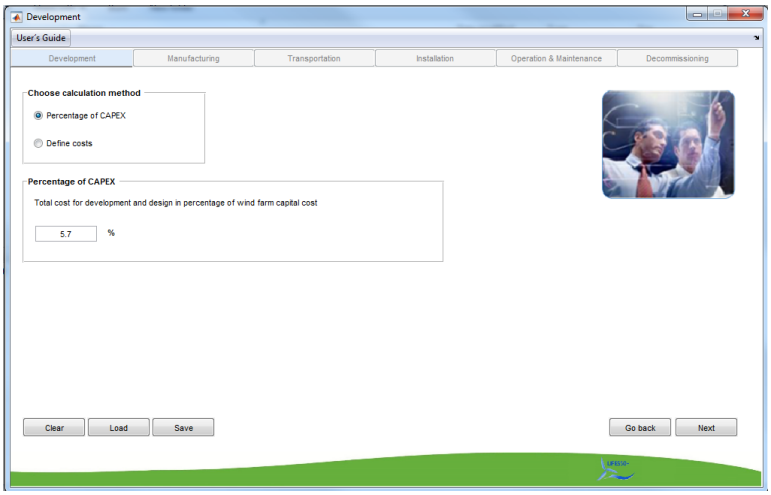

Figure B.17: Development cost.

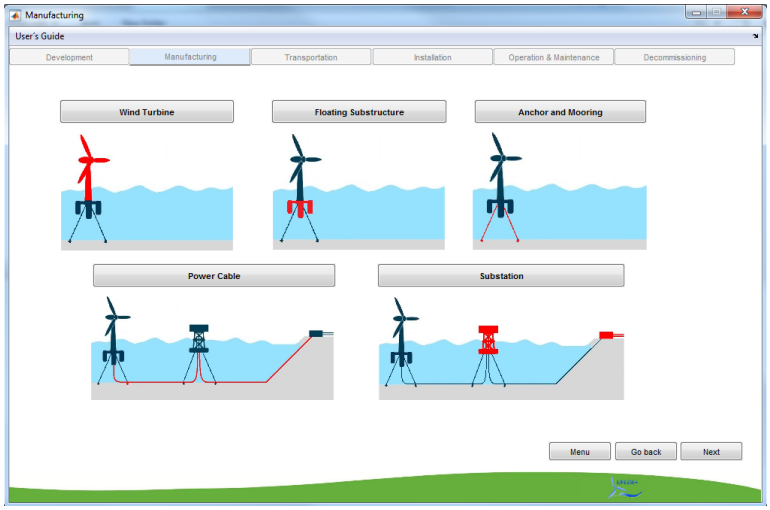

Figure B.18: Manufacturing overview.

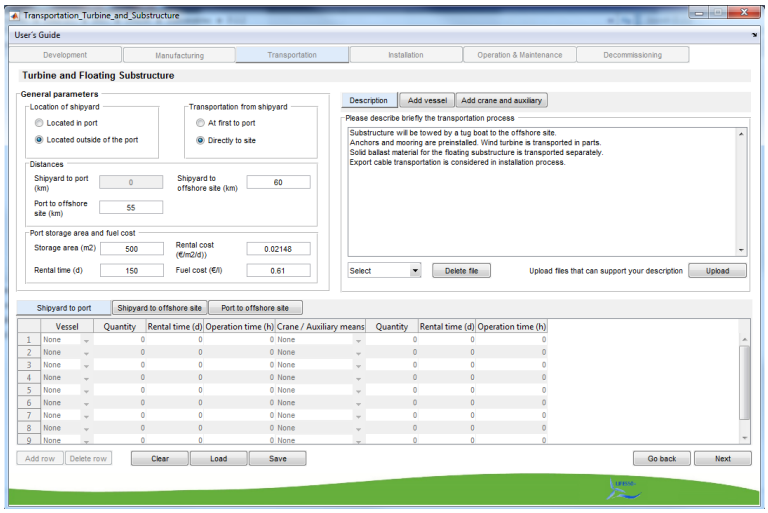

Figure B.19: Substructure transportation.

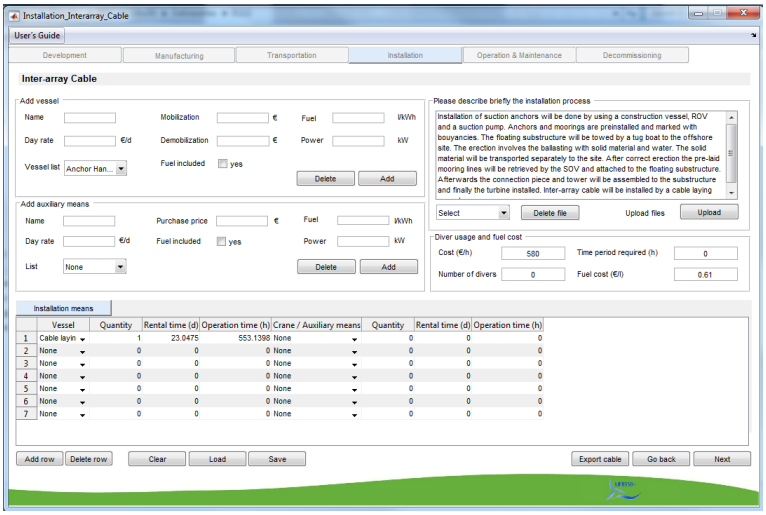

Figure B.20: Cable installation.

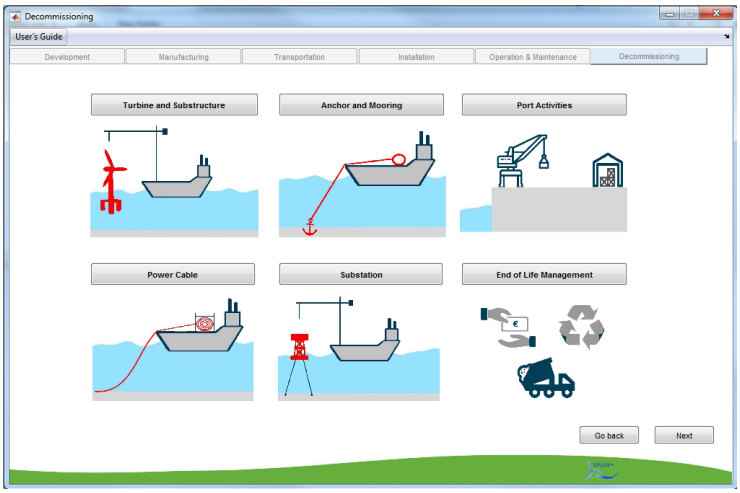

Figure B.21: Decommissioning overview.

The Results section contains the calculated LCOE value as well as the total energy production and life cycle costs considering the entire lifetime of the wind farm. Besides that, graphics are used to illustrate the energy losses in the system as well as the life cycle costs (Figure B.22).

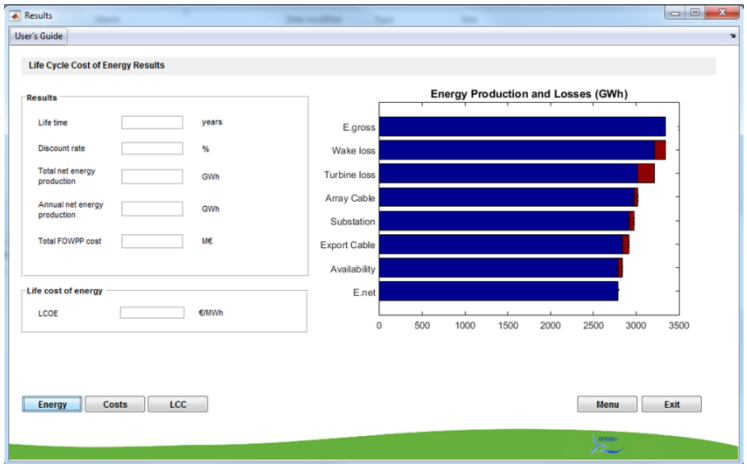

Figure B.22: Results section.

B.2 Dynamic Analysis module

The Dynamic Analysis module has been used in Chapter 4 to analyze the dynamic behavior and performance of a Spar-type FOWT with respect to different met-ocean conditions. A graphical user-interface has been developed also for this module. After starting the module, the user has to select at first the location and then the FOWT concept similar to the Multi-Criteria Evaluation module.

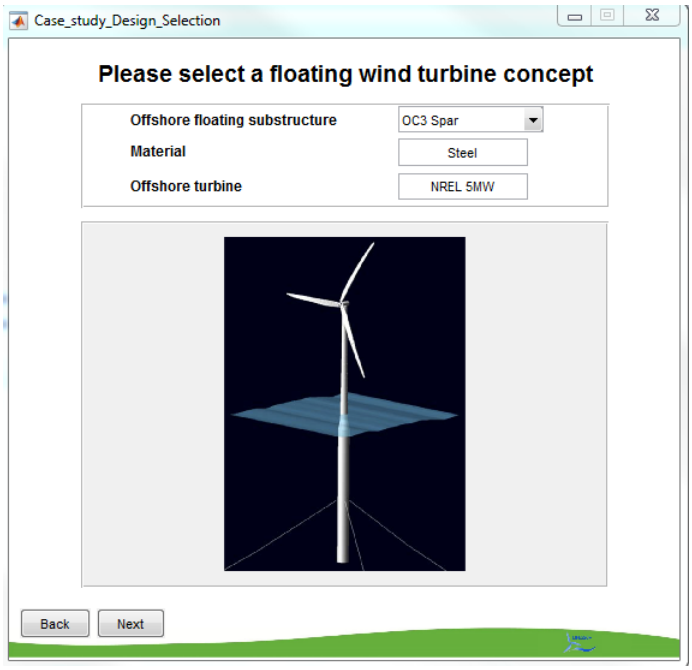

Figure B.23: Concept selection.

Then, the menu of this module opens as shown in Figure B.24. It consists of the sections Definition, Modules and Results, which are further explained next.

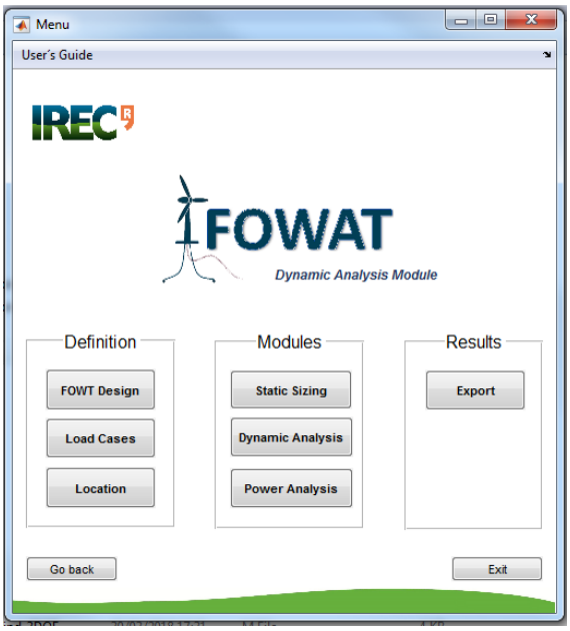

Figure B.24: Menu.

In the Definition section the user can modify the FOWT design and the offshore site as well as review the load cases as presented in Figure B.25 and Figure B.26.

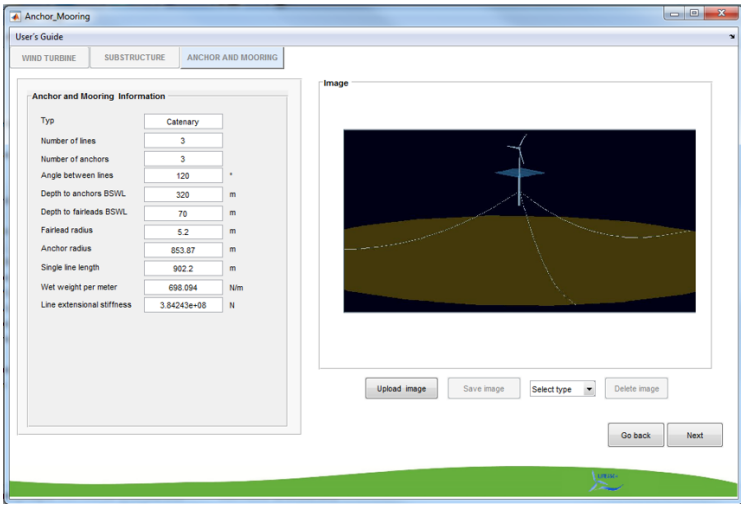

Figure B.25: Mooring system.

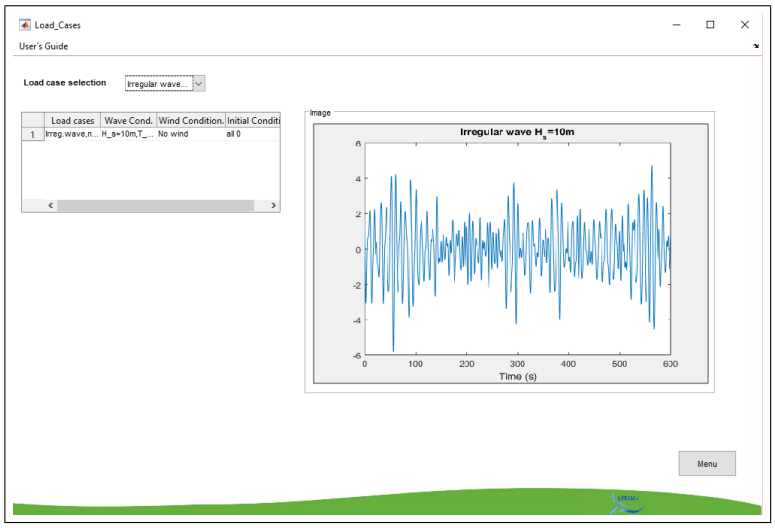

Figure B.26: Load cases.

The main features of the tool are the Static sizing, Dynamic Analysis and Power Analysis, which can be performed by clicking on the respective buttons in the Menu. The following figures illustrate the sections of the tool.

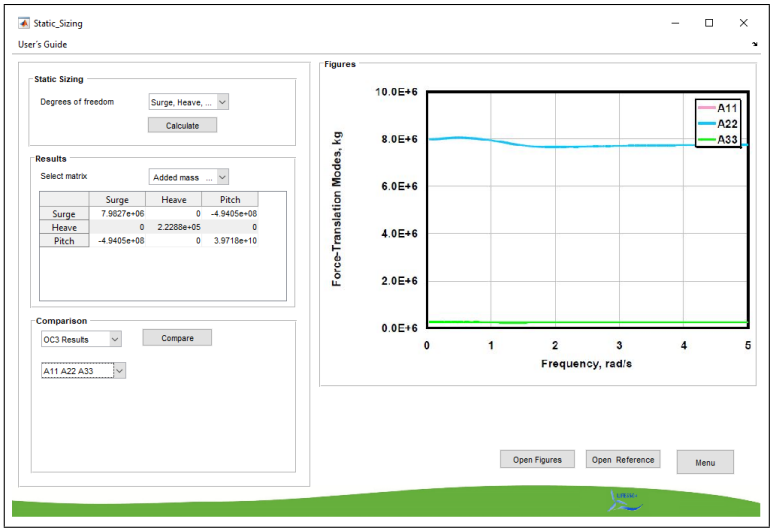

Figure B.27: Static sizing.

In the Static Sizing, the tool computes the main structural properties of the FOWT.

In the Dynamic Analysis, the tool computes for a chosen load case the dynamic response of the FOWT.

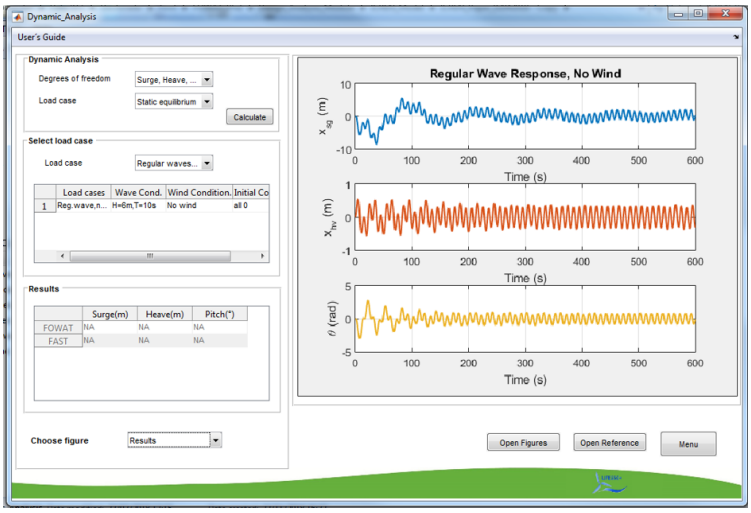

Figure B.28: Dynamic analysis.

The Power Analysis section (Figure B.29) allows to compute the energy generation for a specific site considering the dynamic behavior of the structure. Furthermore, the tools displays the response in each degree of freedom and allows to perform a sensitivity analysis for different threshold limits.

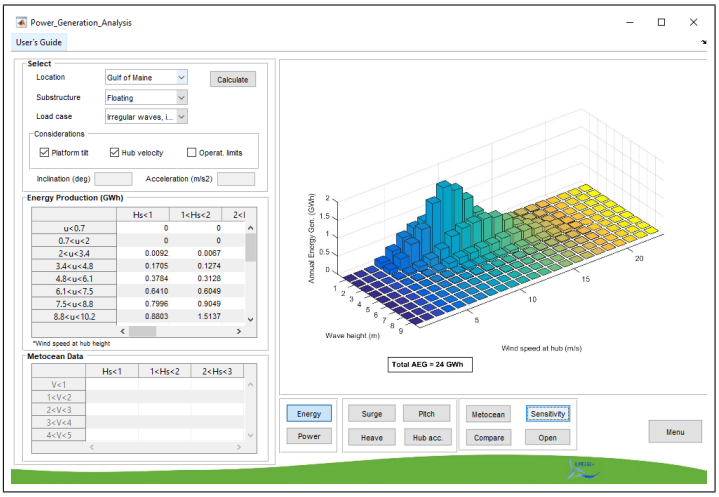

Figure B.29: Power analysis.

B.3 Electrical Layout Optimization module

The Electrical Layout Optimization Module has been used in Chapter 6 to optimize the collection grid of a FOWF. The code of the optimization algorithm has been written in MATLAB. A graphical user interface has not been developed for this module yet. However, the main results of the optimization can be displayed in figures as shown in Figure B.30 and Figure B.31.

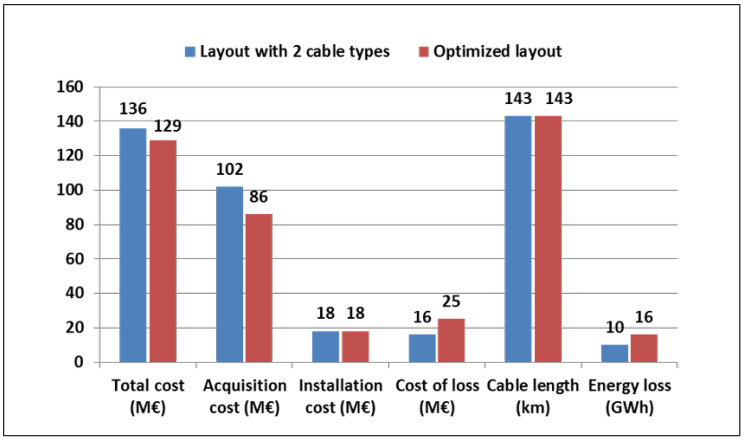

Figure B.30: Optimized costs.

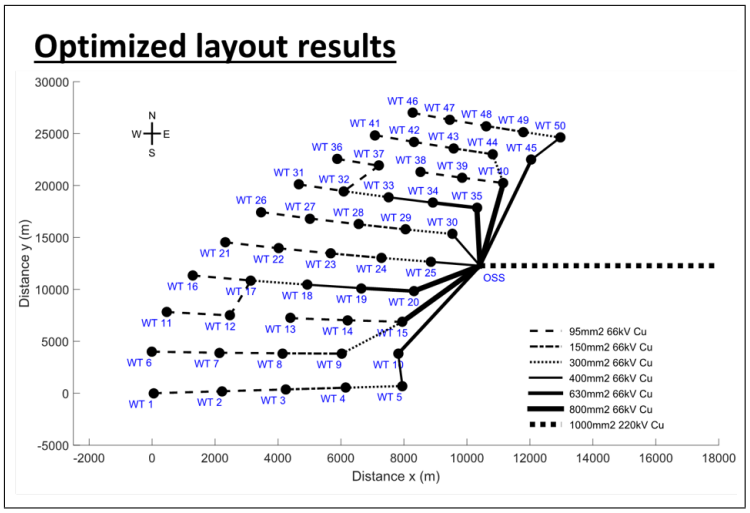

Figure B.31: Optimized layout.